

**Quantum Dots-Amplified Electrochemical Cytochrome
P450 Phenotype Sensor for Tamoxifen,
a Breast Cancer Drug**



UNIVERSITY *of the*
WESTERN CAPE



By

UNIVERSITY *of the*
WESTERN CAPE

Usisipho Feleni

(MSc Nanoscience)

A thesis submitted in fulfilment of the requirements for the degree of

Doctor of Philosophy

Faculty of Science, Department of Chemistry

University of the Western Cape

Cape Town, South Africa

Supervisor: Prof Emmanuel I. Iwuoha

May 2017

ABSTRACT

Breast cancer is regarded as the most common cancer in South Africa and its rate of occurrence is increasing. About one in every 31 South African women are at the risk of developing breast cancer and early diagnosis and treatment guarantee 90% survival rate. Tamoxifen is the drug of choice for the treatment of all stages of breast cancer. The drug binds with estrogen receptor (ER) to minimize the transcription of estrogen dependent genes. However, nearly 50% of ER-positive breast cancer patients either become resistant or fail to respond to tamoxifen resulting in a serious clinical challenge in breast cancer management. The Grand Health Challenges of South Africa includes the development of cost effective diagnostic systems suitable for early detection of diseases and drug resistivity for timely invention and better patient management. Though HIV and Tuberculosis (TB) are focussed on in South African Health management system, breast cancer (which happens to be responsible for as much death among women as TB and HIV combined) is also included as a priority disease. There are currently serious controversies among clinical oncologists and pharmacologists on the role of genetic polymorphism of cytochrome P450 (CYP) enzymes (CYP2D6 and CYP3A4) on the effectiveness of tamoxifen, the most prescribed breast cancer drug. The cost of genotype-based tamoxifen therapeutic monitoring protocols (expected to distinguish between poor, moderate and ultra-rapid metabolisers of tamoxifen) is exorbitant, though genotype alone does not determine a patient's dose-response profile. This thesis focussed on the development of next generation phenotype-based diagnostic nanobiosensors (*b-canceranosens*) for signalling a breast cancer patient's complete response profile for tamoxifen. The signalling protocol is an electrochemical mono-oxygenation reaction involving the enzymes that metabolise tamoxifen's biotransformation. The biosensors were developed with biocompatible palladium telluride-quantum dots (PdTeQDs) and genetically engineered CYP2D6 and CYP3A4 on gold electrode. The quantum dots were synthesised as

colloidal poly-dispersed materials (by a simple, inexpensive and reproducible aqueous method) capped with 3-mercaptopropionic acid (3-MPA), thioglycolic acid (TGA) or 3, 3'-Dithiodipropionic acid (3,3'-DTDPA), to improve their stability, solubility and biocompatibility. The effect of the capped ligands on the QDs was investigated by microscopic, spectrophotometric and electrochemical analysis. The capping of PdTeQDs was confirmed by Fourier transform infrared spectroscopy (FTIR) via the specific COOH and CH₂ signature bands of 3-MPA, TGA and 3,3'-DTDPA. High resolution transmission electron microscopy (HR-TEM) and small angle X-ray scattering (SAXS) revealed that the PdTeQDs materials have average diameters of 3-5 nm. The optical properties of the QDs materials were studied by ultraviolet-visible spectroscopy (UV-Vis) which produced an absorbance band at 320 nm that corresponded to energy band gap values of 3 eV, 3.87 eV and 2.2 e V for 3-MPA-, TGA- and 3,3'-DTDPA-capped PdTeQDs, respectively. The quantum dots were immobilized on electrodes together with CYP3A4 or CYP2D6, and the resultant bioelectrode was shown to undergo monooxygenation. The effectiveness of the CYP-based phenotype biosensor was first tested with indinavir, a protease inhibitor anti-retroviral (ARV) drug which is physiologically metabolised by CYP3A4. The limit of detection (*LOD*) of CYP3A4/3-MPA-PdTeQDs/Cyst/Au biosensor was 40×10^3 ng/mL indinavir for cyclic voltammetric (CV) detection at 0.25 V. The corresponding value for CYP3A4/TGA-PdTeQDs/Cyst/Au sensor obtained at 0.9 V was 90×10^3 ng/mL indinavir. In the case of tamoxifen sensing, 4 biosensors were tested, which differed on the capping agents and enzymes used. CYP2D6/TGA-PdTeQDs/Cyst/Au gave a detection limit of 9.52×10^{-5} ng/mL tamoxifen at a square wave voltammetry (SWV) potential of 0.3 V, while CYP3A4/TGA-PdTeQDs/Cyst/Au gave an *LOD* value of 1.75×10^{-5} ng/mL tamoxifen at a SWV potential of 0.28 V. The tamoxifen phenotype sensors developed with 3,3'-DTDPA produced best signals by differential pulse voltammetry (DPV) transduction but with higher

detection potentials than other sensor formats. The *LOD* of CYP2D6/3,3'-DTDPA-PdTeQDs/Cyst/Au at a DPV signalling voltage of 0.96 V was 1.95×10^{-4} tamoxifen. On the contrary CYP3A4/3,3'-DTDPA-PdTeQDs/Cyst/Au, which contained CYP3A4, exhibited greater sensitivity characterised by low *LOD* (6.88×10^{-5} tamoxifen) and low DPV detection potential (0.46 V). Generally, the *LOD* values obtained with the various phenotype sensors were lower than tamoxifen's maximum steady state plasma concentration (C_{max} 40 ng/mL), thereby indicating that the sensing device, in principle, would be suitable for real time monitoring the drug at point-of-care. The phenotype based biosensor system designed in this project, holds the potential for monitoring proper dosages of tamoxifen for breast cancer patients.



KEYWORDS

Breast cancer

Capping agents

Cyclic voltammetry (CV)

Cytochrome P450 enzymes

Differential pulse voltammetry (DPV)

Electrochemical phenotypic sensors

Indinavir

Limit of detection (LOD)

Palladium telluride

Quantum dots

Square wave voltammetry (SWV)

Tamoxifen



DECLARATION

I declare that *Quantum Dots-Amplified Electrochemical Cytochrome P450 Phenotype Sensor for Tamoxifen, a Breast Cancer Drug* is my own work and has not been submitted before for any degree or examination in any other university, and that all the sources I have used or quoted have been indicated or acknowledged as complete references.



Usisipho Feleni

May 2017

Signed

A handwritten signature in black ink, appearing to be "U. Feleni", written over a horizontal line.

ACKNOWLEDGEMENT

I would like to thank God for giving me faith, good health, wisdom and strength, dedication and courage to finish this work.

“For I know the thoughts that I think towards you, says the Lord, thoughts of peace and not evil, to give you a future and a hope” JERIMIAH 29: 11.

To my supervisor: Prof Emmanuel Iwuoha; thank you for your guidance, support and encouragement throughout this study and thank you for being my source of inspiration.

To my Family: To my grandmother and mother, **Nonkuthalo Beauty Feleni** and **Sindiswa Ngoza Feleni**, thank you for all your unconditional love, support, and courage. Thank you for all the sacrifices you have made, I owe all my success to you. To my one and only son **Samkelo Onothando Feleni**, thank you for being the centre of my life and for coping in my absence. You have made my life to be meaningful.

To Unathi Sidwaba: Thank you for being my big sister and my friend. Thank you for your support, motivation and love for all these years. I wish you all the best in future.

To Chemistry Department: Mrs Wilhemina Jackson, thank you very much for your willingness to assist in solving all the academic and technical problems.

SensorLab Researchers: To Dr Tesfaye Waryo, Dr Abd Baleg, Dr Milua Masikini, Dr Natasha Ross, Dr Rachel Fanelwa Ajayi, Dr Abongile Jijana, Dr Chinwe Ikpo, Dr Mawethu Bilibana, Dr Hlamulo Makelane, and Dr Christopher Sunday, thank you for sharing your opinions and experience through which I received the required information for my project.

To SensorLab Colleagues: Nomxolisi Dywili, Nomaphelo Ntshongontshi, Anne Lurtgarde Djoumessi, Keagen Pokpas, Francis Ntumba Muya, Meryck Ward, Vivian John Suru, Sinazo

Qakala, Lerato Phelane, Lindsay Wilson, Candice Franke, Al Cerillio Farao, Laura Pacoste, thank you for being such good colleagues and friends.

To sponsors: My sincere gratitude goes to the National Research Foundation (NRF) for Doctoral Scholarship, and the EU Marie Curie IRSES Directorate for the award of a fellowship under the SmartCancerNanosens project for research exchange visits to the Centre for Biosensors and Bioelectronics, Linköping University, Sweden. I am also grateful to the L'Oréal-UNESCO for Women in Science, for the Doctoral Fellowship Award I received in 2016. I will like to thank the Department of Science and Technology (DST) of South Africa for the Women in Science TATA Doctoral Fellowship Award of 2016. Finally, I am grateful for The Royal Society of the United Kingdom and the National Research Foundation of Singapore Award, to attend the Commonwealth Science Conference 2017 in Singapore. The conference provided me an opportunity to present my work to an international audience of 400 leading scientists from across the Commonwealth.

UNIVERSITY of the
WESTERN CAPE

DEDICATION

This dissertation is dedicated to:

My late Grandfather, Uncle and Aunt

Swaphi John Feleni, Mbonisi Feleni and Nomgqibelo Sindisiwe Feleni.

May your wonderful souls rest in peace.

To my Grandmother and Mother

Nonkuthalo Beauty Feleni and Sindiswa Ngoza Feleni.

My siblings

Lwandisolomntu Feleni, Ofentse Feleni and Uligwiba Abena Feleni.

Finally, to my lovely son

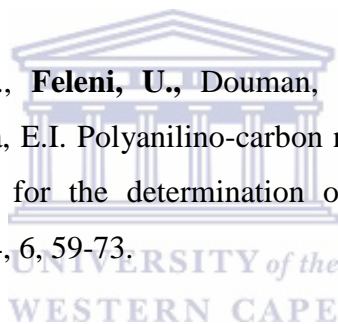
Samkelo Onothando Feleni.

UNIVERSITY of the
WESTERN CAPE

LIST OF PUBLICATIONS

1. **Usisipho Feleni**, Valerio Beni, Anthony P.F. Turner, Emmanuel I. Iwuoha. Phenotype biosensor for signaling tamoxifen activation in breast cancer patients *Electrochemistry Communications*, In Press.
2. **Usisipho Feleni.**, Unathi Sidwaba., Samantha Douman., Emmanuel I. Iwuoha. Palladium telluride quantum dots biosensor for the determination of indinavir drug. *Sensors and Actuators B: Chemical*, In Press.
3. **Feleni, U.**, Ajayi, F., Jijana, F., Sidwaba, U., Douman, S., Baker, P. and Iwuoha, E. Tin selenide quantum dots electrochemical biotransducer for the determination of indinavir-a protease inhibitor anti-retroviral drug. *Journal of Nano Research* 2017, 45, 12-24.
4. Samantha Douman, **Usisipho Feleni**, Natasha Ross, Xolile Fuku, Rachel Ajayi, Ezo Nxusani, Nomaphelo Ntshongontshi, Unathi Sidwaba, Candice Rassie, Abongile Jijana, Priscilla Baker, Avril Williams, Emmanuel Iwuoha. New generation nanoelectrochemical biosensors for disease biomarkers: 1. Indium telluride quantum dots signaling of telomerase cancer biomarker. *Journal of Nanoscience and Nanotechnology*, 2016, 16, 12844-12850.
5. Masikini, M., Ndangili, P.M., Ikpo, C.O., **Feleni, U.**, Douman, S., Sidwaba, U., Waryo, T.T., Baker, P.G. and Iwuoha, E.I., 2016. Optoelectronics of stoichiometrically controlled palladium telluride quantum dots. *Journal of Nano Research*, 2016, 40, 29-45.
6. Rachel F. Ajayi, Ezo Nxusani, Samantha F. Douman, Anovuyo Jonnas, Nomaphelo Ntshongontshi, **Usisipho Feleni**, Keagan Pokpas, Lindsay Wilson, and Emmanuel I. Iwuoha. Silver nanoparticle-doped poly (8-anilino-1-naphthalene sulphonic Acid)/CYP2E1 nanobiosensor for isoniazid - a first line anti-tuberculosis drug. *Journal of Nano Research*, 2016, 44, 229-251.

7. Nomaphelo Ntshongontshi, Abd Almonam A. Baleg, Rachel F. Ajayi, Candice Rassie, Ezo Nxusani, Lindsay Wilson, **Usisipho Feleni**, Unathi Sidwaba, Sinazo Qakala, Samantha Duoman, Priscilla Baker and Emmanuel Iwuoha. Cytochrome P450-3A4/copper-poly (propylene imine)-polypyrrole star co-polymer nanobiosensor system for delavirdine - a non-nucleoside reverse transcriptase inhibitor HIV drug. *Journal of Nano Research*, 2016, 44, 265-280.
8. Unathi Sidwaba, **Usisipho Feleni**, Hlamulo Makelane, Ezo Nxusani, Lindsay Wilson, Sinazo Qakala, Candice Rassie, Milua Masikini, Tesfaye Waryo, Rachel F. Ajayi, Priscilla Baker, and Emmanuel Iwuoha. A novel polyaniline nanocomposite with doping effects of poly (methyl methacrylate) and TiO₂ nanoparticles. *Journal of Nano Research*, 2016, 44, 281-292.
9. Sidwaba, U., Ajayi, R.F., **Feleni, U.**, Douman, S., Baker, P.G., Vilakazi, S.L., Tshikhudo, R. and Iwuoha, E.I. Polyanilino-carbon nanotubes derivatised cytochrome P450 2E1 nanobiosensor for the determination of pyrazinamide anti-tuberculosis drugs. *Nano Hybrids*, 2014, 6, 59-73.



LIST OF CONFERENCE PRESENTATIONS

Title: Smart Bio-electrochemical Sensing and Signalling of Inter-Individual Responses to Breast Cancer Treatment. **Poster presentation** at The Royal Society Commonwealth Science Conference in Singapore, Matrix Building, 30 Biopolis Street, Biopolis district close to the National University of Singapore, **13-16 June 2017**. Authors: Usisipho Feleni, Valerio Beni, Anthony Turner, Emmanuel Iwuoha.

Title: Smart Bio-electrochemical Sensing and Signalling of Inter-Individual Responses to Breast Cancer Treatment. **Oral presentation** at the Symposium on Nanomedicine and Cancer in South Africa, National Zoological Garden (NZG), Pretoria Zoo, 232 Boom St, South Africa, **25 October 2016**. Authors: Usisipho Feleni, Valerio Beni, Anthony Turner, Emmanuel Iwuoha.

Title: Palladium Telluride Quantum Dots-Based Phenotype Biosensor for Breast Cancer Drugs. **Oral presentation** at Nanoscience Platform Symposium in Hotel Verde, Cape Town Airport, South Africa, **03 October 2016**. Authors: Usisipho Feleni, Valerio Beni, Anthony Turner, Emmanuel Iwuoha.

Title: Smart Bio-electrochemical Sensing and Signalling of Inter-Individual Responses to Breast Cancer Treatment. **Oral presentation** at the L'Oréal-UNESCO for Women in Science Sub-Saharan Africa 2016 Award, Johannesburg, South Africa, **28 September 2016**. Authors: Usisipho Feleni, Valerio Beni, Anthony Turner, Emmanuel Iwuoha.

Title: Responses of Palladium Telluride Quantum Dots-Based b-Cancernanosens. **Oral presentation** at African Nanoscience and Nanotechnology Initiative (AANNI), University of the Western Cape, Cape Town, South Africa, **20-22 September 2016**. Authors: Usisipho Feleni, Valerio Beni, Anthony Turner, Emmanuel Iwuoha.

Title: Chalcogenide quantum dots bioelectrode system for determining the metabolism of protease Inhibitor anti-retroviral drugs. **Oral presentation** at The International Conference on Pure and Applied Chemistry (ICPAC 2016) in Mauritius, **18-22 July 2016**. Authors: Usisipho Feleni, Unathi Sidwaba, Pricilla Baker, Emmanuel Iwuoha.

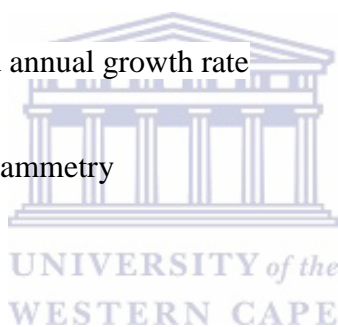
Title: Cytochrome P450 enzyme electrodes for bio-marking breast cancer drug metabolism. **Poster presentation** at An International Workshop on Microsystems Technologies for African Health (μ -Med-A 2015) in Protea Hotel Stellenbosch, South Africa, **16-19 September 2015**. Authors: Usisipho Feleni, Valerio Beni, Anthony Turner, Emmanuel Iwuoha.

Title: Palladium Telluride Quantum Dots-Cytochrome P450 Biosensor for the detection of breast cancer drug – Tamoxifen. **Poster presentation** at the 3rd International Symposium on Electrochemistry under on “Materials, Analytical and Physical Electrochemistry Today” (MAPET’15)”, University of the Western Cape, Cape Town, South Africa, **26-28 May 2015**. Authors: Usisipho Feleni, Valerio Beni, Anthony Turner, Emmanuel Iwuoha.

Title: Palladium telluride-CYP450 biosensor for the determination of tamoxifen breast cancer drug. **Poster presentation** at Japan-Sweden Seminar on Nanomaterials and Nanotechnology, Linköping University, Linköping, Sweden, **10-11 March 2015**. Authors: Usisipho Feleni, Valerio Beni, Anthony Turner, Emmanuel Iwuoha.

LIST OF ABBREVIATIONS AND ACRONYMS

AIDS	Acquired immune deficiency syndrome
ARV	Anti-retroviral drugs
ATR-FTIR	Attenuated total reflection- Fourier transformation infrared spectroscopy
BC	Breast cancer
CANSA	Cancer association of South Africa
CISN	Cancer information support network
CAGR	Compound annual growth rate
CV	Cyclic voltammetry
Cyst	Cystamine
CYP450-2D6	Cytochrome P450-2D6
CYP450-3A4	Cytochrome P450-3A4
DPV	Differential pulse voltammetry
3, 3'-DTPA	3, 3'-Dithiodipropionic acid
DLR	Dynamic linear range
END	Endoxifen
EDS	Energy dispersive spectrometry
ER α	Estrogen receptor alpha



EDC	1-ethyl-3(3-dimethylaminopropyl) carbodiimide hydrochloride
FDA	Food and drug administration
FT-IR	Fourier transformation infrared spectroscopy
AuE	Gold electrode
HIV	Human immunodeficiency virus
HR-SEM	High resolution scanning Electron microscopy
HR-TEM	High Resolution transmission electron microscopy
HR	Hormone Receptor
4-OHT	4-Hydroxytamoxifen
IDV	Indinavir drug
LOD	Limit of detection
3-MPA	3-Mercaptopropionic acid
NDMT	N-DesmethylTamoxifen
NHS	N-Hydroxysuccinimide
PdTeQDs	Palladium telluride quantum dots
PBS	Phosphate buffer solution
PL	Photoluminescence spectroscopy
PIs	Protease inhibitors
SAED	Selected area electron diffraction



SERM	Selective estrogen receptor modulator
SWV	Square wave voltammetry
TAM	Tamoxifen
TB	Tuberculosis
TDM	Therapeutic drug monitoring
TGA	Thioglycolic acid
UV-Vis	Ultraviolet-Visible spectrophotometry
WHO	World health organisation
XPS	X-ray photoelectron spectroscopy
XRD	X-ray diffraction

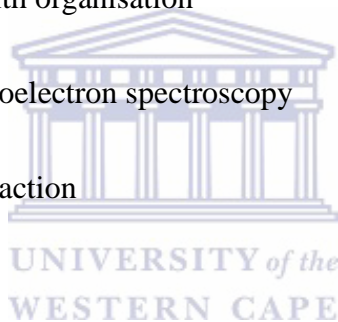
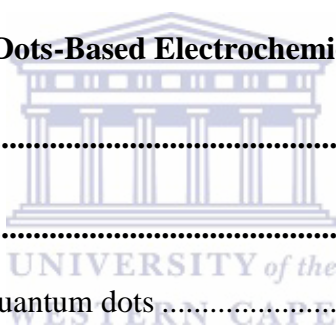


TABLE OF CONTENTS

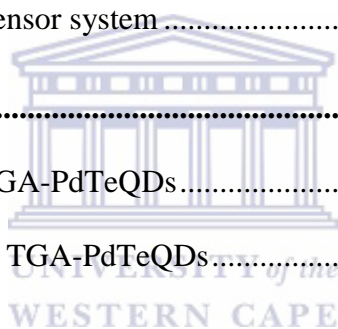
TITLE PAGE	i
ABSTRACT	ii
KEYWORDS	v
DECLARATION	vi
ACKNOWLEDGEMENT	vii
DEDICATION	ix
LIST OF PUBLICATIONS	x
LIST OF CONFERENCE PRESENTATIONS	xii
LIST OF ABBREVIATIONS AND ACRONYMS	xiv
TABLE OF CONTENTS	xvii
LIST OF FIGURES	xxiv
LIST OF TABLES	xxx
CHAPTER ONE	1
Introduction	1
Summary	1
1.1 Background	2
1.1.1(a) Prevalence of breast cancer (BC) and Tamoxifen	2
1.1.1(b) Problem statement	4
1.1.2(a) Prevalence of human immunodeficiency virus and Indinavir metabolism	6
1.1.2 (b) Problem statement	9

1.2 Rationale and motivation of the study	10
1.3 Aim of the project.....	13
1.3.1 Fabrication of CYP3A4 or CYP2D6 biosensor: 3,3'-DTDPA or TGA-PdTeQDs/Cyst/Au biosensor system for tamoxifen involved:.....	13
1.3.2. Fabrication of CYP3A4 biosensor: 3-MPA or TGA-PdTeQDs/Cyst/Au biosensor system for indinavir involved:	14
1.4 Thesis outline	15
CHAPTER TWO	28
Literature review	28
Palladium Telluride Quantum Dots-Based Electrochemical Biosensors.....	29
Abstract.....	29
2.1 Quantum dots	30
2.1.1. Nanotechnology and quantum dots	30
2.1.2 Synthesis of quantum dots	31
2.1.3 Role of surface modification and bioconjugation of quantum dots.....	32
2.2 Applications of quantum dots	34
2.2.1. Quantum dots-based electrochemical sensors	34
2.2.2 Enzyme-based electrochemical biosensors	35
2.3 Electrochemical biosensors for tamoxifen	37
2.3.1 Biosensors for tamoxifen.....	37
2.4 Breast cancer and tamoxifen metabolism	41
2.4.1 Breast cancer.....	41
2.4.2 Tamoxifen metabolism.....	42



2.5 Conclusion.....	44
CHAPTER THREE.....	55
Summary.....	55
Palladium Telluride Quantum Dots Phenotype Sensor for Indinavir	56
Abstract.....	56
3. Introduction.....	57
3.1 Experimental.....	58
3.1.1 Chemicals and sample preparation	58
3.1.2 Instrumentation.....	59
3.1.3 Synthesis of water-soluble 3-MPA-capped PdTeQDs.....	60
3.1.4 Preparation of 3-MPA-PdTeQDs/Au modified electrode	60
3.1.5 Preparation of the biosensor system	61
3.2 Results and discussion.....	61
3.2.1. Crystal structure of 3-MPA-PdTeQDs	61
3.2.2 Morphological properties of 3-MPA-PdTeQDs	63
3.2.3 Optical properties of 3-MPA-PdTeQDs	64
3.2.4 Structural properties of 3-MPA-PdTeQDs	65
3.3 Electrochemical properties of the biosensor materials.....	66
3.3.1 Electrochemistry of 3-MPA-PdTeQDs	66
3.3.2 Biosensor responses to indinavir drug.....	68
3.4 Conclusion.....	70
CHAPTER FOUR.....	78
Summary.....	78

Biocompatible Thioglycolic Acid-Palladium Telluride Quantum Dots-Based Indinavir Sensor	79
Abstract.....	79
4. Introduction.....	80
4.1 Experimental.....	81
4.1.1 Chemicals and sample preparation	81
4.1.2 Instrumentation	82
4.1.3 Synthesis of water-soluble TGA-PdTeQDs	83
4.1.4 Preparation of cysteamine monolayer onto the gold electrode surface	84
4.1.5 Preparation of the biosensor system	84
4.2 Results and discussion.....	85
4.2.1 Optical properties of TGA-PdTeQDs.....	85
4.2.2 Structural properties of TGA-PdTeQDs.....	86
4.3 Electrochemistry of the biosensor platform.....	88
4.3.1 Electrochemistry of cysteamine and TGA-PdTeQDs on gold electrode.....	88
4.3.2 Direct electron transfer of CYP3A4 on gold electrode	91
4.3.3 Electrocatalytic responses of the biosensor system.....	93
4.3.4 Stability of the biosensor	95
4.4 Microscopic measurements of the biosensor materials	96
4.4.1 Microscopic properties of the biosensor.....	96
4.5 Conclusion.....	98
CHAPTER FIVE	109
Summary.....	109



Palladium Telluride Quantum Dots Phenotype Biosensor for Tamoxifen.....	110
Abstract.....	110
5. Introduction.....	111
5.1 Experimental.....	112
5.1.1 Chemicals and sample preparation	112
5.1.2 Instrumentation	112
5.1.3 Preparation of CYP (3A4 or 2D6)/TGA-PdTeQDs/Cyst/Au phenotype biosensors	113
5.1.4 Procedure for tamoxifen metabolic pathway experiment.....	114
5.2 Results and discussion.....	114
5.2.1 Electronic transitions in TGA-PdTeQDs.....	114
5.2.2 Optical properties of TAM and its active metabolites.....	119
5.2.3 Spectroscopic properties of biosensor materials	122
5.2.4 Crystal structure of TGA-PdTeQDs	126
5.2.5 Optical vibrational modes of TGA-PdTeQDs	127
5.2.6 Electronic transitions of TGA-PdTeQDs	128
5.2.7 Structural properties of sensor materials	130
5.3 Electrochemical properties of the biosensor system	133
5.3.1 Biosensor's electrochemical responses	133
5.3.2 Conversion of tamoxifen to its active metabolites	138
5.4 Conclusion.....	144
CHAPTER SIX	157
Summary.....	157

Electrochemical Dithiodipropionic Acid-Palladium Telluride Quantum Dots Phenotype Sensor for Tamoxifen	158
Abstract.....	158
6. Introduction.....	159
6.1 Experimental.....	159
6.1.1 Chemicals and sample preparation	159
6.1.2 Instrumentation	160
6.1.3 Synthesis of 3,3'-DTDPA-capped PdTeQDs	161
6.1.4 Preparation of CYP (3A4 or 2D6)/TGA-PdTeQDs/Cyst/Au phenotype biosensors	162
6.1.5 Pathways for TAM metabolism.....	162
6.2 Results and discussion.....	163
6.2.1 Crystal structure of 3,3-DTDPA-PdTeQDs.....	163
6.2.2 Optical properties of 3,3'-DTDPA-PdTeQDs	166
6.3 Introduction to small angle x-ray scattering (SAXS).....	168
6.3.1 SAXSpace experimental procedure	168
6.3.2 SAXSpace for 3,3-DTDPA-PdTeQDs	169
6.4 Electrochemistry of the biosensor systems.....	171
6.4.1 Biosensor responses to tamoxifen	171
6.4.2 Conversion of tamoxifen to its active metabolites	174
6.5 Conclusion.....	177
CHAPTER SEVEN.....	183
Conclusions and Recommendations	183

7.1 Conclusions184

7.2 Recommendations for future studies.....187



LIST OF FIGURES

Figure 1: Molecular structure of tamoxifen	3
Figure 2: Mechanism of action for tamoxifen	4
Figure 3: HIV prevalence by age and sex in South Africa [60].	7
Figure 4: Molecular structure of indinavir drug (IDV).....	8
Figure 5: Mercapto Acids	33
Figure 6: Graph of the world market for medical biosensor assessment from diverse commercial sources and anticipated for the future in US\$ millions [48].	36
Figure 7: Schematic diagram for the preparation of biosensor systems for determination of tamoxifen.	40
Figure 8: Reaction scheme for the biotransformation of tamoxifen.	43
Figure 9: HR-TEM micrographs of (a) 3-MPA-PdTeQDs, (b) inserted (zoomed) region 3-MPA-PdTeQDs at 5 nm scale view. (c) HR-TEM-EDS spectrum of 3-MPA-PdTeQDs revealing chemical composition.	62
Figure 10 (A): HR-SEM micrograph of 3-MPA-PdTeQDs. (B) HR-SEM-EDX spectrum of 3-MPA-PdTeQDs and an insert region (C) reveal elemental composition of a selected region.	63
Figure 11: (A) UV-Vis spectrum of 3-MPA-PdTeQDs in the region of 200-800 nm in 0.1 M PBS, (pH 7.4) and (B) Normalized PL spectra of 3-MPA-PdTeQDs recorded at different refluxing times for (a) 20 min, (b) 30 min, (c) 40 min, (d) 50 min, (e) 60 min, respectively. 65	
Figure 12: FT-IR spectra of (a) 3-MPA capping agent and (b) 3-MPA-PdTe QDs.....	66
Figure 13: CVs of A(b) 3-MPA-PdTeQDs/Au modified electrode and (B) Bare Au electrode measured at a potential window (1.5 to -1.5 V), scan rates 5-21 mV/s in 0.1 M PBS, pH 7.4, performed under anaerobic conditions.....	68

Figure 14: (A) CV responses of CYP3A4/3-MPA-PdTe QDs/Cyst/Au to indinavir in 0.1 PBS (pH 7.4) at 500 mV/s. (B) Calibration curves drawn from linear region of the biosensor system.	70
Figure 15: (A) UV-Vis of TGA-PdTeQDs in the region of 200-800 nm in 0.1 M PBS (pH 7.4) and (B) normalized PL for TGA-PdTeQDs excited at 360 nm for (a, black line) 30 min, (b, red line) 40 min, (c, green line) 50 min and (d, blue line) 60 min, respectively.	86
Figure 16: FTIR spectra for (a) TGA capping agent and (b) TGA-PdTeQDs.	88
Figure 17: CVs of biosensor platform measured at a potential window (0.2 to -0.85 V) in 0.1 M BBS (pH 7.4) under anaerobic conditions for (A, red line) Bare Au and (A, black line) Cyst/Au. (B) CV measurement for (B, black line) Au and (B, red line) TGA-PdTeQDs, respectively.	90
Figure 18: CVs measured at a potential window -1.5 V to +1.5 V in 0.1 M PBS at a scan rate of 500 mV/s under aerobic conditions for (a) CYP3A4/Au modified electrode and (b) CYP3A4/TGA-PdTeQDs/Cyst/Au biosensor system.	92
Figure 19: CVs measured at a potential window -1.5 V to +1.5 V in 0.1 M PBS at a scan rate of 500 mV/s under aerobic conditions for (a) CYP3A4/TGA-PdTeQDs/Cyst/Au modified electrode and (b) calibration curve drawn from a linear regression of the biosensor.	94
Figure 20: CVs measured at a potential window -1.5 V to +1.5 V in 0.1 M PBS at a scan rate of 500 mV/s under aerobic conditions for (a) CYP3A4/TGA-PdTeQDs/Cyst/Au modified electrode and (b) calibration curve drawn from a linear regression of the biosensor.	96
Figure 21: HR-SEM micrographs of (a) cysteamine, (b) TGA-PdTeQDs, (c) TGA-PdTeQDs/Cyst and (d) CYP3A4/TGA-PdTeQDs/Cyst on aluminium stub at 200 nm scale view.	98
Figure 22: HR-TEM image showing clearly the inter-plane spacing SAED (insert) pattern of TGA-PdTeQDs at 5 nm scale view. (B) UV-Vis spectra of biosensor materials in the region	

of 200-800 nm in 0.1 M PBS (pH 7.4) for (a) Cyst, (b) (TGA-PdTeQDs)-cyst, (c) CYP2D6-(TGA-PdTeQDs)-cyst, and (d) CYP3A4-(TGA-PdTeQDs)-cyst. The insert in (B) is the amplified UV-Vis spectra in the region of (310-420 nm). (C) UV-Vis spectra of (a) TAM, (b) 4-OHT, (c) N-DMT, and (d) END. (D) UV-Vis spectra of substrate-enzyme systems in 0.1 M PBS (pH 7.4) at 25 °C presented for (a) 4-OHT-CYP2D6, (b) NDMT-CYP2D6, (c) END-CYP2D6 and (d) END-CYP3A4, respectively. 118

Figure 23: (A and B): UV-Vis absorption spectra of drug-enzyme complex recorded in a 200-800 nm range as a function of time (0-20 min) in 0.1 M PBS (pH 7.4) for (a) TAM, (b) TAM-CYP2D6 and (a) TAM, (b) TAM-CYP2D6, and (c) TAM-CYP2D6-CYP3A4, respectively. (C and D) represented UV-Vis spectra of (a) Cyst-(TGA-PdTeQDs)-TAM, (b) Cyst-(TGA-PdTeQDs)-TAM-CYP2D6 and (a) Cyst-(TGA-PdTeQDs)-TAM-2D6, (b) Cyst-(TGA-PdTeQDs)-CYP2D6-CYP3A4, respectively. (E and F) shows calibration curves taken at 260 nm as a function of incubation time (0-20 min) in 0.1 M PBS for (A, B, C and D), respectively. 121

Figure 24: PL emission spectra of sensor platform excited at 260 nm in 0.1 M PBS (pH 7.4) for (a) Cyst, (b) TGA-PdTeQDs, (c) Cyst-(TGA-PdTeQDs), (d) Cyst-(TGA-PdTeQDs)-TAM, (e) Cyst-(TGA-PdTeQDs)-TAM-CYP2D6 and (f) Cyst-(TGA-PdTeQDs)-TAM-CYP2D6-CYP3A4, respectively. (B and C) PL emission spectra excited at 360 nm for (a) 4-OHT, (b) TAM, (c) END, (d) NDMT and (a) CYP3A4-END, (b) CYP3A4-NDMT, (c) CYP3A4, (d) CYP2D6-4-OHT, and (e) CYP2D6, respectively. (D and E) PL emission spectra measured at different time interval (0-20 min) for (a) TAM, (b) CYP2D6-TAM at (0-20 min) and (a) CYP2D6-TAM, (b) CYP3A4-CYP2D6-TAM, respectively. (F and an insert E) Calibration curves taken at excitation wavelengths 365 nm and 367 nm as a function of incubation time (0-20 min) in 0.1 M PBS for (D and E), respectively. 125

Figure 25: XRD pattern of TGA-PdTeQDs..... 127

Figure 26: Raman spectra of TGA-PdTeQDs.....	128
Figure 27: XPS of TGA-PdTeQDs: Palladium 3d (A), tellurium 3d (B), thioglycolic acid C1s and O1s (C and D). (E) revealing an overview XPS spectrum of TGA-PdTeQDs.....	130
Figure 28: (A) ATR-FTIR interferograms accumulated over the spectral range s of 500-4500 cm^{-1} for (a) TGA-PdTeQDs, (b) TGA-PdTeQDs-cyst, (c) CYP2D6-TGA-PdTeQDs-Cyst and (d) CYP3A4-TGA-PdTeQDs-Cyst. (B) ATR-FTIR spectra of (black line) TAM, (red line) CYP2D6, (green line) CYP3A4, (blue line) TAM-CYP2D6-(TGA-PdTeQDs)-Cyst and (cyan line) TAM-CYP3A4-(TGA-PdTeQDs)-Cyst.	132
Figure 29: (A and B) DPVs of biosensor platform measured at a potential window (0.2 to -0.85 V) in 0.1 M BBS (pH 7.4) at 25 mV/s under aerobic conditions for (a) Bare Au, (b) Cyst (c) TGA-PdTeQDs, (d) CYP2D6/Au, (e) CYP2D6/TGA-PdTeQDs/Cyst/Au and (f) CYP3A4/TGA-PdTeQDs/Cyst/Au electrodes. (C and D) SWV measurements for (CYP2D6/TGA-PdTeQDs/Cyst/Au) and (CYP3A4/TGA-PdTeQDs/Cyst/Au) biosensor systems upon successive addition of tamoxifen concentrations 0.55 pM-11 pM. (E and F) corresponding calibration curves drawn from linear region of the biosensor systems.....	137
Figure 30: Scheme for the electrocatalytic mono-oxygenation reaction of TAM-bound cytochrome P450-3A4 or CYP2D6; where TAM and 4-HydroxyTAM refer to prodrug and its by-product, respectively.....	138
Figure 31: (A and C) DPVs recorded at a potential window 0.2 to -0.85 V in 0.1 M PBS pH 7.4 for (a) TAM, (b) TAM-CYP2D6 and (c) TAM-CYP2D6-CYP3A4 and (C) (black line) TAM- (TGA-PdTeQDs/Cyst/Au), (red line)TAM-CYP2D6-(TGA-PdTeQDs)/Cyst/Au and (green in) TAM -(CYP3A4-CYP2D6-(TGA-PdTeQDs)/Cyst/Au, respectively. (B and D) time dependent studies performed at (0-20 min) for (a) TAM, (b) TAM-CYP2D6 and (c) TAM-CYP2D6-CYP3A4; (a) TAM- (TGA-PdTeQDs/Cyst/Au), (b)TAM-CYP2D6-(TGA-	

PdTeQDs)/Cyst/Au) and (c) TAM -(CYP3A4-CYP2D6-(TGA-PdTeQDs)/Cyst/Au, respectively. 141

Figure 32: (A and C) DPV experiments recorded at a potential window (0.2 to -0.85 V) for (a)TAM, (b) TAM-CYP3A4 and (c) TAM-CYP3A4-CYP2D6. (C) for TAM- (TGA-PdTeQDs)/Cyst/Au modified), (b)TAM-CYP3A4-(TGA-PdTeQDs)/Cyst/Au) and (c) TAM - (CYP2D6-CYP3A4-(TGA-PdTeQDs)/Cyst/Au). (B and D) time dependent studies performed at (0-20 min) for (a) TAM, (b) TAM-CYP3a4 and (c) TAM-CYP3A4-CYP2D6; (a) TAM-(TGA-PdTeQDs)/Cyst/Au), (b)TAM-CYP3A4-(TGA-PdTeQDs)/Cyst/Au) and (c) TAM - (CYP2D6-CYP3A4-(TGA-PdTeQDs)/Cyst/Au, respectively. 143

Figure 33: HR-TEM micrograph of (A) 3,3'-DTDPA-PdTeQDs (insert is an SAED pattern) at 5 nm scale view. (B) HR-TEM-EDS spectrum of 3,3'-DTDPA-PdTeQDs revealing chemical composition. 165

Figure 34: (A) UV-Vis of 3,3'-DTDPA-PdTeQDs (30 min, black line) and (60 min, redline) in the region of 200-800 nm in 0.1 M PBS (pH 7.4). (B) normalized PL for 3,3'-DTDPA-PdTeQDs excited at 325 nm for (black line) 0 min, (red line) 20 min, (green line) 30 min, (blue line) 40 min, (cyan line) 50 min and (pink line) 60 min, respectively. 167

Figure 35: SAXS measurements of (A) Number, (B) volume and (C) intensity weighted size distributions of 3,3'-DTDPA-PdTeQDs, respectively. 171

Figure 36: (A and B) DPV measurements recorded at a potential window (0.2 to -0.85 V) in 0.1 M PBS for (CYP2D6/3,3'-DTDPA-PdTeQDs)/Cyst/Au) and (CYP3A4/3,3'-DTDPA-PdTeQDs)/Cyst/Au) biosensor systems upon successive addition of tamoxifen concentrations 0.55 pM-5 pM. (C and D) corresponding calibration curves drawn from linear region of the biosensor systems..... 173

Figure 37: (A and B) DPVs recorded at a potential window (0.2 to -0.8 V) for (a) TAM-(3,3'-DTDPA-PdTeQDs)/Cyst/Au), (b)TAM-CYP2D6-(3,3'-DTDPA-PdTeQDs)/Cyst/Au)

and (c) TAM -CYP3A4-CYP2D6-(3,3'-DTDPA-PdTeQDs)/Cyst/Au); (a) TAM- (3,3'-DTDPA-PdTeQDs)/Cyst/Au), (b) TAM-CYP3A4-(3,3'-DTDPA-PdTeQDs)/Cyst/Au) and (c) TAM -CYP2D6-CYP3A4-(3,3'-DTDPA-PdTeQDs)/Cyst/Au). (C and D) time dependent studies performed from (0-20 min) for (a) TAM- (3,3'-DTDPA-PdTeQDs)/Cyst/Au), (b)TAM-CYP2D6-(3,3'-DTDPA-PdTeQDs)/Cyst/Au), (c) TAM-CYP3A4-CYP2D6-(3,3'DTDPA-PdTeQDs)/Cyst/Au; (a) TAM- (3,3'-DTDPA-PdTeQDs)/Cyst/Au), (b) TAM-CYP3A4-(3,3'-DTDPA-PdTeQDs)/Cyst/Au) and (c) TAM-CYP2D6-CYP3A4-(3,3'-DTDPA-PdTeQDs)/Cyst/Au), respectively. 176



LIST OF TABLES

Table 1: Electrochemical biosensors for tamoxifen.....	38
Table 2: Detection limits of tamoxifen using different detection methods (the original values are all converted to ng/mL).....	136
Table 3: Phenotype-based biosensor systems for tamoxifen and indinavir using different electrochemical methods (the LOD values are all converted to ng/mL)	185



CHAPTER ONE

Introduction

Summary

There has been an observable burden of diseases such as tuberculosis (TB), human immunodeficiency virus (HIV/AIDS), breast cancer (BC) and malaria worldwide. Though HIV and TB are focused on in the South African health management system, breast cancer happens to be responsible for as much death among women as TB and HIV combined and is regarded as a priority disease. Cytochrome P450 enzymes (CYP) metabolises 73% of drugs cleared through metabolism as primary mechanism before they are excreted or subjected to further metabolism. However, the liver is a metabolically active tissue that is in charge for the great number of drug metabolism. This chapter gives a background information on tamoxifen (a drug used as a first-line therapy for breast cancer) and indinavir metabolism (a drug used in the treatment of HIV), covering all the aspects on their unfavorable impact on human health as well as their existing detection methods. In addition, other important features such as biosensor systems and semiconducting nanomaterials are also discussed. This chapter also includes the problem statement and motivation, aim and objectives of the study.

1.1 Background

1.1.1(a) Prevalence of breast cancer (BC) and Tamoxifen

Worldwide, breast cancer (BC) is regarded to be the most common cause of cancer-related death among women [1–5]. This malignant disease usually occurs in the inner lining of milk ducts or lobules that supply the ducts with milk [6–8]. Although evidence suggests that the growth and spread of these tumors usually depends on the exact cellular site of origin of the cancer, it is a known fact that metastatic breast cancer cells lodge mainly in the axillary lymph nodes [9]. Despite the increasing occurrence and seriousness of breast cancer, global health management has recently focussed on communicable diseases such as HIV/AIDS, malaria and tuberculosis [10,11]. Since 2008, breast cancer incidence grew by more than 20% while mortality increased by 14% with 522 000 deaths in 2012. Worldwide, it is regarded to be the most commonly diagnosed cancer among women around 140 of 184 countries [7,12–14]. Although breast cancer incidence is already staggering, this increment means that breast cancer will continue to be a global threat in the future. It is believed that breast cancer cases and deaths are potentially preventable since 5-10 % of all cancers are caused by inheritance whereas the remaining 90-95% results from various factors such as age group, genetic predisposition, and the kinds of cells within the tumours itself [15–17]. Due to the high incidence and death related with breast cancer, it is a significant public health concern in society and, as such, is appropriate for screening and other preventative techniques [18,19]. Strategies to reduce morbidity and mortality of this enormous health issue include the identification and modification of risk factors, early diagnosis and treatment and improved treatment strategies have been implemented [20,21]. Endocrine treatment has had a groundbreaking contribution to the decrease in the risk recurrence and death rate from breast cancer in women with hormone receptor-positive early breast cancer [22,23].

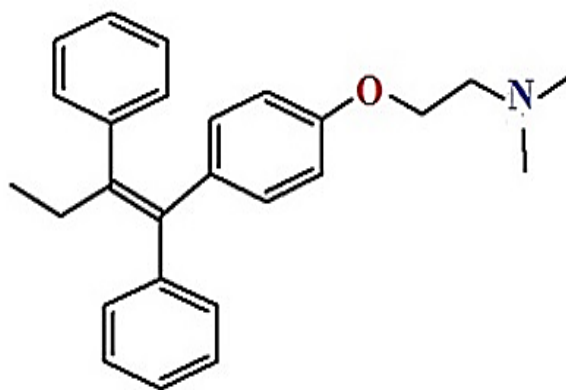


Figure 1: Molecular structure of tamoxifen

Tamoxifen is a selective estrogen receptor modulator (SERM), commonly used for prevention and treatment of hormone receptor-positive breast cancer [24–26]. This drug undergoes a mechanism of action due to its molecular structure that has an extra chain which is responsible for antagonistic action as shown in **(Figure 1)** [27,28]. Tamoxifen binds to complex estrogen receptors (ER) (i.e. a group of proteins found inside the cells) to prevent the transcription of estrogen-dependent genes, which are responsible for cancer cell growth or proliferation as illustrated in **Figure 2** [29,30]. Therefore, the introduction of a long-term TAM therapy resulted in more than 400,000 living breast cancer patients. Since then, the Food and Drug Administration (FDA) also approved tamoxifen as the first cancer chemopreventive drug for the reduction of breast-cancer incidence in women at high risk [31].

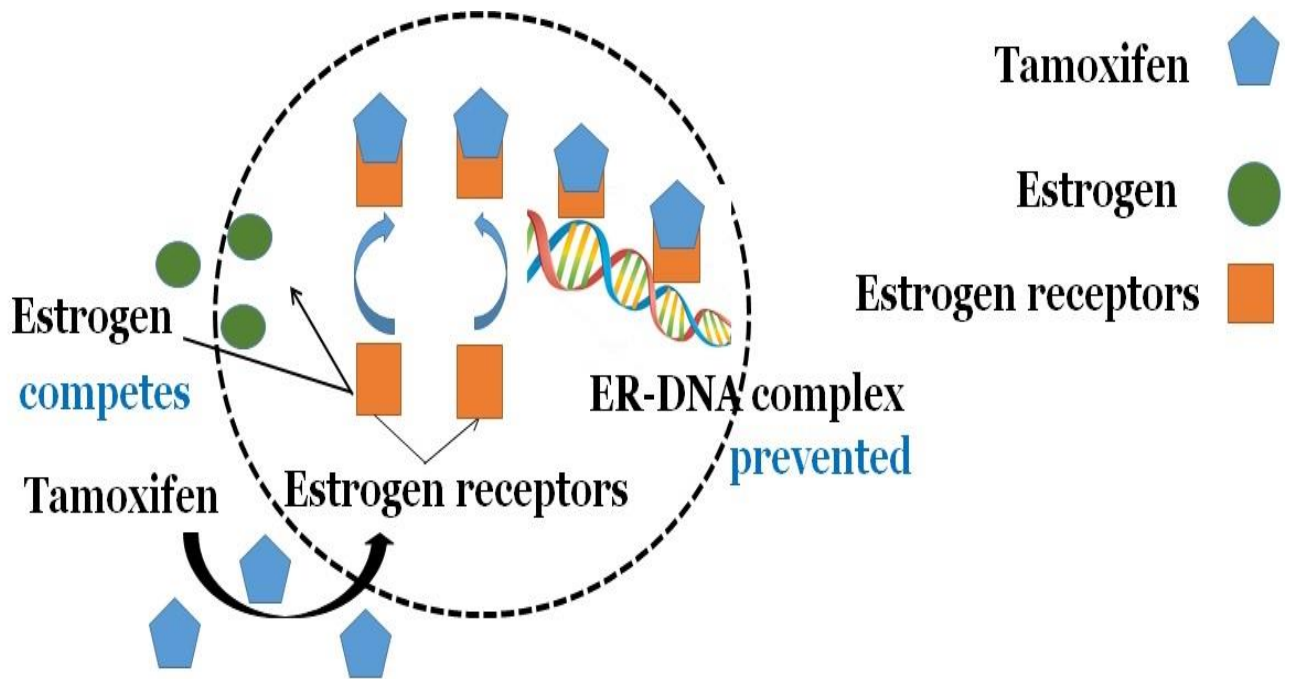


Figure 2: Mechanism of action for tamoxifen

1.1.1(b) Problem statement

According to the Cancer Association of South Africa (CANSA), breast cancer is the most diagnosed of all types of cancer, with the diagnosis rate reaching 21% [32]. The lifetime risk for South African women to develop breast cancer is one in 31 [33]. Based on the South African National Cancer Registry 2008, the number of the female breast cancer patients in the different population groups were as follows: 2,884 cases amongst blacks, 1,976 cases amongst whites, 834 cases amongst coloureds and 330 cases amongst Asians [34]. Drug metabolism is described as one of the major factors contributing to pharmacokinetics, in addition to absorption, distribution and elimination [35]. However, the liver is regarded as the most favourable site of drug metabolism in healthy individuals where the metabolic processes are in homeostasis [36]. Drug metabolising enzymes include both phase I, comprised mainly of cytochromes P450 (CYPs) that catalyse oxidation reactions, and phase II enzymes that catalyse conjugation reactions [37,38]. Cytochrome P450 enzymes (CYPs) are very important

cancer biomarkers due to (i) the selective expression of some variants in tumors; (ii) their role in cancer formation and cancer treatment by the activation of precarcinogens; and (iii) the deactivation as well as activation of anticancer drugs [39,40]. With regards to breast cancer treatment, tamoxifen which requires the two most abundant CYPs in human liver microsomes (CYP2D6 and CYP3A4) for its bioactivity, has been very widely studied by pharmacologists [41]. In comparison with other breast cancer treatments, tamoxifen is regarded as “gold standard” because of its cost effectiveness, lifesaving ability and is devoid of major adverse side effects in majority of breast cancer patients [42,43]. Many studies report that 30-50 % of ER-positive breast cancer patients under long-term treatment with tamoxifen experienced relapse during adjuvant treatment [44]. Relapse could be caused by patient-specific factors, such as genetic variability, patient behaviour, difference in gene expression within the tumour cells and other factors, resulting in a serious challenge in breast cancer management [45,46]. There is currently serious controversy on the role of genetic polymorphism of CYP2D6 on its use in the treatment of breast cancer, particularly since tamoxifen is a prodrug which CYP2D6 mediates its conversion to endoxifen as the active metabolite [47]. Clinical oncologists have argued in favour and against the benefits of genotyping in tamoxifen-related treatment and management of cancer patients, particularly about the risk of inappropriate dosing for poor and ultra-rapid metabolisers. Several analytical techniques have been established for assaying a patient’s metabolic profile including high-performance liquid chromatography (HPLC) [48,49], liquid chromatography-mass spectrometry (LC-MS) [50,51], and gas chromatography-mass spectroscopy (GC-MS) [52]. All the above-mentioned techniques are time consuming and substantial sample preparation steps are required, which results in a very high cost of analysis. Thus, there is an urgent need for the development of detection methods for monitoring the drug resistance of breast cancer patients.

1.1.2(a) Prevalence of human immunodeficiency virus and Indinavir metabolism

Human immunodeficiency virus (HIV) is a retrovirus that leads to the formation of acquired immunodeficiency syndrome commonly known as AIDS [53]. The virus destroys a type of defense cell in the body called a CD4 helper lymphocyte (Host cells), which plays an important role in controlling HIV replication [54]. However, an infected patient becomes more susceptible to contract opportunistic infections which can be caused by whole host of microorganisms leading to a development of symptoms when there is no immune system for prevention [55]. According to World Health Organisation (WHO), there is an estimated number of more than 35.3 million people infected with HIV worldwide which resulted in deaths of more than 25 million people in the past three decades [56]. However, the prevalence of HIV in South Africa varied with age and sex with a higher prevalence noted among females with an age range of 30-34 years in 2012 as shown in **Figure 3** [57]. Over the past decade, an intensive research has been focussed on the HIV-1 protease enzyme since it is regarded as the most critical component of replicative cycle which is responsible for the generation of mature, functional viral enzymes and structural proteins through cleavage of viral Gag and Gag-Pol precursor polyproteins [58]. Based on this, an investigation on HIV protease structure and its substrate has led to a development of antiretroviral (ARV) drugs in the goal of deducing and maintaining maximum suppression of HIV replication and fostering maximum CD4⁺ cell counts to improve the quality of life for people who have HIV infection [59].

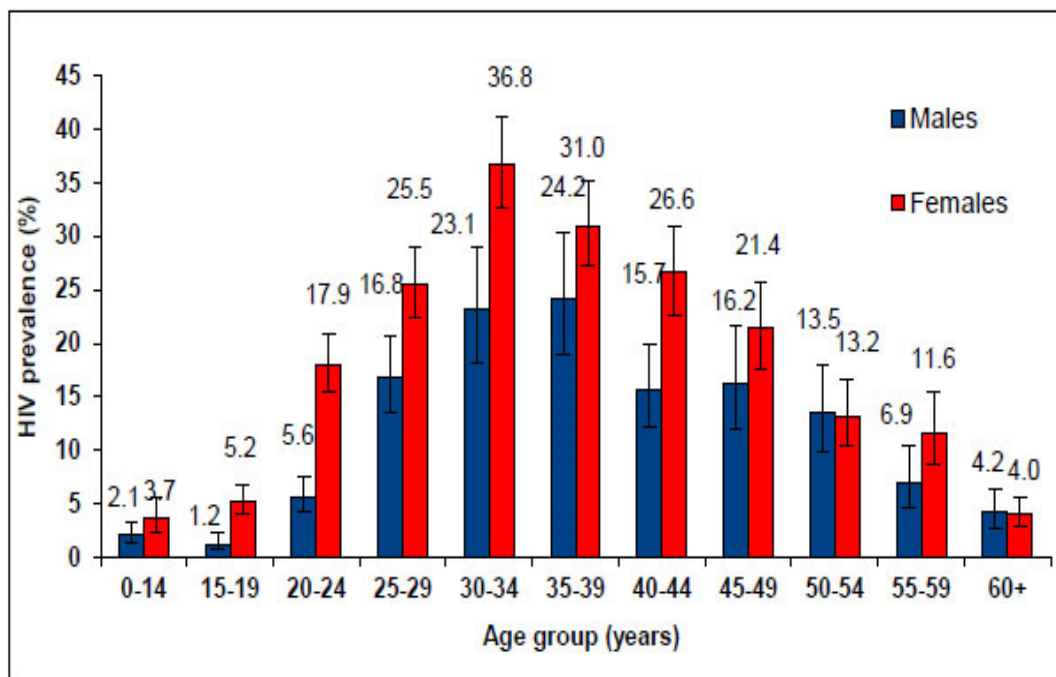


Figure 3: HIV prevalence by age and sex in South Africa [60].

The earliest drugs developed to fight against HIV/AIDS were nucleosides which comprise of the following drugs: zidovudine or didanosine and stavudine but the impact of their long term use is limited by high toxicity levels and a rapid development of viral resistance [61]. Nevertheless, the drawbacks of these drugs resulted in the development of novel therapeutic ARV drugs with unique mechanism of action that can inhibit the viral replication by delaying emergence of viral resistance. These novel developed drugs are called protease inhibitors (PIs) which were designed to mimic the transition state of peptide substrate and compete with them for binding the active site of the protease enzyme i.e. an enzyme that breaks a long chainlike molecule of proteins into shorter fragments. There have been success stories and remarkable achievement based on the therapeutic use of HIV protease inhibitors which represents a unique showcase for the ability and drawbacks of a structure-based drug design in general [62].

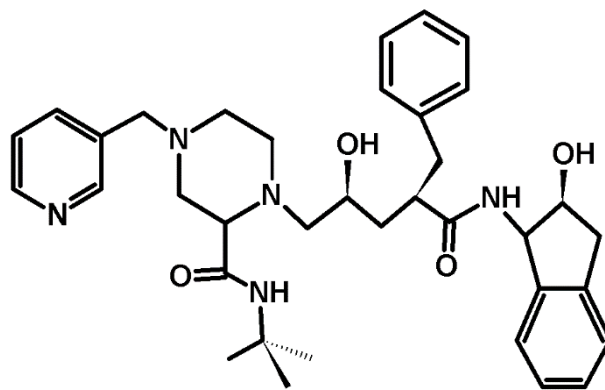


Figure 4: Molecular structure of indinavir drug (IDV).

Indinavir (**Figure 4**) is a potent and well-tolerated protease inhibitor drug administered as part of the drug combination in a treatment regime termed, 'highly active antiretroviral therapy' (HAART), which has become the most effective therapeutic strategy since the discovery of the human immunodeficiency virus (HIV) [63]. These drugs work by binding to the protease HIV-1 active site and delay the activity of the enzyme, which results in the production of non-infectious virions and prevents the consecutive infections of other cells [64,65]. A number of antiretroviral drugs, including indinavir, undergo metabolism that is catalysed by cytochrome P450-3A4 isoform produced in abundance in the liver microsomes [66]. However, it has been shown that inter-individual variability in drug metabolism has substantial effect on clinical outcomes for patients treated with the same dose of a given drug [67,68]. Such effect may be caused by a patient's poor adherence to prescription, virological resistance and pharmacological issues [69]. Therefore, the determination of patient's metabolic profile is very crucial in order to ensure proper dosing of the ARV drugs. However, therapeutic drug monitoring (TDM) during HIV/AIDS treatment has been recommended to play an important role of minimizing the toxicity of the drug and improving individual therapy [70].

1.1.2 (b) Problem statement

Despite the large number of HIV death-related illness, South Africa has made a considerable progress at decreasing HIV incidences during the past decade [71]. Since 2008, there has been great evidence-based intervention focused on HIV prevention, treatment and care for HIV patients [72]. Protease inhibitors (PIs) have played a major role in decreasing the mortality and morbidity among people with HIV infection [73]. According to Cancer Information Support Network (CISN) metabolism of drug is affected by numerous factors of environment and genetic origin i.e. slow metabolizers and normal metabolizers. Slow metabolizer individuals tend to accumulate substantially higher drug concentration which increase the risk for drug related adverse events (life threatening toxicity such as vomiting and kidney stones). Such patients may require smaller dose while normal metabolizers break down drug too quickly and require high dose. The effect of such factors complicates the life of diagnosed patients and there is a need to monitor them. However, there have been several reports in relation with protease inhibitor exposure, their activity and toxicity in combination with wide inter-individual variability in pharmacokinetics which resulted in growing interest in therapeutic drug monitoring of antiretroviral drugs as a tool in management of HIV infected people. The process of drug monitoring can be done by optimization of antiretroviral therapy potent to reduce toxicity and at the same time adequate viral suppression. Several relatively simple techniques which can be used in hospital for measurements of protease inhibitors have been described [74]. Current literature suggested that an assay by Marzolini and co-workers can measure protease inhibitors and non-nucleoside reverse transcriptase which may not be sensitive enough for quantification of concentration in patients on a single protease inhibitor containing regime [75]. Therefore, there is an increased demand for developing analytical devices that can quantitatively and qualitatively allow monitoring of indinavir (and other therapeutic drugs) with high sensitivity, selectivity and faster response

time and lower detection limits. The use of appropriate electrochemical biosensor systems such as the one prepared in this study would be the best option due to their small sizes, capability of continuous measurements. The biosensor can also measure analytes faster and at lower cost than traditional methods.

1.2 Rationale and motivation of the study

The grand health challenges of South Africa include the development of cost effective diagnostic systems suitable for early detection of diseases for timely intervention and effective management. Together with HIV and tuberculosis (TB), in South African health management system breast cancer is regarded as a priority disease. Clinical oncologists and pharmacologists are still trying to understand the effectiveness of tamoxifen, the most prescribed breast cancer drug, in cancer therapy. Modern technologically advances aiding in therapeutic decision making include pharmacogenomics assays to identify patient-based factors in drug metabolism [76]. In addition to using these assays, there is a possibility that they can optimise drug dosing. However, the recommended genotyping of CYP2D6 with a major goal of individualisation of tamoxifen therapy for patients with hormone receptor (HR) positive breast cancer is currently achieved by the available commercial tests [77]. The cost of genotype-based tamoxifen therapeutic monitoring protocols, such as Roche's AmpliChip CYP450 Test (expected to distinguish between poor, moderate and ultra-rapid metabolisers of tamoxifen) is exorbitant (USD1300 per test), though genotype alone does not determine a patient's dose/response profile. On the other hand, Roche has been used as a reliable diagnostic system for monitoring HIV infected patients since 1986 [78]. However, there are several criticisms of this approach among oncological clinicians: (i) CYP2D6 is a Class II xenobiotic metabolizing enzyme with about 105 variants and the existing commercial test kits (e.g. Roche's AmpliChip CYP450 Test and the Luminex xTAG CYP2D6 Kit v3) detect only

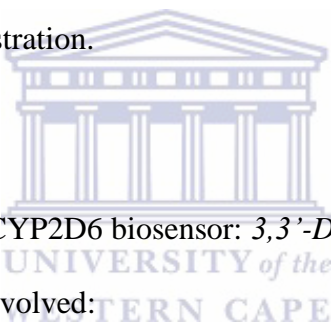
major genotypes and do not cover all phenotypes (e.g. ultra-rapid metabolisers (URMs) with extra copies of the CYP2D6 genes); (ii) CYP2D6 genotype obtained from tumor (somatic) genome is not necessarily the same as those of the host genome (germline DNA); (iii) apart from CYP2D6, other host and tumor factors affect drug metabolism; (iv) CYP3A4 (mainly) and other CYPs play prominent role in the formation of N-desmethylTamoxifen intermediate and the conversion of 4-hydroxytamoxifen intermediate to endoxifen [79]. Though genotyping assays have molecular basis and are fast, their interpretation in predicting a patient's phenotype and consequently response to tamoxifen is left solely to the physician's judgment. Also, the knowledge that genotype alone does not determine a patient's response to treatment with a drug since cancer is caused by not only genetics but also by diet, hormones and lifestyle [80] makes it necessary to find a phenotype-based system for personalising therapy. Phenotyping techniques that use a probe drug that is solely metabolised by CYP2D6 to determine a patient's metabolic profile may be faulty as a drug such as tamoxifen involves other CYP enzymes (but mainly CYP2D6 and CYP3A4) in the formation of its active metabolite, endoxifen [81,82]. It is noteworthy that the metabolism of tamoxifen to produce the active metabolite involves the two predominant drug metabolism enzymes, namely, CYP2D6 whose variability is genetic and CYP3A4 which is a Class I enzyme (with conserved genetics) that exhibits inter-individual variability that cannot be explained by genetic polymorphism. Thus, test kits or devices for the determination of tamoxifen metabolism should include the two enzymes or the intermediate and active products of tamoxifen metabolism in their design.

The development of electrochemical biosensors for clinical diagnostics has recently gained much interest due to lower detection limits, fast response speeds, ease of use and low cost for the detection and management of disease [83,84]. Recent advances in nanotechnology have led to enhanced sensitivity of the devices enabling them to detect small variations in desired

specimen [85]. Semiconductor nanomaterials such as quantum dots (QDs) have been extensively studied due to their unique size-dependent electronic, optical, magnetic and electrochemical properties [86]. In addition, quantum dots have shown a great potential in diverse fields ranging from drug delivery biosensing, solar cells and photovoltaics and light emitting diodes [87]. Several research groups have reported different types of strategies to detect analytes of interest based on nanoparticles [88]. For instance, Guang-Li and co-workers reported a novel strategy for construction of photoelectrochemical sensors based on quantum dots for the detection of dopamine [89]. Based on this, water-soluble and biocompatible palladium telluride quantum dots capped with thioglycolic acid (TGA), 3-mercaptopropionic acid (3-MPA) or 3,3'-dithiodipropionic acid (DTDPA) were employed in this study to harness the signal amplification in the development of bipolar electrochemical nanobiosensors chips (*b-canceranosens*) for the detection and reporting of the rate and extent of metabolism of tamoxifen and its metabolic intermediates. However, the effectiveness of the CYP-based phenotype biosensor was first tested with indinavir, a protease inhibitor anti-retroviral drug which is physiologically metabolised by CYP3A4. For indinavir, the development of electrochemical phenotype-based biosensor system was achieved by incorporating the synthesised palladium telluride (PdTe) quantum dots, capped with thioglycolic acid (TGA) or 3-mercaptopropionic acid (3-MPA) onto a gold electrode that was previously modified with self-assembled cystamine dihydrochloride as a platform for cytochrome P450-3A4 (CYP3A4), an isoenzyme from the cytochrome P450 family of heme enzymes well-known for drug metabolism. Reviews based on the application of QDs as a mediator for biosensor systems applied in the detection of ARV drugs are given in **chapter 3 and 4** in this study.

1.3 Aim of the project

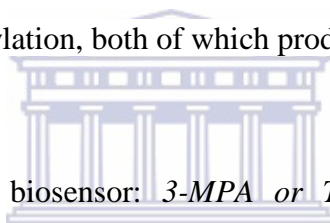
This study focussed on the development of the next generation phenotype-based diagnostic nanobiosensor systems for sensing and signalling breast cancer patient's response profile (poor, moderate or ultra-rapid metaboliser) for tamoxifen, which is the most prescribed breast cancer drug. It involved the development of a bi-polar palladium telluride quantum dots (PdTeQDs) capped with thioglycolic acid (TGA) or 3,3'-dithiodipropionic acid (3,3'-DTPA) bio-reactor on a chip-modified with genetically engineered CYP2D6 and CYP3A4 bi-polar bioelectrodes sensor that promised to be suitable for providing a patient's complete response profile for tamoxifen at point-of-care. This study would benefit women a lot and the b-cancer nanosens would lead to proper drug prescription arising from point of care testing of a patient's response to drug administration.



1.3.1 Fabrication of CYP3A4 or CYP2D6 biosensor: 3,3'-DTPA or TGA-PdTeQDs/Cyst/Au biosensor system for tamoxifen involved:

- Synthesis of palladium telluride quantum dots in the presence of various capping agents including thioglycolic acid (TGA) or 3, 3'-dithiodipropionic acid (3, 3'-DTPA) to form a stable, biocompatible and water-soluble QDs
- Determination of PdTeQDs crystal structure and morphology using microscopic techniques (RH-TEM and HR-SEM).
- Determination of QDs valence shell, crystal structure and optical vibrational modes using X-ray photoelectron spectroscopy, X-ray diffraction and Raman spectroscopy (XPS, Raman and XRD).

- Optical properties and structural properties of QDs using Ultraviolet-visible spectroscopy, photoluminescence spectroscopy and Fourier transformed infra-red spectroscopy (UV-Vis, PL and ATR-FTIR).
- Surface modification of TGA-PdTeQDs and 3-MPA-PdTeQDs on a bare gold electrode followed by determination of electrochemical properties of quantum dots using cyclic voltammetry (CV) and differential pulse voltammetry (DPV).
- Development, optimisation, evaluation and testing of individual phenotype b-cancernanosens for tamoxifen, N-desmethylTamoxifen, 4-hydroxyTamoxfen and endoxifen, which is an active metabolite.
- Conversion of tamoxifen to its active metabolites through two pathway systems; 4-hydroxylation and N-demethylation, both of which produce highly effective metabolites.



1.3.2. Fabrication of CYP3A4 biosensor: *3-MPA or TGA-PdTeQDs/Cyst/Au* biosensor system for indinavir involved:

UNIVERSITY of the
WESTERN CAPE

- Surface modification of gold electrode with cysteamine, resulting in the formation of self-assembled monolayer (SAM) on a gold electrode by taking advantage of strong sulphur-gold interaction.
- Synthesis and characterisation of 3-mercaptopropionic acid capped palladium telluride quantum dots (3-MPA-PdTeQDs) and thioglycolic acid capped palladium telluride (TGA-PdTeQDs) by UV-Vis, PL, XRD, XPS, CV, HR-TEM, HR-SEM
- Development, optimisation, evaluation and testing of biosensor systems in the presence and absence of ARV drugs.

1.4 Thesis outline

The study consists of **seven chapters**

Chapter 1 gives background information on breast cancer and HIV diseases, followed by a brief discussion on semiconducting nanomaterials and the current techniques for the determination of tamoxifen. In addition, the chapter discusses the rationale for the work reported, as well as an outline of the thesis. The scope of the thesis is clearly defined in this chapter.

Chapter 2 introduces quantum dots and their advantages over classical materials. The synthesis and the functionalisation of quantum dots are described, as well as a review of the applications of quantum dots, with specific attention given to electrochemical biosensor applications. The nature of the topic has been adequately interpreted in this chapter, and the literature discussed gave good insight into the problem at hand.

Chapter 3 describes the synthesis, characterisation and application of 3-MPA-PdTeQDs and the electrochemical biosensor system, covering mostly the detection of protease inhibitor, indinavir. Several analytical techniques such as FTIR, CV, UV-Vis, PL and HR-TEM were used to characterize these QDs. The characterization results were sufficiently analysed and discussed, to prove that indeed Pd and Te containing quantum dots was synthesized. These were used as a biosensor for determining indinavir, with the biocompatibility of palladium telluride quantum dots being achieved by surface functionalisation of the quantum dots with 3-mercaptopropionic acid (3-MPA) as a capping agent, which also improved the stability and the solubility of the material. The *LOD* value is lower than indinavir's maximum steady state plasma concentration, thereby indicating that the sensing device, in principle, would be suitable for monitoring the drug in patient.

Chapter 4 describes the fabrication of a biosensor by immobilizing cytochrome P450-3A4 enzymes onto a TGA-PdTeQDs modified gold electrode. The developed electrochemical biosensor and its individual components were characterized using CV, UV-VIS, FTIR and HR-SEM. The electrocatalytic properties of this electrochemical biosensor system were studied by cyclic voltammetry in order to detect the response of the biosensor to indinavir. The obtained detection limit is well below the plasma concentration of indinavir.

Chapter 5 describes the catalytic responses of tamoxifen, the biotransformation of tamoxifen to its primary and secondary active metabolites, as well as the characterization of individual biosensor materials by SWV, UV-Vis, ATR-FTIR, PL, XPS, XRD and Raman spectroscopy. The sensor was based on the combination of novel thioglycolic acid-capped palladium telluride (TGA-PdTe) quantum dots (QDs) and genetically engineered cytochrome P450-3A4 (CYP3A4) or cytochrome P450-2D6 (CYP2D6) enzymes. The *LOD* values are much lower than tamoxifen's maximum steady state plasma concentration, thereby indicating that the sensing device, in principle, could be suitable for monitoring the drug in patients.

Chapter 6 introduces a new thiol-type 3,3'-DTDPA capping agent employed to improve the stability and efficiency of PdTeQDs. The novel 3,3'-DTDPA-PdTeQDs were characterised by HR-TEM, SAXSpace, UV-Vis and PL. The biosensor responses to tamoxifen and the biotransformation of TAM to its primary and secondary metabolites were determined by DPV studies. The tamoxifen biosensors had limit of detection (*LOD*) values for CYP3A4 (CYP2D6) biosensor systems that are much lower than tamoxifen's maximum steady state plasma concentration.

Chapter 7 gives a summary of the work done as well as recommendations for future work.

References

- [1] P. Norman, K. Brain, An application of an extended health belief model to the prediction of breast self-examination among women with a family history of breast cancer., *Br. J. Health Psychol.* 10 (2005) 1–16. doi:10.1348/135910704X24752.
- [2] D.J. MacDonald, L. Sarna, G.C. Uman, M. Grant, J.N. Weitzel, Health beliefs of women with and without breast cancer seeking genetic cancer risk assessment., *Cancer Nurs.* 28 (2005) 372–379. doi:10.1097/00002820-200509000-00006.
- [3] American Cancer Society, Breast cancer facts & figures, *Am. Cancer Soc.* 8 (2010) 16.
- [4] J. Ferlay, H. Shin, F. Bray, D. Forman, C. Mathers, D. Parkin, GLOBOCAN 2008 v2.0, Cancer Incidence and Mortality Worldwide: IARC CancerBase, No. 10 [Internet]. Lyon, Fr. Int. Agency Res. Cancer; 2010. Available from [Http://globocan.iarc.fr](http://globocan.iarc.fr), Accessed Day/month/year. (2010). doi:10.1002/ijc.25516.
- [5] F. Kamangar, G.M. Dores, W.F. Anderson, Patterns of cancer incidence, mortality, and prevalence across five continents: Defining priorities to reduce cancer disparities in different geographic regions of the world, *J. Clin. Oncol.* 24 (2006) 2137–2150. doi:10.1200/JCO.2005.05.2308.
- [6] J. Russo, I.H. Russo, Toward a physiological approach to breast cancer prevention, *Cancer Epidemiol. Biomarkers Prev.* 3 (1994) 353–364. <http://cebp.aacrjournals.org/content/3/4/353.abstract>.
- [7] G.N. Sharma, R. Dave, J. Sanadya, P. Sharma, K.K. Sharma, Various types and management of breast cancer: an overview., *J. Adv. Pharm. Technol. Res.* 1 (2010) 109–26. <http://www.pubmedcentral.nih.gov/articlerender.fcgi?artid=3255438&tool=pmcentrez&rendertype=abstract>.
- [8] J. Makki, Diversity of breast carcinoma: Histological subtypes and clinical relevance, *Clin. Med. Insights Pathol.* 8 (2015) 23–31. doi:10.4137/CPath.s31563.

- [9] N. Schischmanov, NEW HYPOTHESIS ON THE ORIGIN OF METASTASES, Nagoya J. Med. Sci. 75 (2013).
- [10] E. Baca-Garcia, M.M. Perez-Rodriguez, I. Basurte-Villamor, A.L. Fernandez del Moral, M. a Jimenez-Arriero, J.L. Gonzalez de Rivera, J. Saiz-Ruiz, M. a Oquendo, Diagnostic stability of psychiatric disorders in clinical practice., Br. J. Psychiatry. 190 (2007) 210–216. doi:10.1192/bjp.bp.106.024026.
- [11] K.M. De Cock, P.M. Simone, V. Davison, L. Slutsker, The new global health, Emerg. Infect. Dis. 19 (2013) 1192–1197. doi:10.3201/eid1908.130121.
- [12] J. Ferlay, I. Soerjomataram, R. Dikshit, S. Eser, C. Mathers, M. Rebelo, D.M. Parkin, D. Forman, F. Bray, Cancer incidence and mortality worldwide: Sources, methods and major patterns in GLOBOCAN 2012, Int. J. Cancer. 136 (2015) E359–E386. doi:10.1002/ijc.29210.
- [13] P. Release, Latest world cancer statistics Global cancer burden rises to 14 . 1 million new cases in 2012 : Marked increase in breast cancers must be addressed., Int. Agency Res. Cancer, World Heal. Organ. (2013) 2012–2014. doi:223.
- [14] E.E. Chaka, Breast Cancer Incidence , Mortality and Its Risk Factors among Women Worldwide , 2015, 16 (2015) 59–67.
- [15] P. Anand, A.B. Kunnumakara, C. Sundaram, K.B. Harikumar, S.T. Tharakan, O.S. Lai, B. Sung, B.B. Aggarwal, Cancer is a preventable disease that requires major lifestyle changes, Pharm. Res. 25 (2008) 2097–2116. doi:10.1007/s11095-008-9661-9.
- [16] K.A. Ban, C. V. Godellas, Epidemiology of Breast Cancer, Surg. Oncol. Clin. N. Am. 23 (2014) 409–422. doi:10.1016/j.soc.2014.03.011.
- [17] A.L. Fymat, Genetics , Epigenetics and Cancer, 4 (2017).doi:10.19080/CTOIJ.2017.04.555634.
- [18] A. Howell, A.S. Anderson, R.B. Clarke, S.W. Duffy, D.G. Evans, M. Garcia-Closas, A.J. Gescher, T.J. Key, J.M. Saxton, M.N. Harvie, Risk determination and prevention of breast

- cancer., *Breast Cancer Res.* 16 (2014) 446. doi:10.1186/s13058-014-0446-2.
- [19] E.R. Myers, P. Moorman, J.M. Gierisch, L.J. Havrilesky, L.J. Grimm, S. Ghate, B. Davidson, R.C. Montgomery, M.J. Crowley, D.C. McCrory, A. Kendrick, G.D. Sanders, Benefits and Harms of Breast Cancer Screening, *Jama.* 314 (2015) 1615. doi:10.1001/jama.2015.13183.
- [20] R. Peto, J. Boreham, M. Clarke, C. Davies, V. Beral, UK and USA breast cancer deaths down 25% in year 2000 at ages 20-69 years., *Lancet.* 355 (2000) 1822. doi:10.1016/S0140-6736(00)02277-7.
- [21] A. Balmain, J. Gray, B. Ponder, The genetics and genomics of cancer., *Nat. Genet.* 33 Suppl (2003) 238–244. doi:10.1038/ng1107.
- [22] A. Scharl, A. Salterberg, Significance of Ovarian Function Suppression in Endocrine Therapy for Breast Cancer in Pre-Menopausal Women, *Geburtshilfe Frauenheilkd.* 76 (2016) 516–524. doi:10.1055/s-0042-106389.
- [23] G. Schiavon, I.E. Smith, Status of adjuvant endocrine therapy for breast cancer., *Breast Cancer Res.* 16 (2014) 206. doi:10.1007/BF01805884.
- [24] A.J.J. Wood, B.L. Riggs, L.C. Hartmann, Selective Estrogen-Receptor Modulators — Mechanisms of Action and Application to Clinical Practice, *N Engl J Med.* 3487348 (2003) 618–29. doi:10.1056/NEJMra022219.
- [25] E.E. Hennig, M. Piatkowska, J. Karczmariski, K. Goryca, E. Brewczynska, R. Jazwiec, A. Kluska, R. Omiotek, A. Paziewska, M. Dadlez, J. Ostrowski, Limited predictive value of achieving beneficial plasma (Z)-endoxifen threshold level by CYP2D6 genotyping in tamoxifen-treated Polish women with breast cancer., *BMC Cancer.* 15 (2015) 570. doi:10.1186/s12885-015-1575-4.
- [26] Y.C. Lim, Z. Desta, D.A. Flockhart, T.C. Skaar, Endoxifen (4-hydroxy-N-desmethyl-tamoxifen) has anti-estrogenic effects in breast cancer cells with potency similar to 4-hydroxy-tamoxifen, *Cancer Chemother. Pharmacol.* 55 (2005) 471–478. doi:10.1007/s00280-

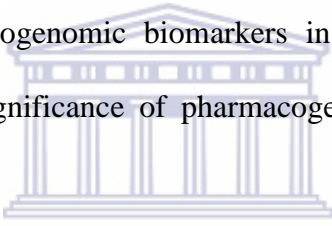
004-0926-7.

- [27] D.S. Goodsell, Oncologist The Molecular Perspective: Tamoxifen and the Estrogen Receptor, (2002) 163–164.
- [28] S.S. Lum, E.A. Woltering, W.S. Fletcher, R.F. Pommier, Changes in serum estrogen levels in women during tamoxifen therapy, *Am. J. Surg.* 173 (1997) 399–402. doi:10.1016/S0002-9610(97)00072-X.
- [29] M. Chang, Tamoxifen resistance in breast cancer., *Biomol. Ther. (Seoul)*. 20 (2012) 256–67. doi:10.4062/biomolther.2012.20.3.256.
- [30] J. Shou, S. Massarweh, C.K. Osborne, A.E. Wakeling, S. Ali, H. Weiss, R. Schiff, Mechanisms of tamoxifen resistance: increased estrogen receptor-HER2/neu cross-talk in ER/HER2-positive breast cancer., *J. Natl. Cancer Inst.* 96 (2004) 926–35. doi:10.1093/jnci/djh166.
- [31] V.C. Jordan, Tamoxifen: a most unlikely pioneering medicine, *Nat Rev Drug Discov.* 2 (2003) 205–213. doi:10.1038/nrd1031.
- [32] I. The, T.S. Cells, L. Cells, S. African, N.C. Registry, Cancer Association of South Africa (CANSAS) Fact Sheet on Testicular Cancer, (2013) 1–11.
- [33] W.M. Kruger, J.P. Apffelstaedt, Young breast cancer patients in the developing world: Incidence, choice of surgical treatment and genetic factors, *South African Fam. Pract.* 49 (2007) 19–24. doi:10.1080/20786204.2007.10873634.
- [34] M.C. Herbst, Cancer Association of South Africa (CANSAS) Fact Sheet on the Top Ten Cancers per Population Group Top Ten Most Common Cancers of Women Top Ten Most Common Cancers of Asian Men, *Cansa.* (2015) 1–6.
- [35] M. Konstandi, E.O. Johnson, M.A. Lang, Consequences of psychophysiological stress on cytochrome P450-catalyzed drug metabolism, *Neurosci. Biobehav. Rev.* 45 (2014) 149–167. doi:10.1016/j.neubiorev.2014.05.011.

- [36] M.W. Robinson, C. Harmon, C. O'farrelly, Liver immunology and its role in inflammation and homeostasis, *Cell. Mol. Immunol.* 13 (2016) 267–276. doi:10.1038/cmi.2016.3.
- [37] L.C. Wienkers, T.G. Heath, Predicting in vivo drug interactions from in vitro drug discovery data., *Nat. Rev. Drug Discov.* 4 (2005) 825–833. doi:10.1038/nrd1851.
- [38] J.A. Williams, R. Hyland, B.C. Jones, D.A. Smith, S. Hurst, T.C. Goosen, V. Peterkin, J.R. Koup, S.E. Ball, Minireview, *Drug Metab. Dispos.* 32 (2004) 1201–1208. doi:10.1124/dmd.104.000794.for.
- [39] C. Rodriguez-Antona, M. Ingelman-Sundberg, Cytochrome P450 pharmacogenetics and cancer., *Oncogene.* 25 (2006) 1679–1691. doi:10.1038/sj.onc.1209377.
- [40] R.D. Bruno, V.C.O. Njar, Targeting cytochrome P450 enzymes: A new approach in anti-cancer drug development, *Bioorg. Med. Chem.* 15 (2007) 5047–5060. doi:10.1016/j.bmc.2007.05.046.
- [41] M.P. Goetz, A. Kamal, M.M. Ames, Tamoxifen pharmacogenomics: the role of CYP2D6 as a predictor of drug response., *Clin. Pharmacol. Ther.* 83 (2008) 160–6. doi:10.1038/sj.clpt.6100367.
- [42] P. Bourassa, T.J. Thomas, J. Bariyanga, H.A. Tajmir-Riahi, Breast anticancer drug tamoxifen and its metabolites bind tRNA at multiple sites, *Int. J. Biol. Macromol.* 72 (2015) 692–698. doi:10.1016/j.ijbiomac.2014.09.022.
- [43] D. Agudelo, S. Sanyakamdhorn, S. Nafisi, H.A. Tajmir-Riahi, Transporting Antitumor Drug Tamoxifen and Its Metabolites, 4-Hydroxytamoxifen and Endoxifen by Chitosan Nanoparticles, *PLoS One.* 8 (2013) 1–11. doi:10.1371/journal.pone.0060250.
- [44] J.M. Dixon, Endocrine Resistance in Breast Cancer, *New J. Sci.* 2014 (2014) 1–27. doi:10.1155/2014/390618.
- [45] B.S. Katzenellenbogen, BIOMEDICINE: Enhanced: Defining the “S” in SERMs, *Science* (80-.). 295 (2002) 2380–2381. doi:10.1126/science.1070442.

- [46] D.P. McDonnell, S.E. Wardell, D.P. McDonnell, S.E. Wardell, D.P. McDonnell, S.E. Wardell, The molecular mechanisms underlying the pharmacological actions of ER modulators: Implications for new drug discovery in breast cancer, *Curr. Opin. Pharmacol.* 10 (2011) 620–628. doi:10.1016/j.coph.2010.09.007.The.
- [47] Q. Zhong, C. Zhang, Q. Zhang, L. Miele, S. Zheng, G. Wang, Boronic prodrug of 4-hydroxytamoxifen is more efficacious than tamoxifen with enhanced bioavailability independent of CYP2D6 status, *BMC Cancer.* (2015) 1–9. doi:10.1186/s12885-015-1621-2.
- [48] S. Carrara, S. Ghoreishizadeh, J. Olivo, I. Taurino, C. Baj-Rossi, A. Cavallini, M.O. de Beeck, C. Dehollain, W. Burseson, F.G. Moussy, A. Guiseppi-Elie, G. De Micheli, Fully integrated biochip platforms for advanced healthcare, *Sensors (Switzerland).* 12 (2012) 11013–11060. doi:10.3390/s120811013.
- [49] F. Rezende, K.K. Prior, O. Lowe, I. Wittig, V. Strecker, F. Moll, V. Helfinger, F. Schnutgen, N. Kurrle, F. Wempe, M. Walter, S. Zukunft, B. Luck, I. Fleming, N. Weissmann, R.P. Brandes, K. Schroder, Cytochrome P450 enzymes but not NADPH oxidases are the source of the NADPH-dependent lucigenin chemiluminescence in membrane assays, *Free Radic. Biol. Med.* 102 (2017) 57–66. doi:10.1016/j.freeradbiomed.2016.11.019.
- [50] M. Mascini, S. Tombelli, Biosensors for biomarkers in medical diagnostics., *Biomarkers.* 13 (2008) 637–657. doi:10.1080/13547500802645905.
- [51] J.M.P.J. Garrido, E. Manuela, P.J. Garrido, A.M. Oliveira-Brett, F. Borges, An electrochemical outlook on tamoxifen biotransformation: current and future prospects., *Curr. Drug Metab.* 12 (2011) 372–382. doi:BSP/CDM/E-Pub/000140 [pii].
- [52] U. Karst, Electrochemistry/mass spectrometry (EC/MS)-a new tool to study drug metabolism and reaction mechanisms., *Angew. Chem. Int. Ed. Engl.* 43 (2004) 2476–2478. doi:10.1002/anie.200301763.
- [53] P.M. Sharp, B.H. Hahn, Origins of HIV and the AIDS pandemic, *Cold Spring Harb. Perspect.*

- Med. 1 (2011). doi:10.1101/cshperspect.a006841.
- [54] P.J. Norris, E.S. Rosenberg, CD4(+) T helper cells and the role they play in viral control., *J. Mol. Med. (Berl)*. 80 (2002) 397–405. doi:10.1007/s00109-002-0337-3.
- [55] R.A. Weiss, Special Anniversary Review: Twenty-five years of human immunodeficiency virus research: Successes and challenges, *Clin. Exp. Immunol.* 152 (2008) 201–210. doi:10.1111/j.1365-2249.2008.03645.x.
- [56] UNAIDS, Global HIV prevalence has levelled off; AIDS is among the leading causes of death globally and remains the primary cause of death in Africa, Update. (2007) 2–4.
- [57] Avert, South Africa HIV & AIDS Statistics, Avert.com. (2012) 1. <http://www.avert.org/south-africa-hiv-aids-statistics.htm>.
- [58] S.K. Lee, M. Potempa, R. Swanstrom, The choreography of HIV-1 proteolytic processing and virion assembly, *J. Biol. Chem.* 287 (2012) 40867–40874. doi:10.1074/jbc.R112.399444.
- [59] O. Oguntibeju, Quality of life of people living with HIV and AIDS and antiretroviral therapy, *HIV/AIDS - Res. Palliat. Care.* 3 (2012) 117. doi:10.2147/HIV.S32321.
- [60] L.A.U.N.C.H. Edition, South African National HIV Prevalence, Incidence and Behaviour Survey, 2012, (2012).
- [61] E.J. Arts, D.J. Hazuda, HIV-1 antiretroviral drug therapy, *Cold Spring Harb. Perspect. Med.* 2 (2012). doi:10.1101/cshperspect.a007161.
- [62] J. Pokorná, L. Machala, P. Řezáčová, J. Konvalinka, Current and novel inhibitors of HIV protease, *Viruses.* 1 (2009) 1209–1239. doi:10.3390/v1031209.
- [63] M.H. Porteus, *HHS Public Access*, 1 (2016) 23–30. doi:10.1007/s40778-014-0003-z.Genome.
- [64] M. Desai, G. Iyer, R.K. Dikshit, Antiretroviral drugs: critical issues and recent advances., *Indian J. Pharmacol.* 44 (2012) 288–98. doi:10.4103/0253-7613.96296.
- [65] C. V Fletcher, K. Staskus, S.W. Wietgreffe, M. Rothenberger, C. Reilly, J.G. Chipman, G.J.

- Beilman, A. Khoruts, A. Thorkelson, T.E. Schmidt, J. Anderson, K. Perkey, M. Stevenson, A.S. Perelson, D.C. Douek, A.T. Haase, T.W. Schacker, Persistent HIV-1 replication is associated with lower antiretroviral drug concentrations in lymphatic tissues., *Proc. Natl. Acad. Sci. U. S. A.* 111 (2014) 2307–12. doi:10.1073/pnas.1318249111.
- [66] S.S. Lakhman, Q. Ma, G.D. Morse, Pharmacogenomics of CYP3A: considerations for HIV treatment., *Pharmacogenomics.* 10 (2009) 1323–39. doi:10.2217/pgs.09.53.
- [67] D. González de Requena, O. Gallego, C. de Mendoza, A. Corral, I. Jiménez-Nácher, V. Soriano, Indinavir plasma concentrations and resistance mutations in patients experiencing early virological failure., *AIDS Res. Hum. Retroviruses.* 19 (2003) 457–9. doi:10.1089/088922203766774496.
- [68] C.L. Ventola, Role of pharmacogenomic biomarkers in predicting and improving drug response: part 1: the clinical significance of pharmacogenetic variants., *Pharm. Ther.* 38 (2013) 545–60.

<http://www.pubmedcentral.nih.gov/articlerender.fcgi?artid=3828931&tool=pmcentrez&rendertype=abstract>
 WESTERN CAPE
- [69] T.R. Cressey, M. Lallemand, Pharmacogenetics of antiretroviral drugs for the treatment of HIV-infected patients: An update, *Infect. Genet. Evol.* 7 (2007) 333–342. doi:10.1016/j.meegid.2006.08.004.
- [70] R.P. van Heeswijk, A. Veldkamp, J.W. Mulder, P.L. Meenhorst, J.M. Lange, J.H. Beijnen, R.M. Hoetelmans, Combination of protease inhibitors for the treatment of HIV-1-infected patients: a review of pharmacokinetics and clinical experience, *Antivir Ther.* 6 (2001) 201–229.
http://www.ncbi.nlm.nih.gov/entrez/query.fcgi?cmd=Retrieve&db=PubMed&dopt=Citation&list_uids=11878403.
- [71] N.P. Simelela, W.D.F. Venter, A brief history of South Africa’s response to AIDS, *South*

African Med. J. 104 (2014) 249–251. doi:10.7196/SAMJ.7700.

- [72] M.J. Rotheram-Borus, D. Swendeman, G. Chovnick, The past, present, and future of HIV prevention: integrating behavioral, biomedical, and structural intervention strategies for the next generation of HIV prevention., *Annu. Rev. Clin. Psychol.* 5 (2009) 143–67. doi:10.1146/annurev.clinpsy.032408.153530.
- [73] E. Anuurad, A. Bremer, L. Berglund, HIV protease inhibitors and obesity., *Curr. Opin. Endocrinol. Diabetes. Obes.* 17 (2010) 478–85. doi:10.1097/MED.0b013e32833dde87.
- [74] V.A. Simon, M.D. Thiam, L.C. Lipford, Determination of serum levels of thirteen human immunodeficiency virus-suppressing drugs by high-performance liquid chromatography, *J. Chromatogr. A.* 913 (2001) 447–453. doi:10.1016/S0021-9673(00)01092-X.
- [75] C. Marzolini, A. Telenti, L.A. Decosterd, G. Greub, J. Biollaz, T. Buclin, Efavirenz plasma levels can predict treatment failure and central nervous system side effects in HIV-1-infected patients., *AIDS.* 15 (2001) 71–75. doi:10.1097/00002030-200106150-00023.
- [76] S.A. Scott, Personalizing medicine with clinical pharmacogenetics., *Genet. Med.* 13 (2011) 987–95. doi:10.1097/GIM.0b013e318238b38c.
- [77] R. Vianna-Jorge, J.S. Festa-Vasconcellos, S.M. Goulart-Citrangulo, M.S. Leite, Functional polymorphisms in xenobiotic metabolizing enzymes and their impact on the therapy of breast cancer, *Front. Genet.* 3 (2013) 1–19. doi:10.3389/fgene.2012.00329.
- [78] F. Pozo, I. Casas, A. Tenorio, G. Trallero, J.M. Echevarria, Evaluation of a commercially available reverse transcription-PCR assay for diagnosis of enteroviral infection in archival and prospectively collected cerebrospinal fluid specimens, *J. Clin. Microbiol.* 36 (1998) 1741–1745.
- [79] I.Y. Gong, W.A. Teft, J. Ly, Y.H. Chen, B. Alicke, R.B. Kim, E.F. Choo, Determination of clinically therapeutic endoxifen concentrations based on efficacy from human MCF7 breast cancer xenografts, *Breast Cancer Res. Treat.* 139 (2013) 61–69. doi:10.1007/s10549-013-

2530-1.

- [80] M. Verma, Personalized Medicine and Cancer, *J. Pers. Med.* 2 (2010) 1–14. doi:10.3390/jpm2010001.
- [81] Y. Jin, Z. Desta, V. Stearns, B. Ward, H. Ho, K.H. Lee, T. Skaar, A.M. Storniolo, L. Li, A. Araba, R. Blanchard, A. Nguyen, L. Ullmer, J. Hayden, S. Lemler, R.M. Weinshilboum, J.M. Rae, D.F. Hayes, D.A. Flockhart, CYP2D6 genotype, antidepressant use, and tamoxifen metabolism during adjuvant breast cancer treatment, *J. Natl. Cancer Inst.* 97 (2005) 30–39. doi:10.1093/jnci/dji005.
- [82] J.P. Kitzmiller, D.K. Groen, M.A. Phelps, W. Sadee, Pharmacogenomic testing: Relevance in medical practice: Why drugs work in some patients but not in others, *Cleve. Clin. J. Med.* 78 (2011) 243–257. doi:10.3949/ccjm.78a.10145.
- [83] L. Weinstein, Infectious diseases., *Hosp. Pract.* 11 (1976) 14–15. doi:10.1586/14737159.2014.888313.Advances.
- [84] S. Campuzano, P. Yáñez-Sedeño, J. Pingarrón, Diagnostics Strategies with Electrochemical Affinity Biosensors Using Carbon Nanomaterials as Electrode Modifiers, *Diagnostics.* 7 (2016) 2. doi:10.3390/diagnostics7010002.
- [85] N.R. Jabir, S. Tabrez, G.M. Ashraf, S. Shakil, G.A. Damanhour, M.A. Kamal, Nanotechnology-based approaches in anticancer research, *Int. J. Nanomedicine.* 7 (2012) 4391–4408. doi:10.2147/IJN.S33838.
- [86] L. Shao, Y. Gao, F. Yan, Semiconductor quantum dots for Biomedical applications, *Sensors.* 11 (2011) 11736–11751. doi:10.3390/s111211736.
- [87] Y.-E. Choi, J.-W. Kwak, J.W. Park, Nanotechnology for Early Cancer Detection, *Sensors.* 10 (2010) 428–455. doi:10.3390/s100100428.
- [88] D. Saikia, P. Dutta, N. Sen Sarma, N.C. Adhikary, CdTe/ZnS core/shell quantum dot-based ultrasensitive PET sensor for selective detection of Hg (II) in aqueous media, *Sensors*

Actuators, *B Chem.* 230 (2016) 149–156. doi:10.1016/j.snb.2016.02.035.

- [89] G.L. Wang, H.J. Jiao, K.L. Liu, X.M. Wu, Y.M. Dong, Z.J. Li, C. Zhang, A novel strategy for the construction of photoelectrochemical sensors based on quantum dots and electron acceptor: The case of dopamine detection, *Electrochem. Commun.* 41 (2014) 47–50. doi:10.1016/j.elecom.2014.01.014.



CHAPTER TWO

Literature review

Electrochemical biosensors are described as portable devices that permit rapid analysis of a substance and are the most recently studied electroanalytical techniques for quantitative and qualitative detection of various drugs such as tamoxifen and indinavir, due to the negative impacts they pose on human health. Moreover, electrochemical biosensors have gained much attention in a wide range of fields such as environmental monitoring, disease screening, water treatment and therapeutic drug monitoring due to their portability, small size, simplicity, low cost and lower detection limits. Similarly, nanomaterials such as quantum dots contain specific features that make them suitable for sensor applications based on their high surface to volume ratio, high reactivity, ease of dispersability and rapid fabrication. This chapter is focussed on the introduction of quantum dots, covering the quantum dots properties, major role played by stabilizing agents during the colloidal synthesis as well as functionalisation strategies of quantum dots. Additionally, the study gives detailed background information on breast cancer and tamoxifen metabolism as well as electrochemical techniques for the determination of tamoxifen.

Palladium Telluride Quantum Dots-Based Electrochemical Biosensors

Abstract

The development of novel quantum dots have attracted enormous attention due to the ability of creating novel diagnostic tools since they display unique and fascinating optical properties including high quantum yield, photostability, narrow emission spectrum, and broad absorption. Stabilising agents play an important role in controlling the particle size and distribution and, hence, the catalytic activity of quantum dots. Among these various stabilizing agents, mercapto acids containing a single mercapto group and a single carboxyl group connected by an alkyl chain are widely used. The application of QDs in electrochemical and biological sensing is regarded as the most active trend due to their high surface-to-volume ratio and high reactivity. Several methodologies from simple to versatile functionalisation of QDs have been discussed in this chapter. In particular, the bioconjugation of QDs via covalent attachment has been found to be very successful and very useful in attaching biomolecules such as enzymes in preparation of an electrochemical sensor. This chapter review highlighted the development of electrochemical sensor system for the determination of breast cancer drug, tamoxifen.

2.1 Quantum dots

2.1 1. Nanotechnology and quantum dots

Over the past decades, nanotechnology field has advanced rapidly since it demonstrated encouraging results in the detection, treatment, and prevention of certain diseases [1,2]. Additionally, further development of nanotechnology has led to significant breakthroughs in the semiconductor industry [3]. Current studies suggest that nanomaterials such as quantum dots (QDs) hold a great potential and promise for different applications due to their superior and fascinating optical properties. Hence, considerable efforts have been made to construct quantum dots for the use in different fields including amplifiers, biosensors, high resolution cellular imaging, tumour targeting, and diagnostics [4,5]. Most semiconducting nanomaterials such as groups II-VI, III-V or IV-VI elements in the periodic table show quantum confinement behaviour in the 1-20 nm diameter range. Based on QDs substantial advantages such as, bright fluorescence, narrow emission, broadband excitation, photostability and extended half-life compared to conventional organic fluorescent probes (organic dyes), scientists and researchers have gained much interest in developing novel semiconducting nanomaterials which could be used for forensic science, biology, electronic technology, environmental science, computer manufacturing, sports facility production as well as food industries [6,7]. Amongst various novel nanomaterials, palladium telluride (PdTe) is an important semiconductor with unique size-dependent optical properties and have attracted attention in recent years due to catalysis and material science relevance. The major role of selecting PdTeQDs is attributed to their preparation which makes them suitable in various fields such as biomedical labelling, solar conversion and photoelectronics [8]. In addition to the important aspect of discovering novel nanomaterials, great attempts are constantly being invented to explore novel synthesis routes and functionalisation [9].

2.1.2 Synthesis of quantum dots

Over the past two decades, numerous reliable methods were developed for the preparation of highly luminescent quantum dots including organic and aqueous synthesis [10]. Additionally, there are several reports based on microwave and hydrothermal methods for rapid synthesis of QDs [11]. Organic synthesis has limited functions to produce QDs that can be used for environmental and biological testing including diagnosis, pathogen and toxin detection [12]. In biological environment, water is regarded as the main solvent and water-soluble QDs becomes an attractive proposition. Due to organic synthesis limitations, Alivisatos and co-workers developed an effective route using a simpler, inexpensive, and highly reproducible method to coat QDs with a cross-linked silica shell, which can be modified using different organic functionalities such as primary amines, carboxylic acids or thiols [13,14]. Since then, researchers have focussed on aqueous colloidal synthesis since it possesses the following properties: monodispersity, chemical integrity and specificity, possibility of further functionalisation, and high degree of crystallinity without any defects [15]. In addition, aqueous growth of QDs occurs at a lower temperature, which indicates that QDs obtain good average crystallinity and lower quantum yield compared to QDs produced with organic synthesis [16]. Recent publication from our lab by Nxusani and co-workers reported colloidal synthesis method which resulted in water-soluble and biocompatible 3-MPA- Ga₂Se₃QDs for biosensing application [17].

2.1.3 Role of surface modification and bioconjugation of quantum dots

Surface capping agents are molecules such as dendrimers, polymers and surfactants with significant advantages in coating the quantum dot outer surface in order to enhance QDs biocompatibility and cause an increase in quantum yield for superior application benefits in biological systems and various fields of chemistry and biological sciences. However, there is an essential need for using proper surface functionalisation of QDs that will be useful for every possible application which determines their interaction with environment or other molecules [18]. A wide variety of different surfactants with different benefits or liabilities have been used to give rise to quantum dots of different optical and chemical properties. However, the surface coatings of quantum dots affect photophysical and physicochemical properties of quantum dots including the emission, profile, and photostability of the particle suspension in biological systems. The main strategies to achieve biocompatible QDs include silanization, phase transfer methods and surface ligand exchange [19]. The ligand exchange method is found to be the best since it is based on the exchange of the bifunctional molecules hydrophobic surfactant molecules (e.g., thiol functional group) with charged ligand molecules including carboxylic or sulphonic acid groups which are found to secure QDs for longer time [20]. Current studies suggest that the growth rate and surface charge of QDs depends on the choice of stabilisers [4]. In addition, the amount of capping agent introduced to the system plays an important role since it can affect the solubility of the QDs and can alter different configurations of the quantum dot nanocrystals [21]. Different thiolated organic surfactants such as 3- mercaptopropionic acid (3-MPA), thioglycolic acid (TGA), 3, 3'-dithiodipropionic acid (3, 3'-DTPA) are commonly used as capping agents during the synthesis of QDs [22]. Such molecules have also been used in this study to bind PdTe quantum dots to thiol group (-SH) while free carboxylic group extends outwards to provide water-solubility, as well as the conjugation to biomolecules to extend the uses and

applications of quantum dots. This is by far the simplest method to achieve solubilisation. Several studies based on functionalisation of QDs have been performed previously from our lab. For instance, Douman and co-workers [23] used indium telluride quantum dots functionalised with 3-mercaptopropionic acid to give rise to water-soluble and biocompatible $\text{In}_2\text{Te}_3\text{QDs}$. The structures of commonly used capping agents for the QDs synthesis are shown below

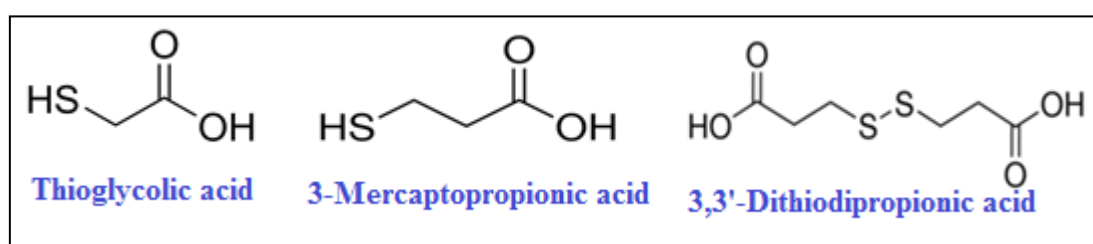


Figure 5: Mercapto Acids

When the solubilisation is achieved, QDs can be functionalised by conjugation to several biomolecules including oligonucleotides, peptides, antibodies, DNA and cytochrome P450 enzymes [24], through surface reactive. Different methods have been used for bioconjugation including noncovalent and covalent conjugation. Covalent linkage maintain an advantage in terms of stability and reproducibility of the surface modification and lowers unspecific physisorption compared to noncovalent conjugation and utilises functional groups on the QDs surface like primary amine, carboxylic acids, and thiols to create a strong bond with groups present on biomolecules or through the use of cross-linker molecules [25,26], such as water-soluble carbodiimide (e.g. EDC) which is used to couple carboxylic group to primary amines and has been used in wide applications such as forming amide bonds in peptide synthesis and an active ester compound (N-Hydroxysuccinimide; NHS) that can be equally used to form amide bonds [27]. Over the past decade, numerous research reviews have been reported based on the synthesis and functionalisation of QDs enabling to have for enormous

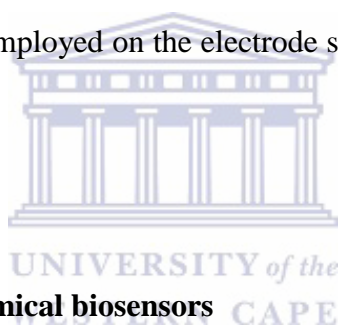
spectacular applications across the biomedical research field, especially in biosensing and bioimaging [28]. Recently, several QDs-based sensors have been developed or fabricated. Publication by Jia and co-workers [29] prepared hybrid structures containing quantum dots for electrochemiluminescence detection of adenosine triphosphate (ATP) and thrombin. In this present work, we report the most significant applications of the functionalised PdTeQDs with (3-MPA), (TGA) or (3,3'-DTPA) for further use as a mediator in electrochemical phenotypic biosensor systems for the determination of various drugs including ARV drugs and tamoxifen.

2.2 Applications of quantum dots

2.2.1. Quantum dots-based electrochemical sensors

Over the past few years, the field of electrochemical biosensors for clinical diagnostics has grown rapidly in order to provide miniaturized platforms with many favorable and fascinating properties, such as reduced sample volume, reducing assay time, portable field-based size, sample or reagent consumptions [30]. Nowadays, the increasing demand for this field has focused on novel sensing strategies with increasing number of publications based on the enhancement of specificity, sensitivity and response time[31,32]. Generally, biosensors are defined as devices that utilise biological components with unique and fascinating specificities and produces an electrical, optical, thermal or magnetic output signal with significant magnitude proportional to the concentration of the analyte [33]. Since the discovery or development of nanoscience and technology, research interest has been focussed on applying nanomaterials in the construction of biosensor systems [34,35]. Among such nanomaterials, gold nanoparticles (GNPs), semi-conductor quantum dots (QDs), polymer nanoparticles, carbon nanotubes (CNTs), fullerene, nanodiamonds, dendrimers and graphene have been intensively studied [36]. However, current studies have demonstrated that QDs provide large

surface area and excellent surface activity thereby enhancing the electron charge transfer across the sensor chip or electrolyte interface [37,38]. For instance, Chad and co-workers presented a nanoparticle-based biosensing system using a variety of nanostructured materials with unique optical electric, magnetic, electrochemical, and thermal signatures for determination of molecular biomarkers with high intensities [39]. Tian and co-workers [40] reported quantum dot-based nanosensor for simultaneous detection of two tumour markers which combines strong luminescence and high photostability of CdSe quantum dots with significant characteristic functions of immunochromatography test strip such as ease of use, relatively low cost fastness. However, there are major challenges based on the immobilisation strategy used to conjugate bio-specific entity onto such nanomaterials. To overcome all these limitations, enzymes should be employed on the electrode surface when developing a reliable biosensor.



2.2.2 Enzyme-based electrochemical biosensors

Over the past decade, Professor Clark Jr. has been regarded as the father of the biosensor concept since he invented the first electrochemical biosensor, known as the ‘enzyme electrode’ [41]. Since then, biosensor field became a fascinating topic since the description by Updike and Hicks [42] who initiated the first functional enzyme electrode based on deposited glucose oxidase on oxygen sensor in 1967. Moreover, the field of biosensors has increased rapidly and appeared in literature with a great number of applications in medical diagnostics [43,44]. Approximately 80% of notable commercial devices based on biosensors are mainly used in commercial devices for determination of glucose produced by Yellow Springs Instrument Company (YSI; Yellow Springs, Ohio, USA incorporated 1975) [45]. However, the literature has revealed the opportunity of the global medical sensors market and the annual growth which was in excess of US\$1,452.8 million in 2015 and is expected to

reach US\$2,476.8 million in 2024, as the market expands at a compound annual growth rate (CAGR) of 6.1% from 2015 to 2024 [46,47] as shown in **Figure 6**. Thus, the increasing biosensors market size is mostly affected by rising demand for disposable, cost-efficient, and user-friendly devices. Hence, electrochemistry has come to play a major role in the field of diagnostics, while optical techniques have found their slot in R&D. Therefore, the field of electrochemical biosensors seem best suited for limited-use and point-of-care application.

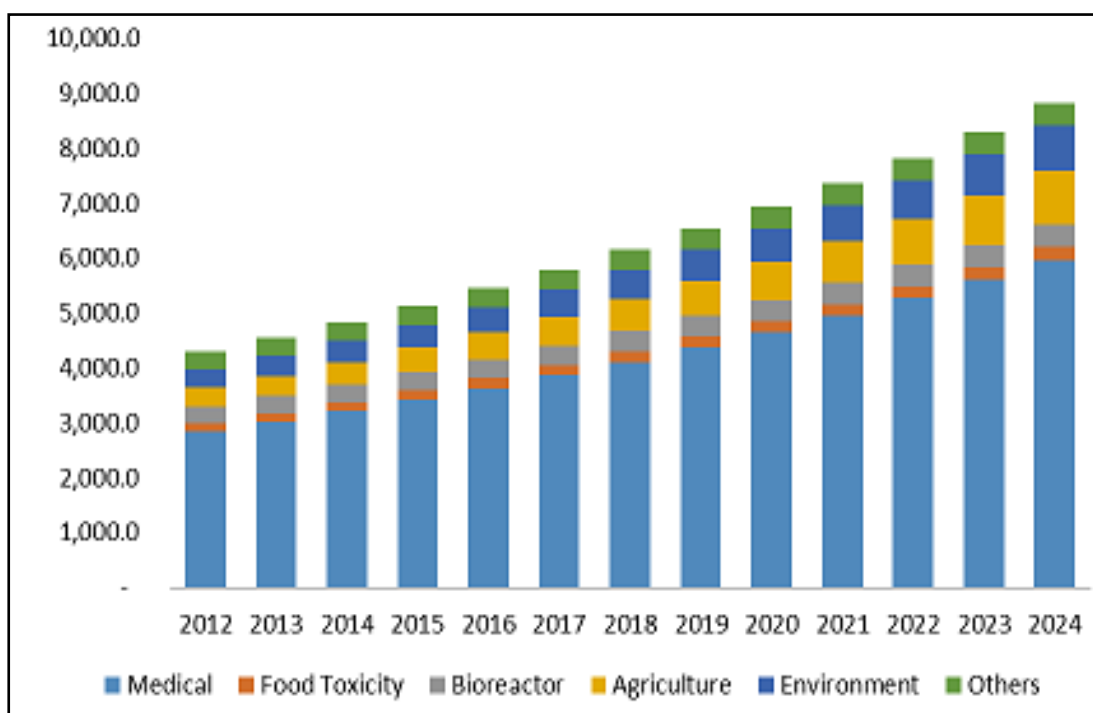


Figure 6: Graph of the world market for medical biosensor assessment from diverse commercial sources and anticipated for the future in US\$ millions [48].

There are several types of biosensors for clinical applications which are categorised according to the nature of recognition including enzyme-based biosensors, immunological biosensors, and DNA biosensors. Even though biosensing devices make use of a different range of recognition elements, electrochemical detection techniques such as electrochemical biosensors mainly use enzymes to develop sensitive, more sophisticated, mature and reliable

biosensor [49]. Moreover, role of enzymes in clinical diagnosis has been known for several years even though they tend to be less stable in solution, it is therefore needed to stabilise them by immobilization method to gain excellent stability and become reusable [47]. Among the enzymes commercially available, the most commonly used are cytochrome P450 enzymes and oxidases, such as glucose oxidase (GOx) and horseradish peroxidase (HRP) [50]. Cytochrome P50 enzymes (CYPs) play an important role in the biotransformation of drugs such as indinavir and tamoxifen drugs. Also, CYPs are associated with different types of reactions such as hydroxylation, epoxidation, dehalogenation, dehydrogenation and N-dealkylation which, together with the monooxygenation capabilities of CYPs, have resulted in their application in biosensors. Recent progress in the development of electrochemical biosensors has been summarised in some excellent reviews. The elaboration of biosensors is considered to be one of the most favourable ways to solve some of the problems concerning sensitive, fast and cheap measurements [51]. Such devices would be very useful for the quick detection of various infectious disease. Furthermore, electrochemical biosensors are nowadays considered to be useful tools for the investigation of electron-transfer reactions and can be used for production of metabolic-redox reactions, as well as applied technique in drug metabolism studies [52].

2.3 Electrochemical biosensors for tamoxifen

2.3.1 Biosensors for tamoxifen

An anticancer drug, tamoxifen has drawn much interest in pharmaceutical field due to its nonsteroidal antiestrogenic effects regardless of its use being associated with a 2–7-fold dignified risk of promoting endometrial carcinoma [51,53]. However, there is still an ongoing research based on the uncertainty of tamoxifen being a consequence of a DNA-damaging (genotoxic) or non-genotoxic mechanism. Therefore, the introduction of electrochemical

methods would highlight some of uncertain issues that have been explored poorly [54]. Additionally, literature has indicated that there are very few reports based on electrochemistry for tamoxifen and its metabolites. Thus, most of the published data in literature has been focussed on the development of simple and rapid electroanalytical methods for the determination of tamoxifen. Innovative electrochemical biosensor strategies could represent an alternative way for reliable tamoxifen testing. Several electrochemical biosensors for the detection of tamoxifen in pure form and in pharmaceutical tablets have been presented in the last few years based on different transduction techniques, from electrochemical as indicated in (**Table 1**).

Table 1: Electrochemical biosensors for tamoxifen

Name of the biosensor	* <i>LOD</i> (M)	Advantages	Disadvantages	References
Adsorptive potential stripping analysis	4×10^{-10}	Relies on the constant-current potentiometric stripping (PSA) mode.	The oxidation mechanism of tamoxifen coincides with literature. No significance in differentiating the parent drug with its active metabolites	[55,56]
Electrochemical MIP sensor		Combine MIPs with enzymes to improve the analytical performance of sensors	The harsh regeneration of MIP is not compatible with the stability of the enzyme The oxidation of TAM brought about a fouling of the electrode surface	[57]
Ultrasensitive flow injection electrochemical sensor	3×10^{-12}	The technology adaptation provides a substantial improvement for rapid analysis	Require very high scan rates	[58]

* Limit of detection

Since tamoxifen is bio-transformed to pharmacologically active metabolites that can remarkably donate to complete adverse effects of the drug. Interestingly, novel electrochemical systems would focus on the relationship between oxidation or reduction chemistry and CYP450-mediated oxidative drug metabolism (Phase I metabolism) to provide a wide variety of information on metabolic characteristics [59,60]. Thus, this study introduces a next generation phenotype-based nanobiosensor for sensing and signaling tamoxifen bioactivity. With regards to phenotype-based biosensor systems, quantum dots are incorporated to create a more sensitive platform and improve the limit of detection for targeted analyte. In addition, phenotype-based biosensor systems differ from and are expected to be more superior than the electrochemical methods mentioned in **Table 1** and genotype-based sensing protocols (such as the very expensive commercial Roche's AmpliChip CYP450 Test) since a patient's drug response profile does not depend on genetics alone. The sensor system would be a low cost reactor on a chip consisting of biocompatible palladium telluride-quantum dots-modified genetically engineered CYP2D6 and CYP3A4 bipolar bioelectrodes for electrochemical sensing and signaling of tamoxifen biotransformation, which aimed to provide a patient's complete response profile at point-of-care. A schematic diagram representing the preparation of electrochemical biosensor systems is shown below **(Figure 7)**.

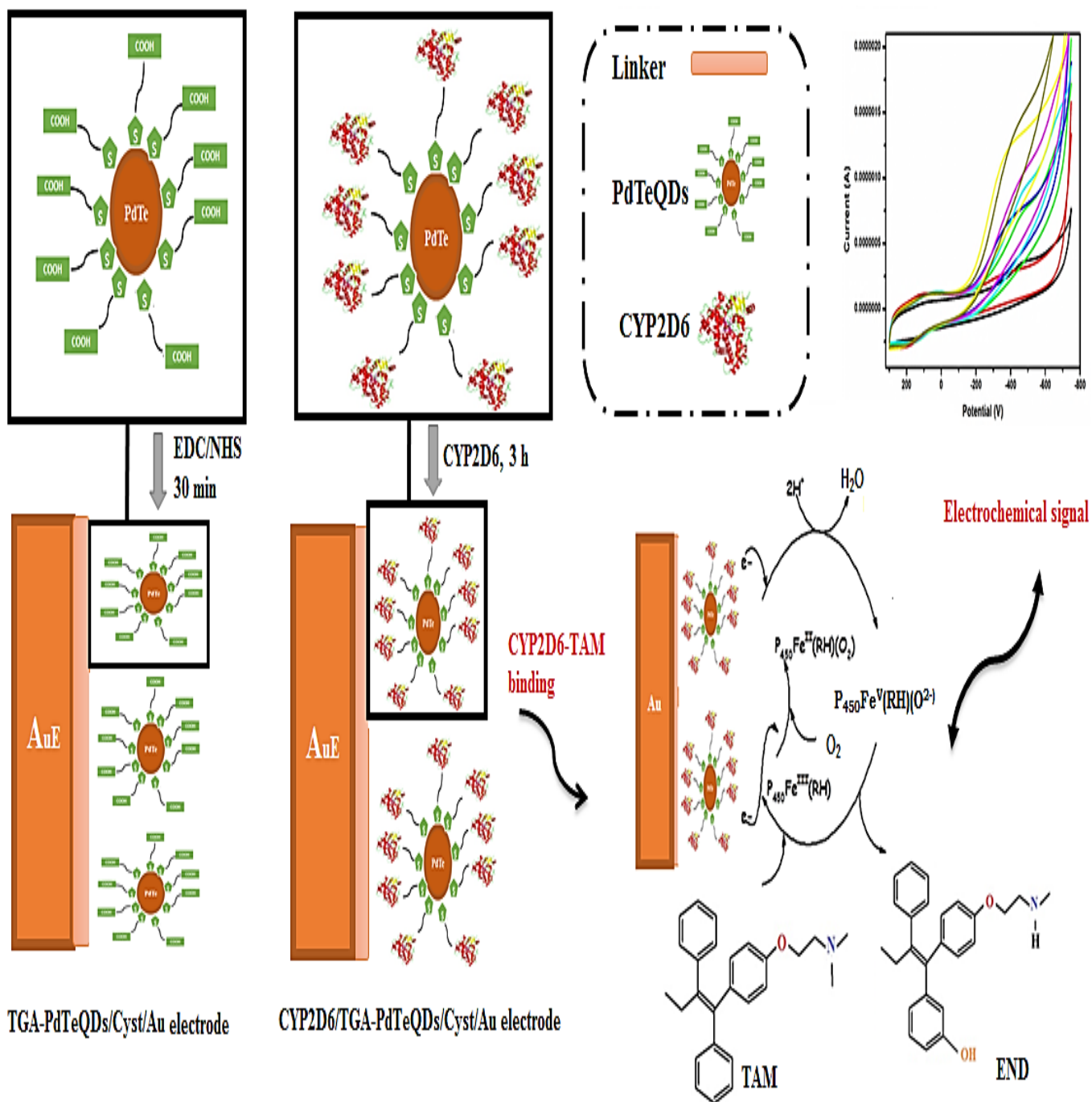


Figure 7: Schematic diagram for the preparation of biosensor systems for determination of tamoxifen.

2.4 Breast cancer and tamoxifen metabolism

2.4.1 Breast cancer

Along with HIV and TB, breast cancer has been regarded as a priority disease and is responsible for as much death among women worldwide. It has been noted that breast cancer was first recognised to be an estrogen-dependent disease as 75% of breast cancers were positive for ER [54]. South Africa ranks 50th on the countries list containing the highest cancer prevalence rates. Furthermore, studies indicate that risks for breast cancer increase with age and that 77% of breast cancer patients are over the age of 50 [61]. It is known that breast tissue growth is estrogen-responsive, usually when the cells becomes tumorous, oestrogen promotes a cancerous reaction that causes cell invasion as well as growth and division [62]. There is, however, a strong connection between early detection and positive patient outcome. The reason for early detection is to improve patient survival and disease prognosis which may lead to cancer prevention [63]. Endocrine therapies have positive adverse-event profile for the treatment of women with hormone receptor-positive (HR+) metastatic breast cancer. Additionally, these therapies are designed to block estrogen signalling [64]. Two endocrine treatments which are mostly used for the treatment of early hormone-responsive breast cancer patients at high risk belongs to a class of drugs called selective estrogen receptor modulators (SERMs) or a different class named aromatase inhibitors (AIs), which has also been shown to be effective for breast cancer prevention, though none are approved for this indication [65]. Despite the development of newer SERMs such as toremifene (an analogue of tamoxifen), and the benzothiophene also known as raloxifene, tamoxifen (brand name: Nolvadex) remains the SERM of first choice and is commonly prescribed for the treatment of hormone responsive breast cancer [66]. There is

currently a development of newer SEMs but none have so far proven to be as effective as tamoxifen in the adjuvant therapy of breast cancer.

2.4.2 Tamoxifen metabolism

Tamoxifen is described as an ER antagonist that has been widely used as a treatment for breast cancer patients since the early 1970s [65]. It is also described as a pro-drug since it is extensively metabolised yielding several metabolites that are more potent antiestrogen than the parent compound [67]. Unlike any other medicine in oncology, TAM is used to treat all stages of breast cancer, in adjuvant therapy as a long-term suppressant of tumor recurrence as well as a chemopreventive agent in women at high risk of developing this type of estrogen-dependent cancer. Several adverse effects have been recognised related with tamoxifen which is either used as a chemotherapeutic or as a chemopreventive agent, against breast cancer [51]. Several studies have shown that benefits of tamoxifen are greater with 5 years of therapy than with 1 or 2 years since it reduces the reoccurrence and the mortality rate by one-third in both pre- and post-menopausal women [68–70]. Interestingly, there may be some additional benefits from tamoxifen including an observed reduction frequency of deaths from myocardial bone loss [53]. Although the adverse effects of tamoxifen have been attributed to its hormonal properties, currently there is a major interest which focusses on the study of TAM bioconversion and recognition of metabolites since they have a tendency of acting as chemical carcinogens [71]. In women, several phase I tamoxifen metabolism mostly occurs through two pathways (**Figure 8**), 4-hydroxylation and N-demethylation, both of which produce a secondary metabolite, endoxifen. Originally, the 4-hydroxylation path, which is catalysed by diversified CYPs including CYP2D6, since it is given major consideration due to the immediately resulting metabolite, 4-hydroxytamoxifen and endoxifen demonstrated its antiestrogen effectiveness with an approximation of ~30–100-fold more than tamoxifen. Both

enzymes participate in the formation of active metabolites. Importantly, N-desmethylTAM comes from the CYP3A4/5-mediated catalysis of tamoxifen, which is regarded as the major primary metabolite and accounts for approximately 92% of primary tamoxifen oxidation. Usually in patients receiving tamoxifen therapy, serum concentrations for endoxifen are found to be 6-12-fold higher than 4-hydroxytamoxifen and is believed that it can play also an important role in vivo [72]. Thus, endoxifen is likely the most important metabolite required for tamoxifen activity.

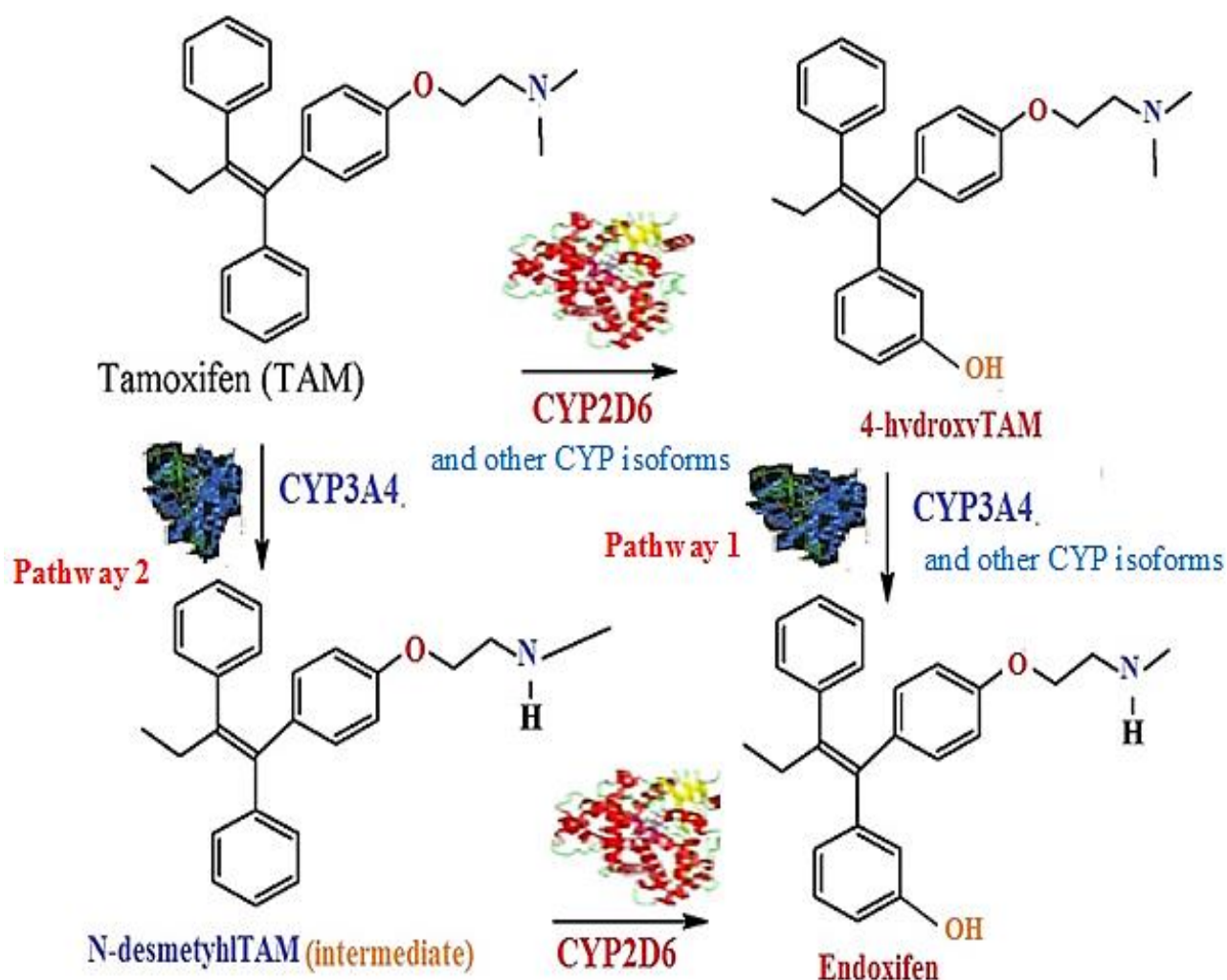
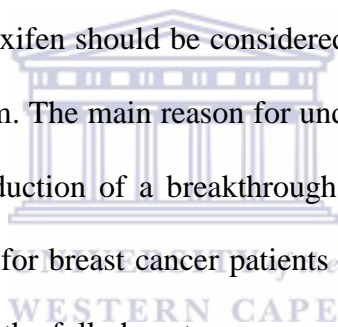


Figure 8: Reaction scheme for the biotransformation of tamoxifen.

2.5 Conclusion

The rapid improvement in nanoscience and nanotechnology have led to the production of several novel nanomaterials including quantum dots which stand unique owing to their biocompatibility and stability. These fascinating properties make them to be very attractive and appropriate for functionalisation of biomolecules such as enzymes in their matrices for biosensor preparation. The growing market of biosensors field in point-of-care diagnostics has aroused the development of novel, inexpensive sensor platforms that can compete effectively to meet consumers' needs. Moreover, the development of novel electrochemical biosensor systems has been found to be extremely promising for improving the efficiency of diagnostic testing and drug monitoring of tamoxifen. However, innovative studies based on voltammetric behaviour for tamoxifen should be considered and accomplished to understand its oxidative/reductive mechanism. The main reason for understanding tamoxifen mechanism is that it would lead to the production of a breakthrough testing protocol for determining appropriate dosing of tamoxifen for breast cancer patients and would be very applicable for use at a doctor's office to supply the full phenotype response pattern of a patient to treatment with tamoxifen.



References

- [1] S. Jain, A.P. Jain, S. Jain, O.N. Gupta, A. Vaidya, Nanotechnology: An emerging area in the field of dentistry, *J. Dent. Sci.* (2013). doi:10.1016/j.jds.2013.08.004.
- [2] C. Dianza, G.P. Zara, G. Maina, P. Pettazzoni, S. Pizzimenti, F. Rossi, C.L. Gigliotti, E.S. Ciamporcero, M. Daga, G. Barrera, Drug delivery nanoparticles in skin cancers, *Biomed Res. Int.* 2014 (2014). doi:10.1155/2014/895986.
- [3] M. Terrones, A. Jorio, M. Endo, A.M. Rao, Y.A. Kim, T. Hayashi, H. Terrones, J.C. Charlier, G. Dresselhaus, M.S. Dresselhaus, New direction in nanotube science, *Mater. Today*. 7 (2004) 30–45. doi:10.1016/S1369-7021(04)00628-5.
- [4] Y. Zhang, A. Clapp, Overview of stabilizing ligands for biocompatible quantum dot nanocrystals, *Sensors*. 11 (2011) 11036–11055. doi:10.3390/s111211036.
- [5] S. Suresh, Semiconductor Nanomaterials, Methods and Applications: A Review, *Nanosci. Nanotechnol.* 3 (2013) 62–74. doi:10.5923/j.nn.20130303.06.
- [6] K.E. Sapsford, T. Pons, I.L. Medintz, H. Mattoussi, Biosensing with Luminescent Semiconductor Quantum Dots, *Sensors*. 6 (2006) 925–953. doi:10.3390/s6080925.
- [7] T. Jamieson, R. Bakhshi, D. Petrova, R. Pocock, M. Imani, A.M. Seifalian, Biological applications of quantum dots, *Biomaterials*. 28 (2007) 4717–4732. doi:10.1016/j.biomaterials.2007.07.014.
- [8] S. Massadeh, M. Alaamery, Nanoparticles Outline :, (n.d.) 357–373.
- [9] P. Mulpur, T.M. Rattan, V. Kamiseti, One-step synthesis of colloidal quantum dots of iron selenide exhibiting narrow range fluorescence in the green region, *J. Nanosci.* 2013 (2013).

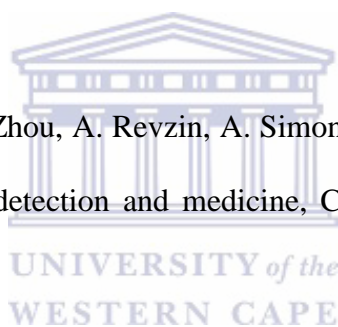
- [10] A. Emamdoust, S.F. Shayesteh, M. Marandi, Synthesis and characterization of aqueous MPA-capped CdS-ZnS core-shell quantum dots, *Pramana - J. Phys.* 80 (2013) 713–721. doi:10.1007/s12043-013-0512-9.
- [11] S.S. Chetty, S. Praneetha, S. Basu, C. Sachidanandan, A.V. Murugan, Sustainable, Rapid Synthesis of Bright-Luminescent CuInS₂-ZnS Alloyed Nanocrystals: Multistage Nano-xenotoxicity Assessment and Intravital Fluorescence Bioimaging in Zebrafish-Embryos, *Sci. Rep.* 6 (2016) 26078. doi:10.1038/srep26078.
- [12] K.D. Wegner, N. Hildebrandt, Quantum dots: bright and versatile in vitro and in vivo fluorescence imaging biosensors., *Chem. Soc. Rev.* 44 (2015) 4792–834. doi:10.1039/c4cs00532e.
- [13] A P. Alivisatos, W. Gu, C. Larabell, Quantum dots as cellular probes., *Annu. Rev. Biomed. Eng.* 7 (2005) 55–76. doi:10.1146/annurev.bioeng.7.060804.100432.
- [14] D. Gerion, F. Pinaud, S.C. Williams, W.J. Parak, D. Zanchet, S. Weiss, P.A. Alivisatos, Synthesis and properties of biocompatible water-soluble silica-coated CdSe/ZnS semiconductor quantum dots, *J. Phys. Chem. B.* 105 (2001) 8861–8871. doi:S1089-5647(01)00548-X.
- [15] M. Venkatesh, G.S. Kumar, S. Viji, S. Karthi, E.K. Girija, Microwave assisted combustion synthesis and characterization of nickel ferrite nanoplatelets, *Mod. Electron. Mater.* 2 (2016) 74–78. doi:10.1016/j.moem.2016.10.003.
- [16] M.Z. Hu, T. Zhu, Semiconductor Nanocrystal Quantum Dot Synthesis Approaches Towards Large-Scale Industrial Production for Energy Applications., *Nanoscale Res. Lett.* 10 (2015) 469. doi:10.1186/s11671-015-1166-y.
- [17] E. Nxusani, P.M. Ndangili, R. a. Olowu, a. N. Jijana, T. Waryo, N. Jahed, R.F. Ajayi,

- P. Baker, E.I. Iwuoha, 3-Mercaptopropionic Acid Capped Ga₂Se₃nanocrystal-CYP3A4 Biosensor for the Determination of 17-Alpha-Ethinyl Estradiol in Water, *Nano Hybrids*. 1 (2012) 1–22. doi:10.4028/www.scientific.net/NH.1.1.
- [18] R.A. Sperling, W.J. Parak, Surface modification, functionalization and bioconjugation of colloidal inorganic nanoparticles., *Philos. Trans. A. Math. Phys. Eng. Sci.* 368 (2010) 1333–1383. doi:10.1098/rsta.2009.0273.
- [19] M. Wang, G. Abbineni, A. Clevenger, C. Mao, S. Xu, Upconversion nanoparticles: Synthesis, surface modification and biological applications, *Nanomedicine Nanotechnology, Biol. Med.* 7 (2011) 710–729. doi:10.1016/j.nano.2011.02.013.
- [20] S.B. Rizvi, S. Ghaderi, M. Keshtgar, A.M. Seifalian, Semiconductor quantum dots as fluorescent probes for in vitro and in vivo bio-molecular and cellular imaging., *Nano Rev.* 1 (2010) 1–15. doi:10.3402/nano.v1i0.5161.
- [21] K. Koç, F.Z. Tepehan, G.G. Tepehan, Growth kinetics of MPS-capped CdS quantum dots in self-assembled thin films., *Nanoscale Res. Lett.* 7 (2012) 610. doi:10.1186/1556-276X-7-610.
- [22] Y. Miao, P. Yang, J. Zhao, Y. Du, H. He, Y. Liu, Photodegradation of Mercaptopropionic Acid- and Thioglycollic Acid-Capped CdTe Quantum Dots in Buffer Solutions, *J. Nanosci. Nanotechnol.* 15 (2015) 4462–4469. doi:10.1166/jnn.2015.9800.
- [23] S. Douman, U. Feleni, N. Ross, X. Fuku, R. Ajayi, E. Nxusani, N. Ntshongontshi, U. Sidwaba, C. Rassie, A. Jijana, P. Baker, A. Williams, E. Iwuoha, New generation nanoelectrochemical biosensors for disease biomarkers: 1. Indium telluride quantum dots signaling of telomerase cancer biomarker, *J. Nanosci. Nanotechnol.* 16 (2016). doi:10.1166/jnn.2016.13648.

- [24] A.S. Karakoti, R. Shukla, R. Shanker, S. Singh, Surface functionalization of quantum dots for biological applications, *Adv. Colloid Interface Sci.* 215 (2015) 28–45. doi:10.1016/j.cis.2014.11.004.
- [25] M. Di Marco, S. Shamsuddin, K.A. Razak, A.A. Aziz, C. Devaux, E. Borghi, L. Levy, C. Sadun, Overview of the main methods used to combine proteins with nanosystems: Absorption, bioconjugation, and encapsulation, *Int. J. Nanomedicine.* 5 (2010) 37–49. doi:10.2147/IJN.S6458.
- [26] Y. Xing, J. Rao, Quantum dot bioconjugates for in vitro diagnostics & in vivo imaging., *Cancer Biomark.* 4 (2008) 307–319.
- [27] E. Valeur, M. Bradley, Amide bond formation: beyond the myth of coupling reagents, *Chem Soc Rev.* 38 (2009) 606–631. doi:10.1039/b701677h.
- [28] Y. Wang, R. Hu, G. Lin, I. Roy, K.T. Yong, Functionalized quantum dots for biosensing and bioimaging and concerns on toxicity, *ACS Appl. Mater. Interfaces.* 5 (2013) 2786–2799. doi:10.1021/am302030a.
- [29] J. Zhang, S.H. Yu, Carbon dots: large-scale synthesis, sensing and bioimaging, *Mater. Today.* 19 (2016) 382–393. doi:10.1016/j.mattod.2015.11.008.
- [30] V. Perumal, U. Hashim, Advances in biosensors: Principle, architecture and applications, *J. Appl. Biomed.* 12 (2014) 1–15. doi:10.1016/j.jab.2013.02.001.
- [31] M. Mehrvar, M. Abdi, Recent Developments, Characteristics, and Potential Applications of Electrochemical Biosensors, *Anal. Sci.* 8 (2004) 14. doi:10.2116/analsci.20.1113.
- [32] E. Bakker, Y. Qin, Electrochemical Sensors, *Anal. Chem.* 78 (2006) 3965–3984. doi:10.1021/ac060637m.Electrochemical.

- [33] M. Holzinger, A. Le Goff, S. Cosnier, Nanomaterials for biosensing applications: a review., *Front. Chem.* 2 (2014) 63. doi:10.3389/fchem.2014.00063.
- [34] E. Katz, I. Willner, Integrated nanoparticle-biomolecule hybrid systems: Synthesis, properties, and applications, *Angew. Chemie - Int. Ed.* 43 (2004) 6042–6108. doi:10.1002/anie.200400651.
- [35] N.L. Rosi, C.A. Mirkin, Nanostructures in biodiagnostics, *Chem. Rev.* 105 (2005) 1547–1562. doi:10.1021/cr030067f.
- [36] M. Farre, L. Kantiani, S. Perez, D. Barcelo, Sensors and biosensors in support of EU Directives, *TrAC - Trends Anal. Chem.* 28 (2009) 170–185. doi:10.1016/j.trac.2008.09.018.
- [37] A.S. Ghreera, C.M. Pandey, M.A. Ali, B.D. Malhotra, Quantum dot-based microfluidic biosensor for cancer detection, *Appl. Phys. Lett.* 106 (2015). doi:10.1063/1.4921203.
- [38] A. Sharma, G. Sumana, S. Sapra, B.D. Malhotra, Quantum dots self assembly based interface for blood cancer detection, *Langmuir.* 29 (2013) 8753–8762. doi:10.1021/la401431q.
- [39] R. Elghanian, Selective Colorimetric Detection of Polynucleotides Based on the Distance-Dependent Optical Properties of Gold Nanoparticles, *Science (80-.).* 277 (1997) 1078–1081. doi:10.1126/science.277.5329.1078.
- [40] J. Tian, L. Zhou, Y. Zhao, Y. Wang, Y. Peng, S. Zhao, Multiplexed detection of tumor markers with multicolor quantum dots based on fluorescence polarization immunoassay, *Talanta.* 92 (2012) 72–77. doi:10.1016/j.talanta.2012.01.051.
- [41] L.C. Clark, Jr. Monitor and control of blood and tissue oxygen tensions, *ASAIO Trans.* 2 (1956) 41-48.

- [42] S.J. Updike, G.P. Hicks, The enzyme electrode., *Nature*. 214 (1967) 986–8. doi:10.1038/214986a0.
- [43] M. Ngoepe, Y.E. Choonara, C. Tyagi, L.K. umar Tomar, L.C. du Toit, P. Kumar, V.M.K. Ndesendo, V. Pillay, Integration of biosensors and drug delivery technologies for early detection and chronic management of illness, *Sensors (Basel)*. 13 (2013) 7680–7713. doi:10.3390/s130607680.
- [44] A. Bard, G. Inzelt, F. Scholz, *Electrochemical dictionary*, 2012. doi:10.1007/978-3-340-74598-3.
- [45] S.J. Setford, J.D. Newman, *Enzyme Biosensors*, 2005. doi:10.1385/1-59259-846-3:029.
- [46] J. Kirsch, C. Siltanen, Q. Zhou, A. Revzin, A. Simonian, Biosensor technology: recent advances in threat agent detection and medicine, *Chem. Soc. Rev.* 42 (2013) 8733. doi:10.1039/c3cs60141b.
- [47] B.D. Malhotra, A. Chaubey, Biosensors for clinical diagnostics industry, *Sensors Actuators, B Chem.* 91 (2003) 117–127. doi:10.1016/S0925-4005(03)00075-3.
- [48] A.P.F. Turner, A.P.F. Turner, *Chemical Society Reviews*, 42 (2013). doi:10.1039/c3cs35528d.
- [49] C. Kokkinos, M. Prodromidis, A. Economou, P. Petrou, S. Kakabakos, Quantum dot-based electrochemical DNA biosensor using a screen-printed graphite surface with embedded bismuth precursor, *Electrochem. Commun.* 60 (2015) 47–51. doi:10.1016/j.elecom.2015.08.006.
- [50] F. Rezende, K.K. Prior, O. Lowe, I. Wittig, V. Strecker, F. Moll, V. Helfinger, F. Schnutgen, N. Kurrle, F. Wempe, M. Walter, S. Zukunft, B. Luck, I. Fleming, N.



- Weissmann, R.P. Brandes, K. Schroder, Cytochrome P450 enzymes but not NADPH oxidases are the source of the NADPH-dependent lucigenin chemiluminescence in membrane assays, *Free Radic. Biol. Med.* 102 (2017) 57–66. doi:10.1016/j.freeradbiomed.2016.11.019.
- [51] J.M.P.J. Garrido, E. Manuela, P.J. Garrido, A.M. Oliveira-Brett, F. Borges, An electrochemical outlook on tamoxifen biotransformation: current and future prospects., *Curr. Drug Metab.* 12 (2011) 372–382. doi:BSP/CDM/E-Pub/000140 [pii].
- [52] U. Karst, Electrochemistry/mass spectrometry (EC/MS)-a new tool to study drug metabolism and reaction mechanisms., *Angew. Chem. Int. Ed. Engl.* 43 (2004) 2476–2478. doi:10.1002/anie.200301763.
- [53] M.N. Singh, H.F. Stringfellow, E. Paraskevaidis, P.L. Martin-Hirsch, F.L. Martin, Tamoxifen: Important considerations of a multi-functional compound with organ-specific properties, *Cancer Treat. Rev.* 33 (2007) 91–100. doi:10.1016/j.ctrv.2006.09.008.
- [54] J.I. MacGregor, V.C. Jordan, Basic guide to the mechanisms of antiestrogen action., *Pharmacol. Rev.* 50 (1998) 151–196.
- [55] J. Wang, X. Cai, J.R. Fernandes, M. Ozsoz, D.H. Grant, Adsorptive potentiometric stripping analysis of trace tamoxifen at a glassy carbon electrode, *Talanta.* 45 (1997) 273–278. doi:10.1016/S0039-9140(97)00129-X.
- [56] A. Schreivogel, J. Maurer, R. Winter, A. Baro, S. Laschat, Synthesis and electrochemical properties of tetrasubstituted tetraphenylethenes, *European J. Org. Chem.* (2006) 3395–3404. doi:10.1002/ejoc.200600123.
- [57] A. Yarman, F.W. Scheller, The first electrochemical MIP sensor for tamoxifen,

- Sensors (Switzerland). 14 (2014) 7647–7654. doi:10.3390/s140507647.
- [58] P. Daneshgar, P. Norouzi, M. Reza, H. Ali, Talanta Ultrasensitive flow-injection electrochemical method for detection of anticancer drug tamoxifen, 77 (2009) 1075–1080. doi:10.1016/j.talanta.2008.08.027.
- [59] W. Lohmann, U. Karst, Biomimetic modeling of oxidative drug metabolism: Strategies, advantages and limitations, Anal. Bioanal. Chem. 391 (2008) 79–96. doi:10.1007/s00216-007-1794-x.
- [60] A. Alvarez-Lueje, S. Bollo, Stability and drug metabolism assessed by electrochemical methods., Comb. Chem. High Throughput Screen. 13 (2010) 712–727. doi:10.2174/138620710791920329.
- [61] R.L. Helms, E.L. O’Hea, M. Corso, Body image issues in women with breast cancer., Psychol. Health Med. 13 (2008) 313–325. doi:10.1080/13548500701405509.
- [62] E.A. Grunfeld, M.S. Hunter, P. Sikka, S. Mittal, Adherence beliefs among breast cancer patients taking tamoxifen, Patient Educ. Couns. 59 (2005) 97–102. doi:10.1016/j.pec.2004.10.005.
- [63] P. Hadji, Improving compliance and persistence to adjuvant tamoxifen and aromatase inhibitor therapy, Crit. Rev. Oncol. Hematol. 73 (2010) 156–166. doi:10.1016/j.critrevonc.2009.02.001.
- [64] S.A. Nazarali, S.A. Narod, Tamoxifen for women at high risk of breast cancer., Breast Cancer (Dove Med. Press. 6 (2014) 29–36. doi:10.2147/BCTT.S43763.
- [65] D.J. Klein, C.F. Thorn, Z. Desta, D.A. Flockhart, R.B. Altman, T.E. Klein, PharmGKB summary: Tamoxifen pathway, pharmacokinetics, Pharmacogenet Genomics. 23 (2013) 643–647. doi:10.1097/FPC.0b013e3283656bc1.

- [66] V.G. Vogel, J.P. Costantino, D.L. Wickerham, W.M. Cronin, R.S. Cecchini, J.N. Atkins, T.B. Bevers, L. Fehrenbacher, E.R. Pajon, J.L. Wade, A. Robidoux, R.G. Margolese, J. James, S.M. Lippman, C.D. Runowicz, P. a Ganz, S.E. Reis, W. McCaskill-Stevens, L.G. Ford, V.C. Jordan, N. Wolmark, Effects of tamoxifen vs raloxifene on the risk of developing invasive breast cancer and other disease outcomes: the NSABP Study of Tamoxifen and Raloxifene (STAR) P-2 trial., *JAMA*. 295 (2006) 2727–2741. doi:10.1097/01.ogx.0000238648.23538.42.
- [67] V.C. Jordan, Tamoxifen as the first targeted long-term adjuvant therapy for breast cancer, *Endocr. Relat. Cancer*. 21 (2014). doi:10.1530/ERC-14-0092.
- [68] M.D. Johnson, H. Zuo, K.H. Lee, J.P. Trebley, J.M. Rae, R. V. Weatherman, Z. Desta, D.A. Flockhart, T.C. Skaar, Pharmacological characterization of 4-hydroxy-N-desmethyl tamoxifen, a novel active metabolite of tamoxifen, *Breast Cancer Res. Treat.* 85 (2004) 151–159. doi:10.1023/B:BREA.0000025406.31193.e8.
- [69] Early Breast Cancer Trialists' Collaborative Group*, Tamoxifen for early breast cancer: an overview of the randomised trials, *Lancet*. 351 (1998) 1451–1467. doi:10.1016/S0140-6736(97)11423-4.
- [70] P. Wegman, L. Vainikka, O. Stål, B. Nordenskjöld, L. Skoog, L.-E. Rutqvist, S. Wingren, Genotype of Metabolic Enzymes and the Benefit of Tamoxifen in Postmenopausal Breast Cancer Patients., *Breast Cancer Res.* 7 (2005) R284-90. doi:10.1186/bcr993.
- [71] M.A. Musa, M.O.F. Khan, J.S. Cooperwood, Medicinal chemistry and emerging strategies applied to the development of selective estrogen receptor modulators (SERMs)., *Curr. Med. Chem.* 14 (2007) 1249–1261. doi:10.2174/092986707780598023.

- [72] Z. Desta, Comprehensive Evaluation of Tamoxifen Sequential Biotransformation by the Human Cytochrome P450 System in Vitro: Prominent Roles for CYP3A and CYP2D6, *J. Pharmacol. Exp. Ther.* 310 (2004) 1062–1075. doi:10.1124/jpet.104.065607.



CHAPTER THREE

Summary

In recent years, semiconductor quantum dots have been regarded as efficient luminescent probes and labels for numerous biological applications since they display fascinating optical and optoelectronic properties. Due to the approach used for the synthesis of QDs, they essentially have organic ligands capping some of the surface atoms. 3-mercaptopropionic acid (3-MPA) is one of the shortest chained mercapto acids and its unique reducing properties make it ideal for use in colloidal quantum dot synthesis. This chapter describes the various chemicals and analytical techniques employed, followed by a detailed experimental procedure based on the synthesis of 3-MPA-PdTeQDs. Some techniques used for QDs characterisation, such as electrochemical, microscopic and spectroscopic methods, are also stated in the chapter. Furthermore, it gives an overview on the design, preparation and application of the 3-MPA-PdTeQDs based electrochemical biosensor system for the detection of indinavir drug. This work was used as a proof of principle for the preparation of electrochemical phenotype biosensor systems.

Palladium Telluride Quantum Dots Phenotype Sensor for Indinavir

Abstract

Biosensor for the determination of indinavir (a protease inhibitor ARV drug) was developed with palladium telluride quantum dots. The biocompatibility of palladium telluride quantum dots was achieved by surface functionalisation of the quantum dots with 3-mercaptopropionic acid (3-MPA) as a capping agent, which also improved the stability and the solubility of the material. The UV-Vis spectrophotometric analysis of the quantum dots revealed a broad absorption band at ~ 320 nm (with a corresponding band gap, E_g , value of 3.87 eV), which falls within the range of values expected for quantum dots materials. FTIR and photoluminescence studies of the QDs confirmed the presence of the capping agent via the specific COOH and CH₂ signature bands; furthermore, the QDs are fluorescent and exhibited emission bands which shifted to shorter wavelengths from 510-460 nm and associated with band gap energies (2.4 eV-2.7 eV). The biosensor was prepared by the self-assembly of cysteamine on a gold electrode that was functionalised with 3-MPA-PdTeQDs, followed by cross-linking with cytochrome P450-3A4 (CYP3A4) using 1-ethyl-3-(3-dimethylaminopropyl) carbodiimide hydrochloride (EDC) and N-Hydroxysuccinimide (NHS). The characteristic properties of cyclic voltammetric reduction peak at -0.25 V was used to detect the response of the biosensor to indinavir. The developed electrochemical biosensor system exhibited high sensitivity ($0.0198 \mu\text{A/nM}$) towards indinavir and gave low limit of detection value of 0.042 mg L^{-1} . The *LOD* value is lower than indinavir's maximum steady state plasma concentration, thereby indicating that the sensing device, in principle, would be suitable for monitoring the drug in patient.

3. Introduction

The synthesis and application of water-soluble QDs have generated great interest in various fields of biology; in-bio-labelling [1], biosensing [2,3]. Compared to traditional organic fluorescent labels, QDs are known to be superior in performance due to numerous advantages such as brightness, extraordinary photostability, broad excitation wavelength range, and size-tunable narrow, symmetric emission spectra ranging from 400 to 2000 nm and multicolour light emission [4]. Their remarkable unique optical properties have inspired scientists and provided an incredible platform for researchers to investigate their applications in different fields such as electronic, molecular, and analytical chemistry. When functionalized with amphiphilic bi-functional molecules such as mercapto carboxylic acids like 3-mercaptotpropionic acid (3-MPA), which is also reported in this study, the small sizes of QDs can enhance the transfer of electrons during analysis [5]. Moreover, the functionalised QDs would open the applications of these materials including health care, biomedical and pharmaceutical industries, as well as bioanalytical chemistry [6]. In general, the issue of biocompatibility should be considered in the construction of biosensors since the biological recognition molecules used in the biosensors such as immobilized enzymes may lose their activity at biologically incompatible environments [7]. Electrochemical detection of indinavir can be improved by conjugation of suitable biomolecule into quantum dot modified electrode due to their high specificity to their target analyte [8]. Thus, in this work we focussed on the optical and electronic properties as well as the biocompatibility of 3-MPA-PdTeQDs, which is applied as an alternative functional bio-materials in the development of electrochemical phenotype biosensors for determination of protease inhibitor, indinavir drug. The development of electrochemical phenotype biosensor was achieved by the incorporating 3-MPA-PdTeQDs with cytochrome P450-3A4 (CYP3A4) enzyme on gold electrode surface for the determination of protease inhibitor-indinavir.

3.1 Experimental

3.1.1 Chemicals and sample preparation

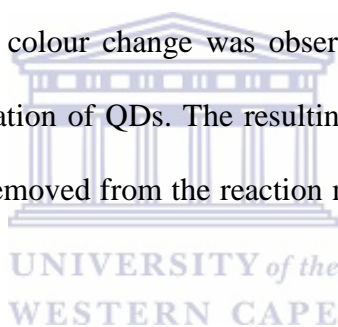
All chemicals used in the experiments were of analytical grade and were used as purchased without further purification. Palladium chloride (PdCl_2 , 99.9%), 3-mercaptopropionic acid [$\text{HSCH}_2\text{CH}_2\text{CO}_2\text{H}$] (3-MPA, $\geq 99\%$), sodium hydroxide (NaOH , $\geq 99\%$), sodium borohydride (NaBH_4 , 98%), hydrogen chloride (HCl , 37 %) 1-ethyl-3-(3-dimethylaminopropyl) carbodiimide hydrochloride (EDC), N-Hydroxysuccinimide (NHS, 98%), sodium phosphate monobasic dihydrate ($\text{H}_2\text{NaPO}_4 \cdot 2\text{H}_2\text{O}$, $> 99\%$), disodium hydrogen phosphate dibasic ($\text{Na}_2\text{PO}_4 \cdot 2\text{H}_2\text{O}$ $> 98\%$), cysteamine ($\geq 98\%$) and human cytochrome P450-3A4 enzyme (≥ 50 units/mg protein based on reductase activity) expressed in *Saccharomyces cerevisiae* were purchased from Sigma Aldrich. 0.1 M phosphate buffer solution, pH 7.4 was prepared from disodium hydrogen phosphate dibasic and sodium dihydrogen phosphate monobasic using Milli Q water purification. The preparation of indinavir solution was achieved by dissolving one capsule of Crixivan 400 mg (M.W. 711.88) purchased from Merck & Co., Inc., NJ, USA, in 0.1 M PBS, pH 7.4. The obtained solution was sonicated for 30 min and stirred at 37°C for 30 min. Clear solution of the drug was attained after filtration using polytetrafluoroethylene PTFE syringe filter of $0.3\ \mu\text{m}$ pore size (Whatman). Millipore ultrapure water (resistivity $\geq 18.2\ \text{M}\Omega\text{cm}$) was used throughout the experiments. The preparations and synthesis of the materials were performed at room temperature ($23 \pm 2^\circ\text{C}$) unless specified.

3.1.2 Instrumentation.

Electrochemical measurements were performed using a 273A Potentiostat/Galvanostat (Princeton Applied Research), wherein gold electrode, platinum wire and Ag/AgCl (3 M NaCl) acted as the working electrode, the counter electrode and the reference electrode, respectively. Cyclic voltammetry (CV) experiments were performed over a potential range of +1.5 V to -1.5 V and scan rate of 500 mV/s. Ultraviolet-visible (UV-Vis) absorption measurements for the prepared PdTeQDs were obtained using 1 cm quartz cuvette on a Nicolet Evolution 100 UV-Visible spectrophotometer (Thermo Electron, UK) over a wavelength range of 200 to 800 nm. The photoluminescence (PL) spectra were recorded using a Nanolog, Horiba NanoLog™ 3-22-TRIAX (USA), with double grating excitation and emission monochromators, plus an imaging spectrograph for a second emission channel. The excitation wavelength used was 340 nm. Fourier transform infrared (FTIR) spectra were recorded on Perkin Elmer FTIR model 100 spectrophotometer, operating between 400 and 4000 cm^{-1} in order to characterise the presence of specific features of 3-MPA on PdTeQDs surface. The high-resolution scanning electron microscopy micrographs (HRSEM) of the QDs were imaged using a Zeiss Auriga SEM operating at 50kV and high resolution-transmission electron microscope (HR-TEM) equipped with an energy-dispersed spectroscopy (EDS) detector was used to study the size and morphology of samples. Copper grid (Cu) was used as sample holder for the immobilisation of (2 μL) solution of 3-MPA-PdTeQDs and the micrographs were recorded at room temperature as presented in **Figure 9**. QDs were well distributed on the copper grid surface, confirming the nature of the zero dimensional structures.

3.1.3 Synthesis of water-soluble 3-MPA-capped PdTeQDs

3-Mercaptopropionic acid-capped palladium telluride quantum dots (3-MPA-PdTeQDs) were synthesized using a modified procedure [9]. First, palladium precursor was prepared in a three necked-round bottomed flask by dissolving PdCl₂ (0.332 g, 1.875 mmol) and 3-MPA (490 μL, 5.625 mmol) in 10 mL of deionised water, under nitrogen atmosphere and constant stirring. The pH was adjusted to 11.4 by addition of 1 M sodium hydroxide (NaOH). In another flask, tellurium precursor was prepared by mixing tellurium powder (Te) (0.319 g, 1.25 mmol) and sodium borohydride (NaBH₄) (0.189 g, 2.5 mmol) in 10 mL deionised water and covered with aluminium foil at room temperature for 30 min until the solution attained a light purple colour. Then, 5 mL of tellurium solution was injected into the nitrogen saturated palladium precursor flask and a colour change was observed from reddish to dark orange indicating the initiation of nucleation of QDs. The resulting solution was stirred and heated (100 °C) and the aliquots were removed from the reaction medium at different time intervals for the UV-Vis and PL analyses.



3.1.4 Preparation of 3-MPA-PdTeQDs/Au modified electrode

Gold disk electrode (AuE) of 3 mm in diameter was used as a working electrode for voltammetric measurements. Prior to each measurement, the AuE was first polished carefully with 1, 0.3 and 0.05 μm alumina slurries, respectively and then thoroughly rinsed with deionised water after each polishing step. Then it was successively ultrasonicated for about 10 minutes with absolute ethanol and distilled water to remove any possible absorbed alumina crystals on the AuE surface. An aliquot 4 μL of 3-MPA-PdTeQDs solution was gradually deposited by drop-casting onto the gold working electrode and allowed to dry for 12 h in the dark at 21°C.

3.1.5 Preparation of the biosensor system

The cleaning procedure for the gold disk electrode has already been described in section 3.1.4. 200 μL of 0.02 M cysteamine aqueous solution was placed on a gold electrode surface and kept in the dark for 24 h to form a monolayer. The Cyst/Au modified electrode was functionalised with a 4 μL of a solution consisting of 3-MPA-PdTeQDs in the presence of 1-ethyl-3-[3-dimethylaminopropyl] carbodiimide/N-Hydroxysuccinimide (EDC/NHS, ratio 1:1) for 12 h. The film of material on the electrode surface was rinsed with 0.1 M PBS, to remove unbound PdTe quantum dots. A 3 μL CYP450-3A4 enzyme solution (used as supplied) was then dropped onto 3-MPA-PdTeQDs/Cyst/Au modified electrode surface and allowed to dry for 3 h, at 4 $^{\circ}\text{C}$. The resulting CYP3A4/3-MPA-PdTeQDs/Cyst/Au was rinsed gently with distilled water to remove any physically adsorbed enzyme and stored at 4 $^{\circ}\text{C}$ in 0.1 M PBS when not in use.



3.2 Results and discussion

3.2.1. Crystal structure of 3-MPA-PdTeQDs

Stabilising agents play an outstanding role in particle size reduction and distribution of quantum dots [10]. In general, a capping agent that binds strongly with quantum dots surface can effectively stabilise and form smaller sizes of as-prepared quantum dots [11–13]. High-resolution TEM was mainly aimed at the determination of structural properties of the material including size, shape as well as the chemical composition and the respective ratios of the synthesised QDs. The 3-MPA-PdTeQDs micrographs observed in **Figure 9 (a)** and an insert **(b)** revealed non-agglomerated, uniformly distributed spherical structures with well-resolved lattice fringes [14–16] and are in diameter range of 3–5 nm [17]. The well resolved lattice fringes confirmed the good crystallinity of 3-MPA-PdTeQDs [18,19]. Moreover, non-agglomeration of nanoparticles resulted from electrostatic repulsion of negatively charged

dehydrogenated carboxylic groups present in 3-MPA capping agent [20,21]. The energy dispersive spectroscopy (EDS) spectrum shown in **Figure 9 (c)**, confirmed the presence of Pd, Te and S in the synthesised 3-MPA-PdTeQDs [22]. Additionally, these results were also confirmed by FTIR measurements (**Figure 12**) [20]. However, the presence of Cu was attributed to the copper grid used during sample preparation. The obtained results are similar to the previous reports performed in our lab by various authors using different QDs capped with 3-mercaptopropionic acid. For instance, Ndangili and co-workers [3] reported 3-MPA-ZnSeQDs which revealed crystallinity and poly-dispersed QDs with average size 4 nm in diameter.

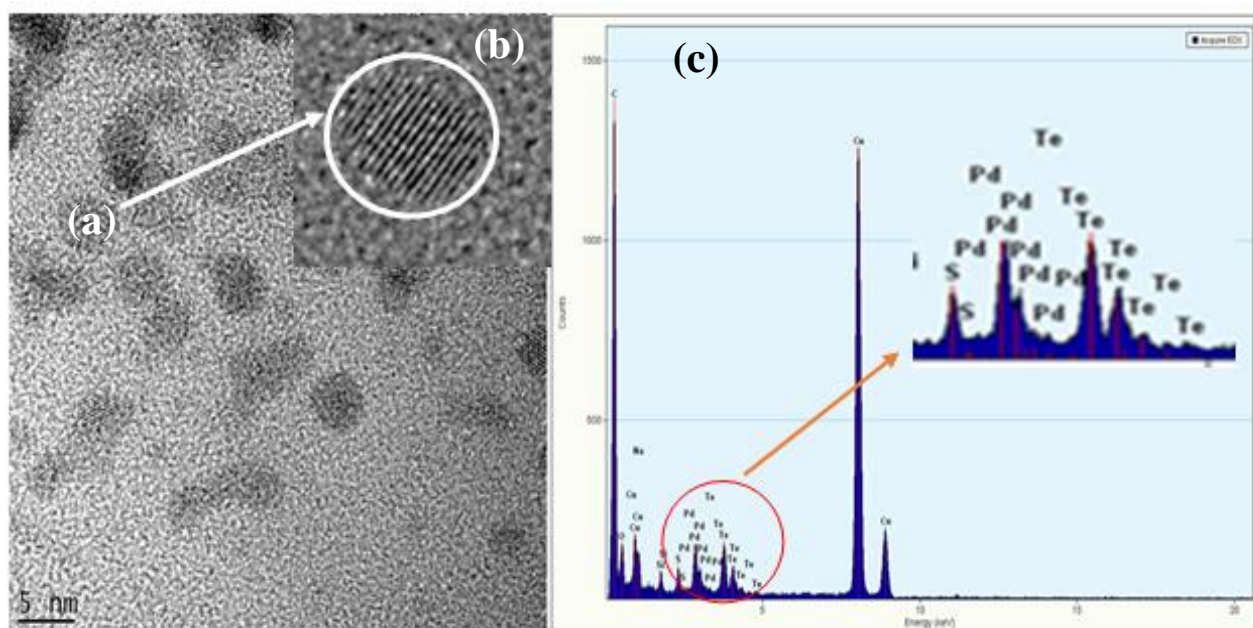


Figure 9: HR-TEM micrographs of (a) 3-MPA-PdTeQDs, (b) inserted (zoomed) region 3-MPA-PdTeQDs at 5 nm scale view. (c) HR-TEM-EDS spectrum of 3-MPA-PdTeQDs revealing chemical composition.

3.2.2 Morphological properties of 3-MPA-PdTeQDs

The HR-SEM micrograph shown in **Figure 10(A)** provided morphological and compositional information of the 3-MPA-PdTeQDs. As shown in **Figure 10(A)**, the 3-MPA-PdTeQDs exhibited agglomerated spherical bubbles with collection of different sizes approximately 200 nm [23]. The observed agglomeration was attributed to a small volume of stabilizing agent used during the synthesis which caused an increase in the surface area to volume ratio and hence increased the attractive forces between the nanoparticles thereby causing them to agglomerate [24]. This observation was further confirmed by energy –dispersive X-ray spectroscopy EDX in **Figure 10(B)**, which revealed the presence of Pd, Te and S in PdTeQDs sample which are the main components of the as-prepared material. These results are in good agreement with results obtained in **Figure 9(c)**.

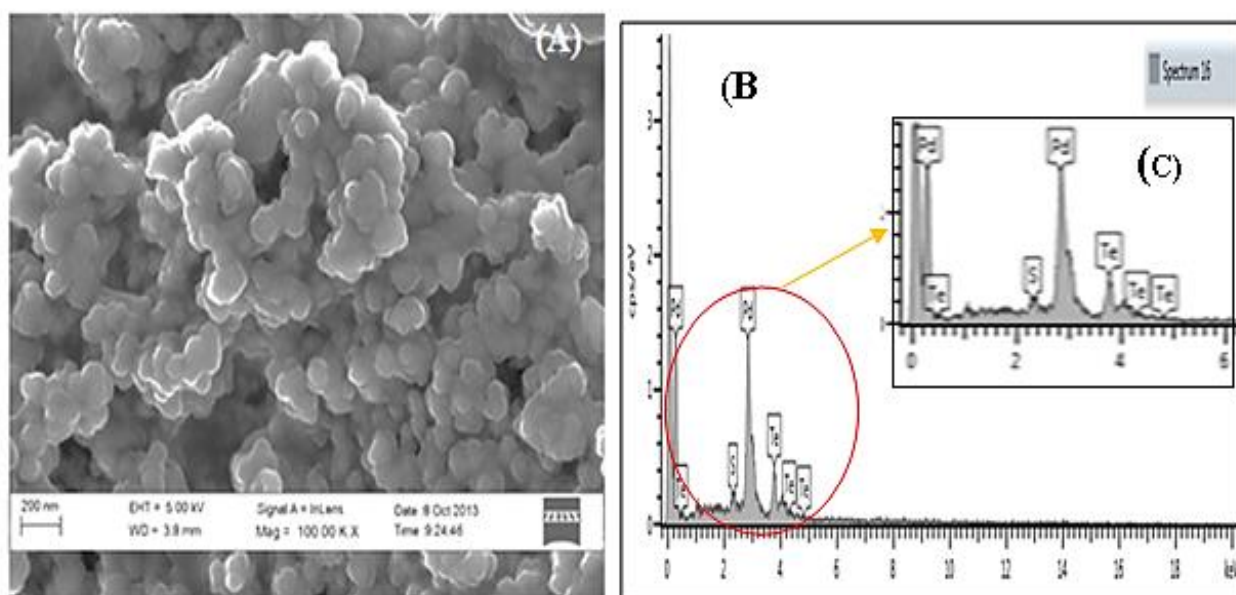


Figure 10 (A): HR-SEM micrograph of 3-MPA-PdTeQDs. (B) HR-SEM-EDX spectrum of 3-MPA-PdTeQDs and an insert region (C) reveal elemental composition of a selected region.

3.2.3 Optical properties of 3-MPA-PdTeQDs

Palladium telluride quantum dots (PdTeQDs) have unique optical, electrical and thermal properties and are being incorporated into various electrochemical biosensors [18]. The UV-Vis and PL analysis were carried out to investigate the absorption, emission and excitation wavelength of 3-MPA-PdTeQDs. The UV-Vis spectrum showing the optical properties of PdTeQDs is illustrated in **Figure 11 A**. Three absorbance bands are observed at 240 nm, 275 nm and 320 nm, respectively. The first absorbance band appearing at higher energy (240 nm) was attributed to the metal-to-ligand charge transfer (MLCT) while the absorbance band at 275 nm was ascribed to $n \rightarrow \sigma^*$ transitions of thiol groups on the 3-MPA [25]. PdTeQDs exhibited a broad absorbance band at 320 which is associated with energy band gap of 3.87 eV (within the E_g value for QDs particles), that confirmed the successful synthesis of the QDs. Due to the broad absorbance band of PdTe QDs distribution, the band gap difference between different sizes of the QDs would be wider and hence result in an improvement of the confinement of electrons and holes [26]. However, the absorption band around 410 nm due to the absorption of Pd(II) ions was not observed (**Figure 11A**), which is an evidence that Pd(II) ions, which were present in PdCl₂, were reduced to Pd⁰ [27].

Fluorescence spectroscopy is a powerful tool in biological research which relies greatly on the availability of sensitive fluorescent probes [28]. The normalized PL spectra for the five aliquots taken during synthesis are shown in **Figure 11 B**. The residual blue shift in emission bands seen around 510–460 nm associated with band gap energies (2.4 eV–2.7 eV) were attributed to the surface defects upon passivation of 3-MPA and PdTeQDs [29]. Additionally, this blue shift of fluorescence emission bands over refluxing period provided an evidence for the occurrence of the band-gap broadening phenomenon due to the quantum size effect which

confirmed the successful coating of the PdTe core [30]. Furthermore, the broad emission peaks observed indicated that the 3-MPA-PdTeQDs have broad dispersity which is in accordance with the information obtained from the absorption spectra of these QDs (**Figure 11A**).

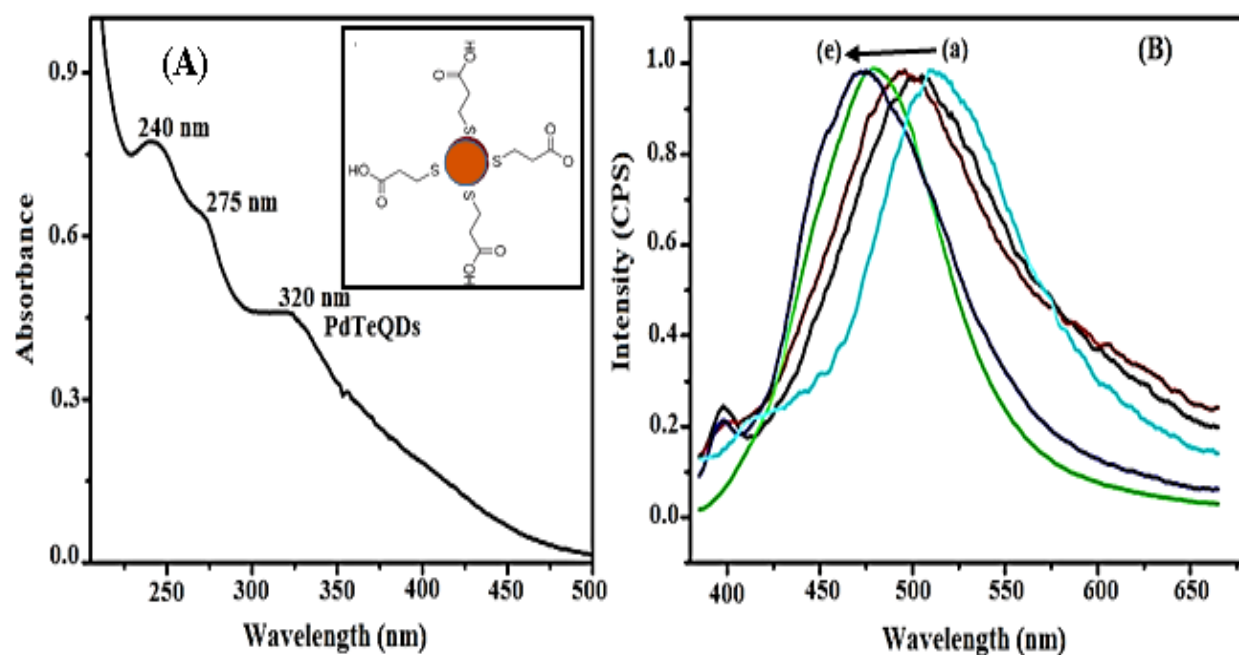


Figure 11: (A) UV-Vis spectrum of 3-MPA-PdTeQDs in the region of 200-800 nm in 0.1 M PBS, (pH 7.4) and (B) Normalized PL spectra of 3-MPA-PdTeQDs recorded at different refluxing times for (a) 20 min, (b) 30 min, (c) 40 min, (d) 50 min, (e) 60 min, respectively.

3.2.4 Structural properties of 3-MPA-PdTeQDs

Further characterisation by FTIR was performed to evaluate structural properties of 3-MPA-PdTeQDs. The FTIR spectral data acquisition was evaluated between 500 cm^{-1} and 4000 cm^{-1} . The IR spectra presented in **Figure 12(a)** revealed three distinct absorption bands at 1650 cm^{-1} , 2550 cm^{-1} and 1502 cm^{-1} , respectively. The exhibited absorption bands are characteristic features of 3-MPA capping and are attributed to (vibration of carboxylic group)

C=O stretch, S-H stretch of the thiol group and CH₂ resulting from the carbon chain of 3-MPA capping ligand [31]. The typical absorption band observed around 3250 cm⁻¹ was ascribed to the stretching and in plane bending vibration of O-H [32]. However, the disappearance of S-H stretch and a decrease in C=O stretch confirmed the formation of S-PdTe bonds between 3-MPA and PdTe core [33] as indicated in **Figure 12(b)**.

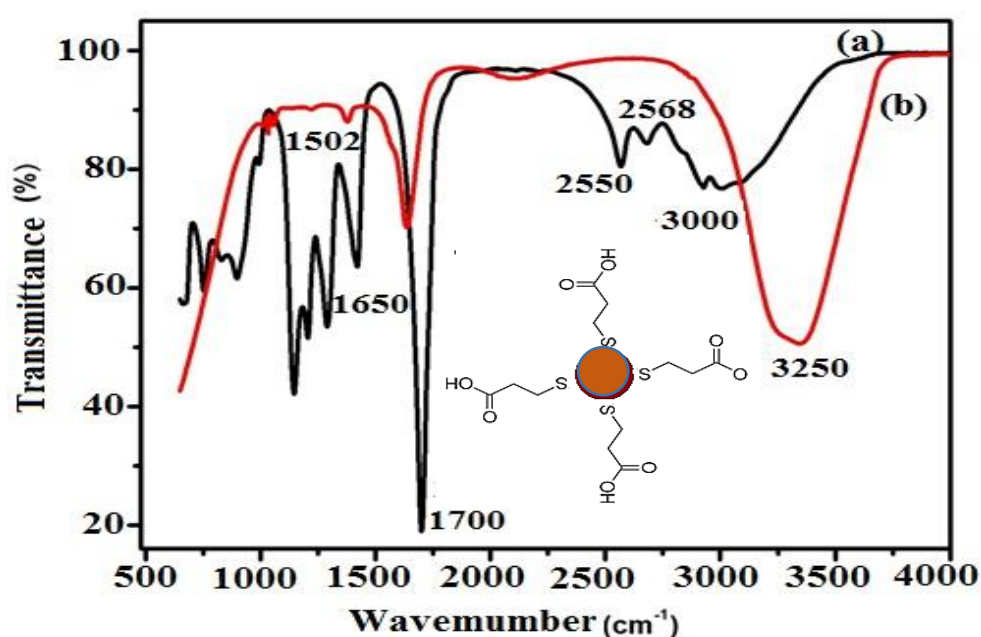


Figure 12: FT-IR spectra of (a) 3-MPA capping agent and (b) 3-MPA-PdTe QDs.

3.3 Electrochemical properties of the biosensor materials

3.3.1 Electrochemistry of 3-MPA-PdTeQDs

The electrocatalytic properties of 3-MPA-PdTeQDs modified electrode and bare Au electrode were studied by cyclic voltammetry (CV). For the bare electrode (**Figure 13B**), the voltammetric response revealed one cathodic peak at $E_{Pc} = 0.46$ V and interestingly one anodic peak around $E_{Pa} = 0.83$ V, which reflected the reduction and subsequent oxidation of the gold oxide [34]. When 3-MPA-PdTeQDs were deposited on a gold electrode surface, a

distinctive number of cathodic peaks were observed $E_{pc} = 0.12$ V (peak A₁), -0.05 V (peak A₂), -0.252 V (peak A₃), -0.75 V (peak A₄) and -1.1 V (peak A₅) (**Figure 13, black line**) while three distinct anodic peaks appeared at {1.2 V (peak C₁), 0.45 V (peak C₂) and -0.33 V (peak C₃)}, respectively. For peak (A₁), the observed cathodic peak was attributed to Te⁴⁺ ions generated from QDs oxidation. Additionally, the observed cathodic peak (A₂) corresponded to the reduction of Te⁴⁺ to Te⁰ while the cathodic peak (A₃) was responsible for further reduction of Te⁰ to Te²⁻ [35]. In contrast, peak (A₂) appeared at higher current than (A₃), thus indicating that both A₂ and A₃ are associated with the reduction of metallic oxidation of the QDs. A characteristic cathodic peak (A₄) observed at about -0.75 V, was most likely associated with the reduction of the PdTeQDs. Literature suggested that the QDs size along with the nature of the capping agent and pH of the electrolyte solution can influence the electrochemistry of the as-prepared QDs material. It should be noted that the observed anodic peaks (C₁) and (C₂) were attributed to Pd²⁺ ions generated from the oxidation of PdTeQDs and the interaction between the metal-to-ligand charge transfer i.e. (PdCl₂-3-MPA) [36], however, the observed anodic peak (C₃) corresponded to the oxidation of PdTeQDs. The obtained results are in good agreement with the obtained UV-Vis results.

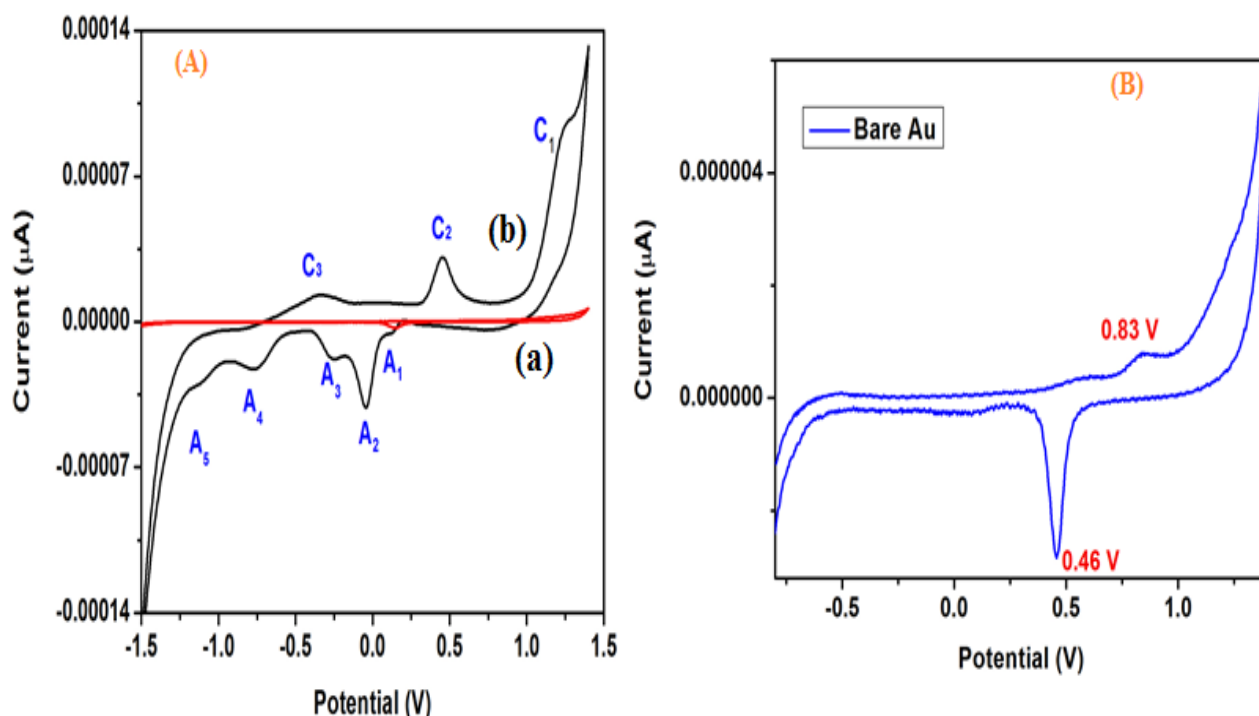
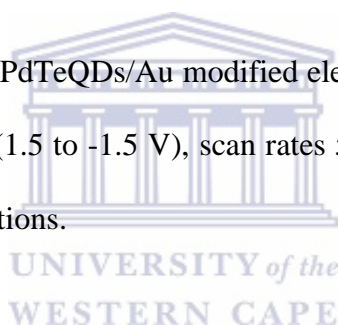


Figure 13: CVs of A(b) 3-MPA-PdTeQDs/Au modified electrode and (B) Bare Au electrode measured at a potential window (1.5 to -1.5 V), scan rates 5-21 mV/s in 0.1 M PBS, pH 7.4, performed under anaerobic conditions.



3.3.2 Biosensor responses to indinavir drug

Figure 14 (A) shows the cyclic voltammetric responses of the biosensor under aerobic conditions, in the presence and absence of indinavir. The aerobic conditions in the reaction was necessary for the monooxygenation reaction to form Fe-O centre [37]. The voltammograms showed that as the potential was scanned from +1.5 V to -1.5 V, the cathodic peak currents steadily increased to a maximum value until the saturation point was reached. As can be seen, the CV responses of the biosensor system in the absence of indinavir consisted of reduction and oxidation waves, with cathodic peaks and anodic peaks, at potential values of (-0.25 V, -0.5 V, -0.75 V and 0.25 V -1.1V) and (0.25 V and 0.5 V), respectively. When different concentrations of indinavir were added, a remarkable

enhancement of the cathodic peak currents and slight shifts were obtained in the presence of oxygen binding to the active site of the (HEME) group of the enzyme [38]. This characteristic process has been documented in literature reports about biosensor studies with P450 [39]. Compared to other reduction peaks, the major cathodic peak considered for indinavir responses appeared at -0.25 V. It is known that the binding of substrates to the ferric CYP (Fe^{III}) changes the spin state from low spin to high spin and makes the redox potential of the enzyme shift towards more positive potentials, thus promoting the electron transfer to and from the electrode system [40,41]. In addition, the CYP3A4-IDV binding at -0.25 V boosted the reduction of CYP to its ferrous form, resulting in a faster oxygen binding. Therefore, the observed characteristic features of the modified electrode offer enormous promise for its sensing applications. The calibration curve drawn from linear regression is shown in **Figure 14 (B)** which exhibited a dynamic linear range (DLR) of 0.001-0.009 nM and the biosensor's sensitivity was determined to be 0.0198 $\mu\text{A}/\text{nM}$. The very low concentration of indinavir tested (0.042 mg L^{-1}) is lower than the median value (10 ng/mL) of the maximum plasma concentration (C_{max}), normally measured 8 h after drug intake. This indicates that the developed biosensor system is suitable for measuring the low concentrations of indinavir and can be customised for higher concentrations.

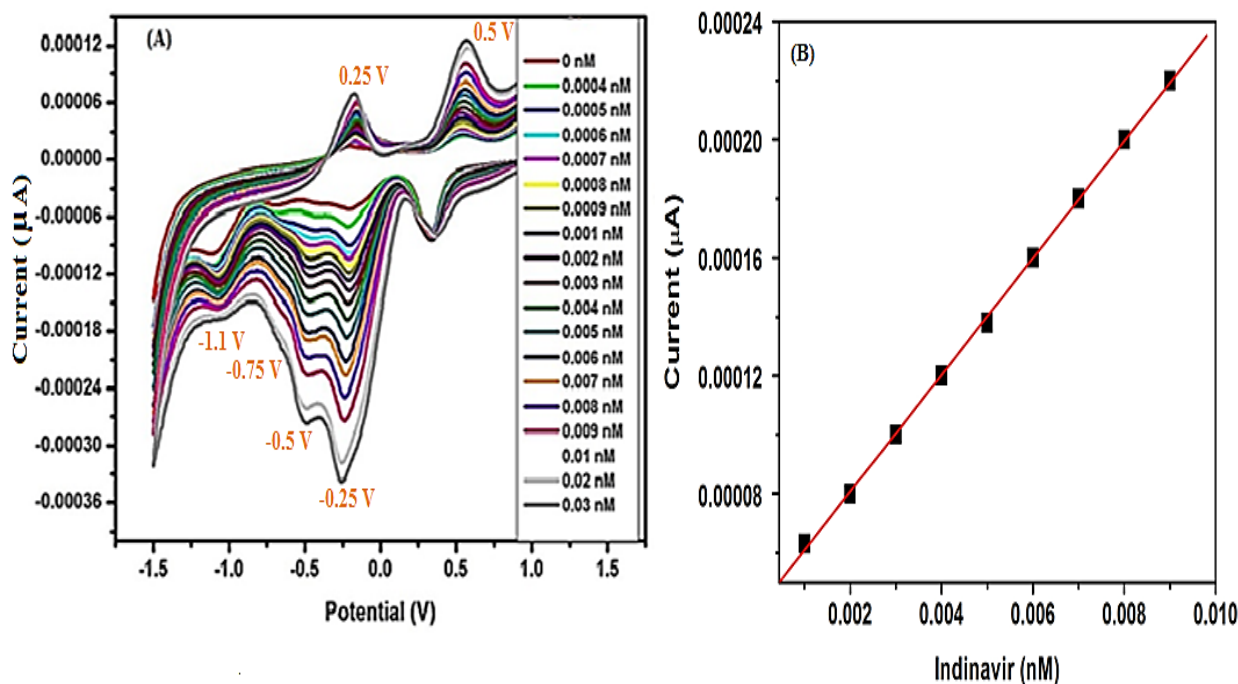
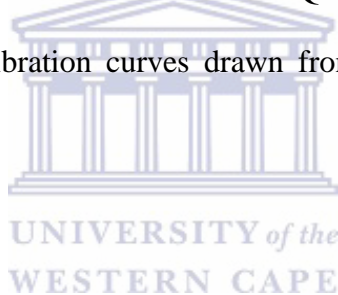


Figure 14: (A) CV responses of CYP3A4/3-MPA-PdTe QDs/Cyst/Au to indinavir in 0.1 PBS (pH 7.4) at 500 mV/s. (B) Calibration curves drawn from linear region of the biosensor system.



3.4 Conclusion

A highly sensitive, selective and producible electrochemical biosensor system based on the combination of 3-MPA-PdTeQDs and CYP3A4 was characterised by a low detection potential of -0.25 V. HR-TEM and HR-SEM studies revealed that the PdTeQDs are spherical in shape with average diameter of 3-5 nm. UV-Vis spectrophotometer, PL and FTIR analysis confirmed the biocompatibility, stability and semiconductivity of 3-MPA-PdTeQDs. The obtained biosensor platform served as an appropriate host for enzyme immobilization for the development of a user-friendly and inexpensive biosensor for Indinavir. Calibration curve drawn from linear region was used to determine the sensitivity ($0.0198 \mu\text{A}/\text{nM}$), dynamic linear range DLR (0.001 nM-0.009 nM) and detection limit (0.042 mg L^{-1}) of the biosensor system. From these results, we can conclude that biosensor construction method developed in

this study possesses excellent acceptable stability and good reliability. Additionally, this indicates that CYP450-based biosensor systems represent a powerful nanotechnology suitable for determining indinavir drug and may be used to develop point-of care and low cost devices for personalized therapy.



References

- [1] M.A. Walling, J.A. Novak, J.R.E. Shepard, Quantum dots for live cell and in vivo imaging, *Int. J. Mol. Sci.* 10 (2009) 441–491. doi:10.3390/ijms10020441.
- [2] L. Hui, Synthesis and Characterization of Aqueous Quantum Dots for Biomedical Applications, *Quantum.* (2008) 1–194. doi:10.1590/S1517-70762007000400005.
- [3] P.M. Ndangili, O.A. Arotiba, P.G.L. Baker, E.I. Iwuoha, A potential masking approach in the detection of dopamine on 3-mercaptopropionic acid capped ZnSe quantum dots modified gold electrode in the presence of interferences, *J. Electroanal. Chem.* 643 (2010) 77–81. doi:10.1016/j.jelechem.2010.03.006.
- [4] I.L. Medintz, H.T. Uyeda, E.R. Goldman, H. Mattoussi, Quantum dot bioconjugates for imaging, labelling and sensing, *Nat. Mater.* 4 (2005) 435–446. doi:10.1038/nmat1390.
- [5] H. Yang, J. Nkeze, R.Y. Zhao, Effects of HIV-1 protease on cellular functions and their potential applications in antiretroviral therapy, *Cell Biosci.* 2 (2012) 32. doi:10.1186/2045-3701-2-32.
- [6] V. Tozzi, Pharmacogenetics of antiretrovirals, *Antiviral Res.* 85 (2010) 190–200. doi:10.1016/j.antiviral.2009.09.001.
- [7] D. Grieshaber, R. MacKenzie, J. Vörös, E. Reimhult, Electrochemical Biosensors - Sensor Principles and Architectures, *Sensors.* 8 (2008) 1400–1458. doi:10.3390/s8031400.
- [8] J. Li, D. Wu, Z. Miao, Y. Zhang, Preparation of quantum dot bioconjugates and their applications in bio-imaging., *Curr. Pharm. Biotechnol.* 11 (2010) 662–671. doi:10.2174/138920110792246582.

- [9] E. Ying, D. Li, S. Guo, S. Dong, J. Wang, Synthesis and bio-imaging application of highly luminescent mercaptosuccinic acid-coated CdTe nanocrystals, PLoS One. 3 (2008). doi:10.1371/journal.pone.0002222.
- [10] Z. Li, J. Gao, X. Xing, S. Wu, S. Shuang, C. Dong, M.C. Paau, M.M.F. Choi, Synthesis and Characterization of n -Alkylamine-Stabilized Palladium Nanoparticles for Electrochemical Oxidation of Methane, J. Phys. Chem. C. 114 (2010) 723–733. doi:10.1021/jp907745v.
- [11] D.Q. Yang, S. Sun, J.P. Dodelet, E. Sacher, A facile route for the self-organized high-density decoration of Pt nanoparticles on carbon nanotubes, J. Phys. Chem. C. 112 (2008) 11717–11721. doi:10.1021/jp802371p.
- [12] R.W. Raut, A.S.M. Haroon, Y.S. Malghe, B.T. Nikam, S.B. Kashid, Rapid biosynthesis of platinum and palladium metal nanoparticles using root extract of asparagus racemosus Linn, Adv. Mater. Lett. 4 (2013) 650–654. doi:10.5185/amlett.2012.11470.
- [13] J. Chen, M. Wang, B. Liu, Z. Fan, K. Cui, Y. Kuang, Platinum catalysts prepared with functional carbon nanotube defects and Its improved catalytic performance for methanol oxidation, J. Phys. Chem. B. 110 (2006) 11775–11779. doi:10.1021/jp061045a.
- [14] J. Duan, L. Song, J. Zhan, One-pot synthesis of highly luminescent CdTe quantum dots by microwave irradiation reduction and their Hg²⁺-sensitive properties, Nano Res. 2 (2009) 61–68. doi:10.1007/s12274-009-9004-0.
- [15] N.A. Hamizi, M.R. Johan, Synthesis and size dependent optical studies in CdSe quantum dots via inverse micelle technique, Mater. Chem. Phys. 124 (2010) 395–398. doi:10.1016/j.matchemphys.2010.06.053.

- [16] T. Van Tam, N.B. Trung, H.R. Kim, J.S. Chung, W.M. Choi, One-pot synthesis of N-doped graphene quantum dots as a fluorescent sensing platform for Fe³⁺ ions detection, *Sensors Actuators, B Chem.* 202 (2014) 568–573. doi:10.1016/j.snb.2014.05.045.
- [17] P. Singh, D. Das, A. Kumar, A.K. Singh, Palladium(II) complexes of N - { 2- (aryltelluro) ethyl } morpholine / piperidine : Synthesis , structure , application in Heck coupling and unprecedented conversion into nano-sized PdTe, *INOCHE.* 15 (2012) 163–166. doi:10.1016/j.inoche.2011.10.015.
- [18] X. Chen, L. Li, Y. Lai, J. Yan, Y. Tang, X. Wang, Microwave-assisted synthesis of glutathione-capped CdTe/CdSe near-infrared quantum dots for cell imaging, *Int. J. Mol. Sci.* 16 (2015) 11500–11508. doi:10.3390/ijms160511500.
- [19] X. Mai, Q. Hoang, The Large-Scale Synthesis of Vinyl-Functionalized Silicon Quantum Dot and Its Application in Miniemulsion Polymerization, 2016 (2016).
- [20] J. Khatei, K.S.R. Koteswara Rao, Hydrothermal synthesis of CdTe QDs: Their luminescence quenching in the presence of bio-molecules and observation of bistable memory effect in CdTe QD/PEDOT:PSS heterostructure, *Mater. Chem. Phys.* 130 (2011) 159–164. doi:10.1016/j.matchemphys.2011.06.023.
- [21] B. Hou, Y. Cho, B.S. Kim, J. Hong, J.B. Park, S.J. Ahn, J.I. Sohn, S. Cha, J.M. Kim, Highly Monodispersed PbS Quantum Dots for Outstanding Cascaded-Junction Solar Cells, *ACS Energy Lett.* 1 (2016) 834–839. doi:10.1021/acsenergylett.6b00294.
- [22] Y. Zhao, X. Yang, J. Tian, F. Wang, L. Zhan, Methanol electro-oxidation on Ni@Pd core-shell nanoparticles supported on multi-walled carbon nanotubes in alkaline media, *Int. J. Hydrogen Energy.* 35 (2010) 3249–3257. doi:10.1016/j.ijhydene.2010.01.112.

- [23] B. Liu, T. Ren, J.R. Zhang, H.Y. Chen, J.J. Zhu, C. Burda, Spectroelectrochemistry of hollow spherical CdSe quantum dot assemblies in water, *Electrochem. Commun.* 9 (2007) 551–557. doi:10.1016/j.elecom.2006.10.030.
- [24] W. Wu, Q. He, C. Jiang, Magnetic iron oxide nanoparticles: Synthesis and surface functionalization strategies, *Nanoscale Res. Lett.* 3 (2008) 397–415. doi:10.1007/s11671-008-9174-9.
- [25] M.S.. P. Bharara Sean; Atwood, David A., Solution behavior of Hg(II)-cystamine by Uv-Vis and Hg NMR, *Main Gr. Chem.* 4 (2005) 217–225. doi:10.1080/10241220600595450.
- [26] J.M. Pietryga, Y.S. Park, J. Lim, A.F. Fidler, W.K. Bae, S. Brovelli, V.I. Klimov, Spectroscopic and device aspects of nanocrystal quantum dots, *Chem. Rev.* 116 (2016) 10513–10622. doi:10.1021/acs.chemrev.6b00169.
- [27] M.R. Shaik, Z.J.Q. Ali, M. Khan, M. Kuniyil, M.E. Assal, H.Z. Alkhatlan, A. Al-Warthan, M.R.H. Siddiqui, M. Khan, S.F. Adil, Green Synthesis and Characterization of Palladium Nanoparticles Using *Origanum vulgare* L. Extract and Their Catalytic Activity., *Molecules.* 22 (2017) 165. doi:10.3390/molecules22010165.
- [28] M.F. Frasco, N. Chaniotakis, Semiconductor quantum dots in chemical sensors and biosensors, *Sensors.* 9 (2009) 7266–7286. doi:10.3390/s90907266.
- [29] A. Kiplagat, N.R.S. Sibuyi, M.O. Onani, M. Meyer, A.M. Madiehe, The cytotoxicity studies of water-soluble InP/ZnSe quantum dots, *J. Nanoparticle Res.* 18 (2016) 1–12. doi:10.1007/s11051-016-3455-5.
- [30] B. Gao, C. Shen, Y. Yang, S. Yuan, G. Chen, Green synthesized CdSe quantum dots capped by 3-mercaptopropionic acid sensitized solar cells, in: *Springer Proc. Phys.*,

2014: pp. 9–17. doi:10.1007/978-3-319-05521-3_2.

- [31] R. Song, Y. Liu, L. He, Synthesis and characterization of mercaptoacetic acid-modified ZnO nanoparticles, *Solid State Sci.* 10 (2008) 1563–1567. doi:10.1016/j.solidstatesciences.2008.02.006.
- [32] Z. Xu, J. Yu, G. Liu, Fabrication of carbon quantum dots and their application for efficient detecting Ru(bpy)₃²⁺ in the solution, *Sensors Actuators, B Chem.* 181 (2013) 209–214. doi:10.1016/j.snb.2013.01.043.
- [33] V. Pilla, S.R. De Lima, A.A. Andrade, A.C.A. Silva, N.O. Dantas, Fluorescence quantum efficiency of CdSe/CdS magic-sized quantum dots functionalized with carboxyl or hydroxyl groups, *Chem. Phys. Lett.* 580 (2013) 130–134. doi:10.1016/j.cplett.2013.07.007.
- [34] S. Y. Rhiu, V. Reipa, Tuning the Size of Gold Nanoparticles with Repetitive Oxidation-reduction Cycles, *Am. J. Nanomater.* 3 (2015) 15–21. doi:10.12691/ajn-3-1-2.
- [35] S. Khene, S. Moeno, T. Nyokong, Voltammetry and electrochemical impedance spectroscopy of gold electrodes modified with CdTe quantum dots and their conjugates with nickel tetraamino phthalocyanine, *Polyhedron.* 30 (2011) 2162–2170. doi:10.1016/j.poly.2011.06.002.
- [36] S.K. Poznyak, N.P. Osipovich, A. Shavel, D. V. Talapin, M. Gao, A. Eychmüller, N. Gaponik, Size-dependent electrochemical behavior of thiol-capped CdTe nanocrystals in aqueous solution, *J. Phys. Chem. B.* 109 (2005) 1094–1100. doi:10.1021/jp0460801.
- [37] E.I. Iwuoha, S. Joseph, Z. Zhang, M.R. Smyth, U. Fuhr, P.R. Ortiz De Montellano,

- Drug metabolism biosensors: Electrochemical reactivities of cytochrome P450(cam) immobilised in synthetic vesicular systems, *J. Pharm. Biomed. Anal.* 17 (1998) 1101–1110. doi:10.1016/S0731-7085(98)00076-4.
- [38] N. Ross, N. Hendricks-Leukes, R.F. Ajayi, P. Baker, E.I. Iwuoha, Conductive Composite Biosensor System for Electrochemical Indinavir Drug Detection, *J. Chem.* 2015 (2015). doi:10.1155/2015/630408.
- [39] C. Baj-Rossi, G. de Micheli, S. Carrara, Electrochemical detection of anti-breast-cancer agents in Human Serum by Cytochrome P450-coated Carbon nanotubes, *Sensors (Switzerland)*. 12 (2012) 6520–6537. doi:10.3390/s120506520.
- [40] K.P. Conner, A.M. Schimpf, A.A. Cruce, K.J. McLean, A.W. Munro, D.J. Frank, M.D. Krzyaniak, P. Ortiz De Montellano, M.K. Bowman, W.M. Atkins, Strength of axial water ligation in substrate-free cytochrome P450s is isoform dependent, *Biochemistry*. 53 (2014) 1428–1434. doi:10.1021/bi401547j.
- [41] J. Belcher, K.J. McLean, S. Matthews, L.S. Woodward, K. Fisher, S.E.J. Rigby, D.R. Nelson, D. Potts, M.T. Baynham, D.A. Parker, D. Leys, A.W. Munro, Structure and biochemical properties of the alkene producing cytochrome p450 OleTJE (CYP15211) from the jeotgalicoccus sp. 8456 bacterium, *J. Biol. Chem.* 289 (2014) 6535–6550. doi:10.1074/jbc.M113.527325.

CHAPTER FOUR

Summary

Over the past few years, there has been an expanded interest in the use of enzyme-based electrochemical biosensors since the attraction has focussed on enzyme electrodes regarding their massive potential for applications in many areas ranging from health care, food safety and environmental monitoring. A rather limited number of enzymes were preferred for the monitoring of clinical metabolites particularly from the group of cytochrome P450 enzymes and oxidases. However, the ongoing research in this field is still focused on the improvement of sensor properties by new sensing approaches. Additionally, the sensitivity and complete performance of enzymatic biosensors has improved enormously because of incorporating nanomaterials such as quantum dots in their fabrication. Hence in this chapter we describe the method of biosensor fabrication by immobilization of cytochrome P450-3A4 enzyme onto TGA-PdTeQDs modified gold electrode. The developed electrochemical biosensor and its individual components were characterized using electrochemical (CV), spectroscopic (UV, and FTIR) and microscopic (HR-SEM) techniques, respectively.

Biocompatible Thioglycolic Acid-Palladium Telluride Quantum Dots- Based Indinavir Sensor

Abstract

An electrochemical drug metabolism biosensor system comprised of cytochrome P450-3A4 (CYP3A4) enzyme and thioglycolic acid capped palladium telluride quantum dots (TGA-PdTeQDs) on a gold disk electrode was developed for the determination of indinavir, a protease inhibitor antiretroviral drug. Optical properties of the novel TGA-PdTeQDs were confirmed by UV-Vis spectrophotometry which produced an absorption band at ~320 nm that corresponded to energy band gap values of 3 eV. Furthermore, the FTIR studies revealed a successful incorporation of thioglycolic acid into PdTe surface due to the disappearance of -SH stretch from PdTeQDs spectra. The electrocatalytic properties of electrochemical biosensor system was studied by cyclic voltammetry (CV) for which the characteristic reduction peak at -0.9 V was used to detect the response of the biosensor to indinavir. The biosensor system was very sensitive towards indinavir and gave sensitivity value of 1.18 $\mu\text{A/nM}$ and low limit of detection (LOD) value of 0.09 mg L^{-1} . The obtained detection limit is well below the plasma concentration (C_{max}) of indinavir (8 h after intake) which range from 0.13 to 8.6 mg L^{-1} .

4. Introduction

Cytochrome P450 enzymes (CYP450s) comprise a super-family of enzymes that play an important role in metabolism of a diverse range of xenobiotics, including therapeutic drugs and countless toxins as well as carcinogens and synthesis of steroid hormones [1–3]. As a member of CYP family, cytochrome P450-3A4 (CYP3A4) is regarded to be a major form of P450 expressed in human liver since it metabolises the majority of therapeutic drugs and was employed in this study for metabolism of a protease inhibitor antiretroviral drug, indinavir [4,5]. The characteristics of this isoform have attracted the field of pharmacology and virology for study of newly developed drugs and their monitorisation [6,7]. Literature suggests that the expression of each CYP is normally influenced by exclusive combination of factors including genetic polymorphisms, induction by xenobiotics, regulation by cytokines, hormones and during disease states, as well as sex, age, and others [8]. However, in the process of drug metabolism which is mainly mediated by CYPs, the interactions between drug-drug and drug-food can result into major effect such as toxicities and lead to specific pharmacogenetic phenotype characteristics termed as poor, intermediate, extensive, and ultrarapid metabolizers [9,10]. Therefore, the characterisation of CYP450 enzymes remains the major issue in pharmacokinetic and toxicokinetic metabolic pathways. Several studies have been conducted to explore the drug metabolic pathway by introducing different systems including biocatalytic systems, electrochemically driven enzymatic system, electrochemical oxidation systems, and other types of in vitro systems [11,12]. Over the past few years, the attention has been focussed on CYP450 enzymes for the development of bioelectrodes for both analytical and bioelectrocatalytic purposes [13,14]. In this case, the use of appropriate biosensor systems would be a good alternative since they are generally of small size, capable of continuous measurements and can measure analytes faster at a very low cost compared to traditional methods. Remarkable achievements in drug metabolism field can be attributed to

applications of QDs since they possess specific features such as, high reactivity, ease of dispersability and good biocompatibility and therefore have great potential applications in biosensors and biomedicine. Previous studies from our lab based on CYP3A4 drug metabolism biosensor systems have been reported. For instance, Nxusani and co-workers [15] and Ignaszak and co-workers [16] employed CYP3A4 enzyme (isoform known to metabolise about 34% of therapeutic drugs which are currently on the market) in conjunction with QDs for the determination of drug metabolite 17 β -estradiol and a protease inhibitor antiretroviral drug, indinavir. This chapter highlight an approach for the determination of indinavir drug using the combination of novel thioglycolic acid-capped palladium telluride quantum dots (TGA-PdTeQDs) and CYP3A4 modified gold electrode system.

4.1 Experimental

4.1.1 Chemicals and sample preparation

All chemicals used in the experiments were of analytical grade and were used as purchased without further purification. Palladium chloride (PdCl₂, 99.9%), thioglycolic acid [HSCH₂CO₂H] (TGA, \geq 99%), sodium hydroxide (NaOH, \geq 99%), sodium borohydride (NaBH₄, 98%), hydrogen chloride (HCl, 37 %) 1-ethyl-3-(3-dimethylaminopropyl) carbodiimide hydrochloride (EDC), N-Hydroxysuccinimide (NHS, 98%), sodium phosphate monobasic dihydrate (H₂NaPO₄·2H₂O, > 99%), disodium hydrogen phosphate dibasic (Na₂PO₄·2H₂O > 98%), cysteamine (\geq 98%) and human cytochrome P450-3A4 enzyme (\geq 50 units/mg protein based on reductase activity) expressed in *Saccharomyces cerevisiae* were purchased from Sigma Aldrich. 0.1 M phosphate buffer solution, pH 7.4 was prepared from disodium hydrogen phosphate dibasic and sodium dihydrogen phosphate monobasic using Milli Q water purification. The preparation of indinavir solution was achieved by dissolving one capsule of Crixivan 400 mg (indinavir sulfate, M.W. 711.88) purchased from Merck &

Co., Inc., NJ, USA, in 0.1 M PBS, pH 7.4. The obtained solution was sonicated for 30 min and stirred at 37 °C for 30 min. Undissolved components were removed by filtering the formed suspension through a Whatman polytetrafluoroethylene (PTFE) syringe filter (pore size 0.3 µm) into a clean storage bottle. The solution was used as stock indinavir solution from which all the other working solutions were prepared using appropriate dilutions with 0.1 M phosphate buffer solution (PBS). Millipore ultrapure water (resistivity $\geq 18.2 \text{ M}\Omega\text{cm}$) was used throughout the experiments.

4.1.2 Instrumentation

Voltammetric experiments were carried out using a Model 273 A Potentiostat/Galvanostat system guarded by the software Model 270/250 (both from EG&G Princeton Applied Research Corporation, USA). A conventional three-electrode system was used with modified gold disk electrode (3 mm diameter) as the working electrode, a platinum wire as the counter electrode, and Ag/AgCl (3 M NaCl) as a reference electrode. To evaluate the electrocatalytic behaviour of the biosensor materials on gold electrode, the cyclic voltammetric experiments were performed in 0.1 M PBS over a potential range of +1.5 V to -1.5 V at a scan rate of 500 mV/s. The morphological evaluation of the biosensor materials including TGA-PdTeQDs, Cyst, and CYP3A4 respectively, was carried out by a high resolution-scanning electron microscopy (HRSEM) (Carl Zeiss Auriga-SEM) system with a Gemini-column and an EDAX EDX-detector operated at 20 kV using various magnifications. Ultraviolet-visible (UV-Vis) absorption measurements for the prepared PdTeQDs were obtained using 1 cm quartz cuvette on a Nicolet Evolution 100 UV-Visible spectrophotometer (Thermo Electron, UK) over a wavelength range of 200 to 800 nm. The photoluminescence (PL) spectra were recorded using a Nanolog, Horiba NanoLog™ 3-22-TRIAX (USA), with double grating excitation and emission monochromators, plus an imaging spectrograph for a second

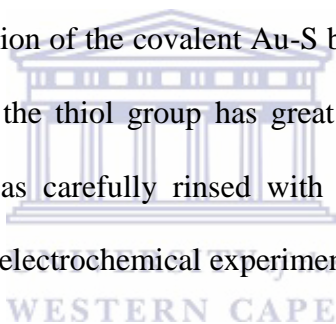
emission channel and excitation wavelength used was 360 nm. Fourier transform infrared (FTIR) spectra were recorded on Perkin Elmer FTIR model 100 spectrophotometer, operating between 4000 and 400 cm^{-1} .

4.1.3 Synthesis of water-soluble TGA-PdTeQDs

Using a bottom-up approach, colloidal TGA-PdTeQDs were prepared according to method described by Zhang and co-workers [17], with some modifications. In a typical synthesis, PdCl_2 (0.332 g, 1.875 mmol) and thioglycolic acid (TGA) (392 μL , 5.625 mmol) were dissolved in 10 mL of deionised water in a three-neck round bottomed flask, followed by adjustment of the pH to (11.2-11.8) by addition of 5 M NaOH solution. The mixture was stirred and bubbled by N_2 gas for 30 min. Then, a freshly prepared NaHTe solution was prepared by mixing tellurium powder (0.254 g, 1.25 mmol) and NaBH_4 (0.151 g, 2.5 mmol) in 10 mL deionised water and heated to 80 $^\circ\text{C}$ for 30 min until the solution attained a light purple colour. In the synthesis of the PdTeQDs, the molar ratio of Pd^{2+} /TGA/Te used was 1.5:3:1. Then, 5 mL of NaHTe solution was injected onto (PdCl_2 and TGA) solution and a colour changed was observed from reddish to orange then greenish colour after some time. After injection, the resulting solution was refluxed at 100 $^\circ\text{C}$ and aliquot portions were collected at defined time intervals for PL measurements. The reaction was quenched by immediately washing the QDs several times with ice cold distilled water, followed by centrifugation to remove any excess starting material. The supernatant was discarded, and the precipitate was re-dispersed in distilled water and stored in the fridge for further use.

4.1.4 Preparation of cysteamine monolayer onto the gold electrode surface

A gold disk electrode of 3 mm diameter used for the experiments was polished carefully with alumina slurry (1 μm , 0.3 μm down to 0.05 μm) respectively, on a polishing cloth and rinsed repeatedly with water to obtain a mirror like surface. The electrode was then subjected to ultrasonic vibration in both absolute ethanol and Milli-Q water to remove residual alumina particles that might be trapped at the surface. The cleanliness of the bare electrode surface was achieved by depositing it in 0.5 M H_2SO_4 and scanning the potential between 0.0 and 1.5 V (vs. Ag/AgCl wire) at a scan rate of 50 mV/s until a reproducible scan was obtained. The Cyst/Au modified electrode was formed by incubating the cleaned Au electrode into 200 μL of 0.02 M cysteamine aqueous solution at room temperature in darkness for 24 h [18]. Gold surfaces are susceptible to formation of the covalent Au-S bond with thiol (S-H) group of the cysteamine monolayers because the thiol group has great affinity for gold metal surfaces. Then, the modified electrode was carefully rinsed with water to remove any physically adsorbed Cyst before conducting electrochemical experiment.



4.1.5 Preparation of the biosensor system

Cysteamine was used as a linking agent for biosensor preparation by forming a monolayer of the linker on the surface of the 0.021 cm^2 gold electrode due to gold-sulphur interaction. The cysteamine-functionalised Au electrode (Cyst/Au) was activated by dipping it into a solution containing EDC and NHS in a ratio 1:1 for 30 min, followed by the drop-casting of 4 μL of TGA-PdTeQDs aqueous solution and keeping it to cure for 12 h affording TGA-PdTeQDs/Cyst/Au electrode [19]. 3 μL of 100 pmol/ μL CYP3A4 enzyme sample (i.e. 300 pmol CYP3A4) was then drop-casted onto the TGA-PdTeQDs/Cyst/Au electrode surface and incubated at 4 $^\circ\text{C}$ for 3 h, allowing the protein to be homogeneously adsorbed onto the TGA-PdTeQDs/Cyst/Au modified electrode. The resulting CYP3A4/TGA-PdTeQDs/Cyst/Au

bioelectrode (biosensor) was rinsed gently with distilled to remove any physically adsorbed enzyme and was kept at 4 °C in 0.1 M PBS, pH 7.4 when not in use.

4.2 Results and discussion

4.2.1 Optical properties of TGA-PdTeQDs

Figure 15 A shows the UV-Vis spectra of TGA-PdTeQDs which revealed three absorbance bands at 245 nm, 320 nm and 410 nm, respectively. The band appearing at 245 nm was attributed to the ligand-to-metal charge transfer i.e. the interaction between thioglycolic acid (TGA) which acts as a stabilizing agent for QDs and palladium (II) ions [20]. In addition, TGA is regarded as one of the most commonly used capping agent for aqueous synthesis of QDs since it binds strongly to the surface of QDs and improves the charge transport [21–23]. Interestingly, palladium telluride quantum dots exhibited a broad absorption band at 320 nm associated with energy band gap of 3 eV. Moreover, the absorbance band appearing at 410 nm corresponded to Pd (II) ions present in the reaction mixture [24].

The major key parameters to be considered during the colloidal QDs synthesis include reaction temperature and time. A longer refluxing time usually shifts the excitonic absorption and PL emission peaks to longer wavelengths indicating the growth of nanocrystals [25].

Figure 15 B revealed absorption characteristics of TGA-PdTeQDs under the excitation wavelength (360 nm). The observed broad emission bands from 411-421 nm revealed an obvious red shift with increasing reaction time leading to quantum confinement size effect [26]. This effect allows the tuning of the energy-band gap with changes in quantum dots size. Moreover, the broad emission bands indicated that the TGA-PdTeQDs have broad dispersity which is in accordance with the information obtained from the absorption spectra of these QDs. Furthermore, the dissolution of the small quantum dots and size increment of the larger

ones indicated that TGA-PdTeQDs colloidal quantum dots experience typical Ostwald ripening [27]. The band gap energies calculated for TGA-PdTeQDs were found to be 2.95 eV for fluorescence and 3 eV for UV-Vis, respectively. The values obtained from the two techniques are significantly comparable and confirmed that the TGA-PdTeQDs are more electrically conductive (semiconductor).

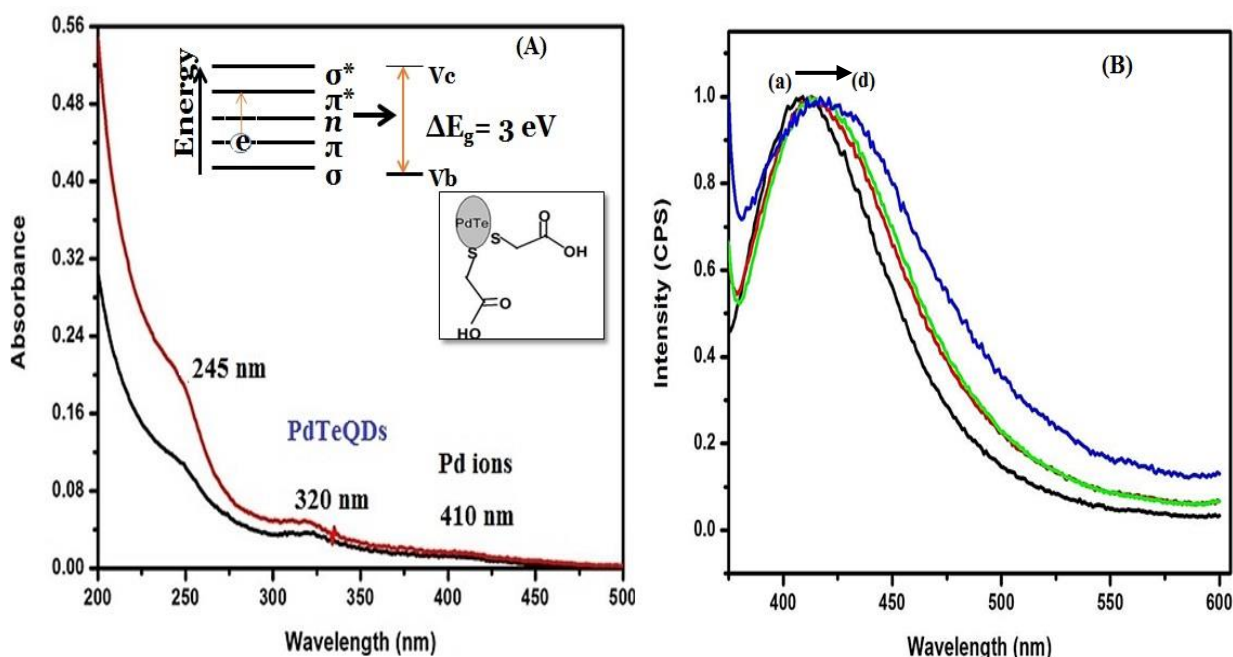
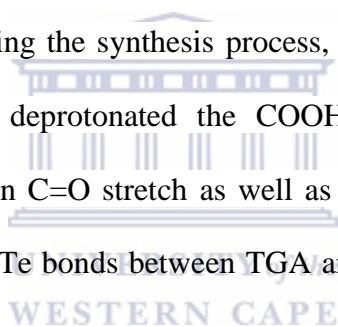


Figure 15: (A) UV-Vis of TGA-PdTeQDs in the region of 200-800 nm in 0.1 M PBS (pH 7.4) and (B) normalized PL for TGA-PdTeQDs excited at 360 nm for (a, black line) 30 min, (b, red line) 40 min, (c, green line) 50 min and (d, blue line) 60 min, respectively.

4.2.2 Structural properties of TGA-PdTeQDs

FTIR spectroscopy was employed to investigate the characteristic features of organic capping agent adsorbed onto the surface of synthesized PdTeQDs. It was expected that the thiol group (-SH) of the thioglycolic acid which is hydrophilic would covalently bind with the

hydrophobic surface of the quantum dot while the carboxylic acid group (-COOH) extends water molecule to make the quantum dot soluble and can be conjugated with bioagents, enabling their application in biosensor fabrication [28]. **Figure 16** represents the FT-IR spectra of (a) TGA (black line) and (b) TGA-PdTeQDs (red line). The spectrum of TGA exhibited five absorption bands at $\sim 2950\text{ cm}^{-1}$, 2550 cm^{-1} , 1660 cm^{-1} , 1402 cm^{-1} and 1213 cm^{-1} , respectively and were attributed to an O-H stretch (which confirmed the good dispersion of the quantum dots in water and other biological media), S-H stretch, C=O stretch, which represents the carboxyl group and existence asymmetric stretching of C-H [29,30]. In contrast, the spectra of the capped PdTeQDs sample displayed absorption bands assigned to the carboxylate anion of the surface ligands. The presence of the carboxylate anion in the QDs developed during the synthesis process, which employed NaOH to adjust the pH to 11.5 and therefore deprotonated the COOH group. However, the shift in wavenumbers and the decrease in C=O stretch as well as the disappearance of S-H stretch confirmed the formation of S-PdTe bonds between TGA and PdTe core [31] as indicated in **Figure 16 (b)**.



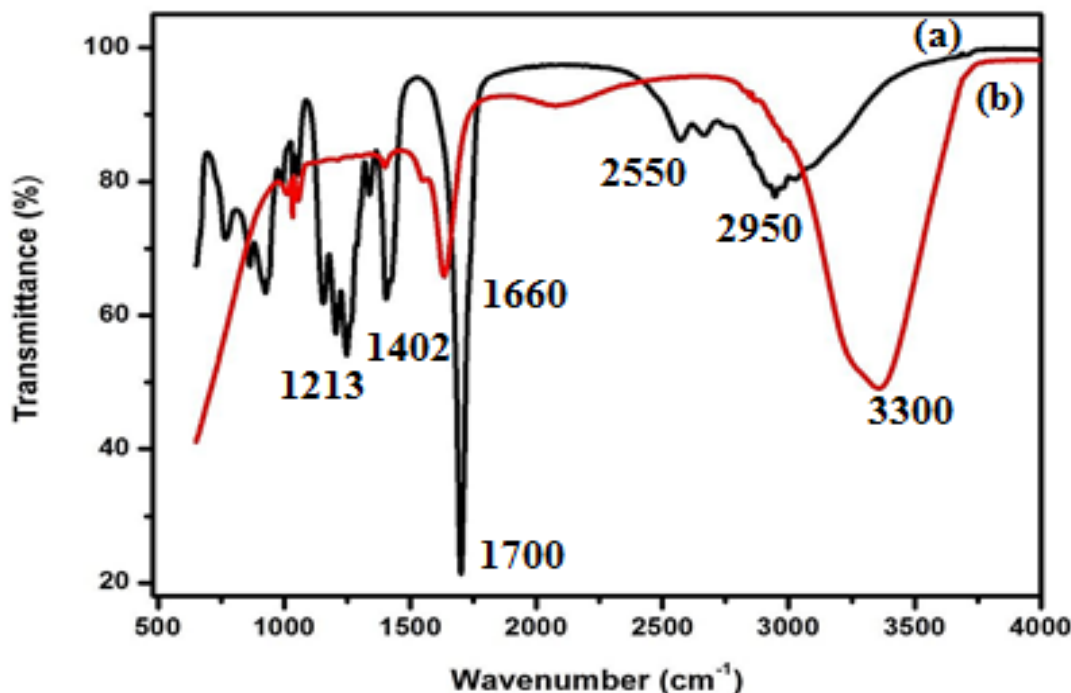


Figure 16: FTIR spectra for (a) TGA capping agent and (b) TGA-PdTeQDs.

4.3 Electrochemistry of the biosensor platform

4.3.1 Electrochemistry of cysteamine and TGA-PdTeQDs on gold electrode

The catalytic properties of TGA-PdTeQDs and Cyst modified electrodes were studied by cyclic voltammetry (CV). **Figure 17A** shows cyclic voltammograms of bare AuE (black line) and Cyst/Au (red line) modified electrode. For the bare electrode, anodic and cathodic peaks emerged at $E_{Pa} = (0.88 \text{ V}, 1.5 \mu\text{A})$ and $E_{Pc} = (0.49 \text{ V}, 7.1 \mu\text{A})$, respectively. The observed peaks corresponded to the reduction of gold oxide and one oxidation peak attributed to the formation of gold oxide during surface oxidation [32,33]. Sulphur compounds such as thiol groups (S-H) have a strong affinity to gold surfaces and their bond strength is approximately 10 kT [34]. In comparison with bare Au, Cyst/Au modified electrode exhibited a pair of redox peaks with slight shift to more negative potential and intensification in peak current because cysteamine accelerated electron transfer rate on the electrode surface [35,36]. The anodic peak observed at $E_{Pa} = (0.77 \text{ V}, 1.65 \mu\text{A})$, was due to adsorption of the thiol group on a gold

surface while the cathodic peak appearing a $E_{pc} = (0.46 \text{ V}, 7.8 \mu\text{A})$ was ascribed to chemisorption of the thiol group [37,38]. Moreover, the background current of Cyst/Au increased greatly because cysteamine formed monolayers at gold surface. Most papers confirmed that there is a strong affinity between gold surface and sulphur atom [39] due to the existence of $-\text{SH}$ in cysteamine which can be adsorbed on the gold surface naturally [40]. Furthermore, the thiol groups are usually employed to attach molecules onto the electrode surfaces for bioanalysis and other modified surface applications such as wetting, corrosion protection and sensor development [41].

When TGA-PdTeQDs were deposited on a gold electrode surface, five reduction peaks were observed at -0.05 V (peak A₁), -0.4 V (peak A₂), -0.75 V (peak A₃), -1.1 V (peak A₄), and -1.4 V (peak A₅) with two anodic peaks which appeared at 0.4 V (peak C₁) and 1.2 V (peak C₂). The observed reduction peak at -0.05 V was attributed to the reduction of Te^{4+} to Te^0 whereas the reduction peak at -0.4 V corresponded to further reduction of Te^0 to Te^{2-} [42]. Moreover, the characteristic reduction peak obtained at -0.75 V was attributed to PdTeQDs. As can be seen in **(Figure 17 B, red line)**, the exhibited reduction peak at -1.1 V was attributed to metal to ligand electron charge transfer (i.e. palladium (II) ions and thioglycolic acid) [43], while the reduction peak at -1.4 V which appeared at more negative potential and overshadowed reduction peaks A₁ to A₄ was attributed to the reduction of Pd^{2+} to Pd^0 [44]. Furthermore, the difference between the anodic and cathodic peak potentials increases on decreasing the size of the QDs, as expected from the quantum confinement of the charges [45]. When the potential was scanned on the forward direction (positive) represented by a (blue dotted line) from -1.5 V to $+1.5 \text{ V}$, the observed anodic peak at 0.4 V was due to oxidation of TGA (S-H group) while the anodic peak observed at 1.2 V corresponded to Pd^{2+} ions which were generated from the oxidation of PdTeQDs and appeared at more positive potential. Literature suggests that the oxidation of transition metals normally occur at more

positive potentials [46]. This, therefore confirmed the proposed structure of TGA stabilizing agent on PdTeQDs with the sulphur atoms of TGA surface bound onto PdTe core [47]. The obtained results are in good agreement with FTIR results.

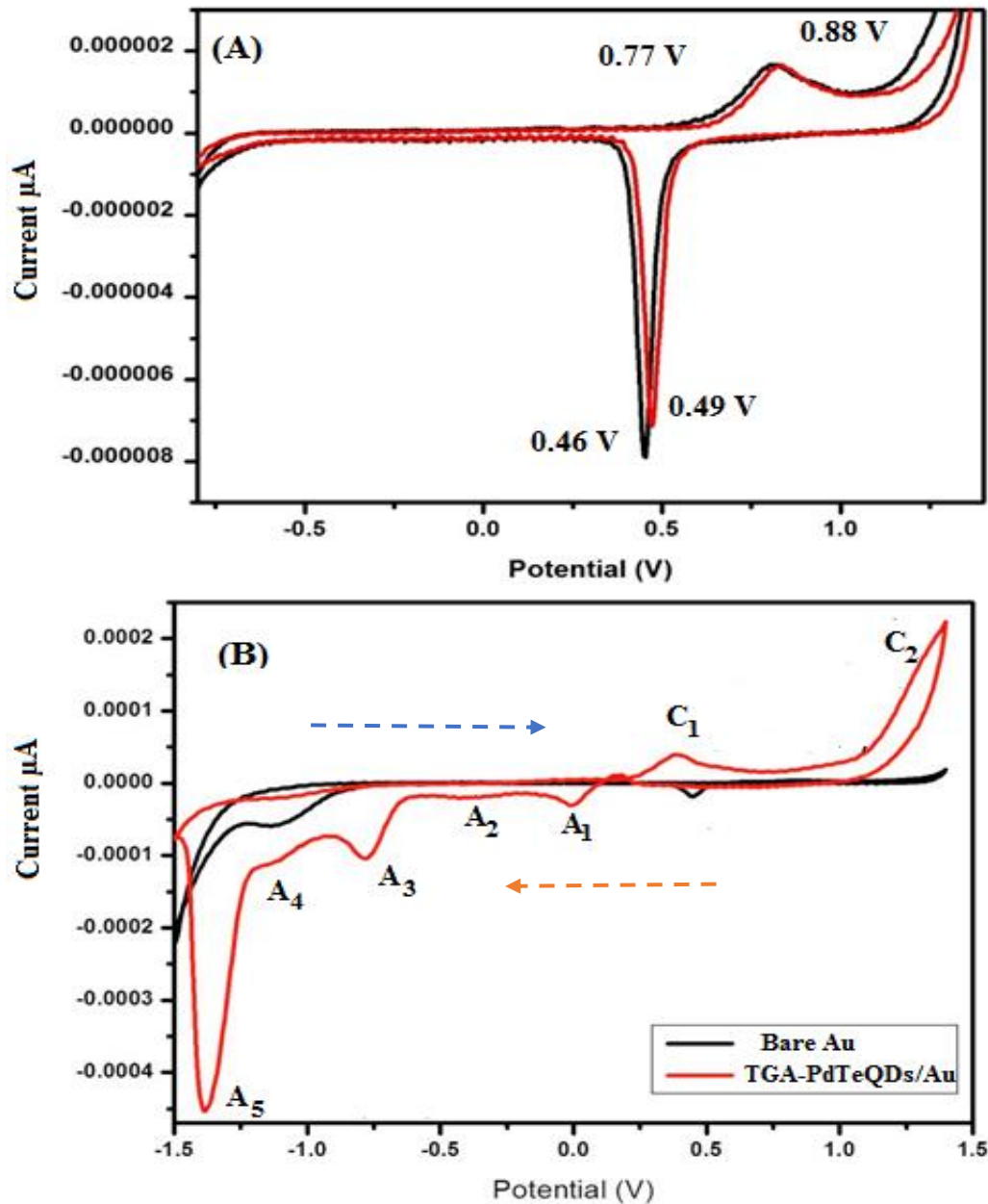


Figure 17: CVs of biosensor platform measured at a potential window (0.2 to -0.85 V) in 0.1 M BBS (pH 7.4) under anaerobic conditions for (A, red line) Bare Au and (A, black line) Cyst/Au. (B) CV measurement for (B, black line) Au and (B, red line) TGA-PdTeQDs, respectively.

4.3.2 Direct electron transfer of CYP3A4 on gold electrode

Direct electrochemistry of proteins can be employed to create a desirable model for fundamental study of the redox behaviour of the proteins in biological systems. This would give a full detailed explanation about the mechanisms of redox transformations of protein molecules as well as their metabolic processes involving redox transformations [48]. Several attempts have been made to improve the electron transfer of heme proteins by modifying electrodes with desirable matrix [49]. In addition, studies of direct electron transfer between proteins and electrodes can provide a platform for fabricating biosensors in patient tailored (personalized) medicine, enzymatic bioreactors, and biomedical devices [50]. However, adsorption of proteins directly to an electrode has proven to be very difficult and often results in denaturation of the biomaterial through the intrinsic instability of such enzymes [51,52]. Even though there are a few reports of useable biosensors, the major key parameter for a successful enzymatic biosensor assembly is the introduction of a mediator which will enhance the electrons transfer process to and from the electrode system [53]. **Figure 18 (a)** shows CV of CYP450-3A4 immobilised on the electrode surface. Two cathodic peaks were observed at -0.05 V (peak C₁) and -0.6 V (peak C₂), respectively with one anodic peak which appeared at -0.08 V (peak D₁). The observed cathodic peak at -0.05 V was attributed to the reduction of the heme group from CYP3A4 (Fe^{III}) to CYP3A4 (Fe^{II}) in the presence of oxygen [54] while the reduction peak at -0.6 V was ascribed to monooxygenation process. Moreover, the oxidation peak at -0.08 V appeared at a very high current intensity due to the re-oxidation of CYP3A4 (Fe^{II}) to CYP3A4 (Fe^{III}). The estimated potential value for the immobilized CYP3A4 enzymes is not the same as other researchers reported [55]. This may be attributed to the possible differences in the heme centre of P450 in solution and its immobilized state.

Quantum dots have been used in biochemistry to provide efficient electron transport and are suitable and stable matrix for enzyme incorporated onto gold electrode. In comparison with CYP3A4/Au, CYP3A4/TGA-PdTe/Cyst/Au exhibited three cathodic peaks at 0.3 V (peak A₁), -0.06 V (peak A₂) and -0.7 V (peak A₃) with three anodic peaks at -0.07 V (peak B₁), 0.5 V (peak B₂) and 1.1 V (peak B₃), respectively. The observed reduction peaks were attributed to the redox of the electroactive heme centre of the immobilized protein coupling between –NH₂ and –COOH of TGA-PdTeQDs acted as a mediator by shuttling electrons to and from the enzyme to speed up the reaction [50]. Such results may be ascribed to characteristic features of TGA-PdTeQDs which allow them to provide favourable microenvironment for the orientation of biomolecules [56]. An investigation regarding the direct electrochemistry of CYP3A4 using mediated films to improve the electron transfer between the heme proteins was done [57].

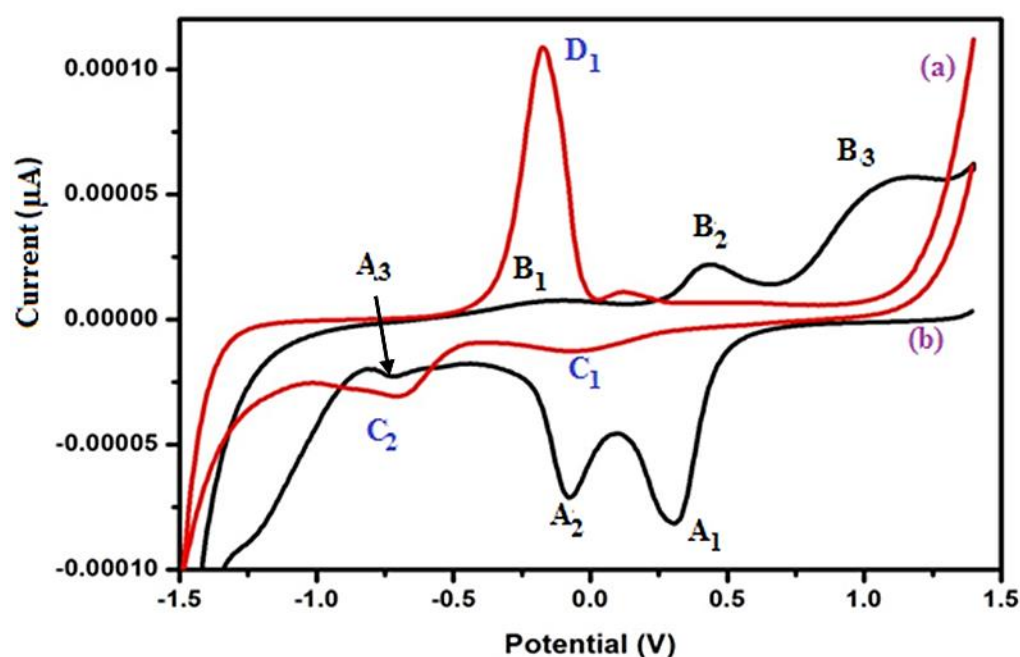


Figure 18: CVs measured at a potential window -1.5 V to +1.5 V in 0.1 M PBS at a scan rate of 500 mV/s under aerobic conditions for (a) CYP3A4/Au modified electrode and (b) CYP3A4/TGA-PdTeQDs/Cyst/Au biosensor system.

4.3.3 Electrocatalytic responses of the biosensor system

Cyclic voltammetry (CV) is regarded as one of the commonly used techniques in electrochemistry for biosensing applications. Compared to other electroanalytical techniques, CV is considered to be the most appropriate in the case of CYP450 enzymes, because of the uncertainty of CYP reduction peak potentials. **Figure 19(a)** shows the cyclic voltammetric responses of the biosensor under aerobic conditions, in the presence and absence of indinavir. The aerobic conditions in the reaction were necessary for the monooxygenation reaction (i.e. the binding of molecular oxygen (O_2) to CYP3A4 (Fe^{2+}) to form Fe-O centre in order to observe enzyme-oxygen substrate interactions. The voltammograms showed that as the potential was scanned from -1.5 V to +1.5 V, the reduction currents steadily increased to a maximum value until the saturation point was reached. About five cathodic peaks were observed at 0.9 V (peak A₁), 0.3 V (peak A₂), -0.3 V (peak A₃), -0.7 V (peak A₄) and -0.9 V (peak A₅) with interestingly four anodic peaks which appeared at -0.2 V (peak B₁), 0.25 V (peak B₂), 0.75 V (peak B₃) and 1.0 V (peak B₄). The catalytic responses were attributed to the biosensor materials present on the electrode surface with slight shifts and increasing currents. The overlapping cathodic responses observed at -0.7 V (peak A₄) and -0.9 V (peak A₅) with increasing indinavir concentrations were ascribed to the filled d-orbital of palladium, since indinavir donates electrons through nitrogen group as well as coupling of the (Fe^{III}) to (Fe^{II}) electrode process to the binding oxygen [58]. Moreover, the obtained cathodic response observed at -0.9 V was chosen as a peak of interest since it obtained much higher peak currents compared to peak A₁-A₃, which were attributed to cysteamine and QDs). The rate of this binding of oxygen increased in the presence of indinavir. Thus it would be possible to observe catalytic signal due to the coupling of the (Fe^{3+}) to (Fe^{2+}) electrode process to the binding oxygen. This binding inhibited the electrochemistry of cysteamine and TGA-PdTeQDs. **Figure 19(b)** shows the calibration plot drawn from the linear region of the

biosensor for indinavir. The biosensor's sensitivity was determined to be $1.18 \mu\text{A}/\text{nM}$, and the detection limit value of 0.09 mgL^{-1} . From in vivo studies, the maximum plasma concentration (C_{max}), of indinavir (8 h after intake) range from 0.13 to 8.6 mgL^{-1} [59]. The C_{max} values fall within the low detection limit of CYP3A4/TGA-PdTeQDs/Cyst/Au biosensor system and its dynamic linear range. This indicates that the biosensor is suitable for measuring the low concentrations of indinavir and can be customised for higher concentrations.

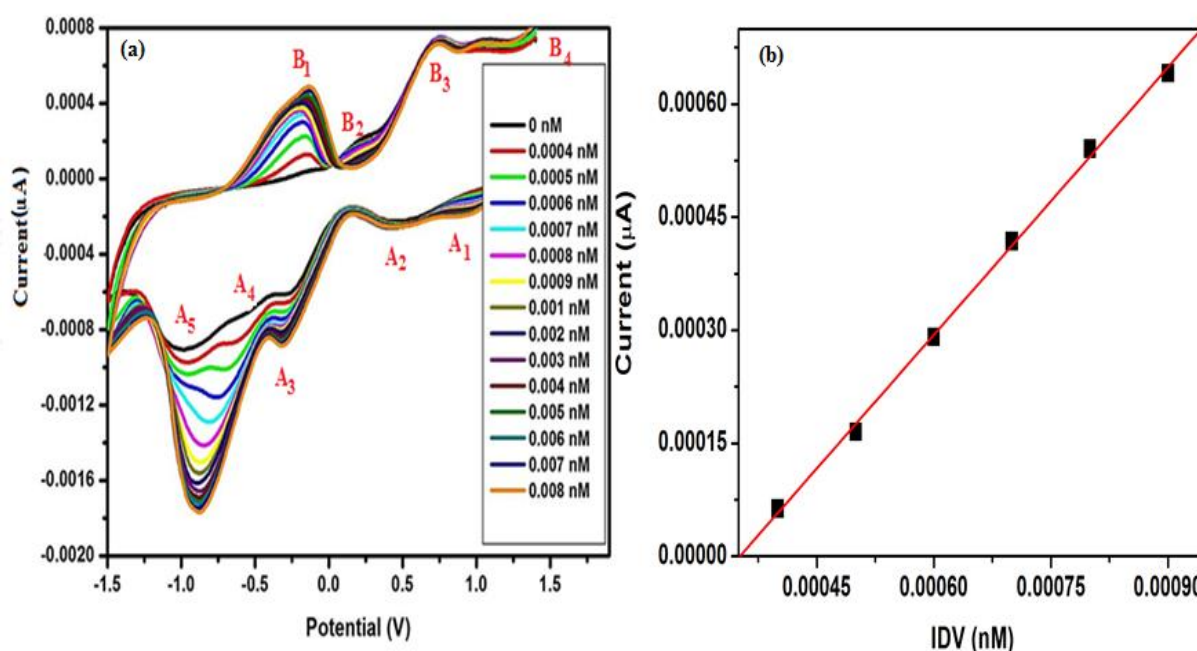


Figure 19: CVs measured at a potential window -1.5 V to $+1.5 \text{ V}$ in 0.1 M PBS at a scan rate of 500 mV/s under aerobic conditions for (a) CYP3A4/TGA-PdTeQDs/Cyst/Au modified electrode and (b) calibration curve drawn from a linear regression of the biosensor.

4.3.4 Stability of the biosensor

The stabilisation and storage of enzymes and other proteins are of great interest in several application areas where shelf life and stability during operation are required [60]. During the last few years, several studies have focused on improving the stability of enzymes for use in biosensors and bioreactors [60], because increasing the long-term stability of enzymes on the electrode may extend the lifetime of biosensors [61]. In this study, the stability and reproducibility of the biosensor was examined by leaving the electrode for hours in the fridge (4 °C) [62]. CV measurements were taken at different time intervals {i.e. initial (black line), 1 h (red line), 3 h (green line) and 7 h (blue line)} to monitor the electrocatalytic responses of the biosensor system as illustrated in **Figure 20(a)**. The magnitude of the cathodic currents observed at -0.35 V (peak A₂) and -0.9 V (peak A₃) were increasing with time whereas the anodic peak currents at -0.6 V (peak C₁) and -0.1 V (peak C₂) were unstable and unresolved which were attributed to the products of the QDs and re-oxidation of CYP3A4 (Fe^{II}) to CYP3A4 (Fe^{III}), respectively. However, the decreasing anodic peak observed at 0.7 V (peak C₃) was attributed to the adsorbed cysteamine. **Figure 20(b)** shows the calibration curve taken at a potential of -0.9 V (characteristic peak of interest) which gave a sensitivity value of 0.01 μA/h, mean value of 3.0, and standard deviation (SD) value of 0.184 and activity response of 6.1%. The loss of the activity response observed may be due to storage and changes of temperature undergone by the biosensor system hourly from the storage temperature to the working temperature [63]. However, the CYP3A4/TGA-PdTeQDs/Cyst/Au biosensor system still improved stability retaining 93% of its initial response up to 7 h. Therefore, these results indicate good reproducibility and stability of the biosensor and have proven that the biosensor can be used for several analysis without losing its activity [64].

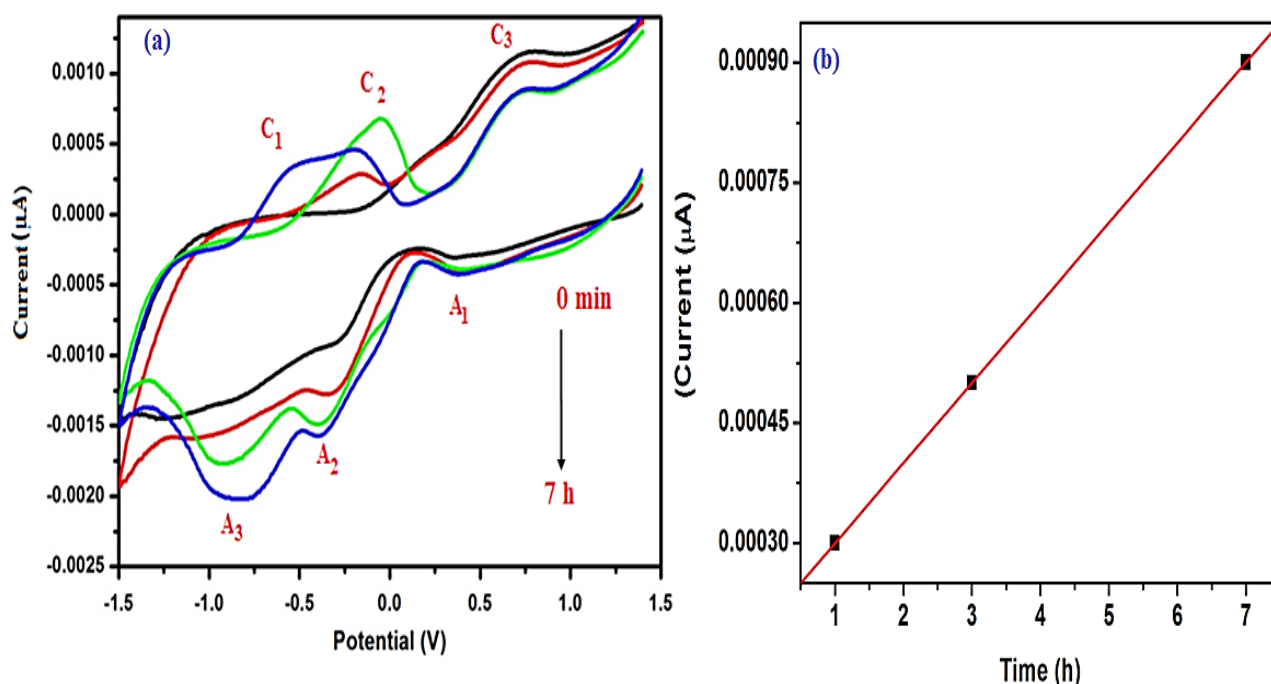
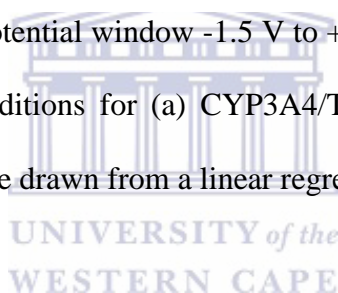


Figure 20: CVs measured at a potential window -1.5 V to +1.5 V in 0.1 M PBS at a scan rate of 500 mV/s under aerobic conditions for (a) CYP3A4/TGA-PdTeQDs/Cyst/Au modified electrode and (b) calibration curve drawn from a linear regression of the biosensor.



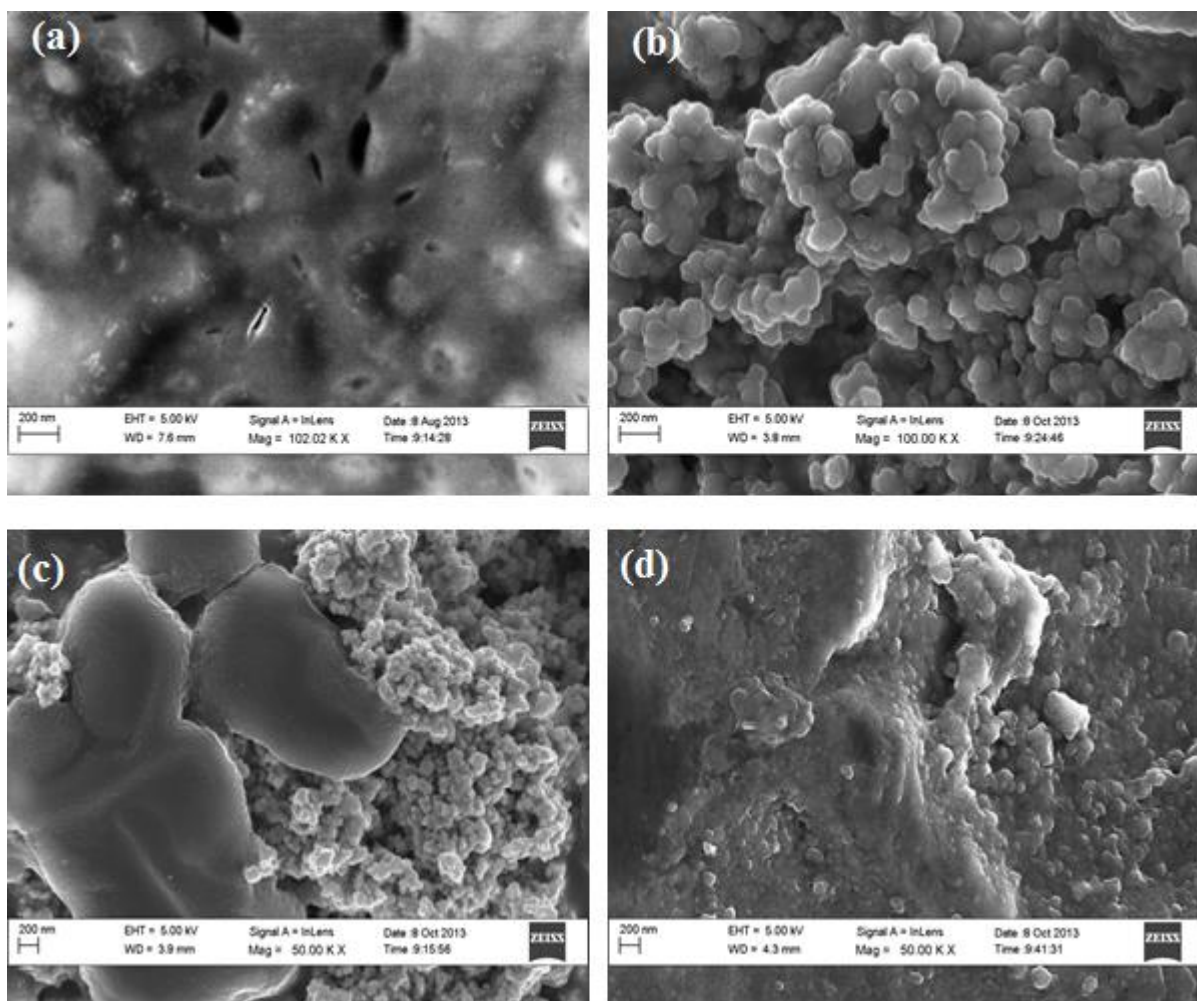
4.4 Microscopic measurements of the biosensor materials

4.4.1 Microscopic properties of the biosensor

In **Figure 21 (a-d)** the high-resolution scanning electron micrographs (HR-SEM) of the various stages of electrode modification are shown. The HR-SEM micrograph in **Figure 21(a)** shows the morphology after the immobilising 3 µL of 0.02 M cysteamine aqueous solution on aluminium stub surface. The morphology resembles a flat surface with holes onto the aluminium stub surface whereas **Figure 21(b)** revealed nonuniform and agglomerated spherical bubbles of PdTeQDs with collection of different sizes approximately 200 nm [65]. When PdTeQDs were combined with cysteamine, noticeable morphological changes were observed which revealed a big irregular shape and unreacted quantum dots, indicating a

strong interaction between amino groups of cystamine and carboxylic acid groups associated with the PdTeQDs as illustrated in **Figure 21(c)** [66]. Moreover, when CYP3A4 enzyme was added onto the QDs-Cyst surface the morphology became smoother with some unreacted PdTeQDs due to the binding of activated carboxylic group from the quantum dots and amine group of CYP3A4 enzyme, which offered a favourable orientation on the aluminium stub surface [67]. Accordingly, this proves the efficient incorporation of CYP3A4 onto QDs-cystamine on aluminium stub and these results are in good accordance with CV measurements of the biosensor system.





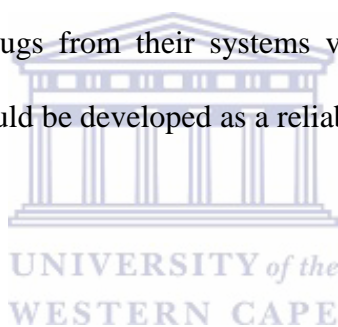
WESTERN CAPE

Figure 21: HR-SEM micrographs of (a) cysteamine, (b) TGA-PdTeQDs, (c) TGA-PdTeQDs/Cyst and (d) CYP3A4/TGA-PdTeQDs/Cyst on aluminium stub at 200 nm scale view.

4.5 Conclusion

The study demonstrated the successful synthesis and application of water-soluble and biocompatible TGA-PdTeQDs in the development of electrochemical biosensor system for indinavir detection. UV-Vis spectrometry showed a broad absorption band at 320 nm associated with a band gap of 3 eV which indicates that TGA-PdTeQDs are semi-conductive and biocompatible. The SEM images revealed a change in morphology after immobilization

of CYP3A4 which confirmed the successful fabrication of the biosensor. When PdTeQDs were immobilized on electrode together with CYP3A4, the resultant bioelectrode was shown to undergo monooxygenation which is a net reduction reaction. Moreover, the developed electrochemical biosensor system gave good stability and high reproducibility retaining 93% of its initial response up to 7 h. A calibration plot from the increasing indinavir concentrations plotted against increasing current was used to determine the sensitivity ($1.18 \mu\text{A/nM}$) and low limit of detection (LOD) (0.09 mg L^{-1}) values. The concentration range studied is much lower than the range found in clinical samples of *moderate drug metabolisers*, where the range of maximum plasma concentration (C_{max}) 8 h after drug intake is 0.13 to 8.6 mg L^{-1} . This means that the biosensor can be applied for drug detection in patients who are *ultra-rapid metabolisers* that clear drugs from their systems very quickly. Thus, there is high expectation that such a device could be developed as a reliable tool for point of care diagnosis for HIV and other diseases.



References

- [1] A.-M. Yu, K. Fukamachi, K.W. Krausz, C. Cheung, F.J. Gonzalez, Potential role for human cytochrome P450 3A4 in estradiol homeostasis., *Endocrinology*. 146 (2005) 2911–9. doi:10.1210/en.2004-1248.
- [2] D.P. Wasalathanthri, V. Mani, C.K. Tang, J.F. Rusling, Microfluidic electrochemical array for detection of reactive metabolites formed by cytochrome P450 enzymes, *Anal. Chem.* 83 (2011) 9499–9506. doi:10.1021/ac202269t.
- [3] Z. Bibi, Role of cytochrome P450 in drug interactions, *Nutr. Metab. (Lond)*. 5 (2008) 27. doi:10.1186/1743-7075-5-27.
- [4] F.J. Gonzalez, Role of gene knockout and transgenic mice in the study of xenobiotic metabolism., *Drug Metab. Rev.* 35 (2003) 319–335. doi:10.1081/DMR-120026496.
- [5] F.P. Guengerich, Cytochromes P450, drugs, and diseases., *Mol. Interv.* 3 (2003) 194–204. doi:10.1124/mi.3.4.194.
- [6] F.P. Guengerich, Cytochrome P450 and chemical toxicology, *Chem. Res. Toxicol.* 21 (2008) 70–83. doi:10.1021/tx700079z.
- [7] U.M. Zanger, M.H. Hofmann, Polymorphic cytochromes P450 CYP2B6 and CYP2D6: Recent advances on single nucleotide polymorphisms affecting splicing, *Acta Chim. Slov.* 55 (2008) 38–44.
- [8] U.M. Zanger, M. Schwab, Cytochrome P450 enzymes in drug metabolism: Regulation of gene expression, enzyme activities, and impact of genetic variation, *Pharmacol. Ther.* 138 (2013) 103–141. doi:10.1016/j.pharmthera.2012.12.007.
- [9] S. Marchetti, R. Mazzanti, J.H. Beijnen, J.H.M. Schellens, Concise Review: Clinical Relevance of Drug Drug and Herb Drug Interactions Mediated by the ABC

- Transporter ABCB1 (MDR1, P-glycoprotein), *Oncologist*. 12 (2007) 927–941. doi:10.1634/theoncologist.12-8-927.
- [10] J.A. Grabowsky, Drug Interactions and the Pharmacist: Focus on Everolimus, *Ann. Pharmacother.* 47 (2013) 1055–1063. doi:10.1345/aph.1R769.
- [11] N. Wang, C. Gao, F. Xue, Y. Han, T. Li, X. Cao, X. Zhang, Y. Zhang, Z.L. Wang, Piezotronic-effect enhanced drug metabolism and sensing on a single ZnO nanowire surface with the presence of human cytochrome P450, *ACS Nano*. 9 (2015) 3159–3168. doi:10.1021/acsnano.5b00142.
- [12] P. Nowak, M. Woźniakiewicz, P. Kościelniak, Simulation of drug metabolism, *TrAC - Trends Anal. Chem.* 59 (2014) 42–49. doi:10.1016/j.trac.2014.02.015.
- [13] A.K. Udit, M.G. Hill, H.B. Gray, Electrochemistry of cytochrome P450 BM3 in sodium dodecyl sulfate films., *Langmuir*. 22 (2006) 10854–7. doi:10.1021/la061162x.
- [14] V.E. V Ferrero, L. Andolfi, G. Di Nardo, S.J. Sadeghi, A. Fantuzzi, S. Cannistraro, G. Gilardi, Protein and electrode engineering for the covalent immobilization of P450 BMP on gold, *Anal. Chem.* 80 (2008) 8438–8446. doi:10.1021/ac8011413.
- [15] E. Nxusani, P.M. Ndangili, R. a. Olowu, a. N. Jijana, T. Waryo, N. Jahed, R.F. Ajayi, P. Baker, E.I. Iwuoha, 3-Mercaptopropionic Acid Capped Ga₂Se₃nanocrystal-CYP3A4 Biosensor for the Determination of 17-Alpha-Ethinyl Estradiol in Water, *Nano Hybrids*. 1 (2012) 1–22. doi:10.4028/www.scientific.net/NH.1.1.
- [16] A. Ignaszak, N. Hendricks, T. Waryo, E. Songa, N. Jahed, R. Ngece, A. Al-Ahmed, B. Kgarebe, P. Baker, E.I. Iwuoha, Novel therapeutic biosensor for indinavir-A protease inhibitor antiretroviral drug, *J. Pharm. Biomed. Anal.* 49 (2009) 498–501. doi:10.1016/j.jpba.2008.10.025.

- [17] F. Zhang, C. Li, X. Li, X. Wang, Q. Wan, Y. Xian, L. Jin, K. Yamamoto, ZnS quantum dots derived a reagentless uric acid biosensor, *Talanta*. 68 (2006) 1353–1358. doi:10.1016/j.talanta.2005.07.051.
- [18] S. Shahrokhian, A. Mahdavi-Shakib, M. Ghalkhani, R. sadat Saberi, Gold Electrode Modified with Self-Assembled Monolayer of Cysteamine-Functionalized MWCNT and Its Application in Simultaneous Determination of Dopamine and Uric Acid, *Electroanalysis*. 24 (2012) 425–432. doi:10.1002/elan.201100545.
- [19] N. Ul H. Alvi, V.J. Gómez, P.E.D. Soto Rodriguez, P. Kumar, S. Zaman, M. Willander, R. Nötzel, An InN/InGaN quantum dot electrochemical biosensor for clinical diagnosis, *Sensors (Basel)*. 13 (2013) 13917–13927. doi:10.3390/s131013917.
- [20] T. Teranishi, M. Miyake, Size Control of Palladium Nanoparticles and Their Crystal Structures, *Chem. Mater.* 10 (1998) 594–600. doi:10.1021/cm9705808.
- [21] J.D. Olson, G.P. Gray, S.A. Carter, Optimizing hybrid photovoltaics through annealing and ligand choice, *Sol. Energy Mater. Sol. Cells*. 93 (2009) 519–523. doi:10.1016/j.solmat.2008.11.022.
- [22] B. Sun, N.C. Greenham, Improved efficiency of photovoltaics based on CdSe nanorods and poly(3-hexylthiophene) nanofibers, *Phys. Chem. Chem. Phys.* 8 (2006) 3557. doi:10.1039/b604734n.
- [23] B. Sun, H.J. Snaith, A.S. Dhoot, S. Westenhoff, N.C. Greenham, Vertically segregated hybrid blends for photovoltaic devices with improved efficiency, *J. Appl. Phys.* 97 (2005). doi:10.1063/1.1804613.
- [24] P.A. Namini, A.A. Babaluo, B. Bayati, Palladium Nanoparticles synthesis using polymeric matrix: poly(ethyleneglycol) molecular weight and palladium concentration

- effects, *Int. J. Nanosci. Nanotechnol.* 3 (2007) 37–43. doi:10.2514/1.22095.
- [25] M. Masikini, P.M. Ndangili, C.O. Ikpo, U. Feleni, S. Duoman, U. Sidwaba, T.T. Waryo, P.G.L. Baker, E.I. Iwuoha, Optoelectronics of Stochiometrically Controlled Palladium Telluride Quantum Dots, *J. Nano Res.* 40 (2016) 29–45. doi:10.4028/www.scientific.net/JNanoR.40.29.
- [26] S.A. Ivanov, A. Piryatinski, J. Nanda, S. Tretiak, K.R. Zavadil, W.O. Wallace, D. Werder, V.I. Klimov, Type-II core/shell CdS/ZnSe nanocrystals: Synthesis, electronic structures, and spectroscopic properties, *J. Am. Chem. Soc.* 129 (2007) 11708–11719. doi:10.1021/ja068351m.
- [27] A. Arshad, R. Akram, S. Iqbal, F. Batool, B. Iqbal, B. Khalid, A.U. Khan, Aqueous synthesis of tunable fluorescent, semiconductor CuInS₂ quantum dots for bioimaging, *Arab. J. Chem.* (2016). doi:10.1016/j.arabjc.2016.10.002.
- [28] X. Mai, Q. Hoang, The Large-Scale Synthesis of Vinyl-Functionalized Silicon Quantum Dot and Its Application in Miniemulsion Polymerization, 2016 (2016).
- [29] J.K. Cooper, A.M. Franco, S. Gul, C. Corrado, J.Z. Zhang, Characterization of primary amine capped CdSe, ZnSe, and ZnS quantum dots by FT-IR: Determination of surface bonding interaction and identification of selective desorption, *Langmuir.* 27 (2011) 8486–8493. doi:10.1021/la201273x.
- [30] N.T. Vo, H.D. Ngo, N. Phuong, D. Thi, K. Phung, N. Thi, A.P. Duong, V. Lam, Stability Investigation of Ligand-Exchanged CdSe / ZnS-Y (Y = 3-Mercaptopropionic Acid or Mercaptosuccinic Acid) through Zeta Potential Measurements, 2016 (2016).
- [31] G.-X. Liang, M.-M. Gu, J.-R. Zhang, J.-J. Zhu, Preparation and bioapplication of high-quality, water-soluble, biocompatible, and near-infrared-emitting CdSeTe alloyed

- quantum dots, *Nanotechnology*. 20 (2009) 415103. doi:10.1088/0957-4484/20/41/415103.
- [32] B.E. Conway, Electrochemical At Noble Metals Oxide Film Formation As a Surface-Chemical Process, *Prog. Surf. Sci.* 49 (1995) 331–452. doi:10.1016/0079-6816(95)00040-6.
- [33] K. De Wael, A. Verstraete, S. Van Vlierberghe, W. Dejonghe, P. Dubruel, A. Adriaens, The electrochemistry of a gelatin modified gold electrode, *Int. J. Electrochem. Sci.* 6 (2011) 1810–1819.
- [34] A. Ulman, Formation and Structure of Self-Assembled Monolayers, *Chem. Rev.* 96 (1996) 1533–1554. doi:10.1021/cr9502357.
- [35] B.R. Kozub, N. V. Rees, R.G. Compton, Electrochemical determination of nitrite at a bare glassy carbon electrode; why chemically modify electrodes?, *Sensors Actuators, B Chem.* 143 (2010) 539–546. doi:10.1016/j.snb.2009.09.065.
- [36] A. ??zer, ??ener Sa??lam, Z. Can, E. Er??a??, R. Apak, Electrochemical determination of food preservativenitrite with gold nanoparticles/p-aminothiophenol-modified gold electrode, *Int. J. Mol. Sci.* 17 (2016). doi:10.3390/ijms17081253.
- [37] T. Łuczak, Gold Electrodes Modified with Self-Assembled Layers Made of Sulphur Compounds and Gold Nanoparticles Used for Selective Electrocatalytic Oxidation of Catecholamine in the Presence of Interfering Ascorbic and Uric Acids, *Int. J. Electrochem.* 2011 (2011) 1–10. doi:10.4061/2011/179474.
- [38] Q. Cheng, A. Brajter-Toth, Selectivity and sensitivity of self-assembled thioctic acid electrodes, *Anal. Chem.* 64 (1992) 1998–2000. doi:10.1021/ac00041a041.
- [39] L.H. Wang, W.S. Huang, Electrochemical oxidation of cysteine at a film gold

- modified carbon fiber microelectrode its application in a flow-through voltammetric sensor, *Sensors*. 12 (2012) 3562–3577. doi:10.3390/s120303562.
- [40] A.I. Gopalan, K.P. Lee, K.M. Manesh, P. Santhosh, J.H. Kim, Gold nanoparticles dispersed into poly(aminothiophenol) as a novel electrocatalyst-Fabrication of modified electrode and evaluation of electrocatalytic activities for dioxygen reduction, *J. Mol. Catal. A Chem.* 256 (2006) 335–345. doi:10.1016/j.molcata.2006.05.027.
- [41] A. Manickam, C.A. Johnson, S. Kavusi, A. Hassibi, Interface design for CMOS-integrated Electrochemical Impedance Spectroscopy (EIS) biosensors, *Sensors (Switzerland)*. 12 (2012) 14467–14488. doi:10.3390/s121114467.
- [42] S.K. Poznyak, N.P. Osipovich, A. Shavel, D. V. Talapin, M. Gao, A. Eychmüller, N. Gaponik, Size-dependent electrochemical behavior of thiol-capped CdTe nanocrystals in aqueous solution, *J. Phys. Chem. B.* 109 (2005) 1094–1100. doi:10.1021/jp0460801.
- [43] M. Grdeń, M. Łukaszewski, G. Jerkiewicz, A. Czerwiński, Electrochemical behaviour of palladium electrode: Oxidation, electrodisolution and ionic adsorption, *Electrochim. Acta.* 53 (2008) 7583–7598. doi:10.1016/j.electacta.2008.05.046.
- [44] K. Yoshii, Y. Oshino, N. Tachikawa, K. Toshima, Y. Katayama, Electrodeposition of palladium from palladium(II) acetylacetonate in an amide-type ionic liquid, *Electrochem. Commun.* 52 (2015) 21–24. doi:10.1016/j.elecom.2015.01.003.
- [45] M. Amelia, C. Lincheneau, S. Silvi, A. Credi, Electrochemical properties of CdSe and CdTe quantum dots, *Chem. Soc. Rev.* 41 (2012) 5728. doi:10.1039/c2cs35117j.
- [46] A. Czerwiński, The adsorption of carbon oxides on a palladium electrode from acidic solution, *J. Electroanal. Chem.* 379 (1994) 487–493. doi:10.1016/0022-

0728(94)87173-6.

- [47] A.L. Rogach, Nanocrystalline CdTe and CdTe(S) particles: Wet chemical preparation, size-dependent optical properties and perspectives of optoelectronic applications, *Mater. Sci. Eng. B Solid-State Mater. Adv. Technol.* 69 (2000) 435–440. doi:10.1016/S0921-5107(99)00231-7.
- [48] A.L. Ghindilis, P. Atanasov, E. Wilkins, Enzyme-catalyzed direct electron transfer: Fundamentals and analytical applications, *Electroanalysis*. 9 (1997) 661–674. doi:10.1002/elan.1140090902.
- [49] S. Liu, Z. Dai, H. Chen, H. Ju, Immobilization of hemoglobin on zirconium dioxide nanoparticles for preparation of a novel hydrogen peroxide biosensor, *Biosens. Bioelectron.* 19 (2004) 963–969. doi:10.1016/j.bios.2003.08.025.
- [50] J.J. Feng, G. Zhao, J.J. Xu, H.Y. Chen, Direct electrochemistry and electrocatalysis of heme proteins immobilized on gold nanoparticles stabilized by chitosan, *Anal. Biochem.* 342 (2005) 280–286. doi:10.1016/j.ab.2005.04.040.
- [51] S.J. Sadeghi, A. Fantuzzi, G. Gilardi, Breakthrough in P450 bioelectrochemistry and future perspectives, *Biochim. Biophys. Acta - Proteins Proteomics*. 1814 (2011) 237–248. doi:10.1016/j.bbapap.2010.07.010.
- [52] V. V. Shumyantseva, S. Carrara, V. Bavastrello, D.J. Riley, T. V. Bulko, K.G. Skryabin, A.I. Archakov, C. Nicolini, Direct electron transfer between cytochrome P450_{scc} and gold nanoparticles on screen-printed rhodium-graphite electrodes, *Biosens. Bioelectron.* 21 (2005) 217–222. doi:10.1016/j.bios.2004.10.008.
- [53] M. Muller, N. Agarwal, J. Kim, A cytochrome P450 3A4 biosensor based on generation 4.0 PAMAM dendrimers for the detection of caffeine, *Biosensors*. 6 (2016).

doi:10.3390/bios6030044.

- [54] M. Yang, J.L. Kabulski, L. Wollenberg, X. Chen, M. Subramanian, T.S. Tracy, D. Lederman, P.M. Gannett, N. Wu, Electrocatalytic drug metabolism by CYP2C9 bonded to A self-assembled monolayer-modified electrode, *Drug Metab. Dispos.* 37 (2009) 892–899. doi:10.1124/dmd.108.025452.
- [55] Z. Dai, J. Zhang, Q. Dong, N. Guo, S. Xu, B. Sun, Y. Bu, Adaption of Au Nanoparticles and CdTe Quantum Dots in DNA Detection, *Chinese J. Chem. Eng.* 15 (2007) 791–794. doi:10.1016/S1004-9541(08)60004-X.
- [56] H. Huang, N. Hu, Y. Zeng, G. Zhou, Electrochemistry and electrocatalysis with heme proteins in chitosan biopolymer films, *Anal. Biochem.* 308 (2002) 141–151. doi:10.1016/S0003-2697(02)00242-7.
- [57] K. Bavishi, T. Laursen, K.L. Martinez, B.L. Møller, E.A. Della Pia, Application of nanodisc technology for direct electrochemical investigation of plant cytochrome P450s and their NADPH P450 oxidoreductase, *Sci. Rep.* 6 (2016) 29459. doi:10.1038/srep29459.
- [58] C.A. Hasemann, R.G. Kurumbail, S.S. Boddupalli, J.A. Peterson, J. Deisenhofer, Structure and function of cytochromes P450: a comparative analysis of three crystal structures, *Structure.* 3 (1995) 41–62. doi:10.1016/S0969-2126(01)00134-4.
- [59] S.C. Piscitelli, A.H. Burstein, D. Chaitt, R.M. Alfaro, J. Falloon, Indinavir concentrations and St John's wort, *Lancet.* 355 (2000) 547–548. doi:10.1016/S0140-6736(99)05712-8.
- [60] Tim D. Gibson, Biosensors: The Stability Problem, *ANALUSIS.* 27 (1999) 630–638. doi:10.1051/analysis:1999270630.

- [61] C. Sarika, K. Rekha, B. Narasimha Murthy, Studies on enhancing operational stability of a reusable laccase-based biosensor probe for detection of ortho-substituted phenolic derivatives, *3 Biotech.* 5 (2015) 911–924. doi:10.1007/s13205-015-0292-7.
- [62] A. Chaubey, B.D. Malhotra, Mediated biosensors, *Biosens. Bioelectron.* 17 (2002) 441–456. doi:10.1016/S0956-5663(01)00313-X.
- [63] F. Ricci, A. Amine, G. Palleschi, D. Moscone, Prussian Blue based screen printed biosensors with improved characteristics of long-term lifetime and pH stability, 18 (2003) 165–174.
- [64] D. Ravi Shankaran, N. Uehara, T. Kato, A metal dispersed sol-gel biocomposite amperometric glucose biosensor, *Biosens. Bioelectron.* 18 (2003) 721–728. doi:10.1016/S0956-5663(03)00005-8.
- [65] H.W. Kim, G. Na, J. Bae, C. Yang, S. Kim, H. Cheong, D. Young, Synthesis and Characterization of Orthorhombic Sb₂O₄ Nanowire Prepared by Heating Sb₂S₃ Powder, 15 (2012) 49–52. doi:10.1149/2.028206esl.
- [66] J. Conde, J. Rosa, J.M. de la Fuente, P. V. Baptista, Gold-nanobeacons for simultaneous gene specific silencing and intracellular tracking of the silencing events, *Biomaterials.* 34 (2013) 2516–2523. doi:10.1016/j.biomaterials.2012.12.015.
- [67] B.I. Ipe, C.M. Niemeyer, Nanohybrids composed of quantum dots and cytochrome P450 as photocatalysts, *Angew. Chemie - Int. Ed.* 45 (2006) 504–507. doi:10.1002/anie.200503084.

CHAPTER FIVE

Summary

Over the past few years, the intensive research activity has been subjected to the interfaces between genetics and drug metabolism. Drug metabolism is generally defined as consisting of phase I oxidation reactions, mainly negotiated by cytochrome P450 enzymes in the liver. However, the composition of each CYP450s in humans varies among individuals because of unique combination of factors including genetic polymorphisms, the influence of diet, as well as sex, age, and other. Notably, the inter-individual differences in response to drug treatment has been linked to the drug metabolism classification or phenotypes (i.e. ultra-rapid, moderate, or slow metabolisers) originating mainly from genetic polymorphism which is regarded as a major problem in clinical practice. Several clinical studies have demonstrated that breast cancer patients treated with adjuvant tamoxifen are influenced mainly by genetic variation in CYP2D6 enzyme which result in an increased risk of recurrence and reductions in disease-free survival. Therefore, innovative test protocols should be made available in order to predict CYP2D6 phenotypes and individualise tamoxifen therapy. Hence, this study focussed on the development of the next generation phenotype-based biosensor systems for sensing and signalling tamoxifen bioactivity and biotransformation. In this chapter, the catalytic responses of tamoxifen, biotransformation of tamoxifen to its primary and secondary active metabolites, as well as, the individual biosensor materials used in this study were characterised by SWV, UV-Vis, ATR-FTIR, PL, XPS, XRD and Raman spectroscopy.

Palladium Telluride Quantum Dots Phenotype Biosensor for Tamoxifen

Abstract

An electrochemical phenotype biosensor for the determination of the metabolism of the most prescribed breast cancer drug, tamoxifen, is presented. The sensor is based on the combination of novel thioglycolic acid-capped palladium telluride (TGA-PdTe) quantum dots (QDs) and genetically engineered cytochrome P450-3A4 (CYP3A4) or cytochrome P450-2D6 (CYP2D6) enzymes. The two heme-thiolate enzymes, to a varying extent, catalyse the activation of tamoxifen to its active form N-desmethyl-4-hydroxytamoxifen (endoxifen) for cancer therapy. Square wave voltammetry (SWV) responses of the CYP3A4 (or CYP2D6) [TGA-PdTeQDs|Cyst|Au] biosensor systems showed catalytic cathodic peaks at -0.28 V (-0.3 V) for the tamoxifen monooxygenation reaction. The tamoxifen biosensor had sensitivity values of 0.00859 $\mu\text{A}/\text{pM}$ (0.0110 $\mu\text{A}/\text{pM}$) and detection limits (*LOD*) of 9.25×10^{-5} ng/mL (1.95×10^{-4} ng/mL) for the CYP2D6- and CYP3A4-based biosensors, respectively. The *LOD* values are much lower than tamoxifen's maximum steady state plasma concentration (C_{max} 40 ng/mL), thereby indicating that the sensing device, in principle, would be suitable for monitoring the drug in patients.

5. Introduction

Tamoxifen is an oral non-steroidal anti-estrogen drug that has been used in the prevention and treatment of breast cancer for the past 28 years [1–4]. The drug binds with estrogen receptor (ER) to minimize the transcription of estrogen dependent genes [5,6]. Cytochrome P450-2D6 (CYP2D6) and cytochrome P450-3A4 (CYP3A4) are the key enzymes that converts tamoxifen to its active metabolites 4-hydroxytamoxifen (4-hydroxyTAM) and N-desmethyl-4-hydroxytamoxifen (endoxifen), both of which have high affinity for estrogen receptor than the parent drug. Studies indicate that up to 50% of ER-positive breast cancer patients treated with tamoxifen experience relapse. Clinical evidence suggests that differences in patients' phenotype (i.e. a combination of the genetic variants of CYP2D6 and CYP3A4 and drug interactions with the inhibitors of the enzymes) determine the variations in the plasma concentrations of the two tamoxifen's active metabolites, and thus whether a patient is a functional, impaired or severely impaired metaboliser of the drug [7–10]. The risk of inappropriate dosing is potentially high for breast cancer patients undergoing tamoxifen therapy who may be impaired or severely impaired metabolisers. In this study, instead of the costly and time consuming analytical techniques [11–14] currently used for quantitative analysis of tamoxifen and its metabolites in biological fluids and pharmaceutical formulations, novel phenotype tamoxifen biosensor systems are being presented. The sensor was developed by the incorporation of thioglycolic acid (TGA)-capped palladium telluride (PdTe) quantum dots (QDs) onto a gold electrode that was previously modified with self-assembled cystamine dihydrochloride (Cyst). CYP3A4 (or CYP2D6) enzyme was then self-assembled onto the modified gold electrode through a reaction mediated by n-3-(dimethylaminopropyl)-n-ethylcarbodiimide hydrochloride, to form the final biosensor.

5.1 Experimental

5.1.1 Chemicals and sample preparation

Tamoxifen citrate (TAM), molecular weight 563.64, human cytochrome P450-3A4 enzyme (≥ 50 units/mg protein based on reductase activity) expressed in *Saccharomyces cerevisiae*, cytochrome P450-2D6 enzyme (1425 units/mg protein based on reductase activity) expressed in *Saccharomyces cerevisiae* were supplied by Sigma-Aldrich Sweden AB, Stockholm, Sweden. (All other reagents were supplied as analytical grade materials by Sigma-Aldrich Sweden AB, Stockholm, Sweden). The preparation of phosphate buffer solution was achieved by dissolving one tablet in 200 mL of deionised water yielding 0.01 M phosphate buffer, 0.0027 M potassium chloride and 0.137 M sodium chloride, pH 7.4, at 25°C. A stock solution of 1 μ M TAM was prepared in absolute ethanol from which a fresh standard solution of 1.6 nM TAM was prepared by dilution with 0.1 M phosphate buffer solution, pH 7.4 (PBS). Both stock and standard TAM solutions were stored at 4 °C. Thioglycolic acid-capped palladium telluride quantum dots (TGA-PdTeQDs) were synthesised in-house by reacting a mixture of thioglycolic acid and PdCl₂ with tellurium powder reduced with sodium borohydride in alkaline medium (pH 11.4). A detailed procedure for TGA-PdTeQDs synthesis was described in **chapter 4 section 4.1.3**, where the stock TGA-PdTeQDs solution was 0.2 M in Pd²⁺.

5.1.2 Instrumentation

Electrochemical measurements were carried out in 0.1 M phosphate buffer, pH 7.4, cell solution using a 3 mm diameter Au disk working electrode, a platinum wire counter electrode and a Ag/AgCl (with 3 M KCl salt-bridge) reference electrode supplied by Bioanalytical Systems, Incorporated (BASi), West Lafayette, IN, USA. The electrochemical signals were recorded with an IviumStat Electrochemical Interface and Impedance Analyser (Ivium

Technologies B.V., Eindhoven, The Netherlands). Differential pulse (DPV) and square wave (SWV) voltammograms were recorded at a scan rate of 20 mV/s. Infrared spectra of the materials were acquired using attenuated total reflectance (ATR) platform by pressing the solid electrodes onto the diamond crystal in a Bruker Model Tensor 27 FT-IR spectrometer (Bruker Optics IFS 66 series) with a scan velocity of 10 kHz and a resolution of 4 cm⁻¹. X-ray diffraction (XRD) patterns of the PdTeQDs were performed on (XRD, Model No D/MAXPC 2500 X-ray, made in UK) operating in the scanning mode (12.082°-90.061°) and using CuK α radiation ($\lambda = 1.5418 \text{ \AA}$) generated at 40 kV and at a current of 30 mA. Steps of 0.034° and step time 192 s employed. X-ray photoelectron spectroscopy (XPS) measurements were performed on a Scienta ESCA 200 spectrometer in ultrahigh vacuum with a base pressure of 10⁻¹⁰ mbar and monochromatic Al (K alpha) x-ray source providing photons with 1486.6 eV. Raman analysis was done with an XPlora Horiba Jobin-Yvon spectrometer equipped with high stability OLYMPUS BX41TF optical microscope and an Ivac CCD detector.

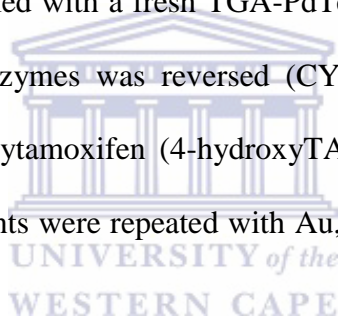
5.1.3 Preparation of CYP (3A4 or 2D6)/TGA-PdTeQDs/Cyst/Au phenotype biosensors

An aliquot (20 μ L) of 0.02 M cystamine (Cyst) was drop-casted on a 3 mm diameter Au disk electrode surface and kept in the dark for 24 h. The Cyst/Au modified electrode was functionalised with a drop of a solution consisting of TGA-PdTeQDs (containing 0.2 M Pd²⁺) and 0.1 M 1-ethyl-3-[3-dimethylaminopropyl] carbodiimide/0.1 M N-Hydroxysuccinimide (EDC/NHS, ratio 1:1) and left to cure for 12 h. The TGA-PdTeQDs-modified electrode was placed in an Eppendorf vial containing 0.5 mL of 0.1 M PBS and gently vortexed (Vortex-Genie 2, Scientific Industries Incorporated, Bohemia, NY, USA) at 10 rpm for 5 min to remove unbound TGA-PdTeQDs. A 3 μ L CYP3A4 or CYP2D6 enzyme solution (used as supplied) was then drop-coated onto the TGA-PdTeQDs/Cyst/Au electrode surface and kept

at 4 °C for 3 h. The resulting CYP3A4/TGA-PdTeQDs/Cyst/Au (or CYP2D6/TGA-PdTeQDs/Cyst/Au) biosensor was rinsed gently with distilled water to remove any physically adsorbed enzyme and stored at 4 °C in 0.1 M PBS when not in use.

5.1.4 Procedure for tamoxifen metabolic pathway experiment

TGA-PdTeQDs/Cyst/Au electrode was prepared and held in an 8 mL electrochemical cell solution containing 0.2 nM TAM in PBS to which 10 µL CYP3A4 enzyme (used as supplied) was added in order to convert TAM to N-desmethylTAM. Then 10 µL of CYP2D6 enzyme (used as supplied) was added to the cell solution to convert N-desmethylTAM to endoxifen. Another experiment was performed with a fresh TGA-PdTeQDs/Cyst/Au electrode in which the order of addition of the enzymes was reversed (CYP2D6 followed by CYP3A4) to produce endoxifen via 4-hydroxytamoxifen (4-hydroxyTAM) intermediate metabolite. For comparison, the above experiments were repeated with Au, Cyst/Au and TGA-PdTeQDs/Au electrodes.



5.2 Results and discussion

5.2.1 Electronic transitions in TGA-PdTeQDs

The morphology and size distribution of the TGA-PdTeQDs were determined through HR-TEM studies and the image is shown in **Figure 22A**. From the micrograph, it is observed that TGA-PdTeQDs are spherical well dispersed particles of average size of 3-5 nm in diameter. The well resolved lattice fringes and the selected area electron diffraction (SAED) patterns (insert **Figure 22A**) confirmed the cubic zinc blende structure of PdTeQDs with three rings attributed to (111), (220) and (311) lattice planes, respectively [15]. These results are comparable with XRD measurements. The optical properties of *TGA-PdTeQDs* material were

investigated to ascertain its suitability for incorporation into the biosensor systems [16]. The UV-Vis absorbance study was first performed for cystamine which exhibited characteristic absorbance bands at 310 and 335 nm associated with the $n \rightarrow \sigma^*$ transitions of the cystamine thiol groups as illustrated in **Figure 22B** (a) [17]. When cystamine was combined with TGA-PdTeQDs solution, a new absorbance band was formed at 357 nm (**Figure 22B** (b)) followed by a decreased in the intensity of the band with time [18]. The 357 nm absorbance band was attributed to $\pi\text{-}\pi^*$ electronic transition arising from a strong interaction between the amino groups of cystamine and the carboxylic acid groups associated of *TGA-PdTeQDs*. Recent studies suggest that proteins such as CYPs exhibit UV-Vis absorptions owing to tryptophan (Trp, 280 nm), tyrosine (Tyr, 280 nm), phenylalanine (Phe, 257 nm) as well as peptide bonds (225 nm) [19]. As illustrated in **Figure 22B** (c and d), the formation of new characteristic bands observed at 260 nm for the UV-Vis of CYP2D6-(TGA-PdTeQDs)-cyst (c) and at 250 nm for the CYP3A4-(TGA-PdTeQDs)-cyst (d). These absorbance bands were attributed to the $\pi\text{-}\pi^*$ and $n\text{-}\pi^*$ electronic transitions of aromatic heterocycle in Phe [19,20]. Moreover, the shifts in the absorbance bands of Phe in the UV-Vis of the CYP-containing systems suggested the occurrence of reactions between the amino groups ($-\text{NH}_2$) of CYP enzymes and the carboxyl groups ($-\text{COOH}$) of the thioglycolic acid capping agent [21].

Figure 22C shows UV-Vis spectra of tamoxifen and its active metabolites. The spectra of the four compounds revealed similar characteristic features indicating that the electronic structure of the boundary orbitals is slightly affected by the atoms in the lateral chain (i.e alkyl amide group) [22]. Three characteristic absorbance bands were observed at 205 nm (6.05 eV), 254 nm (4.88 eV) and 311 nm (3.98 eV), respectively for TAM **Figure 22C** (a), which were attributed to $n\text{-}\pi^*$ (transition of a non-bonding (lone pair) electron on the oxygen up to a π^*) and to $\pi\text{-}\pi^*$ transition due to the extended conjugation of the triphenylethylene

[23]. However, the two active metabolites 4-OHT and END exhibited similar absorbance bands sharing similarities in their molecular structures as illustrated in **Figure 22C** (b and d). The characteristic absorbance bands were observed at 210 nm (203 nm), 244 nm (244 nm) and 291 nm (286 nm) for 4-OHT (END) associated with energy band gap values of 5.91 eV (6.11 eV), 5.08 eV and 4.26 eV (4.34 eV), respectively. In addition, these absorbance bands were attributed to the π - π^* electronic transition in the aromatic ring and a shoulder which appeared at 244 nm corresponded to an $n - \pi^*$ electronic transition involving the formation of a secondary amine group [24]. The presence of an O-H group around the aromatic ring caused a blue shifted transition from 210 nm to 203 nm and 291 nm to 286 nm, respectively. Furthermore, 4-OHT and END obtained larger bandgap values as expected at lower wavelengths than TAM and NDMT [25]. In contrast with TAM, **Figure 22C** (c) exhibited an extended broad absorbance band located at longer wavelength side (544 nm) associated with energy band gap value of (2.28 eV). The characteristic band was attributed to charge transfer migration (CT) involving the whole molecule [26]. Therefore, the obtained energy band gap results are in accordance with clinical studies which indicated that 4-OHT and END exhibited the highest activities and efficiencies compared to TAM or NDMT [23].

Tamoxifen is a pro-drug that requires metabolism to form the pharmacologically active metabolites primarily by the CYP450-3A4 and (CYP450-2D6) enzymes. Although all cytochrome P450 enzymes contain the same heme centre, their optical absorption spectra differ only by a small extent in the different isozymes. Upon the addition of CYP2D6 enzyme in endoxifen aqueous solution, a slight change in absorbance bands was observed from 203 to 212 nm and from 286 nm to 260 nm associated with energy band gap values of 5.85 eV and 4.77 eV, respectively. These changes were attributed to the displacement of coordinated water associated with the active site causing changes in heme-iron spin state (from low-spin

to high spin) as monitored by the shift in the Soret band from 286 to 260 nm [27]. Additionally, it has been suggested that the substrates containing nitrogen or oxygen donor atoms causes the Soret band to shift [28]. Similarly, CYP3A4-END exhibited absorbance bands at 207 nm (5.99 eV) and 260 nm (4.77 eV), respectively. Also, exhibited here was a slight red shift accompanied by a decrease in absorbance intensity due to the main electronic $\pi-\pi^*$ transition of the porphyrin and resulted in the split Soret band indicating that CYP3A4 binds stronger than CYP2D6 due to their difference in their size of the active site and kinetic space as illustrated in **Figure 22D** (d) [29]. **Figure 22D** (b and a), exhibited four absorbance bands at 223 nm (5.56 eV), 260 nm (4.77 eV), 322 nm (3.85 eV) and 543 nm (2.28 eV) while interestingly two characteristic broad absorbance bands were observed at 260 nm (4.77 eV) and 409 nm (3.03 eV) for CYP2D6-4-OHT, respectively. A common feature of all the three compounds was observed at 260 nm indicating that the binding of the enzymes with prodrug and active metabolites occurred at 260 nm.

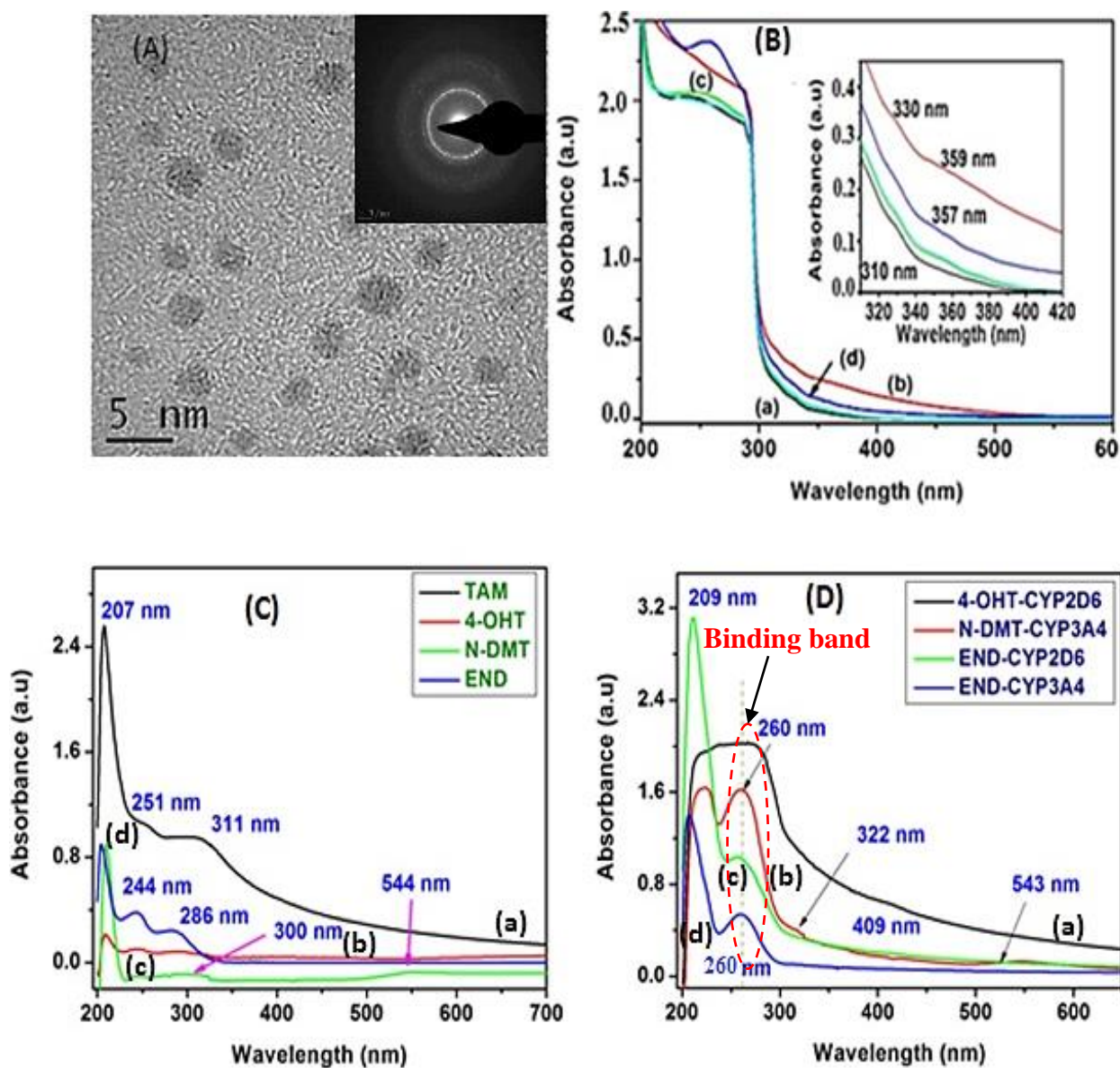


Figure 22: HR-TEM image showing clearly the inter-plane spacing SAED (insert) pattern of TGA-PdTeQDs at 5 nm scale view. (B) UV-Vis spectra of biosensor materials in the region of 200-800 nm in 0.1 M PBS (pH 7.4) for (a) Cyst, (b) (TGA-PdTeQDs)-cyst, (c) CYP2D6-(TGA-PdTeQDs)-cyst, and (d) CYP3A4-(TGA-PdTeQDs)-cyst. The insert in (B) is the amplified UV-Vis spectra in the region of (310-420 nm). (C) UV-Vis spectra of (a) TAM, (b)

4-OHT, (c) N-DMT, and (d) END. (D) UV-Vis spectra of substrate-enzyme systems in 0.1 M PBS (pH 7.4) at 25 °C presented for (a) 4-OHT-CYP2D6, (b) NDMT-CYP2D6, (c) END-CYP2D6 and (d) END-CYP3A4, respectively.

5.2.2 Optical properties of TAM and its active metabolites

Substrate binding to cytochrome P450 enzymes is often monitored by changes in electronic transition using optical absorption spectra. The binding evidence comes from the change in absorbance bands for different incubation periods as illustrated in **Figure 23(A and B)**. With increasing incubation time for **Figure 23A** (b) in the presence of CYP2D6, the absorbance bands decreased to 250 nm (4.96 eV) and 300 nm (4.14 eV) due to the formation of 4-hydroxyTAM and revealed that tamoxifen binding to CYP2D6 exposed the Phe residues of CYP2D6 by extending the peptide bonds (i.e. linking the triphenylethylene of TAM to CYP2D6 via amide bond) [30,31]. Consequently, the energy level of the π - π^* electron transition decreased, which caused a shift from 255 to 250 nm and 310 to 300 nm. Upon the addition of CYP3A4 to TAM-CYP2D6 solution (**Figure 23B** (c)), there is an increase in the absorbance band from 250 nm to 254 nm for which its intensity increases with incubation times due to the formation of the secondary amine in endoxifen (N-desmethyl-4-hydroxytamoxifen) by the demethylation reaction catalysed by CYP3A4 [32]. These results are in good agreement with ATR-FTIR data for the systems, which has a band at 3200 cm^{-1} attributed to be the characteristic band of secondary amides N-H of endoxifen. The presence of cysteamine and QDs mixture in TAM aqueous solution resulted in the shift in absorbance band from 254 nm to 258 nm with an existence of a new characteristic absorbance band at 334 nm as shown in **Figure 23C** (a). However, an increase in absorbance band intensity was observed when CYP2D6 enzyme was introduced in Cyst-TGA-PdTeQDs-TAM solution with increasing incubation time. In addition, the observed increase in absorbance intensity could also be attributed to the presence of QDs which

acted as a mediator and promoted electrons from valence bands to conduction bands. Interestingly, a decrease and a slight shift in absorbance band in the presence of CYP3A4 in Cyst-TGA-PdTeQDs-TAM-CYP2D6 solution was observed as illustrated in **Figure 23D** (b). These findings indicated that both CYP2D6 and CYP3A4 participated in the full conversion of TAM to endoxifen. Calibration plots from the increasing incubation time plotted against absorbance were used to investigate the formation of both primary and secondary metabolites of tamoxifen as indicated in **Figure 23 (E and F)**. Compared to TAM (a), TAM-CYP2D6 (b) and TAM-CYP2D6-CYP3A4 (c) exhibited an increase and a slight shift with increasing incubation time. Furthermore, the use of 0.1 M PBS, pH 7.4 causes the intermediate formed (4-OHTAM) by TAM-CYP2D6 to be neutral and this neutral form of the drug is thought to decompose with increasing incubation time. In contrast with Cyst-TGA-PdTeQDs-TAM (a) and Cyst-TGA-PdTeQDs-TAM-CYP2D6-CYP3A4 (c), TGA-PdTeQDs-TAM-CYP2D6 (red line) appeared at higher absorbance intensity, accompanied by a large decrease from 15 min-20 min, indicating successful conversion of TAM to endoxifen.

CHAPTER 23

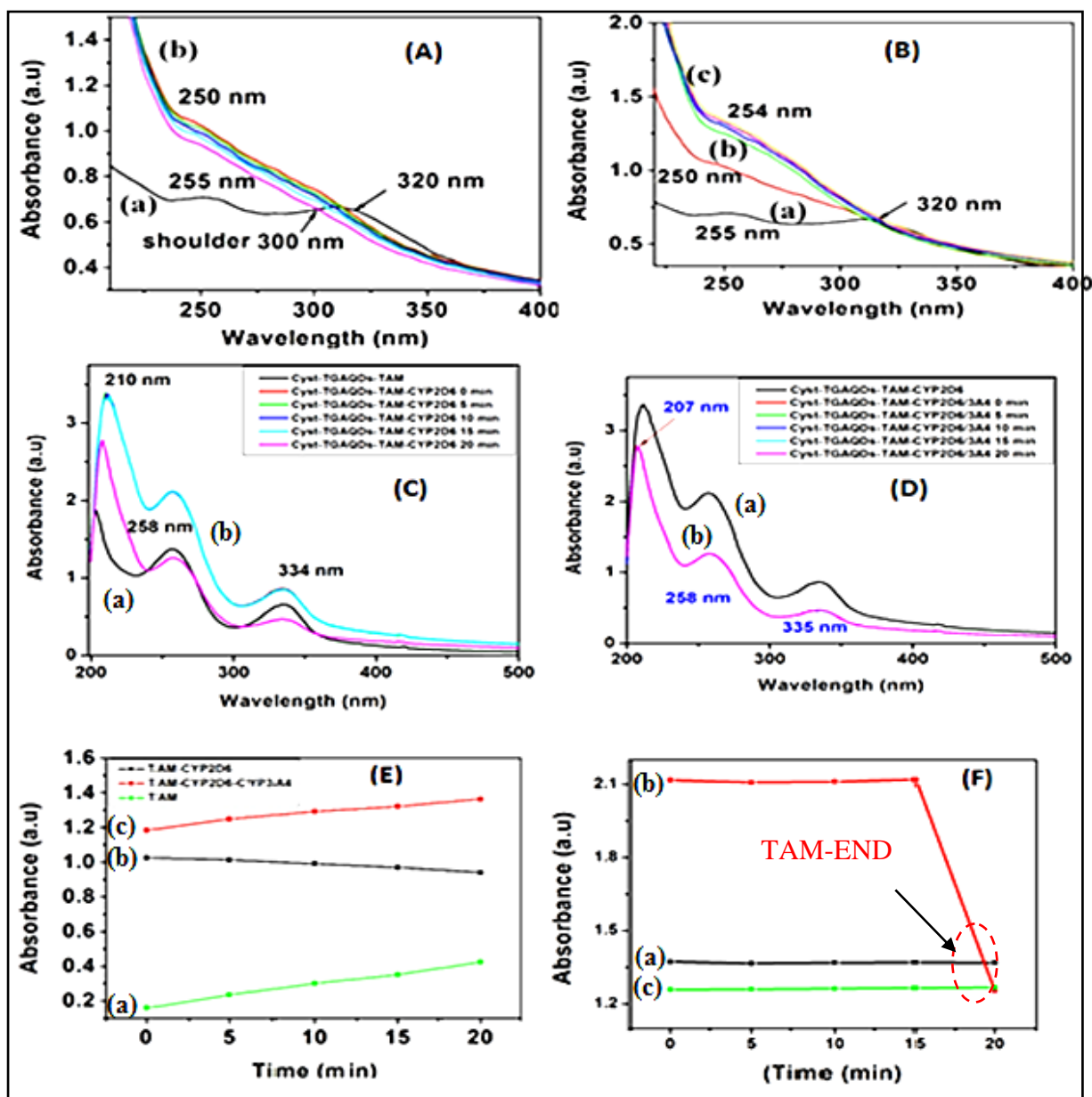


Figure 23: (A and B): UV-Vis absorption spectra of drug-enzyme complex recorded in a 200-800 nm range as a function of time (0-20 min) in 0.1 M PBS (pH 7.4) for (a) TAM, (b) TAM-CYP2D6 and (a) TAM, (b) TAM-CYP2D6, and (c) TAM-CYP2D6-CYP3A4, respectively. (C and D) represented UV-Vis spectra of (a) Cyst-(TGA-PdTeQDs)-TAM, (b) Cyst-(TGA-PdTeQDs)-TAM-CYP2D6 and (a) Cyst-(TGA-PdTeQDs)-TAM-2D6, (b) Cyst-(TGA-PdTeQDs)-CYP2D6-CYP3A4, respectively. (E and F) shows calibration curves taken at 260 nm as a function of incubation time (0-20 min) in 0.1 M PBS for (A, B, C and D), respectively.

5.2.3 Spectroscopic properties of biosensor materials

Different architectures of the biosensor materials were investigated to elucidate the mechanism of the enzymatic recognition event and of the role of the quantum dots. The emission spectra showing the optical properties of cysteamine are illustrated in **Figure 24A** (a). When excited at 260 nm, two maximum emission peaks were observed at 347 nm and 406 nm. These emission bands were attributed to the characteristic features of the thiol (-SH) group and skeletal cysteamine molecules (mainly C–C stretching coupled with the C–N groups [33]). Notably, TGA-PdTeQDs exhibited a shoulder and a broad fluorescence emission peak at 374 nm and 426 nm, respectively. The onset broad emission peak observed at 426 nm was ascribed to different sizes of QDs related to the band gap energy of 2.91 eV while the shoulder was due the metal-ligand-charge transfer (PdCl₂-TGA). In addition, the observed broad PL emission of TGA-PdTeQDs was related to the transitions originating from sulphur vacancies of thioglycolic acid [34]. The combination of cysteamine and TGA-PdTeQDs solution resulted in emission band shifts to longer wavelength with decreasing emission band width at 350 nm (3.5 eV), 378 nm (3.3 eV) and 450 nm (2.75 eV), respectively. These changes in emission bands were attributed to the interaction of cysteamine amine group with the carboxylic functional group offered by TGA-PdTeQDs. When TAM was added in Cyst-TGA-PdTeQDs solution, a noticeable shift accompanied by the enhancement of fluorescence intensity emission peaks was observed due to the donation of nitrogen lone pair of tamoxifen to the d-orbital of palladium metal as indicated in **Figure 24** (c). However, the presence of CYP2D6 in Cyst-TGA-PdTeQDs-TAM solution resulted in narrow emission band which shifted to shorter wavelength accompanied by enhancement in fluorescence emission intensity and this was ascribed to the binding of CYP2D6 heme centre with tamoxifen as shown in **Figure 24** (e) [35]. Similar behaviour was observed when CYP3A4 was introduced

in Cyst-TGA-PdTeQDs-TAM-CYP2D6 solution. These results are in good agreement with UV-Vis measurements.

Figure 24 (B) shows the fluorescence emission spectra of TAM and its active metabolites. When excited at 360 nm, two characteristic fluorescence emission bands were observed at 352 nm and 390 nm associated with energy band gap values of (3.52 eV) and (3.18 eV) for TAM as indicated in **Figure 24(B)** (a). The emission bands were attributed to the excited tertiary amino group and π - π stacking of hydrocarbons in aromatic compounds of tamoxifen [36]. A distinctive number of fluorescence emission bands were observed at 349 nm (3.55 eV), 365 nm (3.39 eV), 377 nm (3.29 eV) and 421 nm (2.95 eV) for NDMT while END exhibited identical characteristic emission peak which appeared at lower emission width as shown in **Figure 24 B** (c and d). In addition, a noticeable blue shift in emission peak observed at 349 nm was attributed to the formation of a secondary amino group [36]. In comparison with TAM, 4-OHT exhibited an emission peak at 421 nm (2.95 eV), accompanied by a quench in emission peak intensity.

Fluorescence spectroscopy was employed to investigate protein-substrate interactions, prior the fluorescent properties of the substrate or the fluorescence of the tryptophan and tyrosine residues of the CYP450s [37]. As illustrated in **Figure 24 C** (e), CYP2D6 enzyme exhibited a well-defined fluorescence emission band at 307 nm and the shoulder around 360 nm which were attributed to characteristic features of two tryptophan residues [38]. Meanwhile, a large red shift of fluorescence emission peak was observed after the addition of CYP3A4 in NDMT solution, implying that the microenvironment around the CYP3A4 (heme centre) has changed [39]. The binding of substrate to CYP450-3A4 enzyme has been extensively studied to monitor the rare oxidation kinetics observed and its dominant involvement in the oxidation of drug molecules [40]. The presence of CYP3A4 in END solution resulted in a slight red shift in emission peak due to the hydrophobic interactions via the aromatic rings and aliphatic side

chains as well as the hydrophobic pockets in CYP3A4 enzyme [39]. as illustrated in **Figure 24 C (a)**. In comparison with CYP2D6, the presence of CYP2D6 in 4-OHT solution resulted in additional number of fluorescence emission peaks at 297 nm, 365 nm, 377 nm, and 420 nm as shown in **Figure 24 C (d)**. The observed characteristic emissions could be attributed to binding of 4-OHT with different tryptophan residues present in CYP2D6 (i.e. the combination of two or more tryptophan residues) [41]. This, therefore indicates that all fluorescent tryptophan residues present in both CYP450 (2D6 and 3A4) enzymes are available for binding with TAM and its active metabolites.

Figure 24 (insert D and F) shows the calibration plots measured at different time intervals (0-20 min) in 0.1 M PBS. When CYP450 enzymes interact with drugs, tryptophan fluorescence intensity may change depending on the effectiveness of the interaction on CYP conformation or via direct quenching effect. In this study, the decrease or increase of fluorescence intensity was monitored at 367 nm and 365 nm for CYP2D6-TAM and CYP3A4-CYP2D6-TAM, respectively. With increasing incubation time (**Figure 24 insert D**) in the presence of CYP2D6 in TAM solution, a major decrease in fluorescence emission peak was observed from 5 min to 20 min typically due to the changes in the tryptophan conformation which resulted in the formation of 4-hydroxyTAM. In contrast, the presence of CYP3A4 in the solution containing CYP2D6-TAM exhibited an increase in fluorescence emission intensity from 0-10 min and equilibrated from 15-20 min. Based on the obtained energy band gap values of 3.55 eV (3.54 eV) for 4-OHT (END) and 3.38 eV (3.4 eV) for CYP2D6-TAM and CYP3A4-CYP2D6-TAM, we can conclude that both CYP450 (2D6 and 3A4) participate in the formation of active metabolites (i.e. 4-OHT and END). Additionally, the obtained results are in good agreement with UV-Vis measurements.

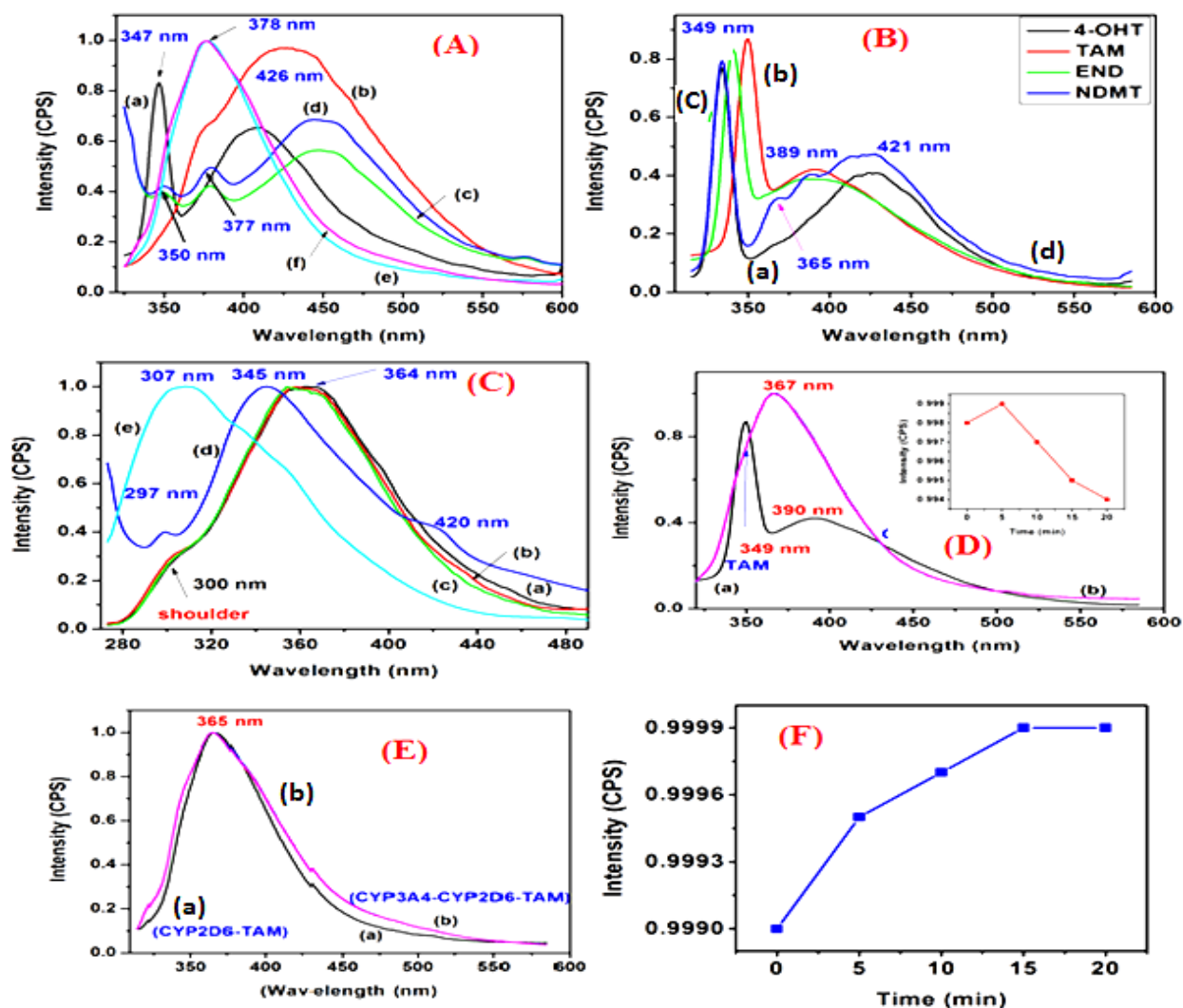
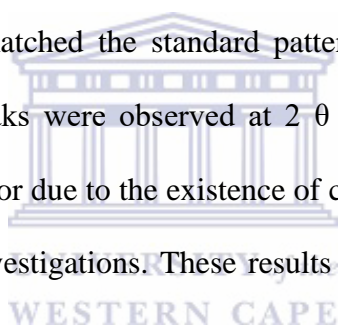


Figure 24: PL emission spectra of sensor platform excited at 260 nm in 0.1 M PBS (pH 7.4) for (a) Cyst, (b) TGA-PdTeQDs, (c) Cyst-(TGA-PdTeQDs), (d) Cyst-(TGA-PdTeQDs)-TAM, (e) Cyst-(TGA-PdTeQDs)-TAM-CYP2D6 and (f) Cyst-(TGA-PdTeQDs)-TAM-CYP2D6-CYP3A4, respectively. (B and C) PL emission spectra excited at 360 nm for (a) 4-OHT, (b) TAM, (c) END, (d) NDMT and (a) CYP3A4-END, (b) CYP3A4-NDMT, (c) CYP3A4, (d) CYP2D6-4-OHT, and (e) CYP2D6, respectively. (D and E) PL emission spectra measured at different time interval (0-20 min) for (a) TAM, (b) CYP2D6-TAM at (0-20 min) and (a) CYP2D6-TAM, (b) CYP3A4-CYP2D6-TAM, respectively. (F and an insert E) Calibration curves taken at excitation wavelengths 365 nm and 367 nm as a function of incubation time (0-20 min) in 0.1 M PBS for (D and E), respectively.

5.2.4 Crystal structure of TGA-PdTeQDs

X-ray diffraction (XRD) technique was employed to investigate the crystal structure of PdTeQDs. As illustrated in **Figure 25**, five distinctive diffraction peaks were observed at $2\theta = 32^\circ$, (111), 45.5° , (200), 56.6° , (220), 66° , (311) and 75° , (222), respectively. These reflection peaks are found to be consistent with the cubic structure of PdTeQDs [42]. The strong and sharp diffraction peak at (111), in contrast with the other four diffractions indicated preferential growth of the PdTeQDs [43]. Moreover, the presence of thioglycolic acid (TGA) capping agent shifted the diffraction peaks toward the cubic crystalline phase due to its strong and effective passivation of PdTeQDs surface [44,45]. This may have also increased sulphur release on the surface of PdTeQDs [46]. The composition of quantum dots was identified as Pd₃Te₂ and matched the standard pattern well (JCP2.2CA:00031-0941). Interestingly, few additional peaks were observed at $2\theta = 39.7^\circ$ and 41.2° and could be attributed to different Te species or due to the existence of chalcopyrite type orderings, which requires further experimental investigations. These results are in good agreement with HR-TEM and XPS measurements.



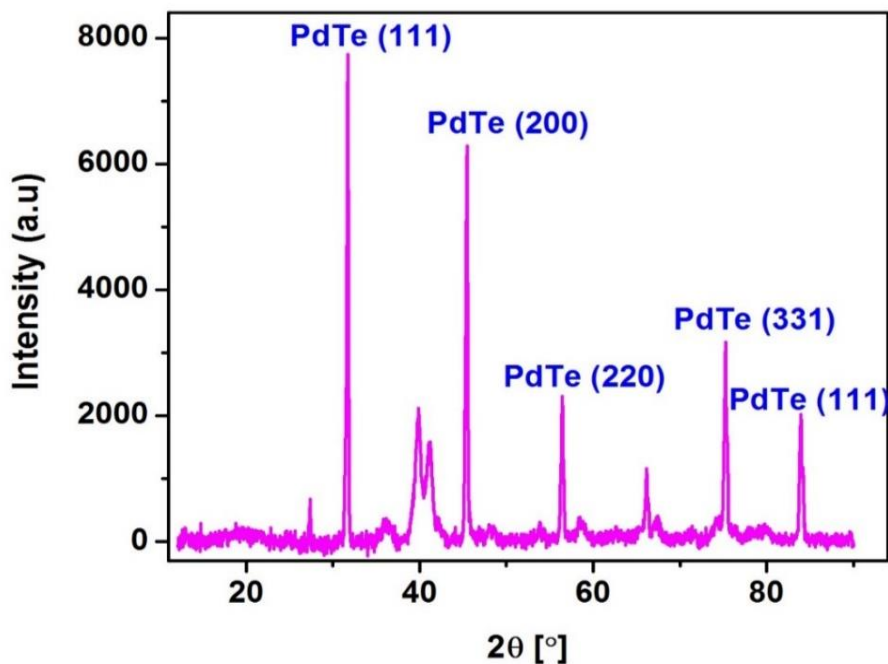


Figure 25: XRD pattern of TGA-PdTeQDs



5.2.5 Optical vibrational modes of TGA-PdTeQDs

Raman spectroscopy is a powerful, non-destructive technique effectively used in the micro-structural characterisation of carbonaceous materials [47]. In this study, Raman spectroscopy technique was employed to investigate photonic properties of PdTeQDs. Measurements were made at room temperature in backscattering configuration excited by a 532 nm line of an Ar⁺ ion laser with power in the range of 1 mW at a wavenumber range 20 to 1500 cm⁻¹. Raman vibrational modes corresponding to the crystalline core and Te defects of the PdTe QDs are illustrated in **Figure 26**. The observed Te vibrational mode at a wavenumber of 99 cm⁻¹ revealed the presence of Te crystals which could either appear within the center of the QDs or at the boundary of the QDs [48–50]. In addition, existence of Te⁰ appeared at only one vibrational mode 300 cm⁻¹ in this range [51]. Furthermore, the presence of excess TGA capping agent in the sample caused an increase in the intensities at 527 cm⁻¹ and 1099 cm⁻¹, respectively. The increase could be attributed to the formation of a ternary Pd–S–Te

interlayer corresponding to the longitudinal optical (LO) photon peak [52], and due to the interaction between TGA and PdTeQDs through mixed banding modes of the $\nu(\text{C-H})$, $\nu(\text{C-C})$, and $\nu(\text{C-O})$, respectively [53]. The occurred interaction can also be described as surface optical photon (SO). Moreover, the exhibited vibrational mode at 800 cm^{-1} could be ascribed to the binding of TGA with PdTe through the sulphur atom [54]. This, therefore revealed that thiolates are strongly passivating the surface of the QDs. The obtained results are comparable with FTIR and XPS measurements.

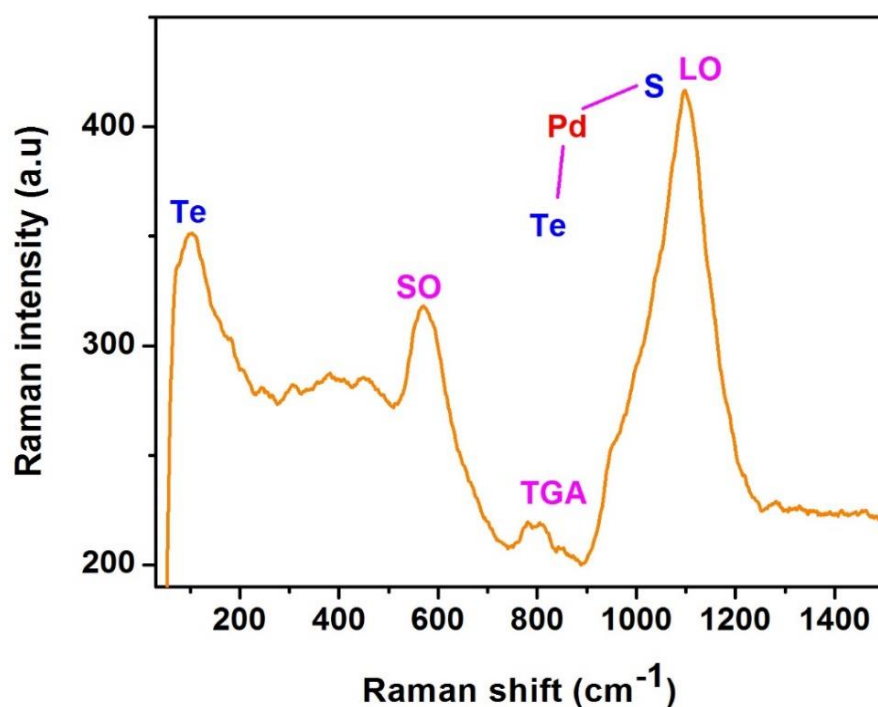


Figure 26: Raman spectra of TGA-PdTeQDs

5.2.6 Electronic transitions of TGA-PdTeQDs

X-ray photoelectron spectroscopy (XPS) was employed to analyse the information on the surface chemical compositions and valence states of PdTe quantum dots. The analysed QDs present the characteristic signal from Pd, Te, O and C photoemission regions [55]. **Figure 27**

shows the XPS spectra of the 3d core-level [56]. The core-levels were analysed with attention to the Pd 3d and Te 3d spin-orbit components, which are of major interest for assessing the particle size effect and oxidation state of Pd atom on PdTeQDs. In **Figure 27A**, three strong peaks with binding energies at 335, 337 and 343 eV were assigned to Pd_{3d5/2} and Pd_{3d3/2} respectively. Such binding energy values are in accordance with those reported for metallic Pd, thus confirming the successful reduction of Pd²⁺ → Pd⁰ [57]. The measured binding energy difference between (Pd²⁺) Pd_{3d5/2} and (Pd⁰) Pd_{3d3/2} was 8 eV, which is consistent with the binding energy observed for stoichiometric PdTe. When inspected carefully, it was observed that each Pd 3d peak was quite broad, implying the possibility of overlapping peaks. As shown in **Figure 27B**, the characteristic peaks at 587, 573 and 567 eV were assigned to Te_{3d3/2} and Te_{3d5/2} respectively [58]. Additionally, the peaks centred at 286 eV and 288 eV were attributed to the alkyl chain of capping agent and the oxidised form of carbons, which are usually detected as (C=O, O-C-O and COO), as shown in **Figure 27C**. Furthermore, the strong peak of O 1s centred at 532.5 eV was due to carboxyl oxygen of thioglycolic acid ligands present in thiol-capped PdTeQDs [59]. As it can be seen in **Figure 27E**, the overview XPS spectrum confirmed the existence of S, Pd and Te in TGA-PdTeQDs.

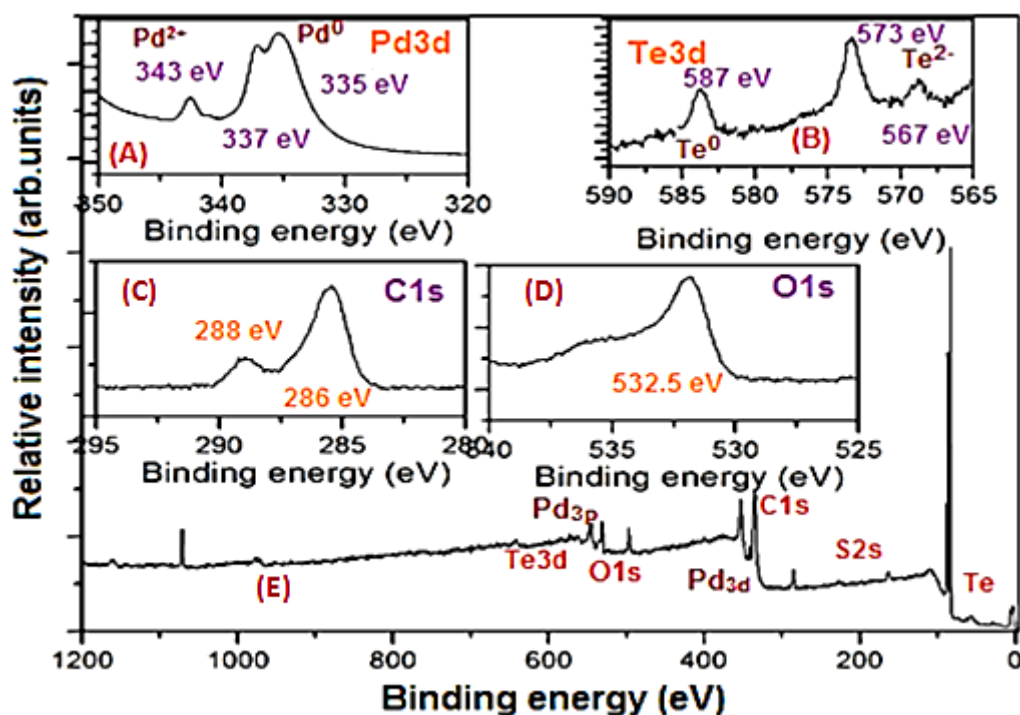
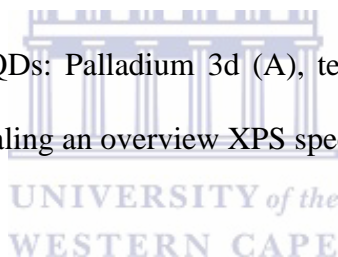


Figure 27: XPS of TGA-PdTeQDs: Palladium 3d (A), tellurium 3d (B), thioglycolic acid C1s and O1s (C and D). (E) revealing an overview XPS spectrum of TGA-PdTeQDs.



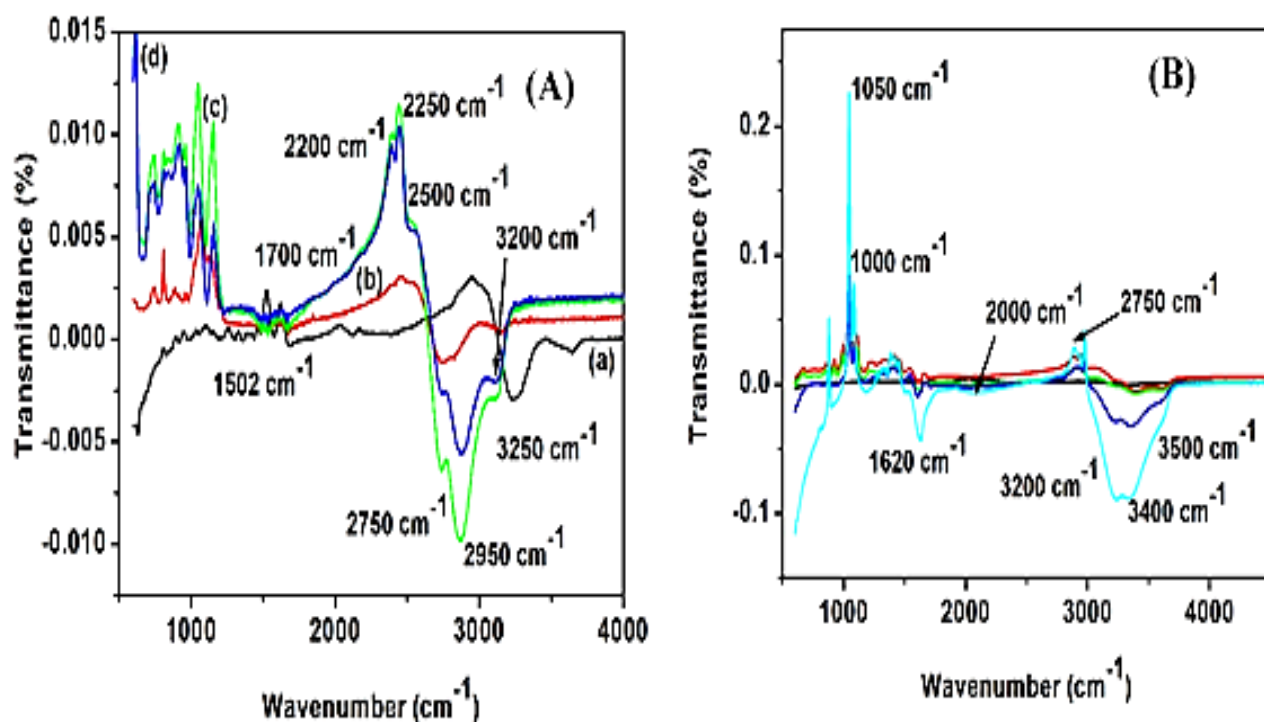
5.2.7 Structural properties of sensor materials

Further characterisation by ATR-FTIR was performed to evaluate the interaction between the TGA-PdTeQDs, Cyst, and CYP450-(2D6 and 3A4) enzymes. The spectra shown in **Figure 28A** (a) was attributed to the successful binding of TGA capping agent on to the PdTe core, this was confirmed by disappearance of S-H broad band stretch at approximately 2550 cm^{-1} indicating the formation of S-PdTe bonds between TGA and PdTe core [60]. The absorption band at 1700 cm^{-1} was ascribed to the vibration of the carboxylic group (COOH) [61]. Furthermore, the band at 1502 cm^{-1} was associated with CH_2 . The difference in band intensity in all the spectra may occur because of intramolecular bonding between the carboxylic group and the amine group in the experimental spectrum. A decrease in C=O stretch of carboxylic acid and a shift in O-H stretch from 3250 cm^{-1} to 2750 cm^{-1} was observed in **Figure 28A** (b),

this shift was due to the interaction between TGA-PdTeQDs and cystamine. However, when the sensor platform, made of CYP2D6-(TGA-PdTeQDs)-cyst was prepared and analysed by FTIR (**Figure 28A c**), two strong absorption bands were observed at 2956.02 cm^{-1} and 2800 cm^{-1} , respectively. The bands at 2956.02 cm^{-1} was attributed to be the characteristic band of primary and secondary amides N-H of the protein backbone and the band at 2800 cm^{-1} was due to C-H stretch [62]. In this work, this band resulted from the reaction of the free carboxylic group (-COOH) in TGA-PdTeQDs and the free amine group (-NH₂) in CYP2D6. Furthermore, a decrease in absorption bands were observed when CYP3A4-TGA-PdTeQDs-cyst was exposed to FTIR spectrum as shown in **Figure 28A (d)**.

There is an infrared spectroscopic evidence for drug binding to CYP450 (2D6 and 3A4) active sites. This evidence for drug binding comes from spectral changes observed from the ATR-FITR of TAM-CYP2D6-(TGA-PdTeQDs)-Cyst and TAM-CYP3A4-(TGA-PdTeQDs)-Cyst with five major absorbance bands of the functional groups present, as shown in **Figure 28B** (green and blue lines). These functional groups include, alcohol O-H stretching, alkane C-H stretching, alkene -C=C- stretching, C=O stretching, protonated COO- stretching, C-N stretching, C-C stretching and N-H stretching with their frequencies appearing at 3200 cm^{-1} , 2950 cm^{-1} , 1620 cm^{-1} , 1770 cm^{-1} , 3400 cm^{-1} , 2000 cm^{-1} , 1050 cm^{-1} , 1000 cm^{-1} and 3500 cm^{-1} respectively [63]. The infrared spectra of free TAM, CYP2D6 and CYP3A4 in the region of 3500 cm^{-1} to 2800 cm^{-1} were compared with those of TAM-CYP2D6-(TGA-PdTeQDs)-Cyst and TAM-CYP3A4-(TGA-PdTeQDs)-Cyst, in order to examine the drug binding to O-H and N-H as well as the existence of hydrophobic contacts in their complexes [64]. Clearly, the presence of TAM in solutions containing CYP2D6-(TGA-PdTeQDs)-Cyst and CYP3A4-(TGA-PdTeQDs)-Cyst had an effect on the spectral absorbance bands intensity with major

shifts indicating a strong tamoxifen binding with CYP3A4 and CYP2D6 enzymes, respectively.



WESTERN CAPE

Figure 28: (A) ATR-FTIR interferograms accumulated over the spectral range s of 500-4500 cm⁻¹ for (a) TGA-PdTeQDs, (b) TGA-PdTeQDs-cyst, (c) CYP2D6-TGA-PdTeQDs-Cyst and (d) CYP3A4-TGA-PdTeQDs-Cyst. (B) ATR-FTIR spectra of (black line) TAM, (red line) CYP2D6, (green line) CYP3A4, (blue line) TAM-CYP2D6-(TGA-PdTeQDs)-Cyst and (cyan line) TAM-CYP3A4-(TGA-PdTeQDs)-Cyst.

5.3 Electrochemical properties of the biosensor system

5.3.1 Biosensor's electrochemical responses

DPV experiments were performed to characterise the surface features of the modified electrodes in 0.1 M PBS, pH 7.4 at 25 mV/s. For the bare gold electrode shown in **Figure 29A** (a), two significant reduction peaks were observed at -0.23 V and -0.45 V, respectively. The reduction peaks were attributed to the reduction of O₂ to H₂O₂ and a further reduction of H₂O₂ [65]. Compared to bare Au electrode, cysteamine exhibited a cathodic peak at -0.8 V which was ascribed to the reduction of the oxidized form of cysteamine as shown in Fig. 25A (b)[66]. Moreover, TGA-PdTeQDs as seen in **Figure 29A** (c), exhibited two cathodic peaks at -0.35 V and -0.75 V, respectively. The first cathodic peak was attributed to the reduction of Te⁰ to Te²⁻ [67] and the second cathodic peak was due to PdTeQDs. Quantum dots have been employed as a mediator to provide efficient electron transfer and as a stable platform for enzyme incorporated onto gold electrode. To understand this, the electrochemical responses of CYP2D6 enzyme immobilised onto Au and quantum dot-modified Au electrodes were studied under aerobic conditions. Notably, two cathodic responses were observed at -0.47 V and -0.64 V for direct immobilisation of CYP2D6 on bare Au. The reduction peaks could be attributed to the cleavage tryptophan residues present in CYP2D6 [68]. These results complemented PL results where tryptophan residues appeared at 307 nm and a shoulder at 360 nm. In comparison, CYP2D6/TGA-PdTeQDs/Cyst/Au exhibited a reduction peak at -0.75 V as shown in **Figure 29A** (e). The cathodic peak was attributed to the coupling between (NH₂) groups from the CYP2D6 enzyme and COOH group from TGA-capped PdTeQDs and an indication that TGA-PdTeQDs had not lost its electro-activity upon enzyme immobilisation. The coupling was also observed in UV-Vis where the energy level of the π - π^* electron transition decreases, and resulted in a shift to more negative potential in DPV measurements. In **Figure 29A** (f), CYP3A4/TGA-PdTeQDs/Cyst/Au revealed one cathodic

peak at -0.8 V which was attributed to monooxygenation. Clearly, the presence of tamoxifen in 0.1 M PBS resulted in an increase in peak current accompanied by a slight shift from -0.23 V to -0.26 V due to the adsorption of tamoxifen on gold electrode surface as illustrated in **Figure 25B** (a). This indicated a slow electron transfer between the electrolyte containing tamoxifen and the gold electrode surface. Compared to TAM-Au, cysteamine-modified electrode revealed two cathodic peaks at -0.5 V and -0.75 V which were attributed to cystamine and tertiary amine group present in tamoxifen's molecule [32,69]. Notably, the disappearance of an overlapping tamoxifen and PdTeQDs cathodic peak at -0.75 V in **Figure 29B** (c) was attributed to the filled d-orbital of palladium, since tamoxifen donated electrons through nitrogen group [70]. When cystamine was chemisorbed onto TGA-PdTe QDs in the presence of TAM in solution **Figure 29B** (d), the QDs on the thiol film had an influence on the interface property of the modified electrode and resulted in a slight shift in cathodic peak observed at -0.49 V due to the interaction between the cystamine and QDs. Further investigation for this interaction was observed in ATR-FTIR spectra. As it can be seen in **Figure 29B** (e) the presence of TAM in CYP2D6/TGA-PdTeQDs/Cyst/Au resulted in a shift followed by a decrease in cathodic peak at -0.21 V whereas TAM-CYP3A4/TGA-PdTeQDs/Cyst/Au gave a very small broad cathodic peak at -0.42 V. Several studies have focussed on addressing the role of CYP2D6 genotypes in patients receiving tamoxifen [71]. For instance, experimental studies by Coller and co-workers have demonstrated that the CYP2D6 genotype has an ability to form 4-OHT [72]. Hence in this study, TAM-CYP2D6-TGA-PdTeQDs/Cyst/Au was easily converted to more potent 4-OHT, since the cathodic peak appeared at less negative potential compared to TAM-CYP3A4-TGA-PdTeQDs/Cyst/Au.

The electrocatalytic responses of CYP2D6/TGA-PdTeQDs/Cyst/Au and CYP3A4/TGA-PdTeQDs/Cyst/Au biosensor systems to successive additions of TAM were studied in the

presence of oxygen in order to examine the interaction between the enzyme-oxygen and substrate at a potential window of 0.2 V to -0.8 V. As illustrated in **Figure 29** (C and D), only one cathodic peak was observed in both biosensor systems at -0.3 V and -0.28 V, which remarkably increased in the cathodic peak current and shifted to less negative potential after each TAM addition. This behaviour was attributed to the coupling of the fast electron transfer on the surface of the electrode with the reduction of TAM or within the biosensor film. Furthermore, these responses were expected since square wave voltammetry (SWV) is a more sensitive and appropriate technique for the detection of analytes at very low concentrations. **Figure 29** (E and F) shows the calibration curves drawn from linear regression of the biosensor responses. The sensitivities were derived from the calibration curve slopes $0.00859 \mu\text{A}/\text{pM}$ ($0.0110 \mu\text{A}/\text{pM}$) and the detection limits (*LOD*) were calculated to be $9.25 \times 10^{-5} \text{ ng/mL}$ ($1.95 \times 10^{-4} \text{ ng/mL}$) for CYP2D6/TGA-PdTeQDs/Cyst/Au (CYP3A4/TGA-PdTeQDs/Cyst/Au) biosensor systems. From these results, the developed biosensor systems can be able to detect samples or material from lower (nM) to higher (μM) concentrations. Since the past few years, suggestions have been made over TAM (approximately 92%) being primary demethylated by CYP3A4/5 to N-desmethylTAM (ND-TAM) followed by hydroxylation to endoxifen by CYP2D6 [10,73]. In contrast, hydroxylation pathway only contributes about 7% of tamoxifen metabolism [27]. This evidence comes from our findings obtained in **Figure 29(D)**, which confirmed that CYP3A4 converted approximately 92% TAM into N-desmethylTAM. The detection limits of the biosensor systems were compared with recent studies using different detection methods. The table below gives the relevant information. It was found that the two biosensor systems exhibited good performance. In addition, the results demonstrated that the two phenotype-based biosensor systems could be used to detect real samples. **Figure 30** describes the binding of TAM onto the active site of the CYP2D6 or CYP3A4 enzymes, followed by

reduction by electron and shift in spin state from low spin to high spin. Monooxygen onto the active site may lead to another electron reduction and formation of by-product

Table 2: Detection limits of tamoxifen using different detection methods (the original values are all converted to ng/mL)

Method	Limit of detection (<i>LOD</i>) (ng/mL)	References
HPLC-DA	55.7	[74]
LC-MS/MS	105	[75]
HF-LPME	0.5	[76]
LD-LC	1	[77]
CYP2D6/TGA- PdTeQDs/Cyst/Au	0.0000952	This work
CYP3A4/TGA- PdTeQDs/Cyst/Au	0.000195	This work

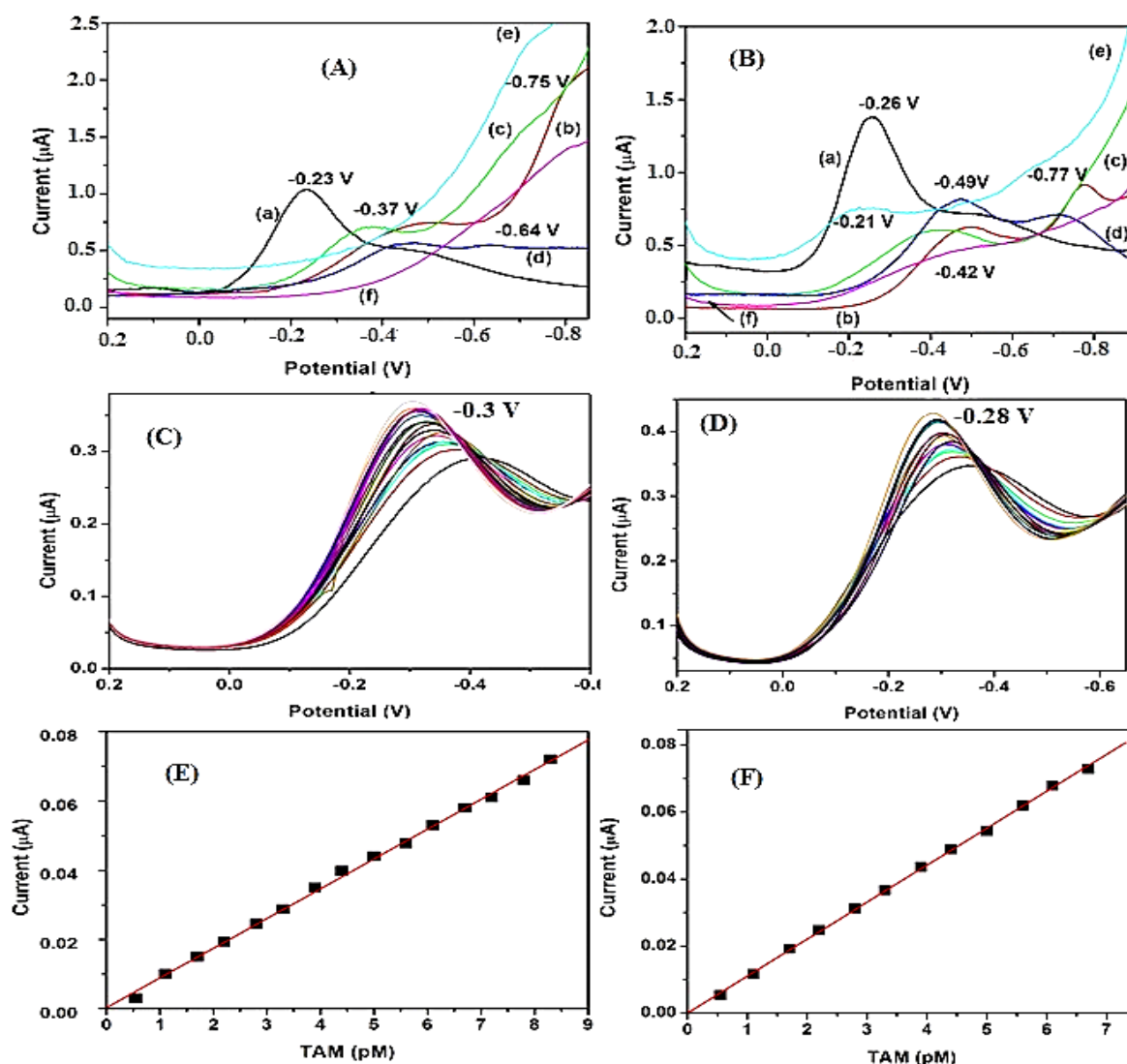


Figure 29: (A and B) DPVs of biosensor platform measured at a potential window (0.2 to -0.85 V) in 0.1 M BBS (pH 7.4) at 25 mV/s under aerobic conditions for (a) Bare Au, (b) Cyst (c) TGA-PdTeQDs, (d) CYP2D6/Au, (e) CYP2D6/TGA-PdTeQDs/Cyst/Au and (f) CYP3A4/TGA-PdTeQDs/Cyst/Au electrodes. (C and D) SWV measurements for (CYP2D6/TGA-PdTeQDs/Cyst/Au) and (CYP3A4/TGA-PdTeQDs/Cyst/Au) biosensor systems upon successive addition of tamoxifen concentrations 0.55 pM-11 pM. (E and F) corresponding calibration curves drawn from linear region of the biosensor systems.

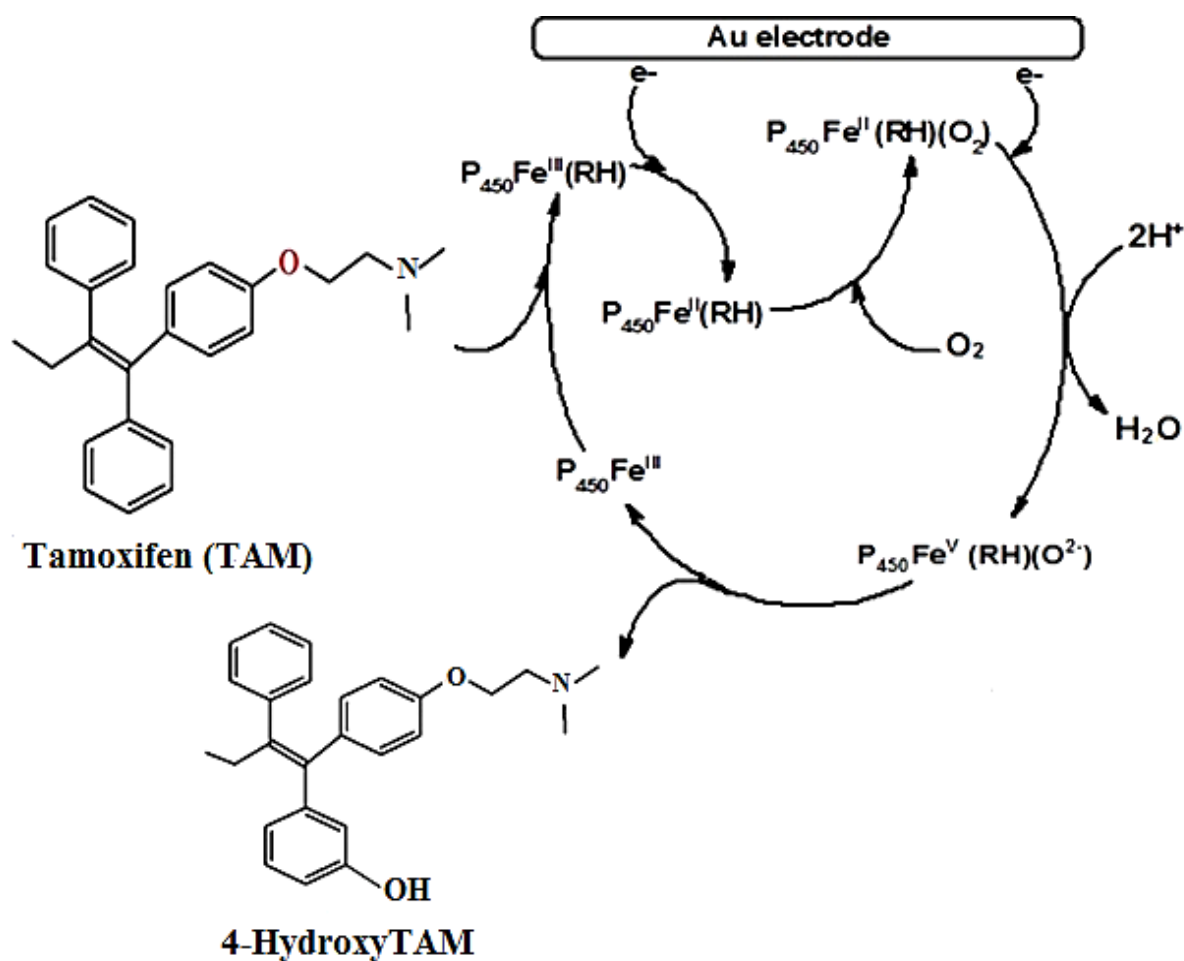


Figure 30: Scheme for the electrocatalytic mono-oxygenation reaction of TAM-bound cytochrome P450-3A4 or CYP2D6; where TAM and 4-HydroxyTAM refer to prodrug and its by-product, respectively.

5.3.2 Conversion of tamoxifen to its active metabolites

The conversion of tamoxifen was performed on a gold electrode surface under aerobic conditions at a potential window (0.2 V to -0.8 V), as shown in **Figure 31A**. The DPV signal of tamoxifen (**Figure 31A** (a)) in 0.1 M PBS exhibited a well-defined cathodic peak current at -0.33 V, which was attributed to the adsorption of tamoxifen onto gold electrode surface. The presence of CYP2D6 enzyme in solution containing TAM revealed three additional cathodic peaks at -0.81 V, -0.40 V and 0.1 5 V accompanied by a slight shift and decrease in

cathodic peak due to the interaction between CYP2D6 and tamoxifen **Figure 31A** (b). Moreover, the cathodic peak observed at -0.4 V was typical for reduction of the (Fe^{III}) to (Fe^{II}) on an electrode surface [78] while the cathodic peak observed at -0.81 V was ascribed to monooxygenation. In addition, DPV measurements revealed that CYP2D6 displayed electrochemical properties that are consistent with other reports of heme-thiolate proteins immobilized on gold electrode surface [79]. Furthermore, the cathodic peak appearing at 0.15 V was due to the reduction for bare gold electrode [80]. Literature suggested that the distance between the protonatable nitrogen atom in tamoxifen and the para position on the adjacent aromatic ring is $> 12 \text{ \AA}$, which is usually 5 \AA greater than the upper limit for CYP2D6 substrate specificity with regards to the currently accepted template model [81]. Interestingly, recent reports have focussed on genetic and environmental factors that causes a change in CYP2D6 activity and affect TAM treatment outcomes. Moreover, fewer suggestions have been made towards CYP2D6 genetic variants which causes a decrease in enzyme's activity resulting in significantly reduction in conversion of TAM to 4-OH-TAM and endoxifen [82,83]. This, therefore provides an evidence for the decrease and a shift to more negative potential obtained in our study. Under aerobic conditions, the presence of CYP3A4 in CYP2D6-TAM solution resulted in a decrease and slight shift in cathodic peak from -0.4 V to -0.42 V due to the formation of an active metabolite endoxifen as shown in **Figure 31A** (c). Palladium telluride quantum dots coated on the bare gold electrode act as an effective layer that promotes electron transfer. When CYP2D6 enzyme was drop-casted on TGA-PdTeQDs/Cyst/Au modified electrode **Figure 31C** (insert black line), two cathodic peaks were observed at -0.69 V, -0.43 V and appeared at lower current intensity than in **Figure 31C** (insert red line). The cathodic peak observed at -0.69 V could be attributed to the interaction between QDs and CYP2D6 enzyme which might result in several conformational changes in the microenvironment surrounding CYP2D6 that may affect the bioactivity and

electrochemical properties of the immobilized protein. However, the electrochemical properties of TGA-PdTeQDs and cystamine showed a decrease in peak current at -0.82 V in the presence of tamoxifen due to $n-\pi^*$ electron transition due to the interaction between strong amide (N-H) bond formed by QDs and cystamine and the lone pair of nitro group present in tamoxifen as shown in **Figure 31C** (a). Time dependent studies were performed to monitor the electrochemical behaviour of tamoxifen in the presence of both enzymes as shown in **Figure 31 (B and D)**. For TAM and TAM-CYP2D6-CYP3A4, a decrease in peak current with increasing time was observed resulting in the formation of an active metabolite endoxifen. Moreover, these results are in good accordance with UV-Vis and PL measurements.



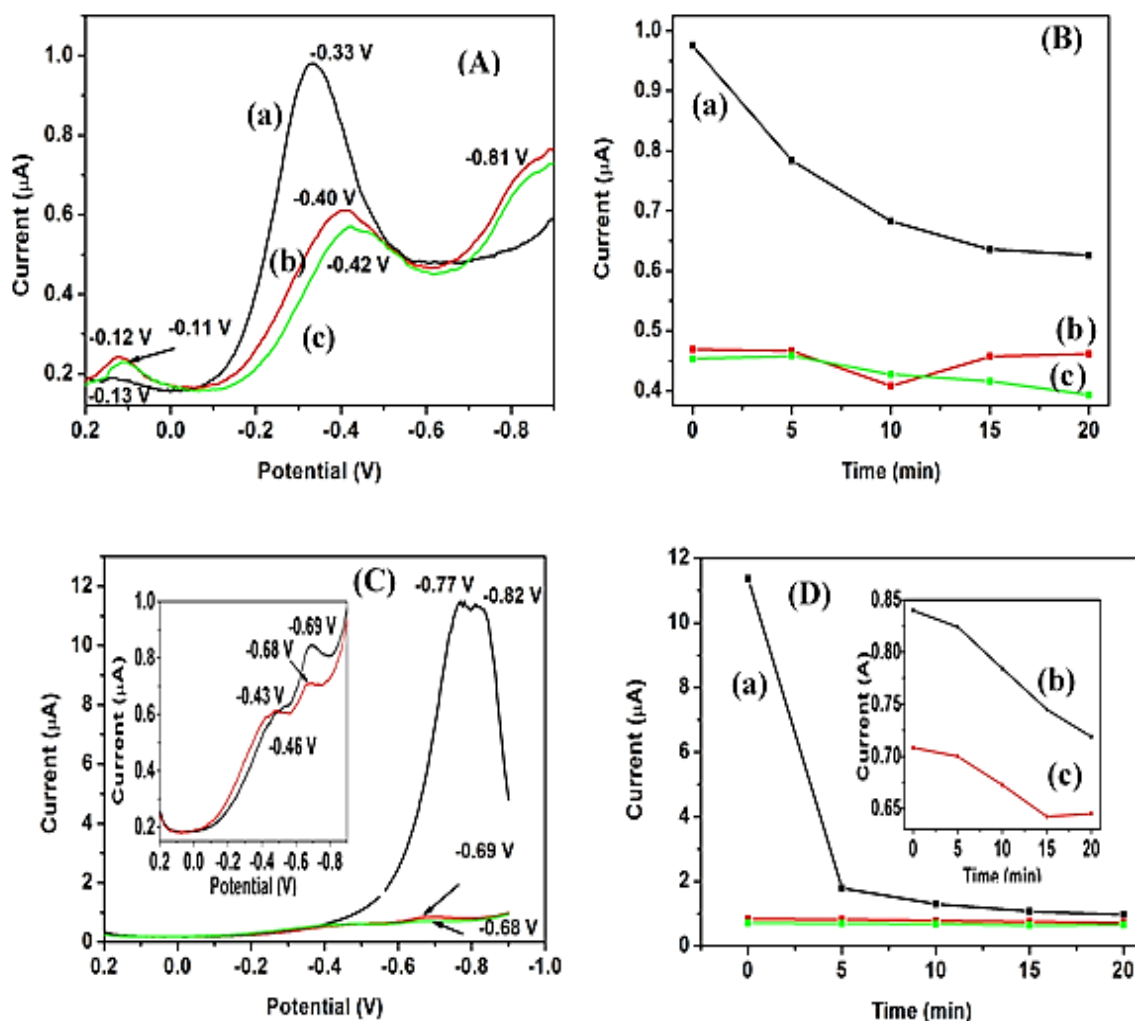


Figure 31: (A and C) DPVs recorded at a potential window 0.2 to -0.85 V in 0.1 M PBS pH 7.4 for (a) TAM, (b) TAM-CYP2D6 and (c) TAM-CYP2D6-CYP3A4 and (C) (black line) TAM- (TGA-PdTeQDs/Cyst/Au), (red line) TAM-CYP2D6-(TGA-PdTeQDs)/Cyst/Au and (green in) TAM -(CYP3A4-CYP2D6-(TGA-PdTeQDs)/Cyst/Au, respectively. (B and D) time dependent studies performed at (0-20 min) for (a) TAM, (b) TAM-CYP2D6 and (c) TAM-CYP2D6-CYP3A4; (a) TAM- (TGA-PdTeQDs/Cyst/Au), (b) TAM-CYP2D6-(TGA-PdTeQDs)/Cyst/Au and (c) TAM -(CYP3A4-CYP2D6-(TGA-PdTeQDs)/Cyst/Au, respectively.

Attempts have been made by several studies trying to define the primary metabolism of TAM in humans. Notably, demethylation of the aminoethoxy side chain to N-desmethylTAM has been regarded as the main route of TAM metabolism [9]. In comparison with CYP2D6, CYP3A4 has a relatively larger active site which could lead to alternative docking interactions for tamoxifen since one side of the heme pocket appears to contain several aromatic amino acid residues that is mainly predicted and competent of binding tamoxifen via its phenyl ring moieties. As illustrated in **Figure 32A** (b and c), the presence of CYP3A4 in TAM solution resulted in a slight shift in cathodic peak current from -0.27 V to -0.3 V. The shift was ascribed to the conversion of TAM to NDMT. In contrast with CYP2D6-TAM and CYP3A4-CYP2D6-TAM as shown in **Figure 31** (b and c), CYP3A4-TAM and CYP2D6-CYP3A4-TAM obtained higher peak current intensities by values of 0.5 μ A and 0.37 μ A, respectively. These values confirmed that CYP3A4 is a major catalyst which converts 92% TAM to its active metabolite NDMT. However, the disappearance of tamoxifen peak observed at -0.82 V in **Figure 32(c)**, was attributed to hydrophobic contact between one of the putative active site aliphatic amino acid residues and the ethyl group of tamoxifen, which gives further support to enzyme-substrate interaction. The presence of both CYP2D6 and CYP3A4 enzymes in TAM-(TGA-PdTeQDs/Cyst/Au) revealed a distinctive number of cathodic peaks at -0.82 V, -0.76 V, -0.31 V and -0.23 V respectively. The changes in peak current were attributed to the conversion of tamoxifen to an intermediate (NDMT) by CYP3A4 followed by hydroxylation by CYP2D6 to the formation of endoxifen. Moreover, the reduction peaks observed at -0.31 V and -0.228 V, indicate that the conversion was faster. This, therefore, provides evidence that CYP3A4 is a major catalyst. Compared to **Figure 31B**, the peak current intensities appeared higher than in TAM alone, as observed in **Figure 32B**.

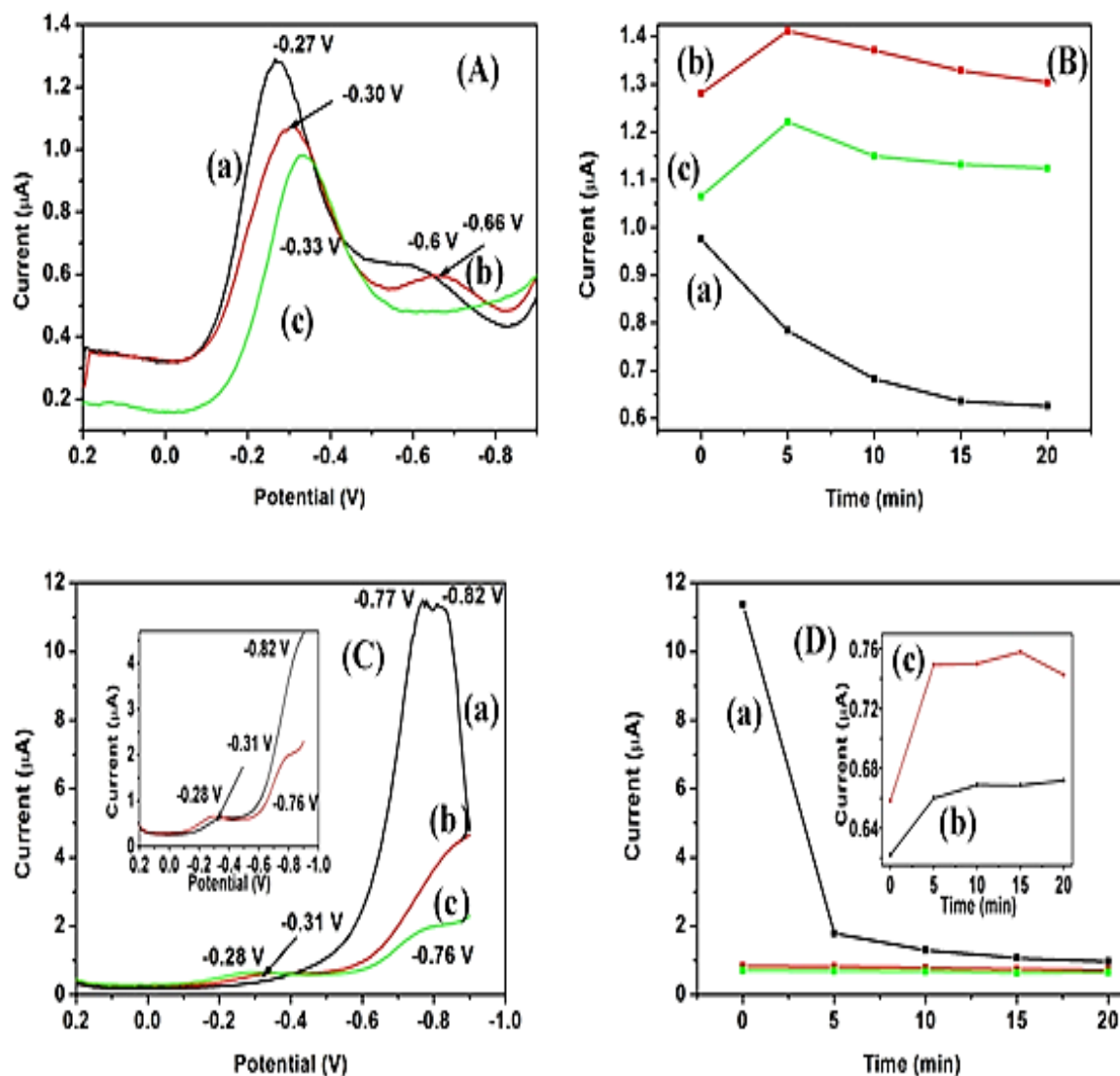


Figure 32: (A and C) DPV experiments recorded at a potential window (0.2 to -0.85 V) for (a)TAM, (b) TAM-CYP3A4 and (c) TAM-CYP3A4-CYP2D6. (C) for TAM- (TGA-PdTeQDs/Cyst/Au modified), (b)TAM-CYP3A4-(TGA-PdTeQDs)/Cyst/Au) and (c) TAM - (CYP2D6-CYP3A4-(TGA-PdTeQDs)/Cyst/Au). (B and D) time dependent studies performed at (0-20 min) for (a) TAM, (b) TAM-CYP3a4 and (c) TAM-CYP3A4-CYP2D6; (a) TAM-(TGA-PdTeQDs/Cyst/Au), (b)TAM-CYP3A4-(TGA-PdTeQDs)/Cyst/Au) and (c) TAM - (CYP2D6-CYP3A4-(TGA-PdTeQDs)/Cyst/Au, respectively.

5.4 Conclusion

This study has been conducted to develop electrochemical phenotype nanobiosensors for detection of breast cancer drug, tamoxifen. The nanobiosensors employed two heme-thiolate enzymes heme enzymes CYP2D6 and CYP3A4 which converted tamoxifen prodrug to its active metabolite, endoxifen. ATR-FTIR, UV-Vis, XPS, Raman, XRD results confirmed a successful synthesis of the novel TGA-PdTeQDs. Calibration curves drawn from linear region were used to determine the sensitivity and detection limits of the biosensor systems. CYP2D6/TGA-PdTeQDs/Cyst/Au gave sensitivity value of 0.00859 $\mu\text{A}/\text{pM}$ and detection limit of 9.52×10^{-5} ng/mL tamoxifen at a square wave voltammetry (SWV) potential of 0.3 V, while CYP3A4/TGA-PdTeQDs/Cyst/Au gave a sensitivity value of 0.0110 $\mu\text{A}/\text{pM}$ and *LOD* value of 1.95×10^{-4} ng/mL tamoxifen at a SWV potential of 0.28 V, respectively. The obtained detection limits are much lower than the allowable daily intake of tamoxifen recommended by the FDA. This, therefore, indicates that CYP450 (3A4 and 2D6) enzymes are suitable for determining tamoxifen and may be suitable for point-of-care analysis. Moreover, approximately 92% of TAM was converted to N-desmethylTAM and hydroxylated by about 7% by CYP2D6 to its active metabolite, endoxifen. Thus, the CYP3A4 enzyme has been found to be a major catalyst for N-desmethylTAM.

References

- [1] V. Craig Jordan, Antiestrogenic Action of Raloxifene and Tamoxifen: Today and Tomorrow, *JNCI J. Natl. Cancer Inst.* 90 (1998) 967–971. doi:10.1093/jnci/90.13.967.
- [2] I.A. Jaiyesimi, A.U. Buzdar, D.A. Decker, G.N. Hortobagyi, Use of tamoxifen for breast cancer: Twenty-eight years later, *J. Clin. Oncol.* 13 (1995) 513–529. doi:10.1200/jco.1995.13.2.513.
- [3] D.C. Tormey, R.M. Simon, M.E. Lippman, J.M. Bull, C.E. Myers, Evaluation of tamoxifen dose in advanced breast cancer: a progress report, *Cancer Treat Rep.* 60 (1976) 1451–1459.
- [4] N. Von Ahsen, C. Binder, J. Brockmoller, M. Oellerich, CYP2D6 and tamoxifen: Pharmacogenetic reinvention of an established drug?, *LaboratoriumsMedizin.* 33 (2009) 293–302.
<http://www.embase.com/search/results?subaction=viewrecord&from=export&id=L355315127>.
- [5] V.C. Jordan, Tamoxifen (ICI46,474) as a targeted therapy to treat and prevent breast cancer, *Br. J. Pharmacol.* 147 (2009) S269–S276. doi:10.1038/sj.bjp.0706399.
- [6] V.C. Jordan, L.J. Dowse, Tamoxifen as an anti tumour agent: effect on oestrogen binding, *J. Endocrinol.* 68 (1976) 297–303. doi:10.1677/joe.0.0680297.
- [7] Y.C. Lim, Z. Desta, D.A. Flockhart, T.C. Skaar, Endoxifen (4-hydroxy-N-desmethyl-tamoxifen) has anti-estrogenic effects in breast cancer cells with potency similar to 4-hydroxy-tamoxifen, *Cancer Chemother. Pharmacol.* 55 (2005) 471–478. doi:10.1007/s00280-004-0926-7.
- [8] J. Gjerde, E.R. Kisanga, M. Hauglid, P.I. Holm, G. Mellgren, E.A. Lien, Identification and quantification of tamoxifen and four metabolites in serum by liquid chromatography-tandem mass spectrometry, *J. Chromatogr. A.* 1082 (2005) 6–14.

- doi:10.1016/j.chroma.2005.01.004.
- [9] Y. Jin, Z. Desta, V. Stearns, B. Ward, H. Ho, K.H. Lee, T. Skaar, A.M. Storniolo, L. Li, A. Araba, R. Blanchard, A. Nguyen, L. Ullmer, J. Hayden, S. Lemler, R.M. Weinshilboum, J.M. Rae, D.F. Hayes, D.A. Flockhart, CYP2D6 genotype, antidepressant use, and tamoxifen metabolism during adjuvant breast cancer treatment, *J. Natl. Cancer Inst.* 97 (2005) 30–39. doi:10.1093/jnci/dji005.
- [10] Z. Desta, Comprehensive Evaluation of Tamoxifen Sequential Biotransformation by the Human Cytochrome P450 System in Vitro: Prominent Roles for CYP3A and CYP2D6, *J. Pharmacol. Exp. Ther.* 310 (2004) 1062–1075. doi:10.1124/jpet.104.065607.
- [11] H.K. Lim, S. Stellingweif, S. Sisenwine, K.W. Chan, Rapid drug metabolite profiling using fast liquid chromatography, automated multiple-stage mass spectrometry and receptor-binding, *J. Chromatogr. A.* 831 (1999) 227–241. doi:10.1016/S0021-9673(98)00956-X.
- [12] M. Furlanut, L. Franceschi, E. Pasqual, S. Bacchetti, D. Poz, G. Giorda, P. Cagol, Tamoxifen and its main metabolites serum and tissue concentrations in breast cancer women., *Ther. Drug Monit.* 29 (2007) 349–52. doi:10.1097/FTD.0b013e318067ded7.
- [13] R.M. Jones, Z.X. Yuan, J.H. Lamb, C.K. Lim, On-line high-performance liquid chromatographic-electrospray ionization mass spectrometric method for the study of tamoxifen metabolism, in: *J. Chromatogr. A*, 1996: pp. 249–255. doi:10.1016/0021-9673(95)00794-6.
- [14] E.A. Lien, E. Solheim, S. Kvinnsland, H. Bile, P.M. Ueland, Identification of 4-Hydroxy- N -desmethyltamoxifen as a Metabolite of Tamoxifen in Human Bile
Identification of 4-Hydroxy- / V-desmethyltamoxifen as a Metabolite of Tamoxifen in, (1988) 2304–2308.

- [15] P. Mushonga, M.O. Onani, A.M. Madiehe, M. Meyer, One-pot synthesis and characterization of InP/ZnSe semiconductor nanocrystals, *Mater. Lett.* 95 (2013) 37–39. doi:10.1016/j.matlet.2012.12.102.
- [16] N.J. Ronkainen, S.L. Okon, Nanomaterial-based electrochemical immunosensors for clinically significant biomarkers, *Materials (Basel)*. 7 (2014) 4669–4709. doi:10.3390/ma7064669.
- [17] M.S. P. Bharara Sean; Atwood, David A., Solution behavior of Hg(II)-cystamine by Uv-Vis and Hg NMR, *Main Gr. Chem.* 4 (2005) 217–225. doi:10.1080/10241220600595450.
- [18] X. Xu, R. Ray, Y. Gu, H.J. Ploehn, L. Gearheart, K. Raker, W.A. Scrivens, Electrophoretic Analysis and Purification of Fluorescent Single-Walled Carbon Nanotube Fragments, *J. Am. Chem. Soc.* 126 (2004) 12736–12737. doi:10.1021/ja040082h.
- [19] J. Shao, J. Chen, T. Li, X. Zhao, Spectroscopic and molecular docking studies of the in vitro interaction between Puerarin and Cytochrome P450, *Molecules*. 19 (2014) 4760–4769. doi:10.3390/molecules19044760.
- [20] F.B. Zhang, Y.. b Ni, A comparison study on the interaction of Sunset yellow and β -carotene with bovine serum albumin, *Acta Chim. Sin.* 70 (2012) 1379–1384. doi:10.6023/A1112156.
- [21] D.J. Boocock, K. Brown, A.H. Gibbs, E. Sanchez, K.W. Turteltaub, I.N.H. White, Identification of human CYP forms involved in the activation of tamoxifen and irreversible binding to DNA, *Carcinogenesis*. 23 (2002) 1897–1901. doi:10.1093/carcin/23.11.1897.
- [22] A. Coletta, S. Castelli, G. Chillemi, N. Sanna, M. Cushman, Y. Pommier, A. Desideri, Solvent Dependency of the UV-Vis Spectrum of Indenoisoquinolines: Role of Keto-

- Oxygens as Polarity Interaction Probes, *PLoS One*. 8 (2013). doi:10.1371/journal.pone.0073881.
- [23] G.Y. Stokes, J.C. Conboy, Measuring selective estrogen receptor modulator (SERM)-membrane interactions with second harmonic generation, *J. Am. Chem. Soc.* 136 (2014) 1409–1417. doi:10.1021/ja409250y.
- [24] S.A. Oladepo, K. Xiong, Z. Hong, S.A. Asher, J. Handen, I.K. Lednev, UV resonance raman investigations of peptide and protein structure and dynamics, *Chem. Rev.* 112 (2012). doi:10.1021/cr200198a.
- [25] W.-J. Yin, J.-H. Yang, J. Kang, Y. Yan, S.-H. Wei, Halide perovskite materials for solar cells: a theoretical review, *J. Mater. Chem. A*. 3 (2015) 8926–8942. doi:10.1039/C4TA05033A.
- [26] E.H. EL-Mossalamy S.A. AL-Thabati, F.M. AL-Nowaiser, Q.A. AL-Sulami, Solvent effects on the electronic absorption spectra and dissociation constants of some sulfa drugs, *Commun Fac. Sci. Univ. Ank. Series B*. 51 (2005) 21-30.
- [27] J. Zhao, A. Das, G.C. Schatz, S.G. Sligar, R.P. Van Duyne, Resonance localized surface plasmon spectroscopy: Sensing substrate and inhibitor binding to cytochrome P450, *J. Phys. Chem. C*. 112 (2008) 13084–13088. doi:10.1021/jp801719c.
- [28] P.J. Mak, I.G. Denisov, Y. V. Grinkova, S.G. Sligar, J.R. Kincaid, Defining CYP3A4 structural responses to substrate binding. raman spectroscopic studies of a nanodisc-incorporated mammalian cytochrome P450, *J. Am. Chem. Soc.* 133 (2011) 1357–1366. doi:10.1021/ja105869p.
- [29] A. Luthra, I.G. Denisov, S.G. Sligar, Spectroscopic features of cytochrome P450 reaction intermediates, *Arch. Biochem. Biophys.* 507 (2011) 26–35. doi:10.1016/j.abb.2010.12.008.
- [30] J. Duan, L. Song, J. Zhan, One-pot synthesis of highly luminescent CdTe quantum

- dots by microwave irradiation reduction and their Hg²⁺-sensitive properties, *Nano Res.* 2 (2009) 61–68. doi:10.1007/s12274-009-9004-0.
- [31] I.F. Sevrioukova, T.L. Poulos, Understanding the mechanism of cytochrome P450 3A4: recent advances and remaining problems, *Dalt. Trans.* 42 (2013) 3116–3126. doi:10.1039/C2DT31833D.
- [32] J.M.P.J. Garrido, E. Quezada, J.L.C. Fajín, M.N.D.S. Cordeiro, E.M.P.J. Garrido, F. Borges, Electrochemical oxidation of tamoxifen revisited, *Int. J. Electrochem. Sci.* 8 (2013) 5710–5723.
- [33] A. Michota, A. Kudelski, J. Bukowska, Influence of electrolytes on the structure of cysteamine monolayer on silver studied by surface-enhanced Raman scattering, *J. Raman Spectrosc.* 32 (2001) 345–350. doi:10.1002/jrs.703.
- [34] P. Sakthivel, S. Muthukumar, M. Ashokkumar, Structural, band gap and photoluminescence behaviour of Mn-doped ZnS quantum dots annealed under Ar atmosphere, *J. Mater. Sci. Mater. Electron.* 26 (2015) 1533–1542. doi:10.1007/s10854-014-2572-0.
- [35] D.R. Davydov, J.A.O. Rumfeldt, E. V Sineva, H. Fernando, N.Y. Davydova, J.R. Halpert, Peripheral ligand-binding site in cytochrome P450 3A4 located with fluorescence resonance energy transfer (FRET)., *J. Biol. Chem.* 287 (2012) 6797–809. doi:10.1074/jbc.M111.325654.
- [36] C. Tamoxifen, D.W. Mendenhall, A. Kobayashi, F. Mel, L. Shih, L.A. Sternson, C. Fabian, Clinical Analysis of Tamoxifen, an Anti-Neoplastic Agent, in Plasma, *Components.* 1524 (1978) 1518–1524.
- [37] I.F. Sevrioukova, T.L. Poulos, Current approaches for investigating and predicting cytochrome P450 3A4-ligand interactions, *Adv. Exp. Med. Biol.* 851 (2015) 83–105. doi:10.1007/978-3-319-16009-2_3.

- [38] N.P. Mullin, A. Gagliardi, L.T.P. Khoa, D. Colby, E. Hall-Ponsele, A.J. Rowe, I. Chambers, Distinct Contributions of Tryptophan Residues within the Dimerization Domain to Nanog Function, *J. Mol. Biol.* (2016). doi:10.1016/j.jmb.2016.12.001.
- [39] P. Bourassa, S. Dubeau, G.M. Maharvi, A.H. Fauq, T.J. Thomas, H.A. Tajmir-Riahi, Binding of antitumor tamoxifen and its metabolites 4-hydroxytamoxifen and endoxifen to human serum albumin, *Biochimie.* 93 (2011) 1089–1101. doi:10.1016/j.biochi.2011.03.006.
- [40] E.M. Isin, F.P. Guengerich, Substrate binding to cytochromes P450, *Anal. Bioanal. Chem.* 392 (2008) 1019–1030. doi:10.1007/s00216-008-2244-0.
- [41] R. Lange, P. Anzenbacher, S. Müller, L. Maurin, C. Balny, Interaction of Tryptophan Residues of Cytochrome P450_{scc} with a Highly Specific Fluorescence Quencher, a Substrate Analogue, Compared to Acrylamide and Iodide, *Eur. J. Biochem.* 226 (1994) 963–970. doi:10.1111/j.1432-1033.1994.00963.x.
- [42] M.R. Shaik, Z.J.Q. Ali, M. Khan, M. Kuniyil, M.E. Assal, H.Z. Alkathlan, A. Al-Warthan, M.R.H. Siddiqui, M. Khan, S.F. Adil, Green Synthesis and Characterization of Palladium Nanoparticles Using *Origanum vulgare* L. Extract and Their Catalytic Activity., *Molecules.* 22 (2017) 165. doi:10.3390/molecules22010165.
- [43] Y. Piao, Y. Jang, M. Shokouhimehr, I.S. Lee, T. Hyeon, Facile aqueous-phase synthesis of uniform palladium nanoparticles of various shapes and sizes, *Small.* 3 (2007) 255–260. doi:10.1002/sml.200600402.
- [44] X. Chen, L. Li, Y. Lai, J. Yan, Y. Tang, X. Wang, Microwave-assisted synthesis of glutathione-capped CdTe/CdSe near-infrared quantum dots for cell imaging, *Int. J. Mol. Sci.* 16 (2015) 11500–11508. doi:10.3390/ijms160511500.
- [45] C.I. do L. Santos, M.S. Carvalho, E. Raphael, C. Dantas, J.L. Ferrari, M.A. Schiavon, Synthesis, Optical Characterization, and Size Distribution Determination by Curve

- Resolution Methods of Water-Soluble CdSe Quantum Dots, *Mater. Res.* 19 (2016) 1407–1416. doi:10.1590/1980-5373-mr-2016-0121.
- [46] F.O. Silva, M.S. Carvalho, R. Mendonca, W. a a Macedo, K. Balzuweit, P. Reiss, M. a Schiavon, Effect of surface ligands on the optical properties of aqueous soluble CdTe quantum dots, *Nanoscale Res. Lett.* 7 (2012) 536. doi:10.1186/1556-276X-7-536.
- [47] Y. Yang, X. Ding, T. Zou, G. Peng, H. Liu, Y. Fan, C.T. Lim, K.P. Loh, K.S. Novoselov, S. Roth, A.K. Geim, Preparation and characterization of electrospun graphene/silk fibroin conductive fibrous scaffolds, *RSC Adv.* 7 (2017) 7954–7963. doi:10.1039/C6RA26807B.
- [48] S.H. Shin, J. Bajaj, L.A. Moudy, D.T. Cheung, Characterization of Te precipitates in CdTe crystals, *Appl. Phys. Lett.* 43 (1983) 68–70. doi:10.1063/1.94123.
- [49] S.J. Byrne, S.A. Corr, T.Y. Rakovich, Y.K. Gun'ko, Y.P. Rakovich, J.F. Donegan, S. Mitchell, Y. Volkov, Optimisation of the synthesis and modification of CdTe quantum dots for enhanced live cell imaging, *J. Mater. Chem.* 16 (2006). doi:10.1039/b605333e.
- [50] H. Borchert, D. V. Talapin, N. Gaponik, C. McGinley, S. Adam, A. Lobo, T. Möller, H. Weller, Relations between the Photoluminescence Efficiency of CdTe Nanocrystals and Their Surface Properties Revealed by Synchrotron XPS, *J. Phys. Chem. B.* 107 (2003) 9662–9668. doi:10.1021/jp0352884.
- [51] S.M. Baesman, T.D. Bullen, J. Dewald, D. Zhang, S. Curran, F.S. Islam, T.J. Beveridge, R.S. Oremland, Formation of Tellurium Nanocrystals during Anaerobic Growth of Bacteria That Use Te Oxyanions as Respiratory Electron Acceptors □, 73 (2007) 2135–2143. doi:10.1128/AEM.02558-06.
- [52] A.G. Milekhin, L.L. Sveshnikova, T. a Duda, N. V Surovtsev, S. V Adichtchev, Y.M. Azhniuk, C. Himcinschi, M. Kehr, D.R.T. Zahn, Resonance effects in Raman scattering of quantum dots formed by the Langmuir-Blodgett method, *J. Phys. Conf.*

- Ser. 245 (2010) 12045. doi:10.1088/1742-6596/245/1/012045.
- [53] J. Heo, C.-S. Hwang, Surface Properties and Photocatalytic Activities of the Colloidal ZnS:Mn Nanocrystals Prepared at Various pH Conditions, *Nanomaterials*. 5 (2015) 1955–1970. doi:10.3390/nano5041955.
- [54] J.S.W. Mak, A.A. Farah, F. Chen, A.S. Helmy, Photonic crystal fiber for efficient Raman scattering of CdTe quantum dots in aqueous solution, *ACS Nano*. 5 (2011) 3823–3830. doi:10.1021/nm200157z.
- [55] Y.F. Liu, J.S. Yu, Selective synthesis of CdTe and high luminescence CdTe/CdS quantum dots: The effect of ligands, *J. Colloid Interface Sci.* 333 (2009) 690–698. doi:10.1016/j.jcis.2009.01.008.
- [56] Z. Li, J. Gao, X. Xing, S. Wu, S. Shuang, C. Dong, M.C. Paau, M.M.F. Choi, Synthesis and Characterization of n -Alkylamine-Stabilized Palladium Nanoparticles for Electrochemical Oxidation of Methane, *J. Phys. Chem. C*. 114 (2010) 723–733. doi:10.1021/jp907745v.
- [57] Z. Sun, Z. Liu, B. Han, S. Miao, Z. Miao, G. An, Decoration carbon nanotubes with Pd and Ru nanocrystals via an inorganic reaction route in supercritical carbon dioxide-methanol solution, *J. Colloid Interface Sci.* 304 (2006) 323–328. doi:10.1016/j.jcis.2006.09.029.
- [58] R.W. Raut, A.S.M. Haroon, Y.S. Malghe, B.T. Nikam, S.B. Kashid, Rapid biosynthesis of platinum and palladium metal nanoparticles using root extract of asparagus racemosus linn, *Adv. Mater. Lett.* 4 (2013) 650–654. doi:10.5185/amlett.2012.11470.
- [59] J. Ma, J. Chen, J. Guo, C.-C. Wang, W.-L. Yang, N.-H. Cheung, P.-N. Wang, Improvement of the photostability of thiol-capped CdTe quantum dots in aqueous solutions and in living cells by surface treatment, *Nanotechnology*. 17 (2006) 5875–

5881. doi:10.1088/0957-4484/17/23/027.
- [60] N.T. Vo, H.D. Ngo, N. Phuong, D. Thi, K. Phung, N. Thi, A.P. Duong, V. Lam, Stability Investigation of Ligand-Exchanged CdSe / ZnS-Y (Y = 3-Mercaptopropionic Acid or Mercaptosuccinic Acid) through Zeta Potential Measurements, 2016 (2016).
- [61] R. Song, Y. Liu, L. He, Synthesis and characterization of mercaptoacetic acid-modified ZnO nanoparticles, *Solid State Sci.* 10 (2008) 1563–1567. doi:10.1016/j.solidstatesciences.2008.02.006.
- [62] R. Xie, Y. Li, L. Liu, L. Yang, D. Xiao, J. Zhu, Aqueous-based route toward Fe:ZnSe semiconductor nanocrystals: Synthesis and characterization, *Mater. Charact.* 62 (2011) 582–587. doi:10.1016/j.matchar.2011.03.016.
- [63] D. Agudelo, S. Sanyakamdhorn, S. Nafisi, H.A. Tajmir-Riahi, Transporting Antitumor Drug Tamoxifen and Its Metabolites, 4-Hydroxytamoxifen and Endoxifen by Chitosan Nanoparticles, *PLoS One.* 8 (2013). doi:10.1371/journal.pone.0060250.
- [64] R. Maji, N.S. Dey, B.S. Satapathy, B. Mukherjee, S. Mondal, Preparation and characterization of tamoxifen citrate loaded nanoparticles for breast cancer therapy, *Int. J. Nanomedicine.* 9 (2015) 3107–3118. doi:10.2147/IJN.S63535.
- [65] P. Phukan, D. Saikia, Optical and structural investigation of cdse quantum dots dispersed in PVA matrix and photovoltaic applications, *Int. J. Photoenergy.* 2013 (2013). doi:10.1155/2013/728280.
- [66] I.S. El-Hallag, A.O. Al-Youbi, A.Y. Obaid, E.H. El-Mossalamy, S.A. El-Daly, A.M. Asiri, Electrochemical investigation of cysteamine at carbon fiber microdisk electrode, *J. Chil. Chem. Soc.* 56 (2011) 837–841. doi:10.4067/S0717-97072011000400003.
- [67] R.K. Sharma, G. Singh, Y.G. Shul, H. Kim, Mechanism of manganese (mono and di) telluride thin-film formation and properties, *Phys. B Condens. Matter.* 390 (2007) 314–319. doi:10.1016/j.physb.2006.08.031.

- [68] A.M.M. Antunes, A.L.A. Godinho, I.L. Martins, M.C. Oliveira, R.A. Gomes, A. V. Coelho, F.A. Beland, M.M. Marques, Protein adducts as prospective biomarkers of nevirapine toxicity, *Chem. Res. Toxicol.* 23 (2010) 1714–1725. doi:10.1021/tx100186t.
- [69] J. Ghilane, P. Martin, H. Randriamahazaka, J.C. Lacroix, Electrochemical oxidation of primary amine in ionic liquid media: Formation of organic layer attached to electrode surface, *Electrochem. Commun.* 12 (2010) 246–249. doi:10.1016/j.elecom.2009.12.005.
- [70] A.C. Sather, H.G. Lee, V.Y. De La Rosa, Y. Yang, P. Müller, S.L. Buchwald, A Fluorinated Ligand Enables Room-Temperature and Regioselective Pd-Catalyzed Fluorination of Aryl Triflates and Bromides, *J. Am. Chem. Soc.* 137 (2015) 13433–13438. doi:10.1021/jacs.5b09308.
- [71] P. Wegman, L. Vainikka, O. Stål, B. Nordenskjöld, L. Skoog, L.-E. Rutqvist, S. Wingren, Genotype of Metabolic Enzymes and the Benefit of Tamoxifen in Postmenopausal Breast Cancer Patients., *Breast Cancer Res.* 7 (2005) R284-90. doi:10.1186/bcr993.
- [72] J.K. Coller, N. Krebsfaenger, K. Klein, K. Endrizzi, R. Wolbold, T. Lang, A. Nüssler, P. Neuhaus, U.M. Zanger, M. Eichelbaum, T.E. Mürdter, The influence of CYP2B6, CYP2C9 and CYP2D6 genotypes on the formation of the potent antioestrogen Z-4-hydroxy-tamoxifen in human liver, *Br. J. Clin. Pharmacol.* 54 (2002) 157–167. doi:10.1046/j.1365-2125.2002.01614.x.
- [73] J.A. De Souza, O.I. Olopade, CYP2D6 genotyping and tamoxifen: An unfinished story in the quest for personalized medicine, *Semin. Oncol.* 38 (2011) 263–273. doi:10.1053/j.seminoncol.2011.01.002.
- [74] M.V. Antunes, D.D. Rosa, T. dos S. Viana, H. Andreolla, T.O. Fontanive, R. Linden,

- Sensitive HPLC-PDA determination of tamoxifen and its metabolites N-desmethyltamoxifen, 4-hydroxytamoxifen and endoxifen in human plasma, *J. Pharm. Biomed. Anal.* 76 (2013) 13–20. doi:10.1016/j.jpba.2012.12.005.
- [75] D.D. Heath, S.W. Flatt, A.H.B. Wu, M.A. Pruitt, C.L. Rock, Evaluation of tamoxifen and metabolites by LC-MS/MS and HPLC methods, *Br. J. Biomed. Sci.* 71 (2014) 33–39. doi:10.1016/j.biotechadv.2011.08.021.Secreted.
- [76] A. Kashtiaray, H. Farahani, S. Farhadi, B. Rochat, H.R. Sobhi, Trace Determination of Tamoxifen in Biological Fluids Using Hollow Fiber Liquid-Phase Microextraction Followed by High-Performance Liquid Chromatography-Ultraviolet Detection, *Am. J. Anal. Chem.* 2 (2011) 429–436. doi:10.4236/ajac.2011.24052.
- [77] E.A. Lien, P.M. Ueland, E. Solheim, S. Kvinnsland, Determination of tamoxifen and four metabolites in serum by low-dispersion liquid chromatography, *Clin. Chem.* 33 (1987) 1608–1614.
- [78] M. Yang, J.L. Kabulski, L. Wollenberg, X. Chen, M. Subramanian, T.S. Tracy, D. Lederman, P.M. Gannett, N. Wu, Electrocatalytic drug metabolism by CYP2C9 bonded to A self-assembled monolayer-modified electrode, *Drug Metab. Dispos.* 37 (2009) 892–899. doi:10.1124/dmd.108.025452.
- [79] K.D. Hagen, J.M. Gillan, S.C. Im, S. Landefeld, G. Mead, M. Hiley, L.A. Waskell, M.G. Hill, A.K. Udit, Electrochemistry of mammalian cytochrome P450 2B4 indicates tunable thermodynamic parameters in surfactant films, *J. Inorg. Biochem.* 129 (2013) 30–34. doi:10.1016/j.jinorgbio.2013.07.039.
- [80] W. Argoubi, M. Saadaoui, S. Ben Aoun, N. Raouafi, Optimized design of a nanostructured SPCE-based multipurpose biosensing platform formed by ferrocene-tethered electrochemically-deposited cauliflower-shaped gold nanoparticles, *Beilstein J. Nanotechnol.* 6 (2015) 1840–1852. doi:10.3762/bjnano.6.187.

- [81] H. Wiseman, D.F.V. Lewis, The metabolism of tamoxifen by human cytochromes P450 is rationalized by molecular modelling of the enzyme-substrate interactions: potential importance to its proposed anti-carcinogenic/carcinogenic actions, *Carcinogenesis*. 17 (1996) 1357–1360. doi:10.1093/carcin/17.6.1357.
- [82] C. Rodriguez-Antona, M. Ingelman-Sundberg, Cytochrome P450 pharmacogenetics and cancer, *Oncogene*. 25 (2006) 1679–1691. doi:10.1038/sj.onc.1209377.
- [83] R. Ferraldeschi, W.G. Newman, The impact of CYP2D6 genotyping on tamoxifen treatment, *Pharmaceuticals*. 3 (2010) 1122–1138. doi:10.3390/ph3041122.



CHAPTER SIX

Summary

The important role played by surface stabilization agents during the colloidal synthesis of quantum dots has been widely studied over the past few years. The choice of the surface ligand and its length play a crucial role with regards to the mobility and the conductivity of the quantum dot films. In general, short chained ligands are the mostly preferred ligands for colloidal synthesis to inhibit nanoparticle overgrowth and aggregation of the prepared QDs. Hence in this study, we introduced a new thiol-type 3,3'-DTDPA capping agent employed to improve the stability and efficiency of PdTeQDs. In this chapter, the novel 3,3'-DTDPA-PdTeQDs were characterised by HR-TEM, SAXSpace, UV-Vis and PL. Also, the biosensor responses to tamoxifen and the biotransformation of TAM to its primary and secondary metabolites were determined by DPV studies.

Electrochemical Dithiodipropionic Acid-Palladium Telluride Quantum Dots Phenotype Sensor for Tamoxifen

Abstract

In this study, we report the development of a highly-sensitive 3,3'-dithiodipropionic acid-capped palladium telluride quantum dots (3,3'-DTDPA-PdTeQDs) phenotype-based biosensor for the determination of tamoxifen. This system comprised of the 3,3'-DTDPA-PdTeQDs deposited on gold electrode surface through the cysteamine sulphur group. 1-ethyl-3-(3-dimethylaminopropyl) carbodiimide/N-Hydroxysuccinimide cross linking agents were used to activate the COOH groups present in 3,3'-DTDPA of the QDs for the attachment of CYP3A4 or CYP2D6 enzyme to form a final biosensor. HR-TEM, SAXSpace and SAED pattern revealed that the PdTeQDs materials are spherical in shape and have average diameters of 3-5 nm. The PL emission spectra revealed a blue-shift from (513nm to 502 nm) with decreasing particle size. The value of band gap energy has been found to be in range of 2.4 eV-2.5 eV. Moreover, this behaviour is related to size quantum confinement attributed to the small sizes of the QDs. The tamoxifen biosensors had a limit of detection (*LOD*) values of 6.88×10^{-5} ng/mL (1.75×10^{-5} ng/mL) for CYP3A4 (CYP2D6) biosensor systems that are much lower than the tamoxifen's maximum steady state plasma concentration (C_{max} 40 ng/mL normally obtained 5 h after drug administration).

6. Introduction

This chapter describes simple, cost-effective preparation and characterization of water-soluble and biocompatible 3,3'-dithiodipropionic acid- capped palladium telluride quantum dots (3,3'-DTDPA-PdTeQDs). The colloidal synthesis of 3,3'-DTDPA-PdTeQDs are important because 3,3'-dithiodipropionic acid (3-3'DTDPA) has been regarded as a novel capping agent used in PdTeQDs [1]. Several reports have focussed on the widely used short ligands such as 3-mercaptopropionic acid (3-MPA), thioglycolic acid (TGA) [2,3]. However, 3,3-DTPA is found to be a very attractive ligand since it has disulphide in the molecular structure and results in low densities of midgap states allowing for collection of charge carriers over relatively long distances outside the depletion region [4] Moreover, this capping agent results in the improvement of optical properties and catalytic performance of QDs [5]. Hence, in this study the functionalised 3,3'-DTDPA-PdTeQDs were conjugated with CYP450 (3A4 or 2D6) enzymes for the development of a highly sensitive and stable phenotype biosensor system for the determination of tamoxifen drug.

6.1 Experimental

6.1.1 Chemicals and sample preparation

Tablets labelled as 20 mg tamoxifen citrate (TAM) molecular weight 563.64 were provided by (City Kem Pharmacy, Cape Town). A stock solution of 1 μ M TAM was prepared in absolute ethanol from which a fresh standard solution of 1.6 nM TAM was prepared by dilution with 0.1 M phosphate buffer solution, pH 7.4 (PBS), for experimental investigations. Both stock and standard TAM solutions were stored at 4 °C. 0.1 M phosphate buffer solution, pH 7.4 was prepared from disodium hydrogen phosphate dibasic and sodium dihydrogen phosphate monobasic using Milli Q water purification. All the reagents were of analytical grade and obtained from Sigma-Aldrich Sweden AB, Stockholm, Sweden including human

cytochrome P450-3A4 enzyme (≥ 50 units/mg protein based on reductase activity) expressed in *Saccharomyces cerevisiae*, cytochrome P450-2D6 enzyme (1425 units/mg protein based on reductase activity) expressed in *Saccharomyces cerevisiae*.

6.1.2 Instrumentation

All electrochemical experiments were carried out in 0.1 M PBS, pH 7.4 using a CHI 760E electrochemical workstation (Shanghai CH Instrument Co., China). The electrochemical measurements of the biosensor systems were conducted in a three-electrode system with modified gold disk electrode (3 mm diameter) as the working electrode, a platinum wire as the counter, and Ag/AgCl (3 M NaCl) as a reference electrode supplied by Bioanalytical Systems, Incorporated (BASi), West Lafayette, IN, USA. To evaluate the electrocatalytic behaviour of the biosensor materials on gold electrode, differential pulse voltammetry (DPV) experiments were performed in 0.1 M PBS over a potential range of 0.2 V to -1.4 V at a scan rate of 100 mV/s. The high-resolution scanning electron microscopy micrograms (HR-SEM) of the QDs were imaged using a Zeiss Auriga SEM operating at 50kV and high resolution-transmission electron microscope (HR-TEM) equipped with an energy-dispersed spectroscopy (EDS) detector was used to study the size and morphology of samples. Ultraviolet-visible (UV-Vis) absorption measurements for the prepared PdTeQDs were obtained using 1 cm quartz cuvette on a Nicolet Evolution 100 UV-Visible spectrophotometer (Thermo Electron, UK) over a wavelength range of 200 to 800 nm. The photoluminescence (PL) spectra were recorded using a Nanolog, Horiba NanoLog™ 3-22-TRIAX (USA), with double grating excitation and emission monochromators, plus an imaging spectrograph for a second emission channel and excitation wavelength used was 325 nm. Small-Angle X-Ray Scattering (SAXS) measurements for PdTeQDs were obtained using a 1 mm thin walled capillary (i.e. liquids that contains mainly water or hydrocarbons) at the beamline ID09B. We used the CCD

detector (Anton Paar, GmbH, Australia, 133 mm diameter, 2048 × 2048 pixels) at a distance of 0.6 m and an X-ray energy of 10 keV.

6.1.3 Synthesis of 3,3'-DTDPA-capped PdTeQDs

The experimental procedure was performed in accordance with previous studies [6], with some modifications, employing a different capping agent. In a typical synthesis experiment, PdCl₂ (0.166 g, 0.938 mmol) and 3,3'-dithiodipropionic acid (3,3'-DTDPA) (196 μL, 2.813 mmol) were dissolved in 10 mL of deionised water in a three-neck round bottomed flask, followed by adjustment of the pH to (11.2-11.8) by addition of 5 M NaOH solution with stirring. The mixture was stirred and bubbled by N₂ gas for 30 min. In a second reaction flask, NaHTe solution was prepared by mixing tellurium powder (0.127 g, 0.625 mmol) and NaBH₄ (0.151 g, 2.5 mmol) in 10 mL deionised water and heated to 80 °C for 30 min until the solution attained a light purple colour. Next, the tellurium precursor solution (NaHTe) was injected onto (PdCl₂ and DTDPA) reaction flask, and the resulting solution was stirred and heated (100 °C). The progress of the QDs synthesis was then followed by removing aliquots from the reaction medium at different time intervals and submitted to UV-Vis and PL for analysis. The reaction was quenched by immediately washing the QDs several times with ice cold distilled water, followed by centrifugation at 15,000 rpm for 20 min to remove impurities and excess reaction products. The obtained solid was re-dispersed in distilled water and stored in the refrigerator for further use.

6.1.4 Preparation of CYP (3A4 or 2D6)/TGA-PdTeQDs/Cyst/Au phenotype biosensors

An aliquot (20 μL) of 0.02 M cystamine (Cyst) was drop-casted on a 3 mm diameter Au disk electrode surface and kept in the dark for 24 h. The Cyst/Au modified electrode was functionalised with a drop of a solution consisting of 3,3'-DTDPA-PdTeQDs (containing 0.2 M Pd^{2+}) and 0.1 M 1-ethyl-3-[3-dimethylaminopropyl] carbodiimide/0.1 M N-Hydroxysuccinimide (EDC/NHS, ratio 1:1) and left to cure for 12 h. The 3,3'-DTDPA-PdTeQDs-modified electrode was placed in an Eppendorf vial containing 0.5 mL of 0.1 M PBS and gently vortexed (Vortex-Genie 2, Scientific Industries Incorporated, Bohemia, NY, USA) at 10 rpm for 5 min to remove unbound 3,3'-DTDPA-PdTeQDs. A 3 μL CYP3A4 or CYP2D6 enzyme solution (used as supplied) was then drop-coated onto the 3,3'-DTDPA-PdTeQDs/Cyst/Au electrode surface and kept at 4 $^{\circ}\text{C}$ for 3 h. The resulting CYP3A4/3,3'-DTDPA-PdTeQDs/Cyst/Au (or CYP2D6/3,3'-DTDPA-PdTeQDs/Cyst/Au) biosensor was rinsed gently with distilled water to remove any physically adsorbed enzyme and stored at 4 $^{\circ}\text{C}$ in 0.1 M PBS when not in use.

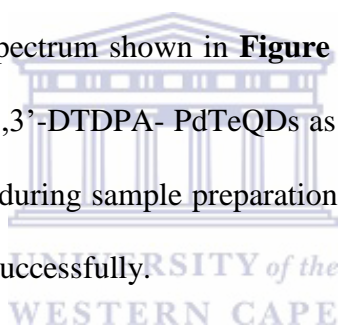
6.1.5 Pathways for TAM metabolism

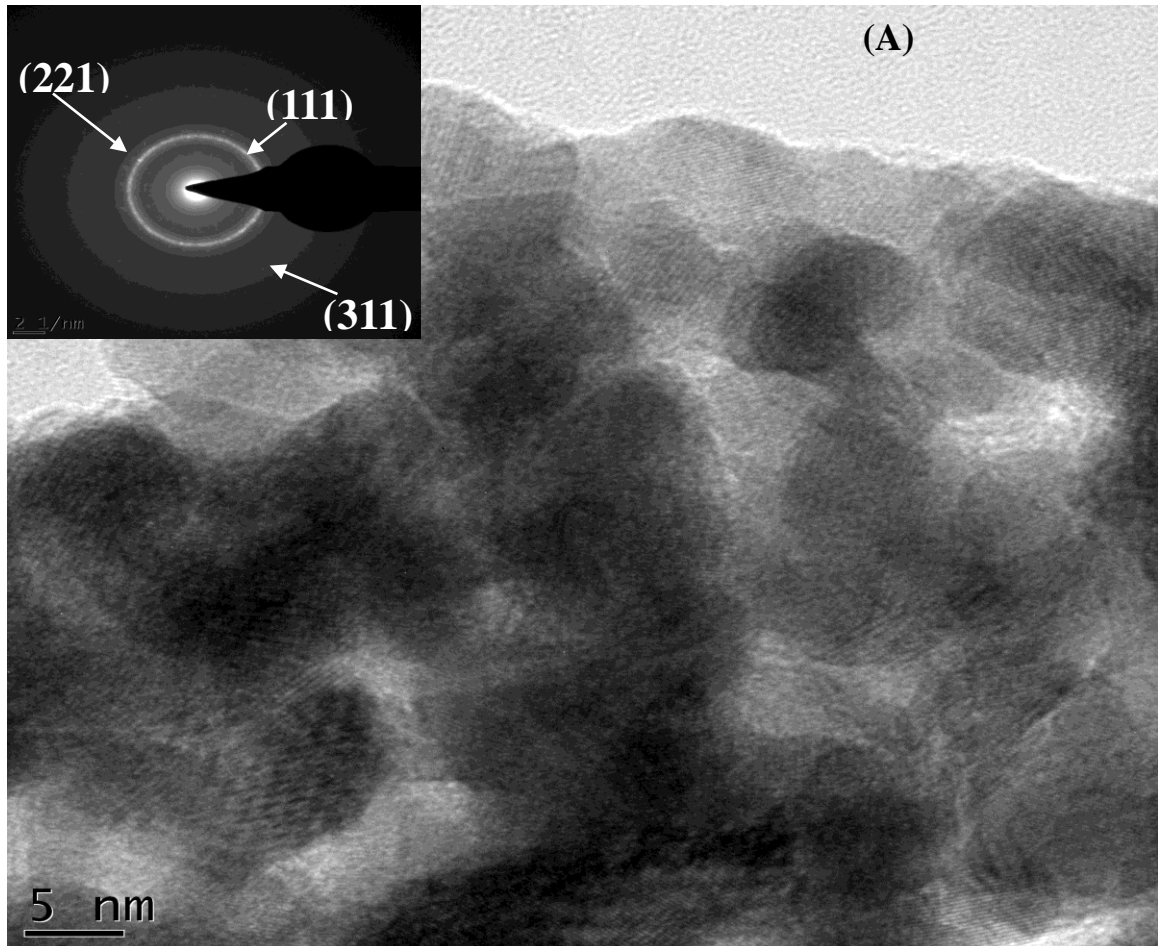
3,3'-DTDPA-PdTeQDs/Cyst/Au electrode was prepared and held in an 8 mL electrochemical cell solution containing 0.2 nM TAM in PBS to which 10 μL CYP3A4 enzyme (used as supplied) was added in order to convert TAM to N-desmethylTAM. Then 10 μL of CYP2D6 enzyme (used as supplied) was added to the cell solution to convert N-desmethylTAM to endoxifen. Another experiment was performed with a fresh 3,3'-DTDPA-PdTeQDs/Cyst/Au electrode in which the order of addition of the enzymes was reversed (CYP2D6 followed by CYP3A4) to produce endoxifen via 4-hydroxytamoxifen (4-hydroxyTAM) intermediate metabolite.

6.2 Results and discussion

6.2.1 Crystal structure of 3,3'-DTDPA-PdTeQDs

HR-TEM technique was employed to investigate the microstructure of 3,3'-DTDPA-PdTeQDs in detail. **Figure 33(A)** depicts the HRTEM micrograph for as-prepared PdTeQDs and electron diffraction pattern (SAED) (insert of **Figure 33(A)**), displaying a broad size distribution and nearly spherically shaped agglomerated QDs, with average sizes of 3-5 nm in diameter [7]. Moreover, the existence of the well-resolved lattice fringes confirmed the good crystallinity of the QDs, which was further supported by the SAED pattern plane spacing (111), (221) and (311) revealing a cubic zinc-blende structure of the QDs [8]. The diameter of the QDs are comparable to that reported by Singh and co-workers [9]. The energy dispersive spectroscopy (EDS) spectrum shown in **Figure 33(B)**, confirmed the presence of Pd, Te and S in the synthesised 3,3'-DTDPA-PdTeQDs as well as the presence of Cu which was due to the copper grid used during sample preparation. Therefore, the results confirmed that PdTeQDs were synthesised successfully.





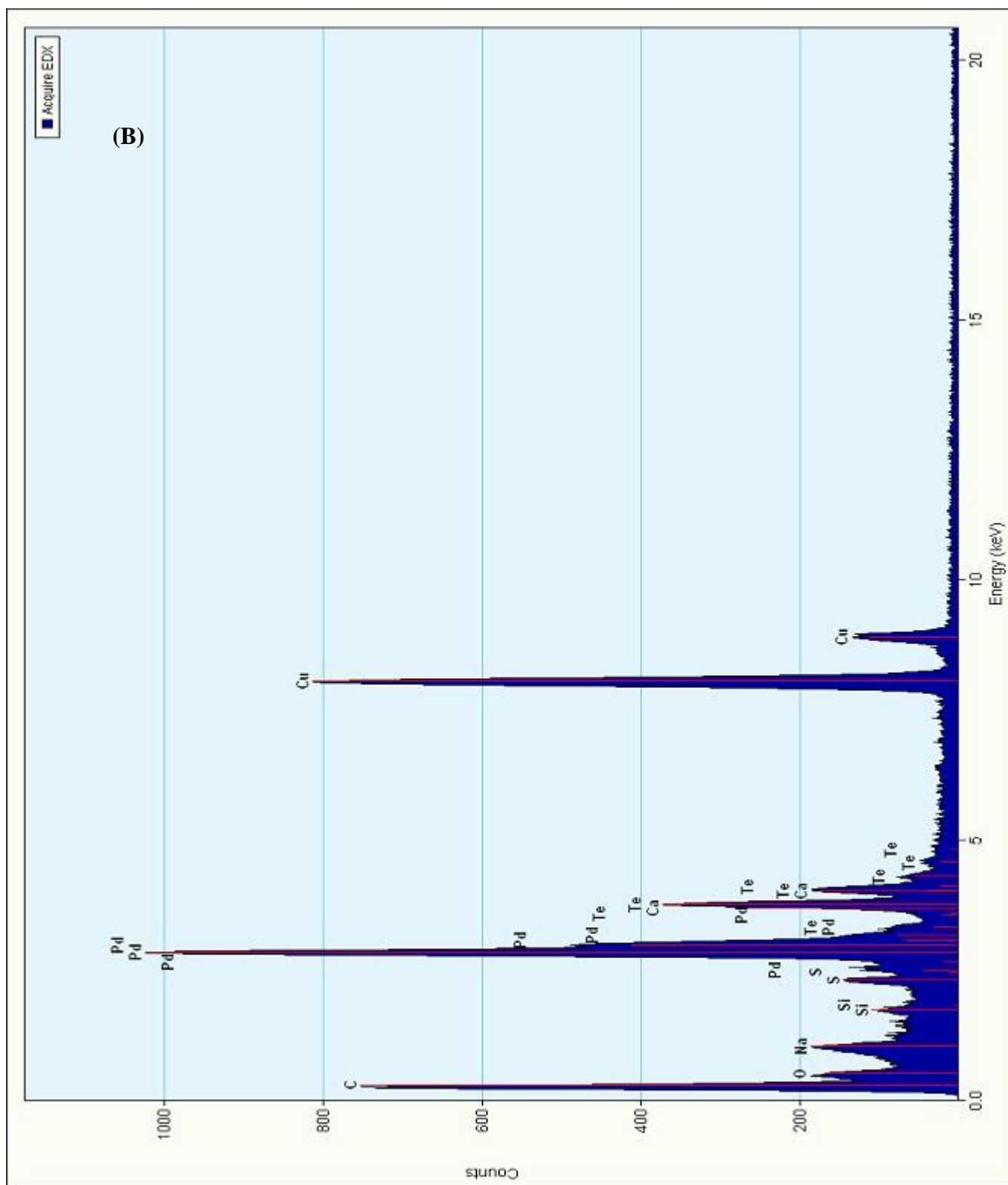


Figure 33: HR-TEM micrograph of (A) 3,3'-DTDPA-PdTeQDs (insert is an SAED pattern) at 5 nm scale view. (B) HR-TEM-EDS spectrum of 3,3-DTDPA-PdTeQDs revealing chemical composition.

6.2.2 Optical properties of 3,3'-DTDPA-PdTeQDs

Figure 34 shows the absorption and emission spectra for PdTeQDs. In this chapter, 3,3'-DTDPA was employed as a new capping agent which efficiently improved the water-solubility and stability by producing a thiol complex around the surface of the PdTeQDs and passivates the surface to sustain high-quality optical properties[10,11]. Interestingly, the presence of DTDPA resulted in a series of characteristic absorbance bands at 212 nm, 250 nm, 267 nm, 320 nm, 415 nm and 563 nm for 30 min and 60 min, respectively, as shown in **Figure 34 A**. The UV-Vis spectra obtained at 60 min appeared at much higher absorbance intensity than 30 min, implying the growth of QDs. Two characteristic absorbance bands observed at 212 nm and 250 nm were attributed to the bond formation of metal-to-ligand charge transfer (PdCl₂-DTDPA) [12]. Tellurium is a toxic metalloid present as a trace constituent in the earth's crust only in about 0.001 parts per million. In the UV-Vis spectrum, the chalcogenide tellurium (Te) is known to exhibit two characteristic absorbance bands[13]. The first characteristic absorbance band observed at 267 nm was ascribed to T⁴⁺ while the second absorbance band at 563 nm was assigned to the reduction of Te⁴⁺ to T⁰ in the visible region [14,15]. PdTeQDs exhibited a characteristic absorbance band at 320 nm, which is consistent with results obtained in **chapter 3 and 4** in the presence of different stabilizing agents. Moreover, the absorbance band appearing at lower energy 415 nm was due to the presence of Pd²⁺ ions in the reaction mixture [16]. **Figure 34 B** shows the normalized photoluminescence spectra (PL) of six aliquots taken during the synthesis of the QDs. Literature suggested that the quantum-confined size effect causes a characteristic change in bandgap energy with decrease in particle size which corresponds to blue shift in emission spectra [17]. Hence, this phenomenon was also observed here, where the excitonic emission bands blue shifted from 513 nm to 502 nm corresponding to widening of the bandgap energies from (2.4 eV-2.5 eV), revealing a decrease in particle sizes. Notably, the QDs

aliquots emitted at similar emission intensity, however, their emission band widths became much broader with prolonging the reaction time, indicating the various sizes of the as-prepared PdTeQDs. Furthermore, the bandgap energies of QDs obtained from UV-Vis (2.2 eV) and PL (2.4 eV) are comparable, indicating that 3,3'-DTDPA-PdTeQDs are semiconductive.

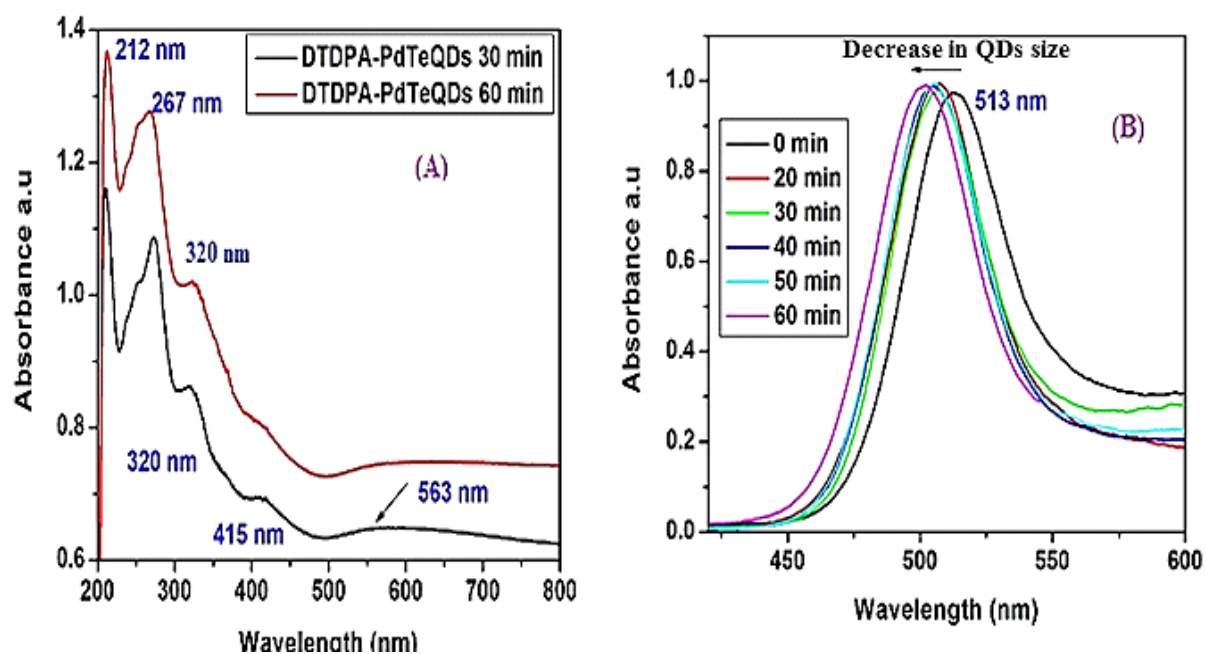


Figure 34: (A) UV-Vis of 3,3'-DTDPA-PdTeQDs (30 min, black line) and (60 min, redline) in the region of 200-800 nm in 0.1 M PBS (pH 7.4). (B) normalized PL for 3,3'-DTDPA-PdTeQDs excited at 325 nm for (black line) 0 min, (red line) 20 min, (green line) 30 min, (blue line) 40 min, (cyan line) 50 min and (pink line) 60 min, respectively.

6.3 Introduction to small angle x-ray scattering (SAXS)

Small-Angle X-Ray Scattering (SAXS) is described as a powerful method employed to determine the structure of particle systems regarding parameters such as averaged particle sizes, shapes, distribution, and surface-to-volume ratio [18]. In contrast with other techniques that provide the information about particle size and shape such as HR-TEM, SAXSpace has an advantage of analysing a variety of materials including aerosols, colloidal suspensions of all types, powders, solids, thin films, biological samples as well as biomolecular interactions[19,20]. Usually, the X-rays are directed through the sample transmission mode and every particle directed into the beam will provide a signal. Literature suggests that the time requirements of the experiments mainly depend on the used instrumentation classified into two groups, (1) line collimation instruments and (2) point collimation instruments.

1. **Line-collimation instruments** confine the beam only in one dimension so that the beam profile is a long but narrow line with typically $20 \times 0.3 \text{ mm}^2$. This instrument is much more compact than the point-collimated systems, and is less expensive and normally illuminates a larger amount of sample to collect more scattering [21].

2. **Point-collimation instruments** have pinholes that usually shape the beam to a small circular or elliptical spot. Moreover, this class of instruments also dominates the small-angle scattering field at synchrotrons as well as neutron sources due to their flexibility [22].

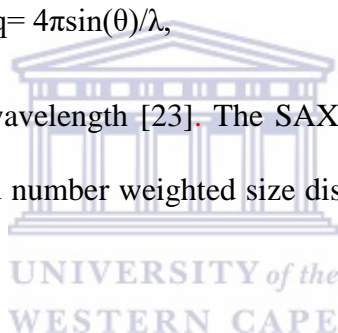
6.3.1 SAXSpace experimental procedure

An aliquot (35 μL) of 3,3-DTDPA-PdTeQDs was loaded in a 1 mm thin walled quartz capillary and was exposed to the beam at a distance of 305.3mm from the CCD and temperature-controlled at 21 $^{\circ}\text{C}$. Measurements were performed with the SAXSpace system (Anton Paar, GmbH, Australia) in line-collimation mode with an accessible q range of

0.0732–1.66nm. For each measurement, six frames were obtained at 100 s exposure time and averaged. Moreover, the deionized water was also measured as a reference under the same conditions as the QDs. Data evaluation/analysis was performed with the GIFT software (generalized indirect Fourier transformation (GIFT) which is a versatile tool for the evaluation of small angle scattering data) in order to determine the particle size and the size distribution of the dispersions [19]. In SAXS, the scattered X-ray intensity is measured as a function of the magnitude of the scattering vector, q , which is related to the scattering angle, 2θ , where by

$$q = 4\pi \sin(\theta) / \lambda, \quad \text{eq (1)}$$

and λ is the incident radiation wavelength [23]. The SAXS curves were then converted by PDDF into intensity, volume and number weighted size distributions as illustrated in **Figure 35**.



6.3.2 SAXSpace for 3,3-DTDPA-PdTeQDs

As can be seen in **Figure 35A**, the majority of poly-dispersed PdTeQDs appeared at small-angle scattering pattern with the average sizes ranging from 3 nm to 5 nm followed by the decreased scattering fraction number of bigger particles observed at larger scattering angles (12.5 nm) [22]. Normally, small angle scattering pattern can be considered as the sum of the scattering patterns of the individual particles contained in the scattering volume fraction. Thus, the scattered intensity generally decreases with scattering angle and the investigation is established on assessment of the scattering by a single particle [24]. **Figure 35B** revealed a series of PdTeQDs weighted by volume fraction at 5 nm, 12.5 nm, 18 nm, 25 nm, 32 nm and 45 nm, [4] respectively. In contrast to other QDs at larger scattering patterns, the volume

fraction of the QDs at small scattering angle pattern (5nm) was more prominent indicating that various QDs sizes mostly occupied at small angle scattering pattern. Moreover, these results are in good accordance with HR-TEM. Literature suggested that the intensity of the scattering signal normally goes with the sixth power of the particle size. Therefore, bigger particles at larger angles obtain much intensity than small particles at small angles [22,24]. Hence, as indicated in **Figure 35C**, the intensity signal obtained by QDs around (5 nm-7nm) was nearly invisible than the intensity at large angles (i.e. the particles ranging from 25 nm to 35 nm in diameter). This, therefore, concluded that larger particles overshadowed the intensity signal of the particles at small angles.



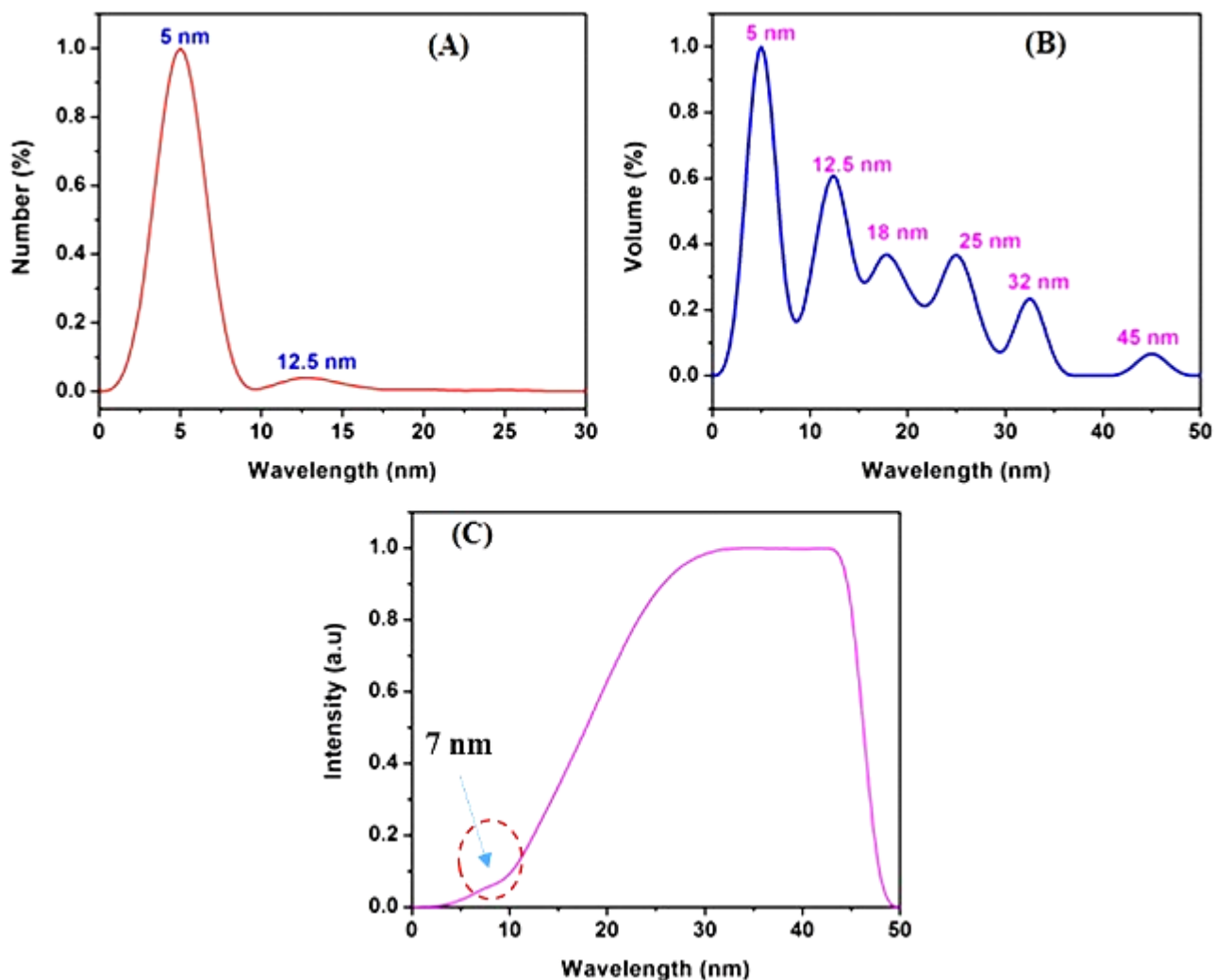


Figure 35: SAXS measurements of (A) Number, (B) volume and (C) intensity weighted size distributions of 3,3-DTDPA-PdTeQDs, respectively.

6.4 Electrochemistry of the biosensor systems

6.4.1 Biosensor responses to tamoxifen

Figure 36 (A and B) illustrates the catalytic responses of CYP2D6/3,3'-DTDPA-PdTeQDs/Cyst/Au and CYP3A4/3,3'-DTDPA-PdTeQDs/Cyst/Au in the absence and presence of tamoxifen at 100 mV/s. In the presence of oxygen, the biosensor system (A) revealed two characteristic cathodic peaks at 0.05 V and -0.99 V while (B) displayed cathodic

peaks at -0.16 V and -0.46 V, respectively. Upon the addition of tamoxifen, a gradual increase in cathodic peaks accompanied by slight shifts to less negative potentials were observed, indicating a more readily reduced species [25]. In general, oxygen is known to be the natural co-substrate of CYP450 enzymes and obviously binds to the ferrous ion of the enzyme's heme centre at a fast rate which results in a major increase in cathodic signal [26]. However, studies have indicated that 4-HydroxyTAM (results from CYP2D6 mediated metabolism) is a minor metabolite even though it is regarded to be more potent antiestrogen than TAM [27]. Hence, the broadness of the cathodic peak observed at -0.96 V in **Figure 36A**, illustrated a weak electron speed compared to biosensor system (**B**) [28]. Based on these results, it can be concluded that CYP3A4 is a major catalyst for N-desmethylTAM. Calibration curves drawn from the linear regression of the biosensor systems are illustrated in **Figure 36** (C and D). The sensitivities were derived from the calibration curve slopes 2.353 $\mu\text{A}/\text{pM}$ (0.614 $\mu\text{A}/\text{pM}$) and the detection limits (*LOD*) were calculated to be 1.75×10^{-5} ng/mL (6.88×10^{-5} ng/mL) for CYP2D6/3,3'-DTDPA-PdTeQDs/Cyst/Au (CYP3A4/3,3'-DTDPA-PdTeQDs/Cyst/Au) biosensor system, respectively.

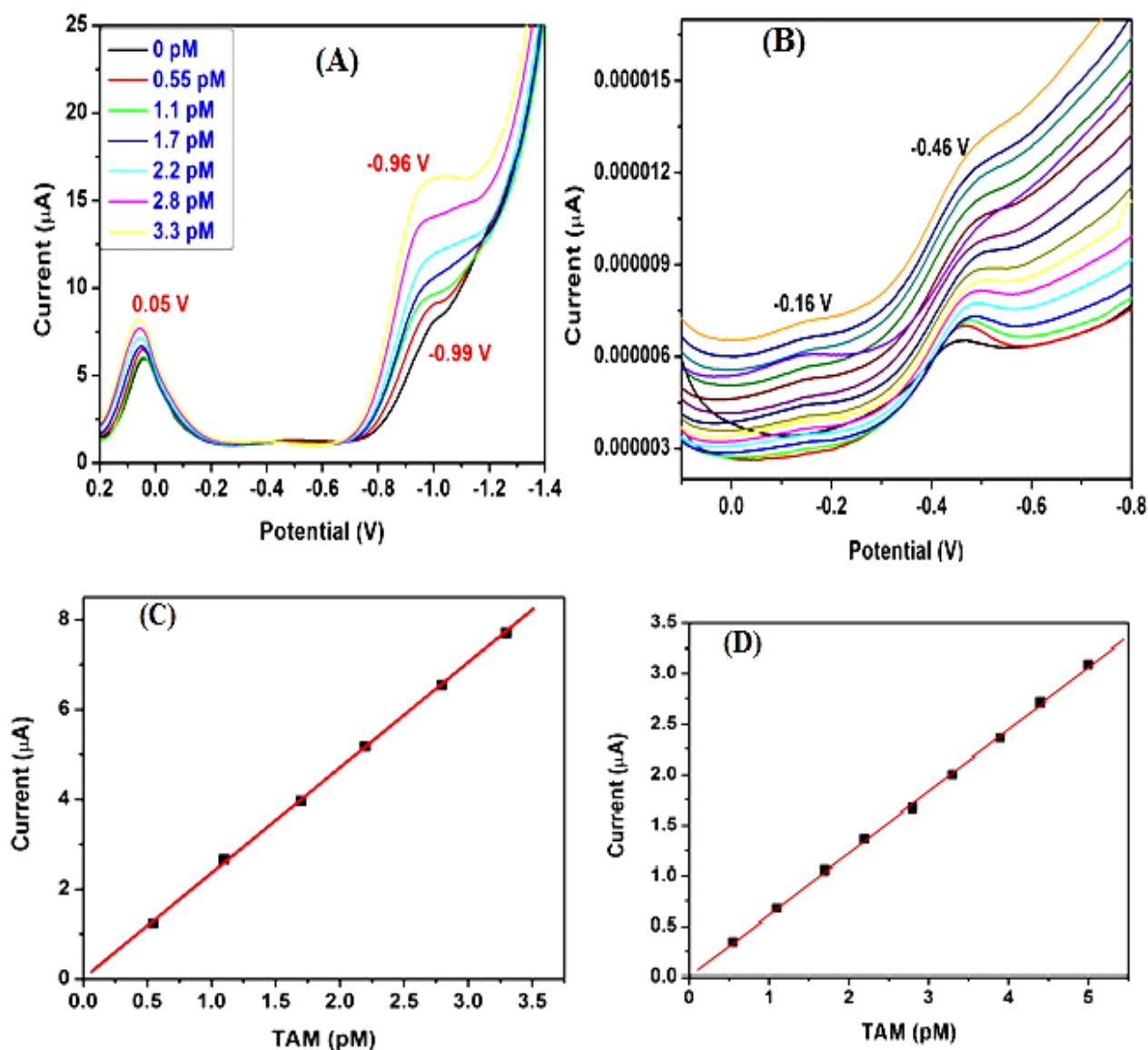
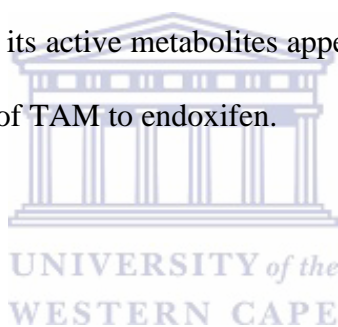


Figure 36: (A and B) DPV measurements recorded at a potential window (0.2 to -0.85 V) in 0.1 M PBS for (CYP2D6/3,3'-DTDPA-PdTeQDs/Cyst/Au) and (CYP3A4/3,3'-DTDPA-PdTeQDs/Cyst/Au) biosensor systems upon successive addition of tamoxifen concentrations 0.55 pM-5 pM. (C and D) corresponding calibration curves drawn from linear region of the biosensor systems.

6.4.2 Conversion of tamoxifen to its active metabolites

Over the past few years, the basic theories about TAM metabolism and responses have been associated with the study by Jordan and co-workers which demonstrated that high first-pass metabolism of TAM exhibits an increase in its activity and further investigated the first active primary metabolite, 4-hydroxyTAM [29]. In this study, DPV was employed to investigate the characteristic features of the modified gold electrode systems in 0.1 M PBS at 100 mV/s. In the presence of TAM in solution, as shown in **Figure 37A**, two characteristic cathodic peaks were observed at -0.016 V and -0.32 V. The first cathodic peaks could be attributed to the adsorption of tamoxifen and the second cathodic peak could be due to the interaction between QDs and cysteamine. When CYP2D6 enzyme was introduced in solution containing TAM-(3,3'-DTDPA-PdTeQDs/Cyst/Au), the enhancement in cathodic peak at -0.06 V and the disappearance of the peak at -0.32 V was observed. This enhancement could be based on the formation of a minor metabolite 4-hydroxyTAM as shown in **Figure 37A** (b). Several studies have suggested that the primary metabolites of TAM can be further oxidized by the human CYP system to a variety of important metabolites [30]. Thus, the presence of CYP3A4 enzyme in TAM-CYP2D6-(3,3'-DTDPA-PdTeQDs/Cyst/Au) solution resulted into a remarkable enhancement of cathodic peak which shifted to more positive potential, indicating a formation of a secondary metabolite endoxifen. In contrast, **Figure 37B** revealed two characteristic cathodic peaks at 0.02 V which appeared at higher current intensity than the cathodic peak at -0.32 V in the presence of TAM in 0.1 M PBS. Interestingly, the cathodic peak slightly increased by a factor of 2 μ A when CYP3A4 enzyme was introduced in solution however, the cathodic peak at -0.32 V decreased in peak current factor of about 4.1 μ A. Furthermore, the presence of CYP2D6 in solution containing CYP3A4-TAM- (DTDPA-PdTeQDs/Cyst/Au) resulted in a major decrease in cathodic current. The observed cathodic peak had properties consistent with a secondary metabolite (endoxifen). The obtained results

suggest that N-desmethyl- and 4-hydroxy-TAM formation accounts for approximately 92% and 7% of primary TAM oxidation respectively [31]. **Figure 37** (C and D) shows the calibration plots measured at different incubation times. It is known that TAM undergoes metabolism, the longer duration of incubation may increase the formation of primary and secondary metabolites which may elucidate the exact contribution of specific metabolic pathway to the overall clearance or activation of the drug[27,32]. Several investigators have tried to use long duration of incubation to observe the sensitivity of the metabolites that are normally made at a slower rate. As it can be seen in **Figure 37C** (c), there was no observable change in cathodic current compared to **Figure 37C** (a and b). However, in **Figure 37 D**, there was an observable change in cathodic currents with increasing incubation time. Interestingly at 20 min TAM and its active metabolites appeared at the same current intensity indicating successful conversion of TAM to endoxifen.



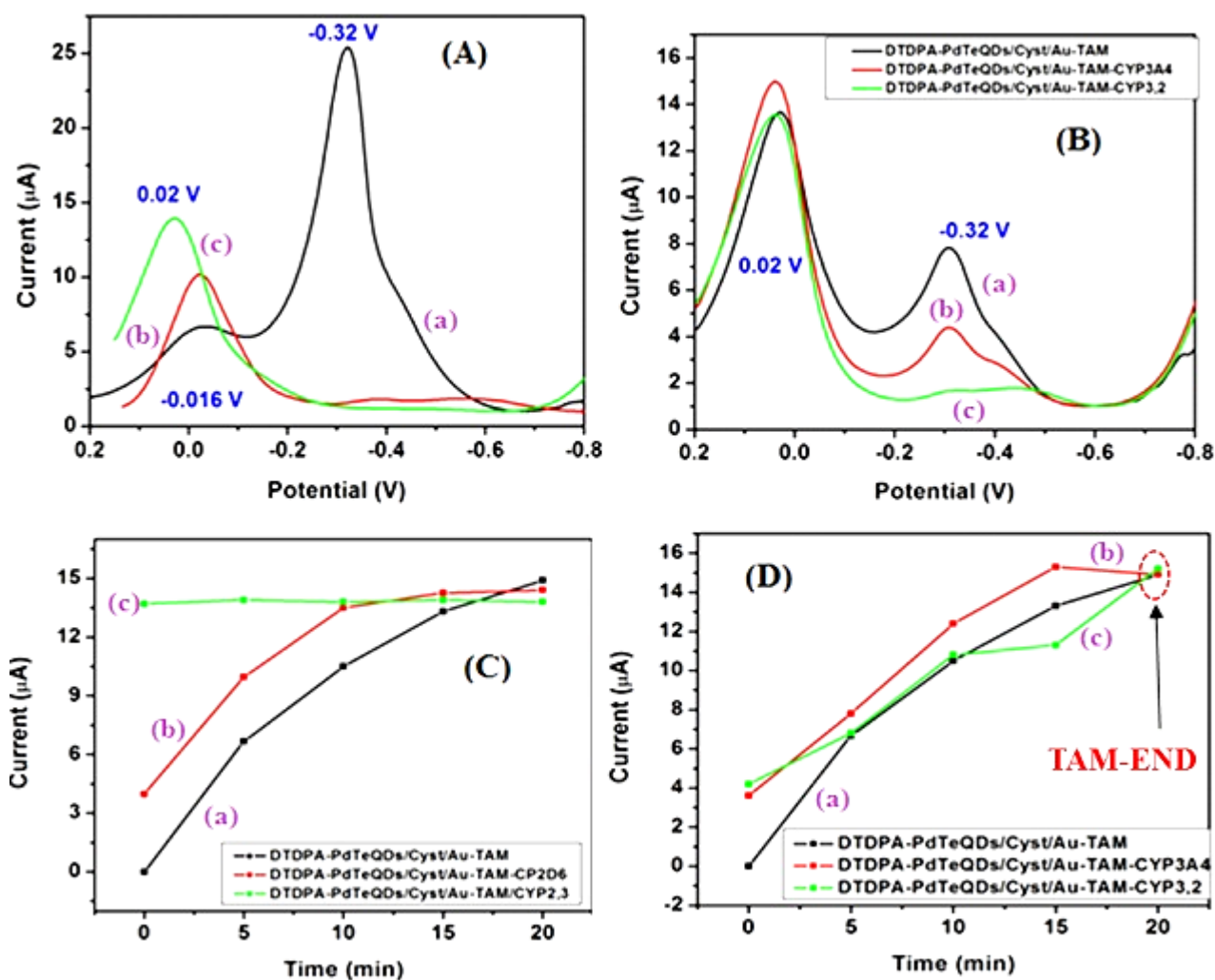
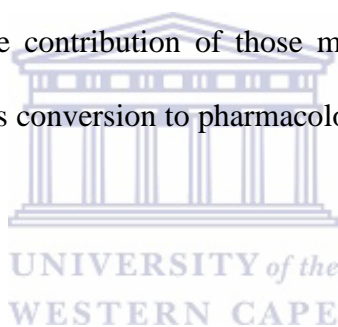


Figure 37: (A and B) DPVs recorded at a potential window (0.2 to -0.8 V) for (a) TAM-(3,3'-DTDPA-PdTeQDs/Cyst/Au), (b) TAM-CYP2D6-(3,3'-DTDPA-PdTeQDs)/Cyst/Au and (c) TAM-CYP3A4-CYP2D6-(3,3'-DTDPA-PdTeQDs)/Cyst/Au; (a) TAM-(3,3'-DTDPA-PdTeQDs/Cyst/Au), (b) TAM-CYP3A4-(3,3'-DTDPA-PdTeQDs)/Cyst/Au and (c) TAM-CYP2D6-CYP3A4-(3,3'-DTDPA-PdTeQDs)/Cyst/Au). (C and D) time dependent studies performed from (0-20 min) for (a) TAM-(3,3'-DTDPA-PdTeQDs/Cyst/Au), (b) TAM-CYP2D6-(3,3'-DTDPA-PdTeQDs)/Cyst/Au, (c) TAM-CYP3A4-CYP2D6-(3,3'-DTDPA-PdTeQDs)/Cyst/Au; (a) TAM-(3,3'-DTDPA-PdTeQDs/Cyst/Au), (b) TAM-CYP3A4-(3,3'-DTDPA-PdTeQDs)/Cyst/Au and (c) TAM-CYP2D6-CYP3A4-(3,3'-DTDPA-PdTeQDs)/Cyst/Au, respectively.

6.5 Conclusion

The study demonstrated the successful synthesis of water-soluble and biocompatible 3,3'-DTDPA-PdTeQDs for the development of phenotype-based biosensor system for tamoxifen detection. Differential pulse voltammetry (DPV) responses of the CYP3A4 (or CYP2D6) 3,3'-DTDPA-PdTeQDs/Cyst/Au biosensor systems indicated -0.46 V (-0.96 V) as the suitable potentials for monitoring the tamoxifen monooxygenation reaction. Consequently, the phenotype biosensor systems have a potential of being an alternative testing tool in comparison to chromatographic methods for determining tamoxifen in pharmaceutical formulation. In addition, this study presents an important application of nanomaterial in medical diagnostics. The biotransformation results obtained in DPV studies may serve as a basis to predict and estimate the contribution of those metabolic pathways and CYP450s relevant to TAM clearance and its conversion to pharmacologically active metabolites in vivo at therapeutic concentrations.



References

- [1] C.C. Reinhart, E. Johansson, Colloidally Prepared 3-Mercaptopropionic Acid Capped Lead Sulfide Quantum Dots, *Chem. Mater.* 27 (2015) 7313–7320. doi:10.1021/acs.chemmater.5b02786.
- [2] P.R. Brown, D. Kim, R.R. Lunt, N. Zhao, M.G. Bawendi, J.C. Grossman, V. Bulovi??, Energy level modification in lead sulfide quantum dot thin films through ligand exchange, *ACS Nano*. 8 (2014) 5863–5872. doi:10.1021/nn500897c.
- [3] R. Azmi, S.-H. Oh, S.-Y. Jang, High-Efficiency Colloidal Quantum Dot Photovoltaic Devices Using Chemically Modified Heterojunctions, *ACS Energy Lett.* (2016) 100–106. doi:10.1021/acsenergylett.6b00070.
- [4] K.M. Clark, Y. Yu, N.M. Marshall, N. Sieracki, M.J. Nilges, N.J. Blackburn, W.A. van der Donk, Y. Lu, Transforming a Blue Copper into a Red Copper Protein: Engineering Cysteine and Homocysteine into the Axial Position of Azurin Using Site-Directed Mutagenesis and Expressed Protein Ligation, *J. Am. Chem. Soc.* 132 (2010) 10093–10101. doi:10.1021/ja102632p.
- [5] M.F. Frasco, N. Chaniotakis, Semiconductor quantum dots in chemical sensors and biosensors, *Sensors*. 9 (2009) 7266–7286. doi:10.3390/s90907266.
- [6] D.S. Mazing, A.M. Brovko, L.B. Matyushkin, O.A. Aleksandrova, V.A. Moshnikov, Preparation of cadmium selenide colloidal quantum dots in non-coordinating solvent octadecene, *J. Phys. Conf. Ser.* 661 (2015) 12033. doi:10.1088/1742-6596/661/1/012033.
- [7] D. Debruyne, O. Deschaume, E. Coutiño-gonzalez, N.H. Nguyen, T.G. Duong, V.N. Hoang, N.T. Pham, coatings Synthesis and application of quantum dots- based biosensor, (n.d.). doi:10.1088/2043-6262/6/1/015015.

- [8] X. Zhou, X. Zeng, X. Yan, W. Xia, Y. Zhou, Shape- and phase-controlled ZnS nanostructures and their optical properties, *Mater. Res. Bull.* 59 (2014) 25–31. doi:10.1016/j.materresbull.2014.06.027.
- [9] P. Singh, D. Das, A. Kumar, A.K. Singh, Palladium (II) complexes of N - { 2- (aryltelluro) ethyl } morpholine / piperidine : Synthesis , structure , application in Heck coupling and unprecedented conversion into nano-sized PdTe, *INOCHE.* 15 (2012) 163–166. doi:10.1016/j.inoche.2011.10.015.
- [10] E.M. Ali, Y. Zheng, H. Yu, J.Y. Ying, Ultrasensitive Pb²⁺ Detection by Glutathione-Capped Quantum Dots, 79 (2007) 9452–9458.
- [11] O. Adegoke, T. Nyokong, Probing the sensitive and selective luminescent detection of peroxy nitrite using thiol-capped CdTe and CdTe @ ZnS quantum dots, *J. Lumin.* 134 (2013) 448–455. doi:10.1016/j.jlumin.2012.08.002.
- [12] R. Seoudi, A. Shabaka, Z.A. El Sayed, B. Anis, Effect of stabilizing agent on the morphology and optical properties of silver nanoparticles, *Phys. E Low-Dimensional Syst. Nanostructures.* 44 (2011) 440–447. doi:10.1016/j.physe.2011.09.018.
- [13] O. Properties, Facile Synthesis of Tellurium Nanowires and Study of Their Third-Order Nonlinear Optical Properties, 28 (2017) 58–67.
- [14] H. Isomaki, J. Isomaki, H. Isomaki, I. Yamamoto, Y. Ohmasa, Optical Absorption of Tellurium, (n.d.).
- [15] S.M. Baesman, T.D. Bullen, J. Dewald, D. Zhang, S. Curran, F.S. Islam, T.J. Beveridge, R.S. Oremland, Formation of Tellurium Nanocrystals during Anaerobic Growth of Bacteria That Use Te Oxyanions as Respiratory Electron Acceptors □, 73 (2007) 2135–2143. doi:10.1128/AEM.02558-06.

- [16] A.J. Kora, L. Rastogi, Green synthesis of palladium nanoparticles using gum ghatti (*Anogeissus latifolia*) and its application as an antioxidant and catalyst, *Arab. J. Chem.* (2015) 0–9. doi:10.1016/j.arabjc.2015.06.024.
- [17] P. Kumar, Effect of Silicon Crystal Size on Photoluminescence Appearance, 2011 (2011). doi:10.5402/2011/163168.
- [18] T. Li, A.J. Senesi, B. Lee, Small Angle X - ray Scattering for Nanoparticle Research, (2016). doi:10.1021/acs.chemrev.5b00690.
- [19] N. Allec, M. Choi, N. Yesupriya, B. Szychowski, M.R. White, M.G. Kann, E.D. Garcin, M. Daniel, A. Badano, Small-angle X-ray scattering method to characterize molecular interactions: Proof of concept, *Nat. Publ. Gr.* (2015) 1–12. doi:10.1038/srep12085.
- [20] A. Agbabiaka, M. Wiltfong, C. Park, Small Angle X-Ray Scattering Technique for the Particle Size Distribution of Nonporous Nanoparticles, 2013 (2013).
- [21] N. Laboratorium, D.N.V.P. Gloeilampenfabrieken, THEORY OF THE STABILITY OF LYOPHOBIC COLLOIDS, (1946) 631–636.
- [22] X. Small-angle, X. Di, B. Fleury, R. Cortes-huerto, O. Tache, F. Testard, N. Menguy, O. Spalla, Gold Nanoparticle Internal Structure and Symmetry Probed by Unified Small-Angle X - ray Scattering and X - ray Diffraction Coupled with Molecular Dynamics Analysis, (2015). doi:10.1021/acs.nanolett.5b02924.
- [23] J. Kimling, M. Maier, B. Okenve, V. Kotaidis, H. Ballot, A. Plech, Turkevich Method for Gold Nanoparticle Synthesis Revisited, (2006) 15700–15707.
- [24] H. Schnablegger, Y. Singh, The SAXS Guide, Anton Paar, (2011),1-99.
- [25] N. Ntshongontshi, A. Almonam, A. Baleg, R.F. Ajayi, C. Rassie, E. Nxusani, L.

- Wilson, U. Feleni, U. Sidwaba, S. Qakala, S. Duoman, P. Baker, E. Iwuoha, Cytochrome P450-3A4 / Copper-Poly (Propylene Imine) -Polypyrrole Star Co-Polymer Nanobiosensor System for Delavirdine - A Non-Nucleoside Reverse Transcriptase Inhibitor HIV Drug, 44 (2016) 265–280. doi:10.4028/www.scientific.net/JNanoR.44.265.
- [26] N. Ross, N. Hendricks-leukes, R.F. Ajayi, P. Baker, E.I. Iwuoha, Conductive Composite Biosensor System for Electrochemical Indinavir Drug Detection, 2015 (2015).
- [27] Z. Desta, B.A. Ward, N. V Soukhova, D.A. Flockhart, Comprehensive Evaluation of Tamoxifen Sequential Biotransformation by the Human Cytochrome P450 System in Vitro: Prominent Roles for CYP3A and CYP2D6, 310 (2004) 1062–1075. doi:10.1124/jpet.104.065607.2001.
- [28] Y. Hu, Z. Zhang, H. Zhang, L. Luo, S. Yao, Talanta Electrochemical determination of l -phenylalanine at polyaniline modified carbon electrode based on β -cyclodextrin incorporated carbon nanotube composite material and imprinted sol – gel film, Talanta. 84 (2011) 305–313. doi:10.1016/j.talanta.2011.01.010.
- [29] F. Forward, Comprehensive evaluation of tamoxifen sequential biotransformation by the human cytochrome P450 system, (2004). doi:10.1124/jpet.104.065607.
- [30] A. Novillo, A. Romero-lorca, M. Rubio, A. Ferna, L.M. Chicharro, A. Tejerina, F. Bandre, Relationship between Genotypes Sult1a2 and Cyp2d6 and Tamoxifen Metabolism in Breast Cancer Patients, 8 (2013) 1–10. doi:10.1371/journal.pone.0070183.
- [31] A. Manuscript, NIH Public Access, 38 (2013) 263–273. doi:10.1053/j.seminoncol.2011.01.002.CYP2D6.

- [32] E.T. Ogburn, D.R. Jones, A.R. Masters, C. Xu, Y. Guo, Efavirenz Primary and Secondary Metabolism In Vitro and In Vivo: Identification of Novel Metabolic Pathways and Cytochrome P450 2A6 as the Principal Catalyst of Efavirenz 7-Hydroxylation □ ABSTRACT :, 38 (2010) 1218–1229. doi:10.1124/dmd.109.031393.



CHAPTER SEVEN

Conclusions and Recommendations

This chapter gives an overview of the main objectives and the achievements of the study. It also outlines the future investigations required for (i) the optimization of the performance of the phenotype biosensor systems and (ii) the determination of the metabolic pathway for tamoxifen biotransformation that will be most beneficial in sensor development.



7.1 Conclusions

This study reported the successful synthesis of water-soluble and biocompatible (PdTeQDs) produced by a simple, inexpensive and reproducible aqueous method capped with 3-mercaptopropionic acid (3-MPA), thioglycolic acid (TGA) or 3, 3'-Dithiodipropionic acid (3,3'-DTDPA), to improve their stability and solubility. Functionalisation of the quantum dots with capping agents is very important in biosensor field and the effect of different capping agents on the surface of the QDs were investigated by microscopic, spectrophotometric and electrochemical analysis. HR-TEM, SAED, XRD and SAXSpace studies revealed the information about the crystallinity and size of the QDs with average sizes of 3-5 nm in diameter. The composition of the quantum dots was verified by EDS, and XPS studies, in which the constituents in Pd, Te, and S were observed. Moreover, XPS gave further details about the valence levels and core/shell structure of the QDs. The presence of the stabilizing capping agent on the QDs surface was successfully confirmed by FTIR and Raman studies, which revealed the specific characteristic features CH₂, COOH, and SH as well as O-H functional groups. The optical properties of the QDs materials were studied by ultraviolet-visible spectroscopy (UV-Vis) showing absorption band edges at 320 nm corresponding to energy band gap values of 3 eV, 3.87 eV and 2.2 eV for 3-MPA-, TGA- and 3,3'-DTDPA-capped PdTeQDs, respectively. The excellent electrochemical transduction characteristics of the three surface bound quantum dots were used as the principle for sensor development. When the quantum dots were immobilized on electrode together with CYP3A4 or CYP2D6, the resultant bioelectrode was shown to undergo monooxygenation which is a net reduction reaction. This procedure can be applied in heme-enzyme linked biosensor system for the determination of not only drug metabolism but also the detection of other analyte of clinical, environmental and nutritional importance. The differences in the detection limits using different techniques (as shown in **Table 3**) of the biosensor systems constructed

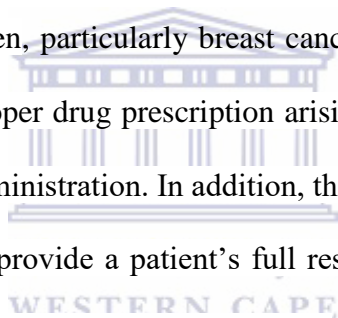
with different capping agents demonstrate one possible method of controlling the performance of this class of biosensor.

Table 3: Phenotype-based biosensor systems for tamoxifen and indinavir using different electrochemical methods (the *LOD* values are all converted to ng/mL)

Techniques	Biosensor	Detection potential (V)	Limit of detection (ng/mL)	Dynamic linear range (pM)	Substrate
CV	CYP3A4/3-MPA-PdTeQDs/Cyst/Au	0.25	40×10^3	1-9	Indinavir
CV	CYP3A4/TGA-PdTeQDs/Cyst/Au	0.9	90×10^3	0.4-0.9	Indinavir
SWV	CYP2D6/TGA-PdTeQDs/Cyst/Au	0.3	9.52×10^{-5}	0.55-8.8	Tamoxifen
SWV	CYP3A4/TGA-PdTeQDs/Cyst/Au	0.28	1.75×10^{-5}	0.55-8.9	Tamoxifen
DPV	CYP2D6/3,3'-DTDPA-PdTeQDs/Cyst/Au	0.96	1.95×10^{-4}	0.55-3.3	Tamoxifen
DPV	CYP3A4/3,3-DTDPA-PdTeQDs/Cyst/Au	0.46	6.88×10^{-5}	0.55-5.6	Tamoxifen

Generally, the *LOD* values obtained with the various phenotype sensors were lower than tamoxifen's maximum steady state plasma concentration (C_{max} 40 ng/mL), thereby indicating that the sensing device, in principle, would be suitable for real time monitoring the drug at point-of-care. This means that the biosensor can be applied for drug detection in patients who

are *ultra-rapid metabolisers* that clear drugs from their systems very quickly. Based on the low DLR values studied, the biosensor systems are very sensitive (down to femto-molar concentrations) and suitable for signalling drug metabolic activity in real time. In this study, two heme-thiolated CYP450 enzymes (CYP3A4 and CYP2D6) participate in biotransformation of TAM to its active metabolite. The obtained results suggest that N-desmethyl- and 4-hydroxy-TAM formation accounts for approximately 92% and 7% of primary TAM oxidation, respectively. The biotransformation results obtained in DPV studies may serve as a basis to predict and estimate the contribution of those metabolic pathways and CYP450s relevant to TAM clearance and its conversion to pharmacologically active metabolites in vivo at therapeutic concentrations. This work is very important and aimed to improve the quality life of women, particularly breast cancer patients. The phenotype based biosensor system will lead to proper drug prescription arising from a point of care testing of the patient's response to drug administration. In addition, the sensing protocol will be suitable for the use at doctor's office to provide a patient's full response pattern for tamoxifen, and therefore, assist the doctor to determine appropriate dose. Hopefully in future the phenotype based biosensor system will be available in pharmacies and hospitals for monitoring a proper dosage of tamoxifen for breast cancer patients.



7.2 Recommendations for future studies

Further studies of phenotype based biosensor systems and applications are discussed below.

- Determination of tamoxifen activation in HeG2 and Hep3B human hepatoma cell lines as well as developing drug toxicity testing protocol for cell lines.
- Individual electrochemical sensing of tamoxifen and its active metabolites (N-desmethylTAM, 4-HydroxyTAM, and endoxifen) using direct electrochemistry or enzyme/aptamer-based biosensors.
- Testing of bi-polar tamoxifen phenotype base biosensor system with clinical samples.
- Application of the phenotype based biosensor for detection of toremifene (an analog of TAM) since it is also taken by breast cancer women at high risk.
- 96-well multichannel robotic electrochemical system must be studied to understand the metabolic pathway (clearance) of tamoxifen drug.
- Integration of tamoxifen metabolism reaction steps using a single microfluidic sensor system that will consist bi-polar reactors for enzymes catalysis and reactors for the detection of metabolites.

